THE UNIVERSITY
of EDINBURGH

Herpes Virus Egress through the Nuclear Envelope and Host Response against Infections

---

Natalia Saiz Ros

Wellcome Trust Centre for Cell Biology
School of Biological Sciences

Doctor of Philosophy – University of Edinburgh – 2017

Declaration

I declare that this thesis has been composed by myself and the work presented herein is my own, except where stated otherwise. This research has not been submitted for any other degree except as specified.

Natalia Saiz Ros

Edinburgh

January 2017

Acknowledgements

Firstly, I would like to express my sincere gratitude to my advisor Dr Eric Schirmer for the continuous support during my PhD, for his patience and for his invaluable guidance. Thanks for always making time for “the princess”.
Together with my advisor, I would like to thank my second supervisor Prof. Sheila Graham for her insightful comments and encouragement.
Many thanks to all the members of the Schirmer and the Principal Scholarship for generously funding my PhD research.
I am thankful to Alba and Mariana, my best friends and colleagues in Edinburgh because without their support and advice during the difficult moments of my PhD I would not be able to write my thesis today. A special mention to all my colleagues of the Wellcome Trust Centre, especially to Mila and Natalia.
My sincere gratitude also to my fellow labmates in la FJD in Madrid, in particular I am grateful to Dr Gabriel Herrero-Beaumont for showing me the first glance of what research is.

Y por último y más importante me gustaría dedicar esta tesis a mi familia y amigos en España porque es lo más valioso que tengo. En primer lugar, a mi madre porque gracias a ella he llegado hasta aquí, por haberme apoyado en todo momento, por sus consejos, por el valor mostrado para salir adelante y por su amor incondicional; a mi hermana pequeña Pau, a quién valoro y aprecio y de la cual aprendí tantas cosas, gracias por las horas de apoyo, gracias por creer en mí; a mi tías, a mis primos, a mi tío, a mi yaya Encarna y a mi yayo Higinio por su humildad y valores transmitidos, a Josema por sus “sabios consejos”, a mis Roncallinas, a mis amigos de Burgos y a todos aquellos que participaron directa o indirectamente en la elaboración de esta tesis porque juntos hemos pasado por un camino de lucha y de esfuerzo. Después de mucha dedicación y no pocos sin sabores y alguna que otra lagrima puedo estar hoy aquí, escribiendo los agradecimientos de mi tesis. Porque esto también os pertenece, ya que sólo vosotros habéis sabido cómo apoyarme, siendo siempre mi principal motivación durante estos tres largos y duros años.

Lay Summary

Viruses are small infectious agents that replicate only inside the living cells of other organisms. Herpesviruses belong to a diverse family of viruses that infect all vertebrates from fish to mammals causing important human health problems associated with the spread of the infection. In order to establish a productive infection, viruses employ a variety of strategies to usurp and control cellular activities and herpesviruses, in particular, commonly take advantage of and use host cell proteins and pathways to support their infections. After using the cell machinery for synthesis and production of new viral particles within the nucleus of infected cells, herpesviruses must overcome the nuclear envelope, a double membrane barrier surrounding the cell nucleus, in order to escape and produce mature viral particles. Previous studies have identified the involvement of three critical viral proteins in the process of herpesvirus egress from the nucleus of infected cells. However little is known about which cellular factors might be aiding this key step in the life cycle of herpesviruses.

The presence of numerous proteins within the nuclear envelope of host cells, and the usurpation of host machinery during different phases of the herpesvirus life cycle led me to investigate the potential contribution of cellular proteins to the escape strategy of herpesvirus from the nucleus of infected cells.

This thesis focuses in the characterization of a specific group of cellular proteins, vesicle fusion proteins, during the escape of new herpesvirus particles from the nucleus of infected cells. These vesicle fusion proteins were identified in a proteomic analysis performed as part of the study presented in this thesis.

Furthermore, this thesis studies the novel role of NET23/STING, a protein localized in part at the nuclear envelope that has been shown to be involved in innate immune signalling pathways protecting infected cells from viral infections.

Abstract

The nuclear envelope is a highly organised double membrane system that separates the activities of the nuclear and cytoplasmic compartments in eukaryotic systems. The wide range of functions recently associated with the NE and the identification of hundreds of proteins associated with this cellular structure indicates that it is a major signalling node for the cell. Recent work indicates NE functions in signalling innate immune responses to herpesviruses. The viruses, on the other hand, often target or usurp NE functions in different ways. The NE is also a physical barrier that must be overcome for viruses like the herpesviridae that assemble capsids in the nucleus. This thesis addresses two important questions: 1) How do herpesviruses cross the NE after new viral particles are produced in the nucleus? and 2) What is the nuclear envelope role of NET23/STING in the activation of immune factors upon herpesvirus infection? To address the first question, I followed two different approaches. The first used the isolation of microsomes from HSV-1 infected cells to identify possible host factors involved during herpesvirus exit through the NE on the prediction that such proteins would disperse into the ER during infection. I identified a group of vesicle fusion proteins that play a role in this herpesvirus exit through the NE. Depletion of three identified vesicle fusion proteins decreased the growth of HSV-1 in host cells, yielding accumulation of viral particles in the nucleus. The second approach was to follow the fate of nuclear envelope transmembrane proteins (NETs) during HSV-1 infection.

To address the question of how NET23/STING is involved in innate immunity I tested the hypothesis that this NET acts as a transport receptor to carry signals through the peripheral channels of the NPC when central channel transport is blocked by pathogens. FRAP was used to quantify the mobility of NET23/STING upon the induction of the innate immune response, finding an increase of the mobility for this protein in the NE. To further elucidate its role within the NE I tested whether some NE-NET23/STING binding partners were being redistributed between the nucleus and cytoplasm during innate immune responses. This revealed

two of these binding partners normally redistribute upon innate immune response activation and this is blocked in cells knocked down for NET23/STING. Finally, I confirmed that NET23/STING contributes to chromatin remodelling during infection involving an increase in the H3K9Me3 epigenetic mark. Collectively, these data argue the identification of novel host proteins involved in herpesvirus nuclear egress and the finding of a new role for NET23/STING within the NE.

Abbreviations

ATP	adenosine-5'-triphosphate	**IRF3/7**	interferon regulatory factor 3 / 7
BSA	bovine serum albumine	**Kb**	kilobase (s)
cDNA	complementary DNA	**LBR**	lamin B receptor
CMV	cytomegalovirus	**mRFP**	monomeric red fluorescent protein
Da	Dalton	**NE**	nuclear envelope
DAPI	4'.6'-diamidino-2-phenylindole	**NET**	Nuclear envelope transmembrane protein
DNA	deoxyribonucleic acid	**NLS**	nuclear localization signal
dNTP	deoxynucleotide triphosphate E	**NPC**	nuclear pore complex
EDTA	ethylenediaminetetraacetic acid	**Nup**	nucleoporin
EM	electron microscopy	**ONM**	outer nuclear membrane
EDMD	Emery-Dreifuss muscular dystrophy	**PA**	(GFP-) Photoactivation
ER	endoplasmic reticulum	**PBS**	phosphate buffered saline
FISH	fluorescence in situ hybridization	**PCR**	polymerase chain reaction
FRAP	Fluorescence Recovery After Photobleaching	**PEP**	primary envelope particles
GFP	green fluorescent protein	**pH**	$-\log_{10}$ (aH+)
HP1	heterochromatin protein 1	**RNA**	ribonucleic acid
HSV-1	Herpes Simplex Virus Type 1	**scr**	scramble
HSV-2	Herpes Simplex Virus Type 2	**SDS**	sodium-dodecyl sulfate
IF	immunofluorescence	**siRNA**	RNA intereference
IIR	innate immune response	**WB**	western blotting
INM	inne nuclear membrane		

List of Figures

List of Tables

Table of Contents

Chapter 1 Introduction

1.1. The Nuclear Envelope (NE)

The nucleus of the host cell is usurped by multiple DNA and RNA viruses for genome replication and/or virion formation. The nuclear envelope (NE), a double membrane system surrounding the nucleus, represents a formidable physical and functional barrier to infection that must be overcome for virus production. Moreover, the NE acts as a signalling structure regulating the transport of molecules and signals in response to viruses. Thus, getting viruses and immune signals across the NE is a highly regulated process that must be understood.

1.1.1. Nuclear envelope and lamina architecture

The NE – also called the nuclear membrane- is a unique organised structure that first appears roughly 3 billion years ago providing a physical barrier between the nucleus and the cytoplasm in eukaryotic cells. The nucleus was the first cell organelle to be discovered by the Dutch microscopy pioneer Anton von Leeuwenhoek in the red blood corpuscles of fish in 1700.

Since the early days of microscopy, our view of the nucleus has developed dramatically. It was in 1833, when the Scottish botanist Robert Brown, named and discovered the nucleus in the cells of an orchid. Additionally, Brown observed by the first time the NE using a light microscope. Later, in the 1940s evidence from electron microscopy (EM) began to accumulate and within a few years the main structural features of the NE became clear. The earliest EM studies specifically focusing on the NE were those of Callan and Tomlin who performed EM on Amphibian oocytes

demonstrating that this structure is a double membrane with layers divided into the inner nuclear membrane *(INM)* and outer nuclear membrane *(ONM)* (Callan and Tomlin 1950).

The two membranes are two concentric lipid bilayers connected at sites where Nuclear Pore Complexes *(NPCs)* are inserted. The NPCs are large protein structures (~60 MDa), composed of multiple copies of approximately 30 different proteins called nucleoporins (Nups) that selectively regulate bidirectional transport between the nucleus and the cytoplasm. The central channel is filled with phenylalanine-glycine (FG)-rich repeat-containing nucleoporins (FG-Nups), which are responsible of limiting the diffusion of molecules with a molecular weight of ~40-60 KDa (Margalit, Vlcek et al. 2005, Eibauer, Pellanda et al. 2015). In addition to central channels, 10 nm peripheral channels are presented between the NPC core and the pore membrane and they can accommodate the diffusion of globular proteins with a mass of < 60 KDa (Hinshaw, Carragher et al. 1992).

The ONM is continuous with the endoplasmic reticulum *(ER)* and it is thought to contain many of the same proteins and lipids (Franke, Scheer et al. 1981, Gerace and Burke 1988). Between the ONM and the INM there is the lumen, a compartment that has been shown to be continuous to the ER lumen. On the other hand, the INM encloses the nucleoplasm, containing the chromosomes and nucleoli (Figure 1).

Both, INM and ONM, contain unique sets of integral membrane proteins called Nuclear Envelope Transmembrane Proteins *(NETs).* Most NETs principally are accumulated in the INM interacting with the lamin intermediate filament polymer maintaining the NE structure. The INM presents a unique enrichment for distinct integral membrane proteins (Schirmer and Gerace 2005, Schirmer and Foisner 2007) that have been identified in several proteomic analyses, most of which are uncharacterized. It is suggested that it contains at least 100 unique components and may contain over 1,000 proteins. Some of these specific INM proteins, apart from interacting with the lamin polymer, also bind chromatin (Mattout-Drubezki and Gruenbaum 2003)

Underneath the INM is the nuclear lamina, a dense meshwork of *lamin polymers* and *lamin associated NETs* that are embedded in the INM and that was first described in vertebrate cells using EM by Fawcett in 1966 (Fawcett 1966) (Figure

1). Lamins are type V intermediate filament proteins that interact with the nucleoplasmic domains of many INM proteins and they include: B-type, lamins encoded by the *LMNB1* and *LMNB2* genes and the A-type, lamins A and C which are different isoforms from the same gene. The lamin filament meshwork is anchored to the INM via interactions with lamin associated NETs such as the Lamin-B Receptor (LBR), emerin, MAN1 and LAP2β. All the interactions between lamin associated NETs, lamin filaments and chromatin, result in the formation of a stable network that supports the architecture of the NE and anchors the INM to chromatin and lamins providing mechanical stability to the nucleus and maintaining nuclear shape.

The lamina network presents a certain nuclear stiffness due to the presence of NETs that stabilize this network and ensure an adequate response to mechanical stress (Dahl, Kahn et al. 2004, Dahl, Ribeiro et al. 2008). The binding of some proteins with lamins depends on the different requirements for nuclear mechanical stiffness and chromatin organization of the cell. The biggest change in lamina architecture occurs during the process of cell division. During mitosis, the NE breaks apart involving the depolymerization of the lamina and the dissociation of proteins from chromatin (Smoyer and Jaspersen 2014). These events are driven by the phosphorylation of lamins and lamin binding proteins such as LBR (Courvalin, Segil et al. 1992) and LAP2 (Dechat, Gotzmann et al. 1998) by protein kinase C (PKC) and cdc2 kinase among others kinases.

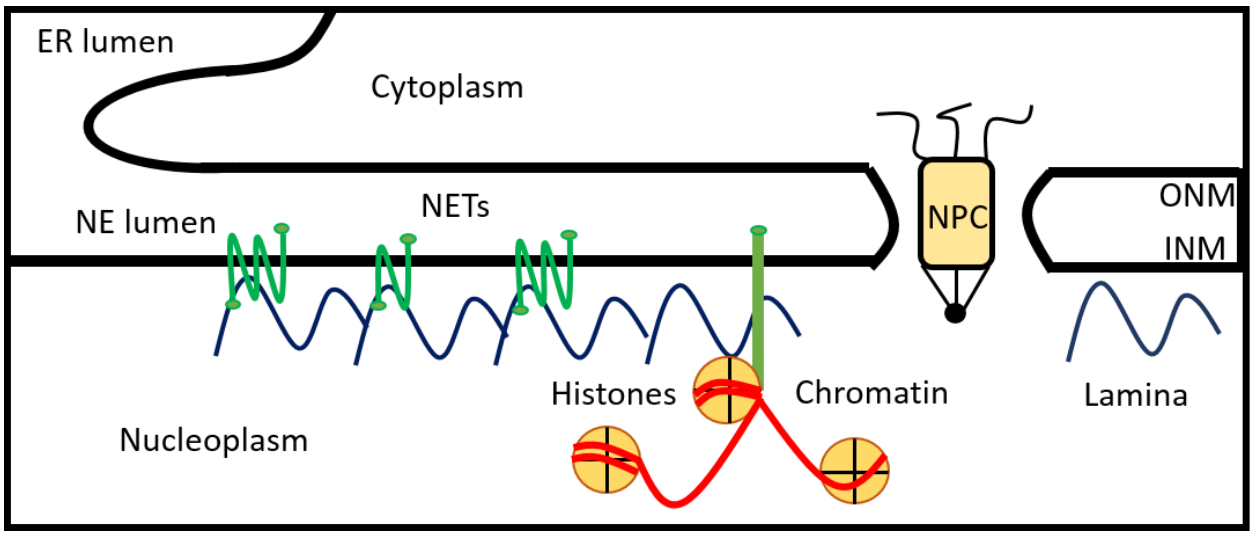

Figure 1. Schematic of the nuclear envelope (NE). *The NE is a double lipid bilayer consisting of the ONM and INM and both lipid membranes are joined at areas where nuclear pore complexes (NPCs) are inserted. Between the INM and ONM there is the NE lumen that is continuous with the ER lumen. The INM presents a unique set of integral membrane proteins (NETs) that together with the lamin filaments constitute the nuclear lamina underlying the INM. At the same time lamins and NETs are known to interact with chromatin.*

1.1.2. Integral proteins of the INM

The INM of eukaryotic cells is a membrane that harbours a unique set of integral membrane proteins required for nuclear structure, chromosome positioning, DNA repair and control of gene expression.

Different proteomic studies have shown the existence of over a hundred different NE proteins that localize to the INM, many of which are expressed in a tissue-specific manner (Dreger, Bengtsson et al. 2001, Schirmer, Florens et al. 2003, Schirmer, Florens et al. 2005, Korfali, Wilkie et al. 2010, Wilkie, Korfali et al. 2011). Notably, only a few of these proteins have been characterized in detail (Olins, Rhodes et al. 2010, Berk, Tifft et al. 2013). LBR, a type II integral membrane protein was the one of the first INM proteins to be identified and it is suggested that the interaction of this protein with chromatin might be important for the attachment of chromatin to the NE (Worman, Yuan et al. 1988, Worman, Evans et al. 1990).

Lamina-associated-polypeptide 1 (LAP1) is a type II integral nuclear membrane protein, that included three variants, LAP1A, 1B and 1C. LAP1A and LAP1B have been shown to specifically interact with lamin A/C *in vitro* (Senior and Gerace 1988). Lamina-associated polypeptide 2 (LAP-2) is another family of lamin binding proteins, including up to six mammalian isoforms. It was show that LAP2 binds lamin B and it presents chromosome-binding properties *in vitro (Foisner and Gerace 1993)*.

Another identified and largely characterized INM protein was emerin. Emerin is a ubiquitously expressed type II integral membrane protein that binds to both A- and B- type lamins *in vitro* and its localization at the NE depends on its interaction with lamin A (Manilal, Nguyen et al. 1996, Maison, Pyrpasopoulou et al. 1997). Emerin as well as LBR, LAP1 and LAP2 appear to have important functions in anchoring the INM to the NE, maintaining the stability of the nucleus (Holmer and Worman 2001).

1.1.3. Interactions of INM proteins with heterochromatin and transcription factors

Recently, it has become increasingly apparent that the genome follows a non-random organisation. It was in 1956 when early EM studies revealed darker stained areas of dense chromatin within the interphase nucleus that were named as heterochromatin and areas presenting an asymmetric distribution of lighter stained regions of chromatin termed euchromatin (Moses 1956).

Heterochromatin tends to dominate proximal areas to the NE while euchromatin tends to be present within the nuclear interior. Previous studies have shown that a small portion of an internal chromosome can stretch out to interact with proteins present in the nuclear periphery (Kupper, Kolbl et al. 2007), suggesting that components present in the NE could contribute in the patterns of chromosome organization. More recent studies have shown that chromosomes follow a discrete non-overlapping territory within the nucleus of interphase cells, occupying a specific radial position. Thus, the NE is considered a tethering point for chromatin in which

NETs might mediate genome organization by interacting with chromatin proteins or epigenetic silent marks.

For instance, A and B-type lamins have been reported to bind directly to telomeric and heterochromatin DNA sequences (Shoeman and Traub 1990, Baricheva, Berrios et al. 1996). Furthermore, lamins can also interact and assemble around chromatin, binding to core histones such as H2A and H2B (Hoger, Krohne et al. 1991, Taniura, Glass et al. 1995, Goldberg, Harel et al. 1999).

In addition to lamins, many NETs bind directly with DNA. For example, MAN1 binds DNA via its C-terminal domain (Caputo, Couprie et al. 2006) while LAP2β binds DNA by its N-terminal domain (Cai, Huang et al. 2001). NETs also associate with DNA indirectly via interactions with chromatin-binding partner proteins; LBR was reported to bind DNA via human HP1-type chromodomain proteins (Ye and Worman 1996) and directly interact with the core histone H3 carrying K9 tri-methylation that promotes gene silencing (Polioudaki, Kourmouli et al. 2001). This implies that LBR acts as a chromatin tethering.

Multiple interactions between NE proteins and transcription factors have also been observed (Heessen and Fornerod 2007). MAN1, for example binds R-SMADs (Osada, Ohmori et al. 2003) whilst Ringer Finger Binding protein (RFBP), a novel INM protein, directly interacts with SWI/SNF transcription factors that model chromatin (Lee, Haraguchi et al. 2001). Similarly, lamin A and lamin B1 interact with transcription factors cFos and Oct-1 (Malhas and Vaux 2009). These observations suggest that the association of chromatin with the NE may directly regulate transcription processes.

Recently studies have identified novel NETs affecting genome organization. Multiple studies carried out in our lab found that ten novel NETs could alter the position of a chromosome or gene locus to the nuclear periphery (Korfali, Wilkie et al. 2010, Zuleger, Boyle et al. 2013, Robson, de Las Heras et al. 2016). In addition, another study aimed to identify NETs involved in chromatin modification, ran visual screens of 31 NE proteins identifying different NETs affecting chromatin compaction (Malik, Zuleger et al. 2014).

1.1.4. Trafficking of nuclear membrane proteins to the INM

The cell has to deal with the problem of transporting proteins in and out the nucleus. This problem was solved for soluble proteins through the use of the NPC. In addition, the transport of transmembrane proteins seems to be more enigmatic. The transport of these proteins includes multiple translocation mechanisms which allow NETs to reach their final destination, the NE.

The NE is a hermetic structure, which covers the whole surface of the nucleoplasm forming a physical barrier interrupted only in areas where NPCs are inserted (Prunuske and Ullman 2006). NPCs are considered to be the gatekeepers of the NE, controlling the trafficking of molecules in and out the nucleus.

The nucleo-cytoplasmic transport of *soluble cargos* has been extensively studied (Gorlich and Kutay 1999). This process takes place in the central channel of the NPC and involves a wide range of transport receptors called karyopherins (also known as importins and exportins) that bind to soluble cargoes via the recognition of targeting information such as nuclear localization sequences (NLSs) for entry or nuclear export sequences (NESs) for exit. These transport receptors interact with phenylalanine/glycine (FG) motifs present in the nucleoporins (nups) of the central channel allowing the diffusion of soluble cargoes up to 60 KDa. This process depends on the small GTPase Ran (Ras-related nuclear protein). A gradient is formed with Ran-GDP in the cytoplasm and Ran-GTP in the nucleus facilitating the binding and release of transport receptors to cargoes and thus allowing the movement of molecules through the central NPC channel (Cook, Bono et al. 2007).

In contrast to the transport of soluble molecules, nuclear transport of NETs remains less understood. The journey for a NET starts in the ER, where NETs are synthesized and inserted into the ER membrane. The observation of the 10 nm peripheral channels together with the ability of a protein to move from the ER to the ONM, as the ER is continuous with the ONM, led to the development of the lateral diffusion-retention hypothesis. This stated that INM proteins freely exchange between the ER-ONM and the INM by simple lateral diffusion through the peripheral channels. Proteins are retained at the INM through their ability to bind lamins and/or chromatin, leading to the accumulation of NETs at this membrane (Figure 2).

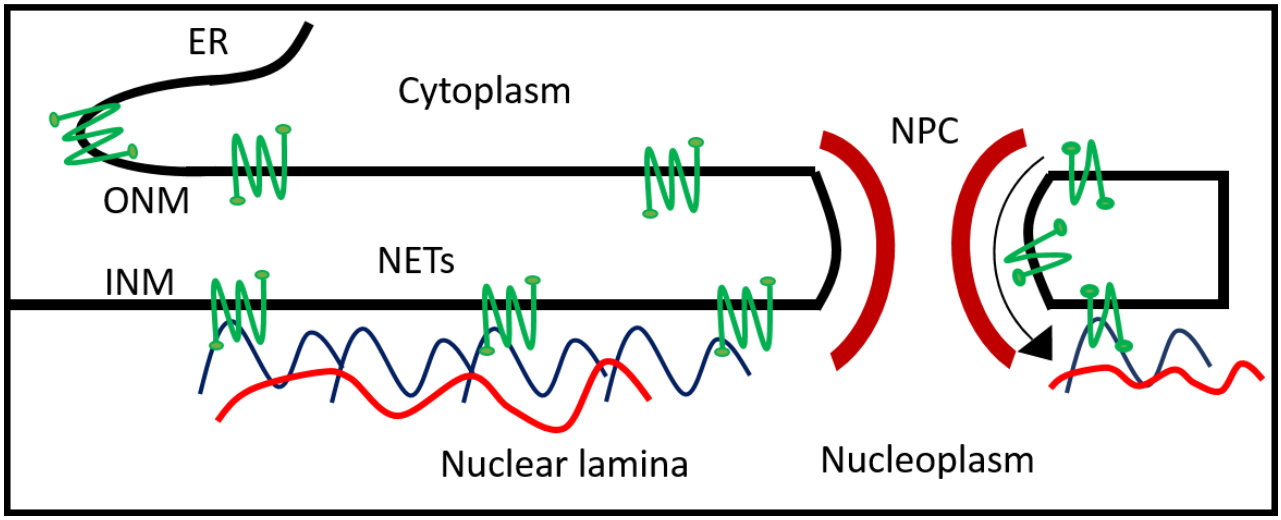

Figure 2. Diffusion-retention hypothesis for NET translocation. *NETs distribute by free diffusion within the continuous membranes of the ER, ONM and INM. After synthesis in the ER, NETs rapidly can diffuse into the ONM and then can further diffuse while still in the membrane into the INM through the peripheral channels of the NPC. Once in the INM, NETs are retained by interactions with lamins and chromatin.*

The first study aimed to test this hypothesis was done by Bruno Soullam and Howard Worman. They fused the nucleoplasmic domain of LBR, which binds to lamin B, with a transmembrane span of chicken hepatic leptin which is a transmembrane protein that is localized in the ER and in the plasma membrane (Chiacchia and Drickamer 1984). After the fusion of these two domains, the chicken hepatic leptin was able to translocate by diffusion from the ER into the INM where it was retained by interaction of the nucleoplasmic domain of LBR with lamin B (Soullam and Worman 1993). Afterwards, two more studies confirmed the lateral diffusion/retention hypothesis using the lamin-binding region of LAP2β (Furukawa 1999) and MAN1 (Wu, Lin et al. 2002).

Moreover, fluorescence recovery after photo-bleaching (FRAP) and photo-activation (PA) studies have confirmed the retention part of the hypothesis. When performing FRAP on NETs fused with GFP present on the INM, the total

fluorescence recovery was never achieved after bleaching. This observation implied that a portion of the NET must be highly immobile within the membrane due to interactions with nuclear elements such as lamins or chromatin (Rolls, Stein et al. 1999, Wu, Lin et al. 2002). Another study published in 2006 showed that emerin presented higher mobility in cells lacking its binding partner, lamin A (Ostlund, Sullivan et al. 2006).

Even stronger support for the retention part of the hypothesis came from observations made in our lab. Zuleger et al. studied the transport of NETs to the INM using FRAP and PA techniques. In this study, they directly compared the diffusion characteristics of multiple NETs. They found two different time recoveries in the ER, one faster than the other, suggesting two types of NETs mobility. The NETs presenting faster recovery likely move freely within the ER without any impediment. On the other hand, the slower set may be clustered with other proteins resulting in a slower diffusion. This could be due to association with proteins that, for example, have roles in targeting NETs to the INM such as transport receptors. Furthermore, the retention part of the hypothesis was additionally supported in this study by the fact that FRAP on NETs in the NE never recovered the prebleach fluorescence levels. For example, SUN2 fluorescence recovery was around 50% of the total signal within the NE. This indicated that a pool of SUN2 might be highly retained at the INM due to interactions with lamins or chromatin.

This study showed that the dynamics of NET exchange between NE and ER compartments creates the presence of several pools of NETs (ER pool, ER-NE pool, INM pool and ONM-INM pool). The fluorescence recovery in the NE is principally due to exchange of NETs between the ER and the INM rather than on movement of the NETs within the INM itself. This was further supported by PA experiments in which different NETs photoactivated within the ER showed a fast accumulation in the NE that was similar to the rate of recovery in NE FRAP experiments. After the translocation of some NETs to the INM, they are trapped and remain in this membrane due to interactions with nuclear components (Zuleger, Kelly et al. 2011).

1.1.5. The NE and disease

Mutations in lamins and NETs have been recently shown to be responsible for at least 20 heritable human diseases, the nuclear envelopathies, that range from muscular dystrophy to neuropathies and progeria syndromes (Worman and Schirmer 2015).

Structural changes of chromatin have been observed in a variety of diseases linked to the NE. The higher-order organization of genomes is functionally important for gene regulation and control of gene expression. Thus, it is not surprising to hypothesize that defects in chromatin organization and distribution might cause disease.

As mentioned before, multiple NETs present direct connections to chromatin and lamins contributing to genome organization and gene regulation. These NE-genome interactions are suggested to be disrupted in some NE human diseases as consequences of mutations in NETs or lamins. The disruption of genome organization and gene regulation together with the alteration of the nuclear and cellular mechanical stability could explained how mutations in NETs cause nuclear envelopathies.

All these disorders are distinct and have restricted tissue pathologies. Several mutations in the LMNA (lamin A) gene are involved in the development of many human diseases. The first human disease identified to be caused by LMNA mutations was Emery-Dreifuss muscular dystrophy, an autosomal dominant disorder that affects muscles (Bonne, Leturcq et al. 1993). LBR has also been linked with an autosomal dominant disorder named Pelger-Huët anomaly (PHA). This disorder is characterized by abnormal nuclear shape and chromatin organization in blood granulocytes. The gene encoding LBR was mutated affecting its expression levels with a corresponding effect on NE-heterochromatin interactions (Hoffmann, Dreger et al. 2002).

1.2. General overview of Herpesviruses

1.2.1. Herpesvirus classification

Herpes Simplex Virus type I (HSV-1) also known as human herpes virus I (HHV-1) is a large enveloped double-stranded DNA virus of 220 nm diameter. The Herpesviridae family includes more than 120 identified members sharing a common virion structure that, in addition to humans, infect other mammals, birds and reptiles. To date, nine human herpesviruses have been identified: herpes simplex virus types 1 and 2 (HSV-1, HSV-2), varicella zoster virus (VZV), Epstein–Barr virus (EBV), cytomegalovirus (CMV), roseolaviruses HHV-6 (A and B) and HHV-7, and Kaposi sarcoma-associated herpes virus (HHV-8) (McGeoch, Rixon et al. 2006, Fossum, Friedel et al. 2009).

In nature, all herpesviruses can establish latent infection within tissues that are characteristic for each virus, reflecting the unique tropism of each member. The Herpesviridae have been classified by the International Committee of Taxonomy of viruses into three subfamilies (Davison 2010): Alpha-, Beta- and Gammaherpesvirinae. HSV-1 and the closely related HSV-2 together with the VZV are members of the human Alphaherpesvirinae subfamily, which are characterized by short replication cycle (hours) with a wide host range and establishment of latency in sensory ganglia. In contrast, members of Betaherpesvirinae, such as CMV, have a restricted host range and their reproductive life cycle is much longer (days) than members in the alpha-subfamily, establishing latent infection in epithelial cells of the secretory glands and kidneys. Lastly, the human Gammaherpesvirinae subfamily present the most limited host range and they are known for their oncogenic potential and their ability to develop human malignancies such as EBV causing leukaemia and KSHV causing Kaposi sarcoma (Reiman, Powell et al. 2003, Wen and Damania 2010).

The classification of the known human herpesviruses, together with the associated diseases is listed in Table 1.

Table 1. Human Herpesvirus classification and associated diseases

Subfamily	Virus	Acronyms	Primary target	Disease
Alpha	Human herpes virus 1	HSV-1/HHV-1	Epithelial and keratinocyte	Herpetic Stomatitis
Alpha	Human herpes virus	HSV-2/HHV-2	Epithelial and keratinocyte	Herpetic Stomatitis and genital herpes
Alpha	Human herpes virus 3	VZV/HHV-3	Epithelial and keratinocyte	Chickenpox,shingles
Beta	Human herpes virus 5	HCMV/HHV-5	Epithelial,endothelial and fibroblast	Mononucleosis
Beta	Human herpes virus 6A	HHV-6A	T-cell	Roseola infantum,encephalitis
Beta	Human herpes virus 6B	HHV-6B	T-cell	Roseola infantum,encephalitis
Beta	Human herpes virus 7	HHV-7	T-cell	Roseola infantum,encephalitis
Gamma	Human herpes virus 4	HHV-4/EBV	B-cell and epithelial	Mononucleosis, Burkitt´s lymphoma
Gamma	Human herpes virus 8	HHV-8/KSHV	B-cell and epithelial	Karposi´s sarcoma, Castleman´s disease

1.2.2. Herpesvirus significance and treatment

As mentioned above, HSV-1 and HSV-2 have a wide tropism allowing these viruses to produce a huge range of clinical manifestations in humans. HSV-1 is the prototypical and best studied member of the alpha subfamily. In contrast to other HHV, HSV-1 is able to infect different animal species in experimental infection due to its broad cell tropism and high infectivity ratio. Therefore, HSV-1 is an attractive biological model to study different aspects of the Herpesviruses.

HSV-1 is a highly successful virus as it is estimated that 45% to 98% of the adult human population is HSV-1 seropositive. The prevalence of the virus depends on demographic factors including age, location and socioeconomic status (Fatahzadeh and Schwartz 2007). A critical factor for herpesvirus infections is the requirement for intimate contact between a person who is carrying the virus and a susceptible host. Typically, in humans, primary infection is acquired during early childhood via direct contact of mucosal membranes. After viral inoculation onto the skin or mucous membranes, a rapid incubation period of four to six days is required for herpes simplex virus replication in epithelial cells. Cell lysis and local inflammation take place resulting in characteristic vesicle lesions. Subsequently, the virus enters nerve cells and is transported along axons to the dorsal root ganglia where it establishes a latent infection for a lifetime (Diefenbach, Miranda-Saksena et al. 2008).

Clinical manifestations produced by HSV-1 infection depend on a variety of factors such as immune status of the infected host, age as well as viral load and viral replication rate. Symptomatic outcomes of HSV-1 infection range from mild orofacial watery blisters also known as cold sores to serious manifestations such as encephalitis. Herpes simplex encephalitis is a severe infection of the central nervous system presenting a 70% mortality rate if left untreated. Other symptoms can vary from ocular infections to genital lesions (Hill, Ku et al. 2014).

HSV is a prevalent virus in the population leading to a huge range of clinical outcomes that can compromise the life of the host. Due to the establishment of latent infection in neurons, herpesviruses are mostly impossible to detect and eradicate from the human population (Whitley and Roizman 2001, Dwyer and Cunningham 2002).

At this time, there are a variety of antiviral drugs such as acyclovir or penciclovir but none of these drugs can eradicate the latent form of the virus, as they only target the replication viral stage (Martinez, Caumes et al. 2008). There is a high need for the development of pharmaceutical treatments that will stop the spread of the infection as well as decrease the toxic side effects of the current medication.

1.2.3. HSV-1 virion structure

Early EM studies together with recent cryoEM studies have shown that a typical HSV-1 mature viral particle is observed as a spherical multilayer particle with a size ranging from 180-200 nm (Bruns 1980, Mettenleiter, Klupp et al. 2009). The HSV-1 mature virion is composed of an icosahedral capsid that stores an electron-dense core, the viral genome. The capsid is surrounded by an amorphous protein layer called the tegument containing 30 or more viral proteins and an outer lipid bilayer envelope derived from the infected cell Golgi apparatus containing glycoproteins that are essential for HSV-1 entry into cells (Reske, Pollara et al. 2007) (Figure 3).

Herpesvirus infection can lead to the production of three viral particle forms within the nucleus of host cells; empty A-, scaffold-containing B- and DNA-containing C-capsids. While C-capsids are capable to produce mature infectious virions, A- and B- capsids are considered to be defective particles; B-capsids failed to package viral DNA, and A-capsids represent empty capsids as they do not contain either scaffold proteins or viral DNA (Tandon, Mocarski et al. 2015).

The herpesvirus genome packaged inside the core is a linear double strand-DNA viral genome that ranges from about 125 to 250 kbp, encoding over 80 viral genes. Upon infection, the linear viral DNA is injected into the nucleus where it circularises to form a viral episome. The herpesvirus genome is characterised by the presence of unique and repeat sequences. Two covalently joined segments S and L form a unique short (US) and a unique long (UL) region respectively.

These regions are flanked by inverted repeat sequences (McGeoch, Dalrymple et al. 1988). The HSV genome contains three origins of replication and it can be divided into three categories depending on the kinetics of their transcription: “immediate early” (IE) that allow the expression of further viral genes; “early” (E), responsible of viral genome replication; and “late” (L), encoding the structural proteins.

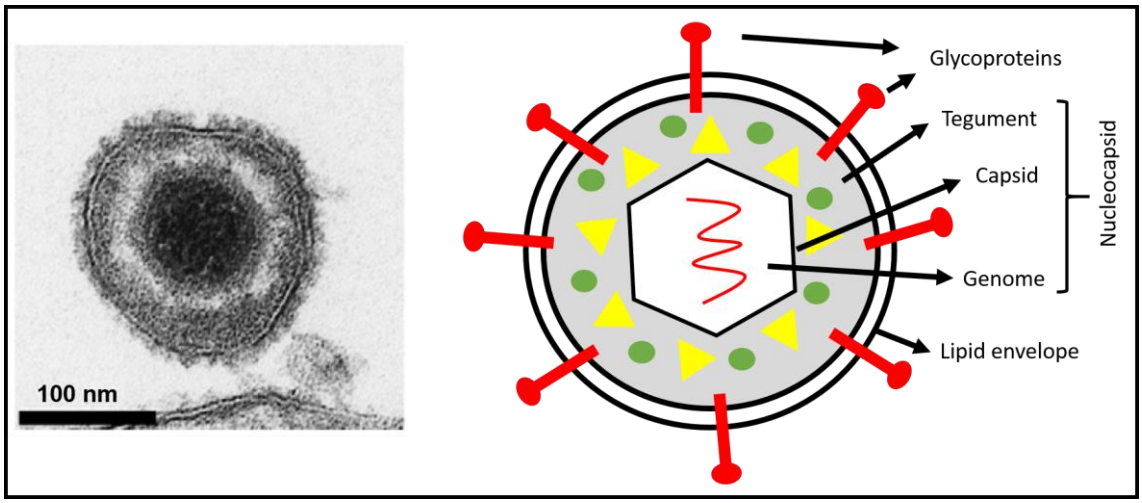

Figure 3. HSV-1 virion structure. *An electron micrograph image showing a HSV-1 mature particle (Mettenleiter, Klupp et al. 2009) next to a schematic representation of a HSV-1 virion. It shows the viral genome enclosed in a capsid that is surrounded by a tegument layer containing multiple tegument proteins. The tegument together with the capsid and the viral genome forms the nucleocapsid. At the same time, the nucleocapsid is encased by a lipid envelope derived from host cell membranes containing viral glycoproteins.*

1.2.4. HSV-1 life cycle: Lytic and latent infection

The life cycle of HSV involves both lytic (productive) and latent (non-productive) infection. A large body of evidence has accumulated over the years dividing the HSV life cycle in 5 major steps: attachment, entry into the host cell, viral replication, virion assembly and egress of new viral progeny.

The HSV life cycle begins as the virus particle recognizes and binds to receptor proteins on the surface of cell membrane presented at the mucosal surface or in the skin. Entry of HSV can vary between cell types and it is driven by the attachment of viral glycoproteins to targets on the host cell surface. Several glycoproteins are known to be involved in this step such as gD, gB, and the heterodimer gH/gL (Connolly, Jackson et al. 2011). These glycoproteins are known to be conserved among herpesviruses (Eisenberg, Atanasiu et al. 2012). gD can bind to different cellular receptors such as nectin-1 and nectin-2, herpes virus entry mediator (HVEM) and 3-O-sulfated heparan sulfate (3-O-S-HS) presented in the plasma membrane of the host cell. This interaction triggers a membrane fusion event which can happen at the plasma membrane or inside endocytic vesicles resulting in the deposition of the capsids directly into the cytoplasm of the cell which are then transported via interactions with microtubules to the NPC (Akhtar and Shukla 2009) (Figure 4).

At the NPC, the viral genome is injected into the nucleus followed by viral genome replication. Viral genome expression is a regulated cascade: IE, E, and L genes (Boehmer and Lehman 1997, Mettenleiter 2002). The nucleus is reorganized to form replication compartments in which viral DNA is replicated and new progeny viral particles are assembled. Subsequently, newly synthesized nucleocapsids acquire tegument proteins and leave the NE in a process called ***primary envelopment/de-envelopment*** (Figure 4)**.** This process leads to the budding of nucleocapsids at the INM forming primary enveloped particles (PEP) within the lumen of the NE. Subsequently, these particles fuse with the ONM releasing nascent capsids into the cytoplasm (Skepper, Whiteley et al. 2001, Simpson-Holley, Colgrove et al. 2005) (*This process will be explained in detail in the next section).*

Virion maturation then takes place in the cytoplasm, where capsids acquire tegument proteins followed by a process called secondary envelopment in which a final enveloped-lipid bilayer is acquired by the virus via budding into the trans-Golgi or in early endosomes coming from the plasma membrane. This process results in a mature and enveloped virion particle inside a vesicle that is transported to the cell surface where it fuses with the plasma membrane releasing progeny enveloped viruses into the extracellular environment (Kelly, Fraefel et al. 2009, Mettenleiter, Klupp et al. 2009) (Figure 4).

Following primary cutaneous or mucosal infection, HSV spreads from the primary site of infection to infect sensory neurons that innervate the affected area by fusion with the neuronal membrane at the axonal termini. Nucleocapsids are then transported by retrograde axonal transport from the site of entry to the nucleus in the cell body of the neuron in the dorsal root ganglia or trigeminal ganglia (Simmons 2002). At this point two events may occur. First, the lytic replicative cycle described above may take place resulting in neuronal death and egress of infectious particles leading to encephalitis. Alternatively, viral DNA released into the nucleus of neurons may persist in a latent state in a circular episomal form that is associated with nucleosomes (Mellerick and Fraser 1987).

Once latency is established, different stimuli such as stress may cause viral reactivation. Reactivation implies the sufficient expression of viral proteins and viral DNA replication to produce progeny virions. Nucleocapsids and other envelope proteins are transported independently by anterograde axonal transport to the peripheral nerve terminals where they are assembled and released to infect new neurons (Taylor, Kobiler et al. 2012).

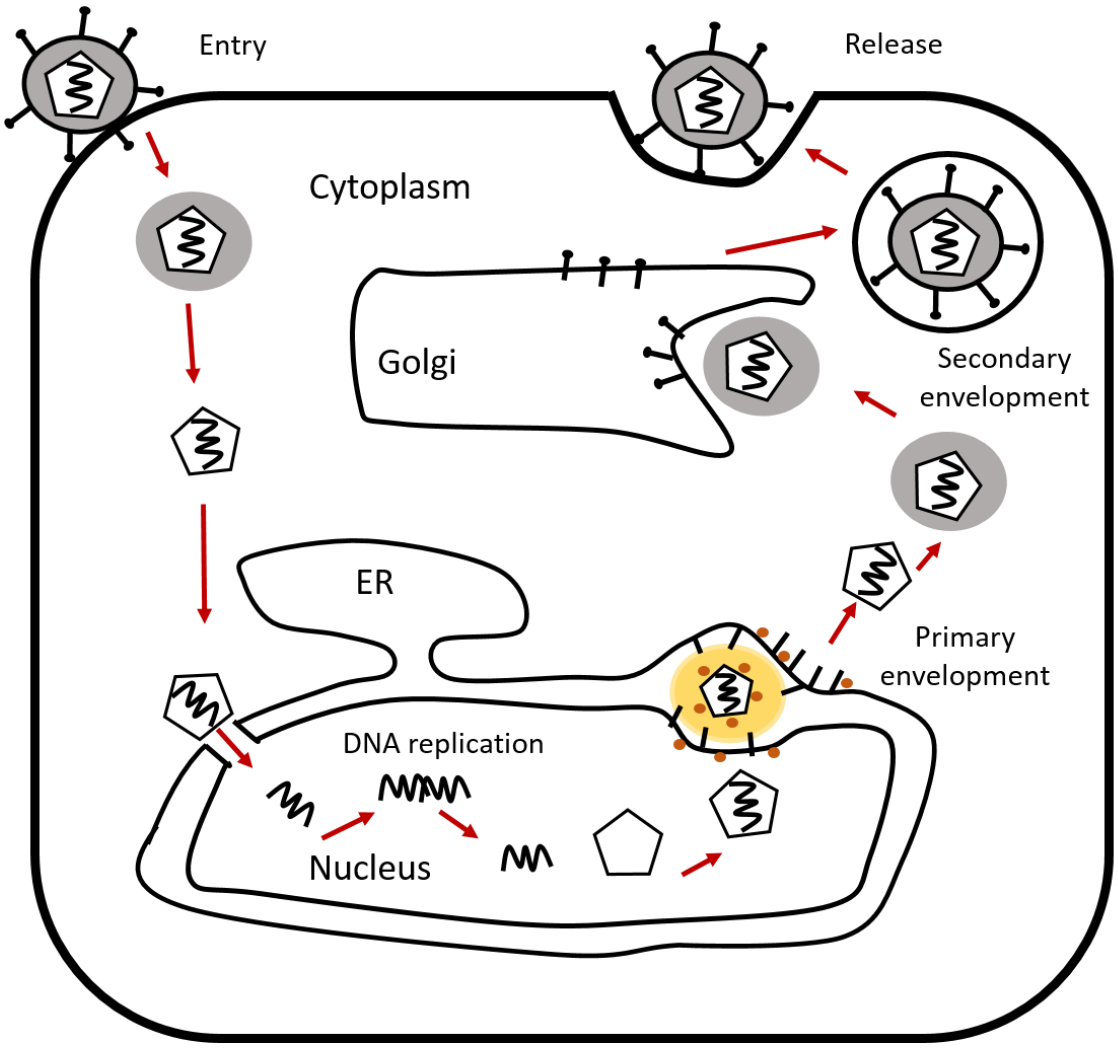

Figure 4. HSV-1 life cycle. *After recognition of specific receptors present in the surface of host cells, the envelope fuses with the plasma membrane releasing the capsids into the cytoplasm. Subsequently, the capsid is transported to the nucleus in where it injects its genome through the NPC. Once in the nucleus, DNA replication and transcription takes place. Single viral genomes are packaged into new viral nucleocapsids and translocated into the cytoplasm in a process called primary envelopment/de-envelopment. In the cytoplasm the final maturation takes place. Released viral capsids acquire the final tegument and bud into membranes from the Golgi (secondary envelopment) resulting in the formation of vesicles. These vesicle containing mature particles fuse with the plasma membrane releasing mature particles from the cell.*

1.2.5. Secondary envelopment

Secondary envelopment is a better understood process compared with primary envelopment/de-envelopment. In order to understand some of the biological processes occurring during primary envelopment, we should first describe how secondary envelopment takes place.

After primary envelopment/de-envelopment at the NE, nascent capsids delivered into the cytoplasm have to acquire the complete set of viral tegument proteins and the final envelope in a process known as secondary envelopment or re-envelopment, a step thought to take place in the trans-Golgi (TGN) (Figure 4). However, recent studies have suggested that HSV-1 particles present in the cytoplasm might acquire its final envelope from endocytic tubules containing glycoproteins derived from the plasma membrane.

Secondary envelopment is driven by interactions between tegument proteins present in the surface of capsids and the cytoplasmic tails of various viral glycoproteins located in the TGN (Owen, Crump et al. 2015). For example, there is evidence that gD, gE-gI (HSV) can interact with the VP22 tegument protein promoting secondary envelopment (Duffy, Lavail et al. 2006). These protein interactions are responsible to pulling the host membranes around viral particles.

Studies have shown that while mutations in single glycoproteins have minimum defects in secondary envelopment, HSV mutants lacking gD and gE-gI accumulate nascent capsids in the cytoplasm (Farnsworth, Goldsmith et al. 2003). Similar phenotypes were observed in double PRV mutants in which both gE-gI and gM were depleted (Brack, Klupp et al. 2000). Moreover, mutations in the cytoplasmic domain of gE and gM (PRV) or gD (HSV) showed the same accumulation defects for secondary envelopment (Farnsworth, Goldsmith et al. 2003).

Once nascent capsids have acquired their final envelope, mature virions within membrane vesicles present in the cytoplasm are transported to the cell surface where the fusion between the vesicle and the plasma membrane results in the release of enveloped particles out of cells or cell lysis.

1.3. The nuclear envelope in viral infection

Viruses are obligate biological pathogens depending on the exploitation of the cellular machinery of their host organism to survive and replicate. To accomplish a successful life cycle including cell entry, replication, assembly and release of new viral particles, viruses must face a number of obstacles that they overcome by the manipulation and usurpation of cellular factors and machinery. One of the biggest barriers viruses need to bypass for productive virus replication, is cellular membranes.

During cell entry, enveloped and non-enveloped viruses have to cross the plasma membrane using different mechanisms. For the viruses that replicate in the nucleus of the cell, the NE is another major barrier that has to be overcome for viral entry and release. The majority of the viruses are unable to cross through the 39 nm central channel of the NPC because of their large size; therefore, different viral families have developed ingenious ways for the nuclear entry of their genomes (Cohen, Au et al. 2011, Kobiler, Drayman et al. 2012, Mettenleiter 2016).

As an example, during herpesvirus infection, the docking of viral capsids at the NPC and the release of the genome through it is thought to be depend on two viral proteins that are highly conserved within the Herpesviridae, UL25 and UL36, and the nuclear pore proteins Nup358 (Copeland, Newcomb et al. 2009) and Nup214, known to interact with UL25 (Pasdeloup, Blondel et al. 2009). Another study has shown that the karyopherin importin-β and the GTPase Ran may also mediate the docking of viral capsids at the NPC allowing the nuclear import of the herpesvirus genome through the central channel of the NPC (Ojala, Sodeik et al. 2000). Other viral families as Papillomaviruses, import their viral DNA into the nucleus taking advantage of the NE breakdown (NEBD) occurring during mitosis (Aydin, Weber et al. 2014).

Once the viral genome gets access to the nucleus, a coordinated series of events takes place producing the assembly of new capsids. Progeny viruses need to escape the nucleus to continue their journey to the external cell environment via complex routing pathways that can involve the NE in various ways. Many viruses leave this cellular compartment by breaching the NE or deforming it for budding

(Mettenleiter 2016). Virus budding at the NE is a complex process that can be defined as the envelopment of new viral capsids within the INM involving membrane deformation around the capsid and subsequent membrane fission with the ONM to release the particle into the cytosol. Some viral families interfere with the integrity of the NE causing cellular lysis to allow the release of infectious particles. This is the case of Polyomaviruses among others; intranuclear particles target the NE by interaction of the JP viral protein with LBR resulting in the destabilization of the NE, facilitating virus egress (Okada, Suzuki et al. 2005). However, new evidence suggests that other viral families have evolved subtler ways of nuclear egress without drastic damage of the nucleus by usurping cellular transport pathways through the NPC or developing new ingenious mechanisms to exit from the nucleus as is the case of the Herpesviridae family.

1.3.1. HSV-1 nuclear egress, primary envelopment

Once herpesvirus genomes are packaged into nucleocapsids, the complex egress pathway by which nucleocapsids move from the nucleus to the extracellular environment takes place. During egress, herpesviruses face multiple obstacles that they solve by restructuring host membranes. While HSV-1 capsid formation and DNA packaging occur in the nucleus, the final virion maturation takes place in the cytosol. As the new viral nucleocapsids (~125 nm) are considered too large to pass through the NPCs, they need to pass through the NE in a process known *viral nuclear egress*.

For a long time, the mechanisms by which the nucleocapsid crosses the NE have been debated. Three different models have been proposed to describe herpesvirus nuclear egress:

The *nuclear pore model* predicts that the NPC can dramatically change conformation to accommodate viral capsids. This is based on NPCs observed to be grossly dilated in the analysis of HSV-1 infected cells using high-pressure freeze-fracturing. This model has been exclusively based on EM observations and no evidence has been obtained using conventional fixation TEM or cryoEM procedures.

It suggests that >100 nm herpesvirus capsids cross the NE by enlarging the NPC (Leuzinger, Ziegler et al. 2005, Wild, Engels et al. 2005, Wild, Senn et al. 2009).

In the *luminal model* (also known as the single envelopment model) credited by Johnson and Spear in 1982, nucleocapsids present in the nucleus become budded at the INM acquiring a primary envelope resulting in the formation of PEP residing in the lumen space (primary envelopment) (Johnson and Spear 1982). PEP travel to the ER, as the lumen space is continuous with the ER lumen, and continue their journey to the trans-Golgi through the secretory pathway (Galdiero, Falanga et al. 2005). This model obtained some conventional EM support in the observation of PEP in the lumen of the ER.

Finally, in the *envelopment/de-envelopment/re-envelopment model* of egress proposed in 1961 by Stackpole in a study of frog herpesvirus, the primary envelopment step is the same as in the luminal model. However, this model proposes that PEP residing in the lumen space fuse with the ONM in a process called de-envelopment by membrane scission, depositing nascent capsids into the cytoplasm while the primary envelope remains fused with the ONM. Nascent capsids released into the cytoplasm travel to the Golgi membranes or TGN where they undergo a secondary envelopment step (re-envelopment) acquiring a final envelope containing glycoproteins that will be part of the final mature particle (Figure 5). This is the most widely accepted model for viral egress at the NE for both HSV and VZV and in recent years there have been growing evidences in favour of it (Jones and Grose 1988, Granzow, Klupp et al. 2001, Mettenleiter 2002, Schulz, Klupp et al. 2015). Moreover, it effectively encompasses the data supporting the luminal model as due to the continuity of the NE and ER lumen any particles that did not immediately fuse with the ONM would be able to fuse anywhere in the ER while traversing the ER lumen.

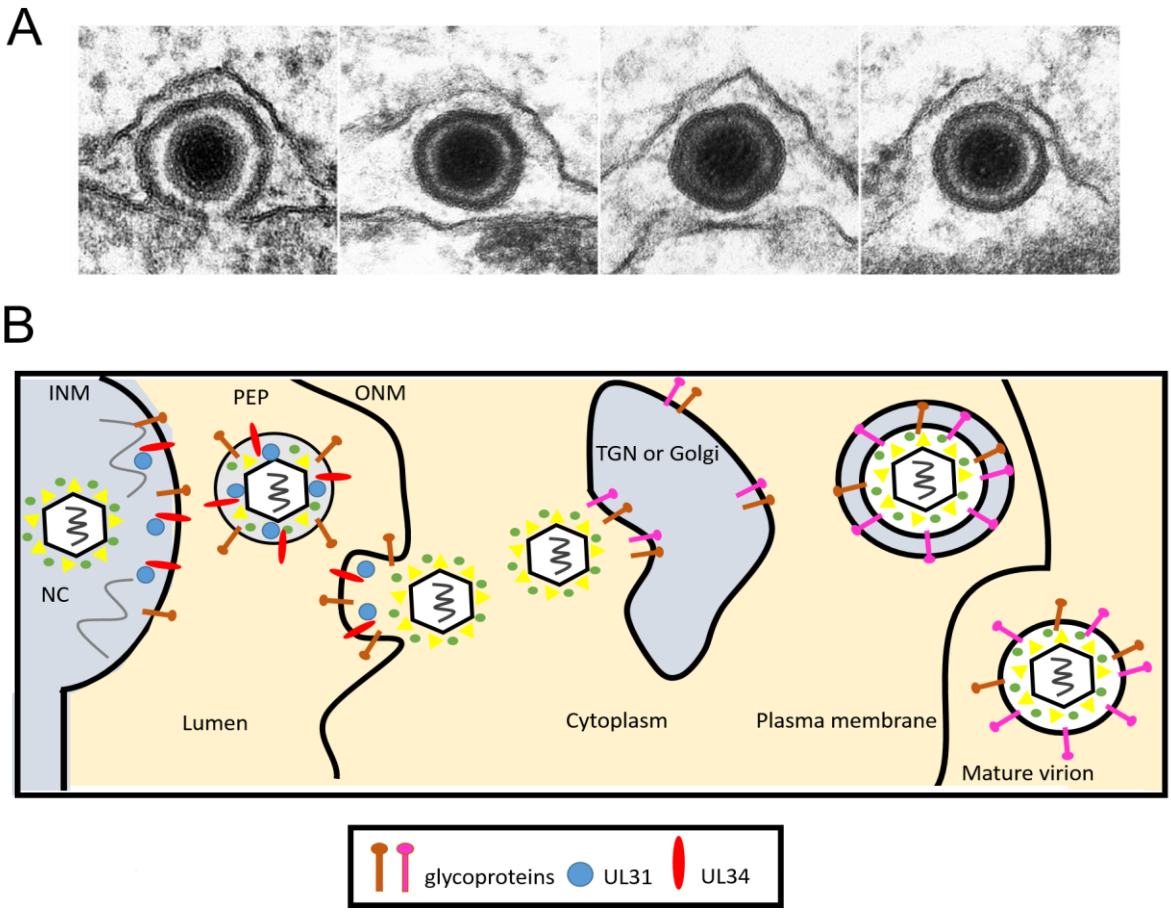

Figure 5. Envelopment/de-envelopment/re-envelopment model for HSV-1 egress. (A) *An electron micrograph image showing a HSV-1 egress at the NE by the formation of primary enveloped particles (PEP) in the lumen(Mettenleiter, Klupp et al. 2009).* ***(B)*** *Nucleocapsids (NCs) synthesized in the nucleus bud at the INM (primary envelopment) resulting in the formation of PEP residing in the lumen. The primary envelope is derived from the INM and it contains multiple viral proteins such as UL31/UL34 or glycoproteins that are incorporated into PEP. These particles fuse with the ONM (de-envelopment) releasing nascent capsids into the cytoplasm while the primary envelope remains fused to the ONM. In the cytoplasm, these particles bud into host membranes from the TGN or Golgi (secondary envelopment or re-envelopment) acquiring viral glycoproteins that will be part of the final mature particle. Finally, enveloped virions are released from the infected cell into the extracellular environment ready to infect new cells.*

A first line of evidence in favour for the envelopment/de-envelopment/re-envelopment model was EM studies made in HSV-1 infected neurons. They found a separate transport of nucleocapsids and viral glycoproteins within axons. The transport of glycoproteins within vesicles was observed in distal regions of the axon which did not co-localize with nucleocapsids. Thus they hypothesized the presence of two pathways of viral transport and assembly within infected cells (Penfold, Armati et al. 1994).

Further evidence in favour for this model came from studies of tegument assembly. These studies provided evidence that the site of assembly for herpesviruses was the cytoplasm. Elliot and colleagues observed that the tegument protein VP22 was exclusively observed in the cytoplasm in a live virus-infected cell, supporting the cytoplasm as the main site of tegument assembly (Elliott, Mouzakitis et al. 1995). Moreover, they showed that VP22 deletion mutant viruses did not hamper virion morphogenesis.

Another study of tegument assembly in PrV further supports the hypothesis that intranuclear capsids presented a different protein composition than cytoplasmic and extracellular virions. UL36 and UL37 were demonstrated to be present in the cytoplasmic capsids while they were absent from primary virions. Moreover, UL36 and UL37 deletions hampered the ability of viral particles released into the cytoplasm to mature into enveloped virus. These observations confirmed the presence of a different viral composition in primary virions versus cytoplasmic and extracellular virions (Klupp, Fuchs et al. 2002).

Immunocytochemistry of rat dorsal root ganglion neurons infected with HSV-1 showed that the tegument assembly took place in the cytoplasm of neurons while the acquisition of the final envelope took place in vesicles of the Golgi and TGN. While tegument proteins such as VP16, VP22 and US9 were present in the nucleus, they were not detected in PEP within the lumen. However, these tegument proteins were detected in viral particles within the Golgi and extracellular mature particles. The same pattern was observed for the viral glycoprotein D (Miranda-Saksena, Boadle et al. 2002).

Recent EM studies have supported the de-envelopment/re-envelopment model. Gillian and colleagues observed by EM that enveloped particles present in the

lumen of HSV-1 and PRV infected cells showed a difference in composition and appearance from viral particles presented in the cytoplasm and virions already released into the extracellular environment. The capsid of these viral particles was surrounded by a uniform electron dense layer; a sharply and thick bordered rim corresponding to tegument proteins. On the other hand, primary virions presented a uniform thinner layer. These studies showed that major components of enveloped herpesvirus particles in the lumen are absent from cytoplasmic virions, indicating an intermediate step between nuclear and extracellular virions (Granzow, Klupp et al. 2001).

Further evidence to support this model came from mutation studies. Viruses carrying deletions in glycoproteins exhibited defects in virus morphogenesis. For example, deletions of gE-gI and gM drastically impaired PRV replication inducing the accumulation of viral particles in cytoplasmic compartments, suggesting the participation of these proteins in secondary envelopment in the cytoplasm (Brack, Dijkstra et al. 1999). gK depleted PRV virus showed defects in viral release of primary virions into the cytoplasm. This found the accumulation of PRV primary virions within the lumen, suggesting the involvement of gK in promoting the fusion of the primary envelope with the ONM (Klupp, Granzow et al. 2001).

The process of budding of herpesvirus nucleocapsids proposed by the luminal model and the envelopment/de-envelopment model require the reshaping of multiple host membranes such as the INM and ONM. Nucleocapsid budding results in the curvature of the INM around the viral particle leading to membrane deformation and scission to allow free access of nucleocapsids to the lumen space (Bigalke, Heuser et al. 2014).

1.3.2. Primary enveloped particles versus cytoplasmic virions

Herpesvirus infection results in the formation of two types of virions within the infected cell. Primary enveloped particles (PEP), also known as primary virions, reside in the lumen and are new viral nucleocapsids surrounded by an envelope derived from the INM. On the other hand, mature virions present in the cytoplasm are secondarily enveloped virions inside Golgi or plasma membrane derived vesicles

PEP have been characterised by exhibiting a uniform size. EM observations revealed that the primary virion nucleocapsid is surrounded by a clear lucent halo, a sharply bordered rim containing the primary tegument and a smooth envelope without surface projections. In contrast, mature virions frequently exhibited a size variation and the presence of visible surface projections (Granzow, Klupp et al. 2001, Mettenleiter 2004, Pignatelli, Dal Monte et al. 2007)

The composition of PEP is largely unknown. This limitation is mainly from the difficulties in isolating primary virions from the perinuclear space because their size and density are similar to mature virions present in the cytoplasm (Loret, Guay et al. 2008, Padula, Sydnor et al. 2009). Furthermore, there is the additional problem of the weakness that the NE presents upon HSV-1 infection making hard the isolation and separation of primary virions from cytoplasmic ones.

The UL31 and UL34 viral proteins known to be present in the NE of infected cells, play a fundamental role during HSV-1 nuclear egress and are generally accepted to be constituents of primary virions but absent from mature virions (Klupp, Granzow et al. 2000, Reynolds, Wills et al. 2002, Reynolds, Liang et al. 2004). In contrast, major tegument and envelope proteins are only present in the cytoplasmic mature particles (Naldinho-Souto, Browne et al. 2006).

The composition of HSV-1 primary enveloped particles is largely unknown

A proteomic study showed the presence of viral proteins that are restricted to primary virions (Padula, Sydnor et al. 2009). This study supports previous EM and immunogold studies suggesting that the composition of PEP partly differs to the composition in mature virions. Padula´s study attempted to analyse by proteomics the composition of PEP (Table 2). For this, they attempted to isolate NE from HSV-1 infected cells and subsequently harvested these virions. To do so, they harvested COS-7 cells after 18 h of HSV-1 infection into a sucrose buffer. After cellular disruption, nuclei were pelleted and subjected to different rounds of DNAase digestions to eliminate chromatin and enrich for NEs (Padula, Sydnor et al. 2009). A caveat to this study is that during HSV-1 infection the NE is partially disrupted allowing nucleocapsids to reach the cytoplasm (Maric, Haugo et al. 2014). The NE becomes weak and it breaks apart making difficult the isolation of this cellular structure from HSV-1 infected cells. Thus, different approaches to study the composition of the primary envelope are required to shed light on potential nuclear proteins involved in primary envelopment at the INM.

Table 2. Proteins identified in Padula´s study as part of PEP

(Padula, Sydnor et al. 2009)

Gene	Protein	Localization
UL17	DNA packaging protein	capsid
UL18	VP23	capsid
UL19	VP5	capsid
UL26	VP24	capsid
UL34	UL34	PEP
UL38	VP19	capsid
UL49	VP22	tegument
US6	gD	PEP/envelope

1.3.3. Heterochromatin modifications during HSV infection

HSV-1 infection is associated with a variety of structural changes in nuclear architecture. The infected cell nucleus is irregular in shape and presents peripheral displacements of chromatin resulting in a significant increase of the nuclear size (Conn and Schang 2013). Monier and colleagues performed different studies using histone H2B-GFP to label host chromatin in Hela cells infected with HSV-1. They attempted to analyse the heterochromatin dynamics and changes that the nuclei suffer upon HSV-1 infection. This study showed that between 8 and 9.5 hpi, the nuclei of HSV-1 infected cells increased to 1.75 times that of uninfected cells. Thus, this study showed that nuclear size increased by nearly two-fold upon HSV-1 infection. Most of the increase in volume is due to the expansion of the interchromosomal space. Additionally, they also demonstrated the marginalization of host chromatin to the nuclear periphery and the disruption of the nucleolar morphology by the presence of viral replication centres (VRC). The formation of VRCs produces the separation of chromatin as it presents low solubility in the concentrated solution of viral replication components resulting in the displacement of the host chromatin towards the nuclear periphery (Monier, Armas et al. 2000).

Another study observed that the nuclei volume of HSV-1 infected Hela cells increased four to five-fold compared with mock cells at 16 hpi. This same study demonstrated that G-actin was essential to produce nuclear expansion and enlargement during HSV-1 infection (Simpson-Holley, Colgrove et al. 2005).

Later studies have shown that the remodelling of the nuclear structures is a main factor to allow nucleocapsids to cross the nuclear space. They used ring-sheet microscopy to image and track the movement of nucleocapsids with super resolution microscopy. This study showed that transport of nucleocapsids within the nucleus is not led by a directed motility and transport. However, the modifications that the nuclear structure suffered upon HSV-1 infection allowed viral nucleocapsids to get access to the NE by the formation of enlarged nuclear spaces (Bosse, Hogue et al. 2015).

1.3.4. Nuclear lamina and NETs during HSV-1 infection

The 20 to 100 nm deep orthogonal filamentous meshwork of the nuclear lamina together with the presence of NETs and attached chromatin present a physical obstacle for capsid budding. This complex network hampers the movement of nucleocapsids to access the INM (Mou et. al., 2008). To access the INM herpesviruses have developed ingenious strategies causing the partial disassembly of the lamina. Disruption of the lamina by HSV-1 infection has been shown to be coupled with the maturation of VRC involving the activation of both cellular and viral proteins (Simpson-Holley, Baines et al. 2004).

Lamina disassembly requires specific phosphorylation of lamins. Furthermore, some NETs have been shown to be hyperphosphorylated during HSV-1 egress such as emerin (Leach, Bjerke et al. 2007, Morris, Hofemeister et al. 2007). Phosphorylation leads to lamin depolymerisation resulting in the release of some NETs associated to lamin as for example LBR (Scott and O'Hare 2001). Multiple cellular kinases are known to be activated during mitosis leading to the phosphorylation of lamins and NETs which facilitates NE disassembly. This process is mediated by the activation of cyclin dependent kinase1 (Cdk1), protein kinase C (PKC), mitogen-activated protein kinase (MAPK), protein kinase A (PKA), casein kinase II, and AKT (Margalit, Vlcek et al. 2005).

Disassembly of the nuclear lamina, as a result of the phosphorylation produced by different kinases, causes the individual filaments to break apart into individual lamin dimers. In consequence, phosphorylation disrupts the lamina protein-protein and protein-DNA interactions (Guttinger, Laurell et al. 2009).

Several pieces of evidence suggest that members of the herpesvirus family have adapted analogous cellular mechanisms for phosphorylating lamins to gain access to the INM (Gonella et. al., 2005; Reynolds, Liang and Baines, 2004; Muranyi et. al., 2002). HSV-1, HSV-2 and HCMV infections promote the phosphorylation of all three types of lamins (lamin A/C, lamin B1 and lamin B2) (Cano-Monreal et al., 2009; Marschall et al., 2005; Mou et al., 2007, 2008; Park and Baines, 2006) while HCMV infection induces phosphorylation of lamin A/C (Lee et al., 2008; Muranyi et al., 2002). Lamin B can be phosphorylated directly by PKC cellular protein and/or other

cellular or viral kinases during HSV-1 infection (Park and Baines 2006). On the other hand, lamins A/C have been reported to be phosphorylated by US3 viral kinase during HSV-1 infection (Mou, Wills et al. 2008) and by PKC in cells infected with HCMV (Muranyi, Haas et al. 2002).

In addition to lamins, NETs have also been reported to be phosphorylated and disrupted during herpesvirus infection. The first evidence that a NET can be targeted during HSV-1 egress was provided by the O'Hare lab (Scott, E. S. 2001). They used live-cell imaging to monitor LBR tagged to GFP during HSV-1 infection showing that LBR is translocated from the INM to the ER of infected cells. Further, they performed FRAP analyses to show an increase in the mobility of LBR within the nuclear rim of infected cells resulting in its partial redistribution from the INM. Hence, this data indicated that LBR becomes increasingly free in order to diffuse laterally from the INM suggesting the disruption of the LBR connection to the lamina network upon viral infection. This provides an easy access for nucleocapsids to bud at the INM (Scott and O'Hare, 2001).

A few years later the O´Hare and Roller labs reported the targeting of another NET during HSV-1 infection. Emerin, a single transmembrane span protein anchored to the INM and interacting with lamins was shown to be hyperphosphorylated in HSV-1 infected cells resulting in an increase of its mobility within the NE. Interestingly, the phosphorylation of emerin led to a loss of connections between emerin and lamins resulting in a greater extractability of this NET from the NE of infected cells (Morris, James B 2007). One last study demonstrated the redistribution of LAP2β in a discountinous and punctuate manner within the NE in HSV-1 infected cells (Reynolds, Liang et al. 2004, Simpson-Holley, Baines et al. 2004). This argued that the same kinases involved in lamin phosphorylation during HSV infection would participate in the phosphorylation of NETs.

All these findings suggested that in order to achieve a successful nuclear egress, HSV-1 must target NETs and lamins resulting in the disruption of protein-protein connections prior to primary envelopment at the INM. These modifications will facilitate the access of nucleocapsids to the INM where they become wrapped by this membrane.

The interactions between NETs and lamins results in the formation of a complex environment for the access of nucleocapsids to the INM. The dismantling of the nuclear lamina by the phosphorylation induced during HSV-1 infection would include the release of lamins and NETs allowing proteins to diffuse into the ER. This diffusion would be caused by the alteration of the tethering of proteins bound to the lamina resulting in an increase of nucleocapsid access to the INM. Emerin as well as LBR and LAP2β have been shown to be targeted during HSV-1 infection resulting in a loss of these proteins from the INM.

The modifications observed in the few transmembrane proteins tested might reflect a more whole-scale effect on NETs during HSV-1 infection. As mentioned before, the INM is a unique structure containing numerous specific resident nuclear transmembrane proteins. Therefore, it is reasonable to deduce that at least some other NETs could be targeted by HSV-1 in order to facilitate viral access to the INM. Most interesting would be to test, if some of them are being affected or modified by the virus during NE egress.

Are there other NETs apart from emerin and LBR being targeted by HSV-1 during NE egress?

To date several viral proteins that will be discussed in the next section have been characterized to regulate HSV-1 primary envelopment from the nuclear membrane. However, little is known about cellular proteins that might be involved in this process. During secondary envelopment, viral capsids present in the cytoplasm acquire their final envelope in either the TGN or the Golgi. As mentioned in the previous section, this budding event between cytoplasmic capsids and cellular membranes is thought to occur as a result of interactions between tegument proteins present in the capsid´s surface and cytoplasmic tails of envelope glycoproteins expressed in cellular membranes (Mettenleiter 2004, Mettenleiter, Klupp et al. 2009). Supporting this hypothesis, several interactions have been identified between tegument proteins and glycoproteins (Elliott, Mouzakitis et al. 1995, Gross, Harley et al. 2003). As an example, VP16 was shown to interact with the cytoplasmic tail of gH (Gross, Harley et al. 2003). These interactions between glycoprotein tails and tegument

proteins might facilitate the budding of capsids into cellular compartments such as the TGN or Golgi bending the host membrane tightly around the viral particle.
Different host cellular proteins have been shown to be utilised by the virus to achieve secondary envelopment. For instance, Rab1A activity was suggested to be important for the trafficking of viral envelope proteins from the ER to the Golgi, where they are incorporated into the virus after glycosylation. During nuclear egress, as in the case of secondary envelopment, protein interactions might be needed to pull the INM around nucleocapsids triggering the formation of PEP.
Thus, we postulated that some host cellular proteins such as Rabs and/or proteins in the NE such as NETs, are likely to be interacting with viral proteins present in nucleocapsids in order to facilitate the budding of these viral particles at the INM.

Are NETs being involved in fusion events facilitating budding at the NE?

1.3.5. Cellular kinases activated during nuclear egress

A variety of cellular kinases are activated during herpesvirus nuclear egress resulting in the disruption of the nuclear lamina in order for capsids to gain access to the INM.
CDK1 also known as cdc2, has been shown to be involved in the disruption of the nuclear lamina during HSV-2 infection via its potential role in emerin phosphorylation (Morris, Hofemeister et al. 2007). In addition, recruitment of PKCs to the NE was also suggested to be involved during HSV-1 infection. PKC is a family of ten serine/threonine kinases involved in a variety of cellular functions (Reyland 2009). Different studies have reported the recruitment of PKC alpha and delta to the nuclear rim of infected cells between 8 and 12 hpi with HSV-1, resulting in an increase in the phosphorylation of lamina components (Park and Baines 2006). The concentration of PKC within the nuclear rim of infected cells depends on the presence of UL31/UL34 at the NE (Park and Baines 2006) and it is known to induce the phosphorylation of lamin B and emerin (Leach, Bjerke et al. 2007, Leach and Roller 2010) (Figure 6). Furthermore, there are studies suggesting that the activation

of PKC during HSV infection is necessary for nuclear lamina breakdown thus facilitating viral egress at the NE (Leach and Roller 2010).

The involvement of PKCs during nuclear egress seems to be a conserved characteristic of herpesviruses. PKCs are also recruited to the nuclear rim of *Murine cytomegalovirus* (MCMV) and Human *cytomegalovirus* (HCMV) infected cells where they phosphorylate lamin proteins, promoting a partial disruption of the lamin meshwork (Muranyi, Haas et al. 2002, Milbradt, Webel et al. 2010, Sharma, Bender et al. 2015).

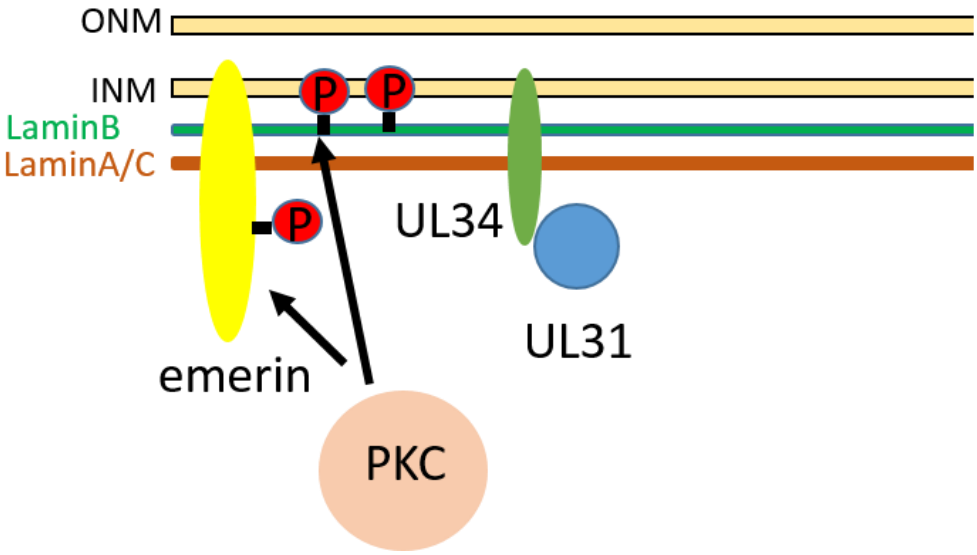

Figure 6. PKC recruitment at the NE during HSV-1 infection. *Lamin B is phosphorylated during HSV-1 infection by PKC cellular kinase as well as emerin. The recruitment of PKC at the NE depends on the presence of UL31 and UL34.*

All these previous studies have pointed out the potential role of only three cellular kinases during HSV-1 nuclear egress. Additionally, to our knowledge, only lamins and three NETs (emerin, LAP2β and LBR) have been shown to be targeted by either cellular or viral kinases during HSV-1 infection.

As lamins and some NETs are phosphorylated by multiple cellular kinases during cellular processes and as NETs present connections with chromatin and lamins, it is reasonable to hypothesize that some other NETs are being targeted during viral infection in order to break connections and mobilize NETs for capsid access to the NE. Moreover, additional cellular kinases might be recruited by the virus to promote nuclear lamina disruption, facilitating the access of nucleocapsids to the INM.

Are there other cellular kinases facilitating HSV-1 nuclear egress?

1.3.6. Viral factors involved in herpesvirus nuclear egress

Various studies including mutagenesis, genetic and ultrastructural analysis, observed the involvement of different viral factors during herpesvirus egress at the NE. Here, I will describe the viral proteins that have been described as being main factors during HSV-1 nuclear egress:

-The Nuclear Egress Complex (NEC) is a heterodimeric complex composed of two conserved viral proteins (UL31/UL34) essential for nuclear budding. Both proteins are conserved throughout the Herpesviridae family, suggesting their importance in herpesvirus life cycle. The NEC is targeted to the NE and it is thought to be involved in various nuclear egress steps such as (1) nuclear lamina disruption by the recruitment of viral and cellular kinases to locally dissolve the nuclear lamina, (2) interaction between nucleocapsid and the INM allowing membrane deformation (3) fusion of PEP with the ONM resulting in the release of naked capsids into the cytosol (Mettenleiter, Klupp et al. 2009).

UL31 is a nuclear phosphoprotein that localizes to the INM via UL34 interaction (Chang and Roizman 1993, Reynolds, Wills et al. 2002). This protein is likely interacting with the nuclear matrix as it has been shown to be resistant to extraction

with detergent and high salt concentrations as are many other nuclear lamina components (Chang and Roizman 1993).

The UL34 protein is a type II integral membrane protein containing a 22 amino-acid transmembrane domain at the C-terminus. This protein is anchored to the INM by its short C-terminal transmembrane domain with only three residues extending into the perinuclear space (Shiba, Daikoku et al. 2000). On the other hand, the 247 amino-acid N-terminal domain of this protein faces the nucleoplasm in where it interacts with the C-terminus of UL31 (Yamauchi, Shiba et al. 2001). UL31 interacts with lamin through its N-terminus (Figure 7). In the absence of UL34, UL31 protein is localized to the nucleus of infected cells but it does not target the NE (Reynolds, Ryckman et al. 2001). Thus, the C-terminus of UL34 is responsible to target the NEC complex to the INM while UL31 is exposed to the nucleoplasm where it associates with the capsid surface of PEP. The unique structure of the NEC reshapes the INM resulting in the deformation and curvature of this membrane ensuring that nucleocapsids are tightly enveloped, leading to viral budding and formation of PEP. Next, fusion with the ONM releases nascent capsids into the cytoplasm while the NEC remains in the ONM where it is exposed to the cytoplasm (Bigalke, Heuser et al. 2014, Funk, Ott et al. 2015).

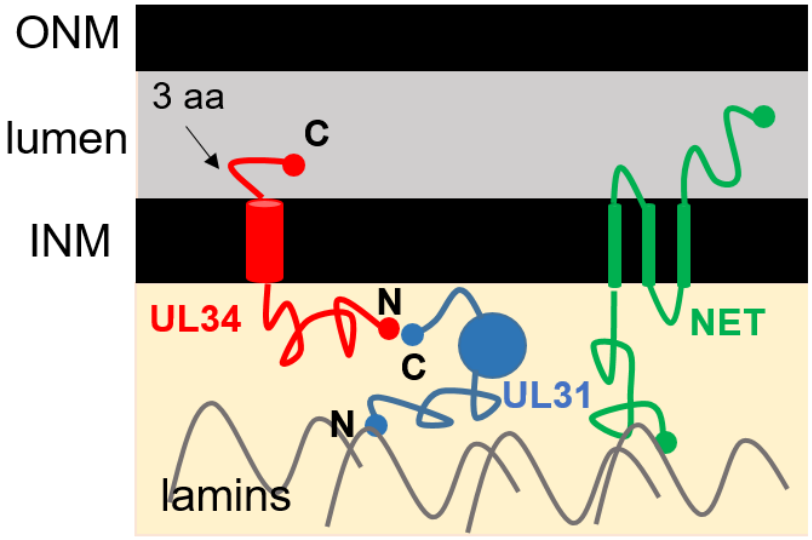

Figure 7. NEC viral complex. *The heterodimer complex of UL31 and UL34 are involved in HSV primary envelopment. UL31 protein is a phosphoprotein that is recruited to the nuclear membrane by the interaction of its C-terminus with the N terminus of UL34. At the same time UL31 interacts with lamins through its N-terminus. UL34 is an integral membrane protein with an N-terminal nucleoplasmic domain and a short C-terminal transmembrane domain TM embedded in the INM extending only 3 amino-acids into the lumen. Opposite to UL34, nuclear integral proteins (NETs) contain multiple TM domains strongly anchoring these proteins to the NE.*

Different studies have shown that in the absence of the NEC, viral egress is partially impaired resulting in the accumulation of nucleocapsids in the nucleoplasm. Interestingly, some viral particles were able to reach the cytoplasm after UL31/UL34 silencing indicating that there is an independent pathway by which viral particles cross the NE in the absence of this complex (Fuchs, Klupp et al. 2002, Klupp, Granzow et al. 2007, Passvogel, Klupp et al. 2015). Fuchs and colleagues showed the impairment in viral titres produced by a UL31 deleted mutant PRV virus (Fuchs, Klupp et al. 2002). This mutant showed a decreased plaque formation of more than 100-fold from those of wild type. In this same study, ultrastructural analyses demonstrated that particles undergoing budding at the INM and cytoplasmic or

extracellular virions were absent from cells infected with UL31 mutant PRV virus. These defects were also observed in a similar study with a UL34 mutant PRV virus (Fuchs, Klupp et al. 2002).

Moreover, both proteins have been associated with PEP in the lumen and at the INM and ONM but are absent from cytoplasmic and extracellular virions. In an ultrastructural study performed by Reynolds and colleagues, UL31 and UL34 were observed to associate with perinuclear virions but not with extracellular virions in HSV-1 infected cells. These observations further support the envelopment/de-envelopment model of virion egress (Reynolds, Wills et al. 2002).

The NEC was also shown to be sufficient to drive the formation of vesicles from the nuclear membrane in an *in vitro* study. In (Klupp, Granzow et al. 2007) cell lines stably expressing both UL31 and UL34 of the alphaherpesvirus PRV were generated. These cells showed the formation of membranous vesicles from the NE containing both proteins, UL31 and UL34, localizing at the lumen. These results suggested that UL31 and UL34 can induce the formation of perinuclear vesicles that mimic PEP without a nucleocapsid in an artificial system.

The importance of the UL31/UL34 complex has increased the interest in elucidating its structural and mechanical features for designing specific drugs targeting the complex. Recently cellular electron cryo-tomography has revealed the NEC coat architecture. This study argued that only electron density for UL31 and UL34 was observed at sites of fusion between the INM and PEP suggesting these two proteins function alone during nuclear egress in order to promote viral egress (Hagen, Dent et al. 2015). However, this might be an over-interpretation of the results as no immunogold EM studies were performed in order to confirm the presence of UL31 and UL34. Nevertheless, this study does not exclude the possibility of host proteins being involved in nuclear egress because there would be no visible electron density for a multispanning transmembrane NET with short nucleoplasmic region that might be aiding herpesvirus nuclear egress. Another study arguing that UL31 and UL34 are sufficient for primary envelopment showed that membrane invaginations can be induced by mixing these two viral proteins with liposomes in a completely artificial system (Bigalke, Heuser et al. 2014). Neither of these papers

measured the efficiency of membrane budding compared to a normal infection and neither excluded the possibility of other proteins participating in the egress process. It is highly unlikely that primary envelopment will be driven by only these two viral proteins as UL31 is not a transmembrane protein and its location at the INM depends on its interaction with UL34 and UL34 is targeted to the INM by the presence of one single transmembrane domain containing only three residues extending into the lumen space (Shiba, Daikoku et al. 2000). Thus, this protein presents a weak association to the membrane as compared with other membrane proteins presenting multiple transmembrane domains within the NE.

During HSV budding, the INM must undergo deformation to create membrane curvature and budding around nucleocapsids. The generation of curvature in the membrane is an enthalpy-driven process that is mediated by protein-protein interactions, resulting in the change of membrane topology. Protein interactions apply forces to flat membranes surfaces pulling membranes around a cargo (Zimmerberg and Gawrisch 2006).

Thus, there are still lot of questions to be answered in regards to the function of the NEC in membrane budding. Does UL34/UL31 complex recruit host proteins (as yet unidentified) during in vivo HSV-1 infections or are these two viral proteins able to mediate curvature and membrane budding directly without the presence of any other host cellular proteins?

UL31/UL34 might interact with host proteins driving INM deformation

Taken together, it is unlikely that the short C-terminal transmembrane domain of UL34 would act as a single driving factor of viral budding at the INM unless its density in the nuclear membrane at sites of egress becomes sufficiently high for protein-protein interactions to bend the membranes. To achieve this density, would also require the removal of hundreds of different NETs.

The involvement of cellular proteins in other steps of viral nuclear egress suggests the high possibility of the contribution of other cellular factors in order to facilitate membrane budding during HSV nuclear egress. Furthermore, protein-protein interactions are needed to help pulling the membrane around the viral particles, as

in the case of secondary envelopment where tegument proteins on the surfaces of the capsids present in the cytoplasm bridge with viral glycoproteins expressed in the TGN or Golgi, resulting in the formation of enveloped particles.
Thus, we postulate that the NEC complex is interacting with other proteins within the NE resulting in the formation of tight interactions allowing the tethering of the viral complex at the INM. These protein interactions will pull the INM into a bud resulting in the formation of PEP residing in the lumen.

-pUS3 is a viral protein presenting kinase activity that is only found in the alpha-herpesvirus subfamily and it distributes throughout the infected cell. It has been proposed to phosphorylate UL34, as well as other cellular and viral factors involved in nuclear egress. US3 kinase is required for a correct distribution of UL34 at the nuclear rim of infected cells where it localizes with US3.
Different studies have shown that infection of cells with a US3-null virus results in a punctuate distribution of UL34 at the NE, as compared with the uniformly even distribution presented in cells infected with a wild type HSV-1 (Reynolds, Ryckman et al. 2001, Reynolds, Wills et al. 2002).
Furthermore, US3-null virus infection produces the accumulation of PEP in an expanded perinuclear space indicating that this kinase has an important role in de-envelopment at the ONM (Wagenaar, Pol et al. 1995, Reynolds, Wills et al. 2002).
In contrast to UL31 and UL34, US3 is a tegument protein not only found on PEPs but on cytosolic capsids and in mature extracellular virions (Granzow, Klupp et al. 2004, Loret, Guay et al. 2008)

-Viral glycoproteins: While the role of viral glycoproteins during HSV entry is well characterised, the contribution of these proteins during primary and secondary envelopment remains unclear mainly due to a high functional redundancy of these proteins.
Multiple viral glycoproteins such as gM, gB, gH-gL and gD are found in the INM and in PEP (Stannard, Himmelhoch et al. 1996, Baines, Wills et al. 2007, Johnson, Wisner et al. 2011). After synthesis in the ER, they are laterally transported to the ONM. How these proteins reach the INM has not been proved at the moment but it

is thought they exploit similar mechanisms as NETs by the use of peripheral channels of the NPC. Additionally, immunogold EM studies have found the presence of gB, gC, gD and gM in PEP (Torrisi, Di Lazzaro et al. 1992, Jensen and Norrild 1998).

Another study showed that the recruitment of gM and gD to the INM depends on the presence of NEC (Table 3, Table 4). They showed that UL34 interacted directly or indirectly with gD and these interactions were needed for the retention of the glycoprotein at the INM (Wills, Mou et al. 2009). Interestingly, other studies did not observe the presence of these glycoproteins in the primary envelope of PRV virions, suggesting that different members of the same family might utilize different mechanisms for de-envelopment at the ONM (Klupp, Altenschmidt et al. 2008)

All the studies showing the presence of viral glycoproteins at the INM and PEP open the possibility of the involvement of glycoproteins during herpesvirus nuclear egress. As mentioned in the previous section, secondary envelopment is driven by interactions between tegument proteins of the cytoplasmic viral particles with glycoproteins present in the Golgi or TGN. These interactions drive the deformation of the host membrane allowing the viral budding. Thus, it is likely that a similar process is taking place during primary envelopment where glycoproteins by interactions with other proteins might be anchoring the nucleocapsids at the INM resulting in the curvature of the INM.

There are also evidences pointing out the participation of glycoproteins during de-envelopment at the ONM. PEP decorated with viral glycoproteins fuse with the ONM in an apparently similar process as herpesvirus entry into cells. As mentioned in the previous section, gB, gD and the heterodimer gH-gL are necessary for membrane fusion during viral entry. These three glycoproteins are also found in PEP as well as in the INM and ONM. Evidence for the involvement of these glycoproteins in de-envelopment came from studies in which infection with a HSV-1 mutant lacking both gB and gH showed a decrease in the number of viral particles able to cross the NE reaching the cytoplasm suggesting their role in promoting fusion between the primary virions and the ONM (Farnsworth, Wisner et al. 2007). Depletion of these two glycoproteins increased the number of PEP in the lumen but there are still viral particles reaching the cytoplasm.

Other viral glycoproteins found in PEP such as gD and gM might promote fusion with the ONM although there are studies suggesting the contrary (Johnson, Wisner et al. 2011). Thus, there might be other mechanisms by which viral particles fuse with the ONM.

Table 3 contains a list of the known HSV-1 glycoproteins and where they have been found to be localized. Table 4 contains different steps in HSV-1 life cycle and the glycoproteins known to be involved.

The NEC complex present in the PEP might be promoting de-envelopment, however it is unlikely that UL31 and UL34 could by themselves direct fusion events as UL34 only extends three residues from the surface of the PEP and UL31 interacts with tegument proteins without any extension from the surface. This opens the possibility of roles for glycoproteins during primary envelopment and de-envelopment at the NE during nuclear egress as the NEC seems to be insufficient to drive this process by itself. Are there other viral glycoproteins involved in these viral steps? Furthermore, it is likely that host proteins such as ESCRT proteins might be involved in membrane curvature and scission helping during virus budding into the lumen (Lee, Liu et al. 2012).

Table 3. HSV-1 glycoproteins and their known localization

Gene	Protein	Envelope	PEP	INM
UL1	gL	YES	YES	YES
UL10	gM	YES	YES	YES
UL22	gH	YES	YES	YES
UL27	gB	YES	YES	YES
UL53	gK	YES	?	?
US4	gG	YES	?	?
US5	gJ	YES	?	?
US6	gD	YES	YES	YES
US7	gI	YES	?	?
US8	gE	YES	?	?

Table 4. HSV-1 glycoproteins and their involvement in viral life cycle steps

Viral life cycle step	Glycoproteins involved
Primary envelopment	n/a
De-envelopment	gB, gH/gL
Secondary envelopment	gB,gD,gE/gI
Direct release from cell	gE/gI

1.3.7. Membrane fusion events during viral infections

As previously mentioned, it is reasonable to suggest the potential interaction between UL31/UL34 and host proteins in order to drive budding events at the INM. These as yet not identified cellular proteins, could contribute together with the NEC complex in the formation of vesicles at the INM resulting in the release of PEP into the lumen or in the fusion with the ONM releasing nascent capsids into the cytosol. Intracytoplasmic transport between cellular compartments is mainly mediated by vesicles. Vesicles are a basic tool for the cell; they are involved in a variety of physiological events such as the secretory and endocytic pathways as well as transport of cargo molecules between organelles (Bonifacino and Glick 2004).

Vesicle formation is a highly regulated but conceptually straightforward mechanism in which the integrity and composition of the involved organelles is not compromised. This process starts with the selection of cargo molecules by cargo receptor proteins. After this, coat proteins recruited to the site of assembly impose a curvature on the membrane, generating buds that result in the formation of vesicles containing the selected cargo. *Clathrin, COPI and COPII* are the best known coat proteins involved in the selection of cargo resulting in vesicle formation and membrane deformation into the cytosol, cleaving membrane necks by constricting them from the outside (Zeev-Ben-Mordehai, Vasishtan et al. 2014).

In contrast to this, the *ESCRT machinery* participates in membrane scission from inside the neck and mediates membrane deformation in the opposite direction (away from the cytosol) such as secretory body formation or egress of enveloped viruses as HIV at the plasma membrane (Wollert, Yang et al. 2009)

Once vesicle formation has finished, vesicle transport must be selective in order to only recognize in an orderly way the correct target membrane to fuse with in a process called vesicle docking. This crucial recognition step is controlled by *SNARE proteins* and *Rab GTPases* (Zerial and McBride 2001, Geumann, Barysch et al. 2008, Bhuin and Roy 2014, Wandinger-Ness and Zerial 2014).

There are 20 SNARE proteins in eukaryotic cells associated with specific membrane-organelles (Ungar and Hughson 2003). These transmembrane proteins work in combination with Rab GTPases. There are over 60 human Rabs that regulate and coordinate multiple cellular processes such as vesicle budding, fusion and tethering and vesicle transport. Specific Rabs are associated with distinct organelles and transport vesicles to enable a highly regulated delivery of vesicle membranes and cargo to specific target compartments. Thus, Rabs have been shown to be key regulators of intracellular membrane trafficking by regulating two main processes: fusion and transport of vesicle membranes.

In recent years, a number of studies have provided evidence for the exploitation of Rabs function by viruses during budding and secondary egress pathways in the cytoplasm, as is the case for HSV-1 (Manna, Aligo et al. 2010, Caillet, Janvier et al. 2011). Different studies have identified Rab proteins as key players in herpesvirus secondary envelopment for the transport of virus glycoproteins from the TGN to the PM and vice versa (Zenner, Yoshimura et al. 2011, Hollinshead, Johns et al. 2012, Johns, Gonzalez-Lopez et al. 2014).

One study showed the involvement of Rab6 in a specific exocytosis pathway to transport virus glycoproteins from the Golgi/TGN to the PM and how this step was essential in HSV-1 secondary envelopment (Gonzalez-Lopez et al. 2014). Another study performed by the same group showed a new mechanism for the recruitment of glycoproteins by endocytosis from the PM into endocytic tubules in which Rab11 was involved (Hollinshead, Johns et al. 2012). Finally, a few years later, Rab1a/b and Rab43 were shown to be essential for the traffic of viral glycoproteins from the ER to the assembly compartment in the cytoplasm of HSV-1 infected cells (Johns, Gonzalez-Lopez et al. 2014).

Recently, vesicle trafficking has been reported to regulate nucleocytoplasmic transport of large cargo such as ribonucleoprotein particles (RBP) (Speese, Ashley

et al. 2012). This nuclear transport pathway involves vesicle formation at the INM and scission from the nucleoplasm into the lumen space of the NE prior to fusion with the ONM. This process is similar to herpesvirus egress at the NE. Therefore, it is not surprising that vesicle transport might represent a potential mechanism for transport of large cargo from the nucleus to the cytoplasm, which viruses such as HSV have usurped and exploited during evolution.

So far, the only vesicle fusion pathways linked to nuclear egress are the involvement of ESCRT pathway proteins for EBV nuclear egress. Dominant-negative mutations in Vps4, a protein component of the ESCRT machinery that contributes to the release of ESCRT complex from membranes and Chmp4b involved in scission, result in the reduction of virion release from the nucleus. Interestingly, the cellular ESCRT machinery was shown to be recruited by EBV BFRF1, (homologous of UL34 in alphaherpesviruses), suggesting its participation in the scission of the nucleus-associated membrane during EBV primary envelopment. However, the involvement of ESCRT in the induction of vesicle formation was not found for HSV-1, suggesting that alphaherpesviruses require alternate mechanisms for NE egress (Lee, Liu et al. 2012).

Vesicle fusion pathways are used by EBV during primary envelopment

Hence, this study opens the possibility that vesicle fusion pathways might be exploited by other herpesvirus types during nuclear egress. It is therefore reasonable to think that, as for other physiological processes in the cell, vesicle formation from the INM will require the presence of vesicle fusion proteins that either interact with UL31/UL34 to aid in pulling the INM around nucleocapsids promoting viral budding or will act following an independent pathway resulting in membrane curvature to ensure that viral capsids are tightly enveloped.

1.4. The NE and its role in innate immunity

1.4.1. The STING / NET23 pathway and its role in innate immunity

In vertebrates, there are two complementary systems that have evolved to detect, fight and protect the cell against microbial pathogens: the innate and adaptive immune systems. Innate immunity is the first and most rapid line of host defence against invasion by multiple pathogens.

The detection of pathogen invasion occurs via the recognition of pathogen-associated molecular patterns (PAMPs) that are present in all microorganisms, such as viral nucleic acids or bacterial cell wall components as lipopolysaccharides, through a set of host pattern recognition receptors (PPRs) that in turn induce anti-pathogen genes. PPRs can be divided into two groups; the first group includes several members of the Toll-like receptor (TLR) family that mainly localize in the lumen of endosomes and lysosomes allowing the detection of pathogen nucleic acids. The second group of receptors are the cytosolic nuclei acid sensors including the cytoplasmic DNA sensors as well as the RIG-I like receptors (RLR) family able to detect pathogen-derived RNA in the cytosol. RLRs, including RIG-I, MDA5 and LGP2 are sensors of viral RNAs in the cytoplasm such as hepatitis C virus (HCV). After viral RNA is detected, RLRs associate with MAVs/VISA, an integral protein present in the mitochondria, facilitating the activation of Tank Binding Kinase 1 (TBK1) leading to the phosphorylation of IRF3/7 that then induce type I IFN genes (Akira, Uematsu et al. 2006, Wu and Chen 2014, Dempsey and Bowie 2015) (Figure 8).

Besides innate immune response activation by RNA, accumulation of foreign DNA in the cytosol can also induce dramatic activation of type I IFNs. STING (stimulator of interferon genes), also known as TMEM173, MPYS, MITA, ERIS and NET23 is a transmembrane protein localized in the ER, mitochondria and NE, that was found in 2008 to be an adaptor protein exhibiting a vital role in DNA signalling in the cytosol (Ishikawa and Barber 2008).

cGAS is a recent identified cytosolic DNA sensor that upon DNA binding catalyses the production of cGAMP which acts as a second messenger binding to and activating STING on the surface of the ER. In response to cGAMP binding, STING dimerizes and relocalizes from the ER to the Golgi and further to perinuclear vesicles. Following STING activation, the downstream kinase TBK1 is recruited to STING leading to subsequent phosphorylation of STING and IRF3. Consequently, phosphorylated IRF3 dissociates from TBK1 and dimerizes before translocating into the nucleus to activate innate immunity genes (Zhong, Yang et al. 2008, Liu, Li et al. 2015).

It has been recently shown, that STING interacts with both TBK1 and IRF3, suggesting STING acts as a scaffold protein to promote the phosphorylation of IRF3 by TBK1 (Tanaka and Chen 2012). The repertoire of genes induced upon cytosolic-DNA detection such as type I interferon (IFN) or tumor necrosis factor alpha (TFN-α) are activated via IRF3 and NF-KB pathways (Paludan and Bowie 2013) (Figure 8).

Although the activation of STING by cytosolic DNA is well established, the role of this protein in response to RNA is less clear. Different studies have suggested STING as a key scaffolding protein that links RIG-I (cytosolic RNA sensor) to the mitochondrial protein MAVS, key element of the RNA-sensing pathway. Activated MAVS interacts with STING resulting in its dimerization and subsequent IRF3 activation (Zhong, Yang et al. 2008).

In 2011, Chen Huihui and colleges demonstrated that RNA virus infection triggers the activation of STING via STING interaction with MAVs leading to the recruitment of STAT6 (signal transducer and activator of transcription 6), which is phosphorylated by TBK1 leading to its nuclear translocation. Once inside the nucleus, STAT6 acts as a transcription factor activating multiple genes involved in innate immunity (Chen, Sun et al. 2011) (Figure 8).

The importance of STING in the innate immune defence against RNA viruses has been also supported. Different studies involving RNA viruses have reported the role of RNA viral proteins as cGAS-STING antagonists. For example, the yellow fever virus (YFV), a RNA virus belonging to the Flaviviridae family has been reported to directly interact with STING and block STING and RIG-I dependent signalling by the

non-structural protein NS4B (Ishikawa, Ma et al. 2009). Another study has shown the importance of cGAS in the activation of the IIR to HIV and other retroviruses by detecting reverse-transcribed viral cDNA (Maelfait, Seiradake et al. 2014). A recent study published by Holm and colleagues has shown the stimulation of a cGAS-independent STING pathway by enveloped RNA viruses to block the host IIR activation. In particular, they observed that the HA2 FP protein of Influenza A virus (IAV) targeted this pathway by its direct binding to STING, resulting in the inhibition of STING dimerization and therefore TBK1 activation (Holm, Rahbek et al. 2016). Despite the fact that STING might be interacting with some proteins involved in RNA cascade signalling, the basis for the involvement of STING in controlling RNA defence mechanisms remains unclear.

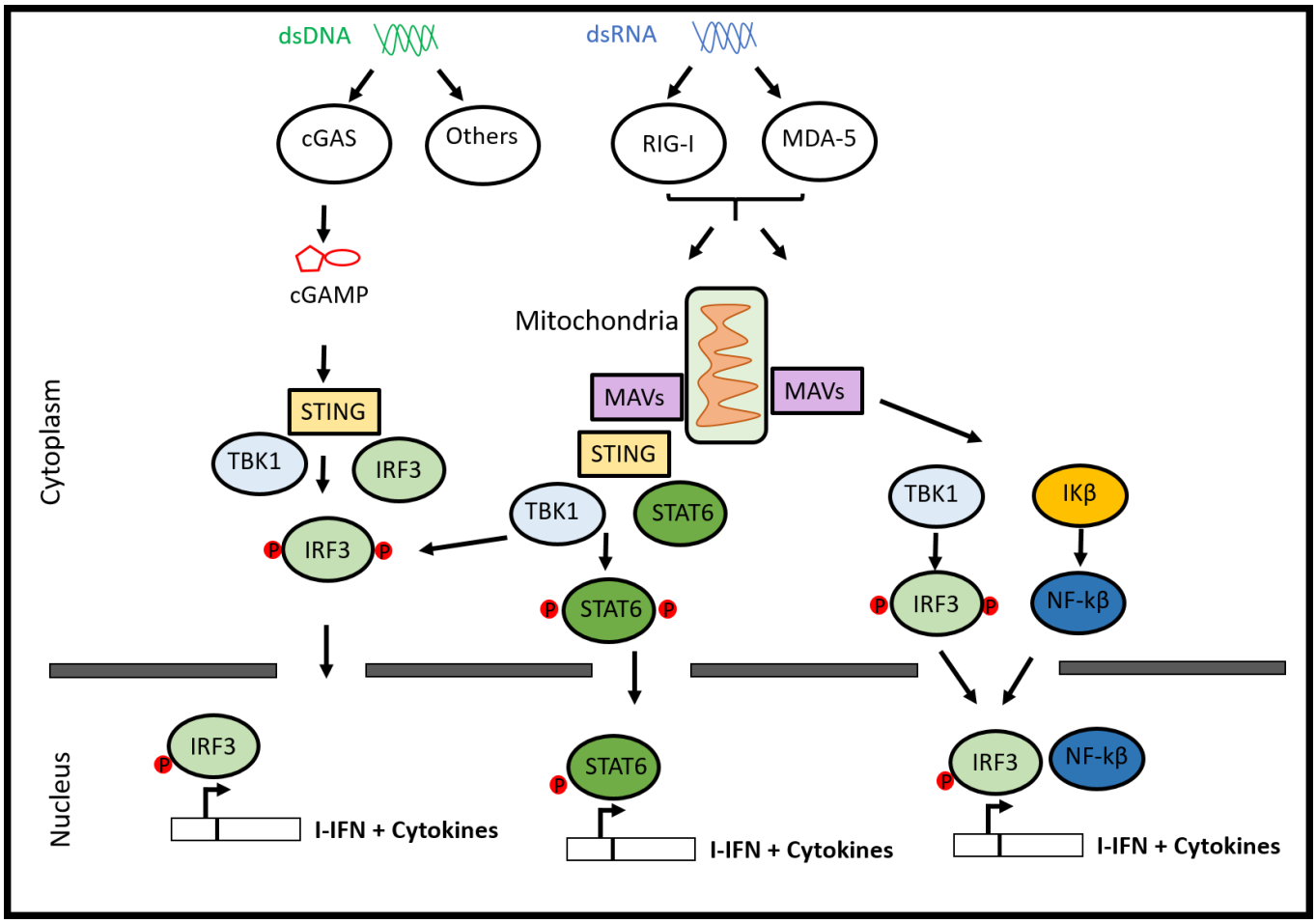

Figure 8. Overview of IIR activation in response to cytosolic nucleic acids. *Cytosolic DNA is sensed directly by cGAS or by alternative cytoplasmic sensors leading to the activation of STING. STING interacts with TBK1 and IRF3 leading to the phosphorylation of IRF3 by TBK1. Once IRF3 is phosphorylated, it translocates into the nucleus where it activates IFN and cytokines production. Double stranded RNA generated from multiple viral infections is sensed by RIG-1 and MDA-5. These two proteins bind directly to dsRNA leading to the activation of MAVs, a protein tethered to the mitochondrial membrane. At this point two pathways have been described: (1) MAVS can either activate TBK1 and IKβ kinases leading to the activation of IRF3 and NF-kβ inducing the secretion of I-IFN and cytokines (2) Recently it has been shown (Chen, Sun et al. 2011) that RNA viruses trigger the activation of STING through a STING-MAVS interaction. Subsequently STING recruits STAT6 and TBK1, leading to the phosphorylation and activation of STAT6 resulting in I-IFN and cytokines activation*.

1.4.2. Role of NET23/STING in HSV-1 infection

While host cells have developed various strategies to battle against viruses and initiate a robust immune response, over time viruses are also evolving distinct mechanisms to escape the host immune responses.

Different studies have shown that multiple DNA and RNA viruses have gained strategies to counteract the cGAS-STING pathway. Some of these viruses, present similar mechanisms to inhibit STING-TBK1 binding, while others use more sophisticated mechanisms involving STING cleavage and degradation.

For example the Hepatitis B virus (HBV), a DNA virus, was found to inhibit the STING-triggered IFN promoter activation by the HBV polymerase by dampening its K63-linked ubiquitination (Liu, Li et al. 2015). Another study identified that oncoprotein E7 from Human papillomaviruses (HPV) and EA1 oncoprotein from adenovirus bound to STING acting as an antagonist for the cGAS-STING pathway preventing the activation of the antiviral response. They showed that the LXCXE motif of these oncoproteins, essential for blockade of the retinoblastoma tumor suppressor, was also important for antagonizing DNA sensing. Furthermore, the absence of E7 resulted in a significant induction of type I interferon (Lau, Gray et al. 2015).

The Herpesviridae family has also been reported to evade the cGAS-STING pathway. HSV-1 was the first DNA virus reported to activate STING in vivo and *in vitro*. Thus, this virus is widely used in investigations as an activator of the cGAS-STING pathway. In 2009, Ishikawa and colleges found that STING is necessary for the production of type I IFN after HSV-1 infection. They used a STING knockout mouse model demonstrating that these mice were more sensitive to HSV-1 infection than the wild-type mice, due to the lack of a successful activation of type I interferon response (Ishikawa and Barber 2008). Multiple proteins of different viruses belonging to the Herpesviridae family have been described to target the cGAS-STING pathway. For instance, HSV-1 ICP0 E3 ubiquitin ligase was reported by Orzalli and colleges in 2012 to degrade the nuclear interferon gamma inducible protein 16 (IFI16), inhibiting cytoplasmic STING and IRF3 activation. IFI16 localizes in the nucleoplasm and nucleoli and interacts with p53 and retinoblastoma-1 tumor suppressors regulating its function (Orzalli, DeLuca et al. 2012).

Another study performed a screen using 90 KSHV open reading frames (ORFs) to identify potential proteins from KSHV that could inhibit the activation of the cGAS-STING pathway. They found that the viral interferon regulatory factor 1 (Virf1) interacts with STING preventing its binding to TBK1. Consequently, STING phosphorylation is inhibited resulting in an overall repression of the DNA sensing. In another study, Kaposi's sarcoma- associated herpesvirus ORF52 protein was found to directly inhibit the enzymatic activity of cGAS (Gillen, Li et al. 2015). All these studies showed different mechanisms by which the Herpesviridae family evades the cGAS-STING pathway to mitigate the host immune response.

Recently, ICP27, an essential multifunctional protein for HSV-1 replication (Rice and Knipe 1990) and conserved among all herpesviruses (Sandri-Goldin 2011), has been shown to directly interfere with the TBK1 activated STING signalosome (Christensen, Jensen et al. 2016). They found that ICP27 translocated from the nucleus to the cytoplasm, where it interacts with the TBK1-STING activated complex resulting in a reduction in the phosphorylation and activation of IRF3 via the cGAS-STING pathway.

Viruses have co-evolved with their host developing mechanisms to overcome and evade host immune responses. The role of STING in host protection from HSV has

been clearly demonstrated by different studies indicating the essential role of this protein in IIR pathways.

1.4.3. What is known about NET23/STING within the Nuclear Envelope?

STING was originally identified and introduced as NET23 from a proteomic study to identify NETs in crude NE carried out in my supervisor´s lab (Schirmer, Florens et al. 2003). Since then, multiple studies have also located this protein in the ER and mitochondria where it has been described to play a pivotal role in innate immunity (Ishikawa and Barber 2008, Zhong, Yang et al. 2008, Sun, Li et al. 2009, Chen, Sun et al. 2011, Ishikawa and Barber 2011).

Different studies have shown the accumulation of NET23/STING in perinuclear vesicles once innate immunity is activated by its interaction with TBK1. However, it is uncertain why this translocation takes place, and the authors of these studies have presumed it to stay in the ER and not enter the nucleus (Ishikawa, Ma et al. 2009, Holm, Jensen et al. 2012, Tanaka and Chen 2012). Despite the distinct functions and localisations suggested for STING during innate immunity, the potential nuclear role for this protein has been largely unaddressed.

1.4.3.1. NET23/STING and chromatin organization from the NE

NET23/STING has been subjected to multiple studies carried out in our lab since it was first identified in a proteomic study in crude NE fractions. NET23/STING is resistant to detergent extraction from cells, suggesting association with the lamin polymer (Malik, Korfali et al. 2010).

To determine whether NET23/STING is in the INM or ONM, three-dimensional structured illumination microscopy (OMX) studies were done. Interestingly, while other previously NETs tested with this method were exclusively detected in the INM or ONM, NET23/STING was found in some cells to be restricted to the INM and in other cells restricted to the ONM (Figure 9).

NET23/STING is found in both, ONM and INM

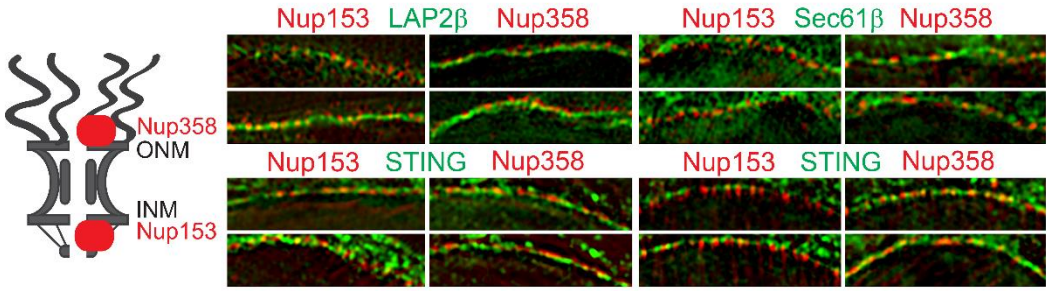

Figure 9. NET23/STING localises at the INM and ONM. *Super resolution microscopy Nup153 colocalisation indicates INM localisation while Nup358 colocalisation indicates ONM localisation. Top panel images from control NETs. Lap2β is present in the INM and Sec61β in the ONM. Bottom panel shows images from NET23/STING presented in the INM in some cells and in the ONM in others. Taken from de las Heras et al, in preparation.*

Another study carried out in our lab aimed to identify NETs involved in chromatin organization, found NET23/STING as a strong promoter of chromatin compaction. In this study, different NETs identified in proteomic studies were tested by microscopy techniques to identify potential NETs that could promote chromatin compaction. Most of the analysed NETs showed little compacted chromatin. However, NET23/STING seemed to induce a very strong increase in the quantity of visually dense chromatin.

NET23/STING expression promotes high levels of chromatin compaction

Previous studies published by multiple groups have studied the role of NET23/STING as an ER and a mitochondria protein. Whether this population of NET23/STING is functional at the NE is also unclear.

The identification of NET23/STING as a NET together with the strong chromatin compaction effect induced by this protein, opened the possibility of a potential new role of NET23/STING within the NE. But, how does NET23/STING promote

chromatin compaction from the NE? Is NET23/STING interacting with chromatin proteins?

To our knowledge this was the first time where the function of NET23/STING within the NE was being addressed. This and another aspects regarding the role of NET23/STING in chromatin compaction from the NE will be addressed in *chapter 3* as a continuation of the study started in my supervisor´s lab.

1.4.3.2. Some NET23 nuclear binding partners are highly involved in innate immunity

Although NET23/STING was first discovered in a proteomic study for nuclear proteins in the Schirmer lab, different studies have shown the involvement of this protein in intracellular DNA-mediated and HSV-1-activated type I IFN production. However, its potential role in mediating IIR activation from the NE has been largely neglected.

As previously mentioned, NET23/STING binds to the lamin polymer, resulting in a highly insoluble protein. Earlier studies aimed to identify NET23/STING binding partners might have missed NET23/STING specific binding partners at the NE due to the insolubility of this protein pool within the NE. Thus, in order to address the limitations of standard co-IPs, and with the aim of identifying NET23/STING specific binding partners at the NE that might be missed in earlier studies, a NET23-NE co-IP was done in our lab. To do so, NEs were isolated from cells previously transfected with NET23/STING-GFP and treated with reversible cross-linker (Figure 10). After, cross-linked NEs were fragmented by sonication, immunoprecipitated, and crosslinks reversed with, then potential NET23/STING partners were identified by mass spectrometry.

The NET23/STING-NE co-IP was highly enriched for proteins with Gene Ontology (GO) terms for chromatin and chromosome organisation and RNA/DNA binding factors. Specifically, they found that one of the most abundant NET23/STING-binding partners were bromodomain proteins that might mediate the previously mentioned involvement of NET23/STING in chromatin compaction and other

epigenetic alterations associated with its role in IIR (Figure 10). Interestingly, there was a pool of NET23/STING binding partners enriched for the GO term of proteins involved innate immunity.

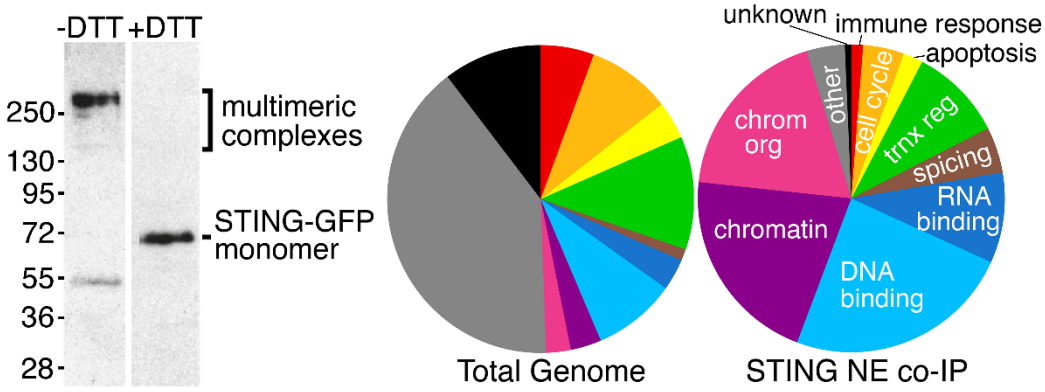

Figure 10. NET23/STING binding partner proteins identified by co-IP within the NE. *Left panel shows the cross-linking of NEs with orthophenanthroline copper chasing NET23/STING to multimeric protein complexes while the treatment with DTT reversed the crosslinked protein into its expected molecular weight (NET23/STING-GFP 70 KDa). The right panel represents the Gene ontology (GO) classification for NET23 partners identified by mass spectrometry of cross-linking NE-co-IP proteins. Notably, chromatin, DNA binding and chromosome organization terms are enriched. Taken from de las Heras et al, in preparation.*

Predicting that the relationship between NET23/STING nuclear binding partners and its effect on gene expression might be interrelated, gene expression changes were analysed upon reduction or gain of NET23/STING. As previously shown for a NET23/STING knockout mouse, some of the genes that were affected upon NET23/STING silencing were targets of IRF3/7 transcription factors involved in IIR. Importantly, the NET23/STING nuclear partners and the genes affected by the manipulation of NET23/STING were highly represented for GO terms for nucleotide binding partners, specifically for ss and dsRNA binding partners, suggesting that

NET23/STING might be involved in sensing a wide variety of pathogen nucleic acids though these binding partners, consistent with what has been shown for its functioning in IIR to RNA viruses.

Further analysis of the pool of NET23/STING NE-binding proteins using the HPRD interactome database and Cytoscape, revealed the presence of 17 direct binding partners that present interactions with six IRF3/7-binding partners, some of which are RNA-binding proteins. This suggested that NET23/STING might be indirectly affecting the regulation of the expression of genes involved in IIR by interactions with some of these 17 NE-binding partners (Figure11) suggesting a highly redundant pathway by which NET23/STING can participate in IIR activation.

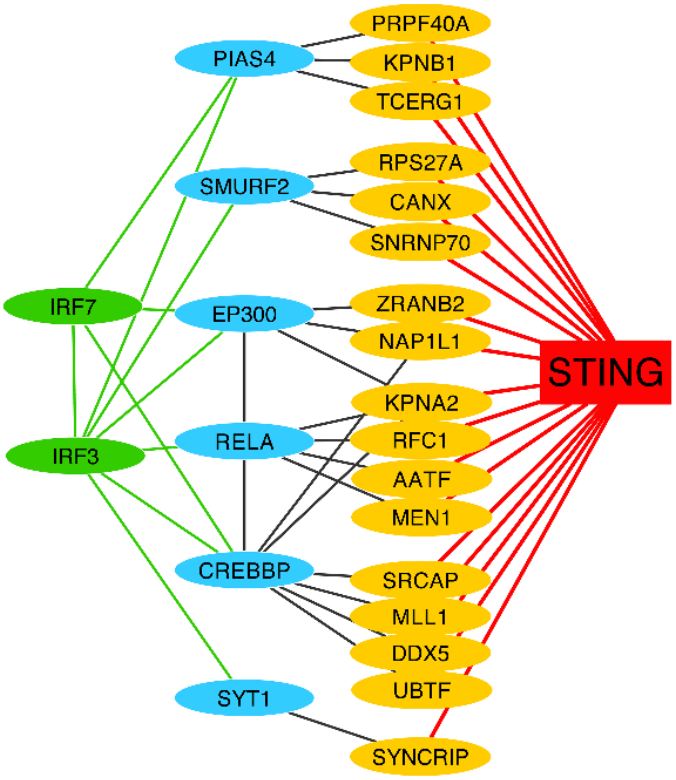

Figure 11. NET23/STING binding partners present connections with IRF3/7. *Interactome analysis of NET23/STING NE binding partners showed indirect connections to IRF3/7 transcription factors involved in IIR. Taken from de las Heras et al, in preparation*.

Based on all these observations, we postulated that NET23/STING might be acting as a nucleocytoplasmic transporter for some NET23/STING-NE co-IP partners facilitating the activation of IRF3/7 transcription factors to further activate IIR. Many viruses are able to inhibit nuclear transport through the central channels of the NPC upon infection. NET23/STING, as a NET, might be able to navigate the peripheral channel of the NPC. Thus, the multiple NET23/NE binding partners that are linked with IRF3/7 transcription factors, and the potential ability of this protein to travel through the peripheral channels, opens the possibility of NET23/STING acting as a nucleocytoplasmic transporter for transcription factors and proteins involved in IIR.
This would not exclude the activation of signalling cascades that navigate through the central channel of the NPC, but it would provide a backup mechanism for the host for activating IIR through the peripheral channels.

NET23/STING could be acting as a nucleocytoplasmic transporter

Additionally, the function of NET23/STING in sensing RNA nucleic acids is not well understood. Interestingly, in the study carried out in our lab, proteins involved in ssRNA and dsRNA were highly affected by the manipulation of NET23/STING. This opens the possibility of NET23/STING having an important role for sensing RNA nucleic acids in addition to DNA.
Thus, the function of NET23/STING acting as a chromatin regulator together with its potential novel role in IIR activation from the NE will be investigated as part of my thesis project. Answering all these questions could have an important impact in human health as NET23/STING is known to be essential for host defence against pathogens and it could potentially facilitate the adjuvant activity of pathogen nucleic acid-based vaccines by enhancing immunization procedures through the production of type I IFNs.

1.5. Outstanding questions

One purpose of this research is to establish a more comprehensive understanding of the *role of the NE during herpesvirus nuclear egress*. The wide range of functions recently linked to the NE and the identification of hundreds of proteins associated with this cellular structure, indicates that it is a much more complex physical barrier to herpesvirus infection than previously thought, and it must be overcome to ensure infection and production of virus progeny.

At the present, the most widely accepted model for herpesvirus egress at the NE is the envelopment/de-envelopment model in which it is thought that UL31/UL34 viral proteins are involved in the initial budding of herpesvirus nucleocapsids at the INM, resulting in the formation of PEP. Different studies have suggested that UL31/UL34 are sufficient to drive the formation of perinuclear vesicles without the presence of other cellular proteins. However, all these experiments left the function of the NEC in membrane budding at the INM unclear. It is difficult to understand how these two viral proteins could directly drive membrane fusion events during primary envelopment without any other host protein interaction, as UL31 is not associated with the membrane and UL34 presents a short transmembrane domain attached to the INM with only three residues extending into the perinuclear space. Furthermore, there are a hundred of NETs in the INM and membrane fusion typically requires a close apposition of proteins that could be impeded by the presence of all these NETs.

I postulate that NETs might be targeted during egress at the NE by either degradation or modification by the virus. For example, just as the UL31/34 complex recruits cellular kinases to depolymerise the lamin polymer it could also phosphorylate NETs to break their interactions with chromatin. (1) To test this hypothesis, different NETs were screened by immunofluorescence as tagged fusions to determine whether they are degraded or redistributed during HSV-1 infection.

As an alternative, host proteins might be recruited to the NE in where they could interact with viral proteins to enhance membrane association assisting viral fusion events during primary envelopment. During HSV-1 primary envelopment,

nucleocapsids acquire their envelope from the INM that contains potential host proteins that might be driving/contributing to membrane budding. During de-envelopment at the ONM, nascent capsids are released into the cytoplasm while the primary envelope derived from the INM remains fused with the ONM. Thus, it might be expected that during de-envelopment, host proteins involved in membrane budding and other primary envelope proteins, would be released into the ONM and will diffuse into the ER, as it is continuous with the ONM. (2) To achieve the detection of host proteins that might be assisting viral fusion events during nuclear egress, microsomal membranes (MMs) and NEs from mock and HSV-1 infected cells were isolated to compare the relative distribution of associated proteins between the two fractions.

If successful, this study will provide novel insights into herpesvirus life cycle, revealing proteins mediating herpesvirus egress at the NE that could be potentially targeted therapeutically. Furthermore, elucidating the protein composition of primary envelope particles will provide new insights into HSV-1 biology.

The second purpose of this research is to continue the study started in my supervisor´s lab regarding *the role of NET23/STING within the NE*. NET23/STING was firstly identified in my lab as a NE integral membrane protein. Since then, different studies have linked this protein with an IIR function in the ER and mitochondria; however, whether this protein harbours a role within the NE was completely ignored.

In a screen performed in our lab for NETs that promote chromatin compaction, NET23/STING was found to have a very strong effect indicating a potential novel nuclear function for this protein in IIR within the NE. Furthermore, the identification of NET23/STING NE-binding partners linked with a chromatin/chromosome organisation and IIR functions, supported the potential involvement of this protein in chromatin regulation and IIR signalling events within the NE.

Our main hypothesis was that NET23/STING might have a separate role within the NE. To investigate some of these aspects, I used different approaches such as FRAP to study if the translocation of NET23/STING was being affected upon IIR within the NE. This will indicate a potential nucleocytoplasmic transport role of this protein. In addition, some NET23/STING NE-binding partners identified by co-IP

were observed by immunofluorescence staining to analyse if after NET23/STING depletion their redistribution fails to occur in IIR induced cells. This study allowed me to elucidate the role of NET23/STING within the NE upon IIR activation.

Chapter 2

Materials and Methods

2.1. Materials

2.1.1. Bacterial strains and genotypes

DH5alpha

F- endA1 glnV44 thi-1 recA1 relA1 gyrA96 deoR nupG Φ80dlacZΔM15 Δ(lacZYA-argF) U169 hsdR17(rK- mK+) λ–

StrataClone SoloPack

F- endA1 glnV44 thi-1 recA1 relA1 gyrA96 deoR nupG Φ80dlacZΔM15 Δ(lacZYA-argF) U169 hsdR17(rK- mK+) λ–. (Stratagene, 240207)

2.1.2. Buffers and solutions

Table 5. Composition of Buffers used in this study.

Name	Composition
LB	1% tryptone; 0.5% yeast extract; 10mM NaCl; pH7.4
PBS	65mM Na2PO4; 8.8mM KH2PO4; 137mM NaCl; 2.7mM KCl; pH7.4
TAE	40mM Tris-acetate; 1mM EDTA
SDS PAGE buffer	25 mM Tris; 192 mM glycine; 0.1% SDS; pH 8.3
Transfer buffer	80% SDS-page buffer; 20% methanol
Denaturation buffer (FISH)	70% formamide, 2xSSC

Hybridization buffer (FISH)	50% formamide, 2xSSC, 1%Tween20,10% Dextran Sulphate
SSC 20x	300mM Sodium Citrate pH 7.2, 3M NaCl
ImmunoFISH blocking buffer	2% BSA, 2xSSC
FISH wash buffer 1	0.1% Tween20, 2X SSC
FISH wash buffer 2	0.1% Tween20, 0.1X SSC
Opti-MEM	Opti-MEM® I Reduced Serum Medium (Gibco, 31985062)
Hypotonic lysis buffer	10 mM HEPES pH 7.4, 1.5 mM MgCl2, 10 mM KCl, 2 mM DTT
SHKM	50 mM HEPES pH 7.4, 25 mM KCl, 5 mM MgCl2, 1 mM DTT and 1.8M sucrose
GMEM	GMEM, Invitrogen, UK (51492C)
DMEM	Dulbecco's Modified Eagle's Medium (Lonza, 12-604F)

2.1.3. Primary antibodies

Table 6. Primary antibodies used in this study

Antigen	Host	WB dilution	IF dilution	Source
NET5	Rabbit	1:250	N/A	Millipore (06-1013)
α-tubulin	Mouse	1:1000	N/A	Sigma
Tmem38A	Rabbit	1:250	N/A	Millipore (06-1005)
Tmem214	Rabbit	1:250	N/A	Proteintech (20125-1-A)
WFS1	Rabbit	1:250	N/A	Proteintech (11558-1-AP)
Lamin A/C	Rabbit	1:250	N/A	(Schirmer et al, 2001)
Emerin	Rabbit	1:250	N/A	Dr Glenn Morris
Calnexin	Rabbit	1:100	N/A	Stressgen, SPA-860
Rab11b	Rabbit	1:100	N/A	NBP2-15085
Rab18	Rabbit	1:100	N/A	IHC-plus ^{TM} LS-B9430
VAPB	Mouse	N/A	1:400	ProteinTech

VAPB	Rabbit	1:1000	N/A	Dr Christopher C.J. Miller
Rab24	Rabbit	1:200	N/A	BD bioscience
Rab1A	Rabbit	1:200	N/A	Santa Cruz Biotechnology
Nup153	Rabbit	N/A	1:200	Covance
Nup358	Rabbit	N/A	1:200	Dr. F. Melchior
NET23/Tmem173	Rabbit	1:400	N/A	ProteinTech
gD	Mouse	1:500	1:200	Abcam (ab41197)
GM-130	Rabbit	1:1000	N/A	Abcam (EP892Y)
ICP27	Mouse	1:2,000	N/A	Virusys Corp
GADPH	Rabbit	1:500	N/A	E1C604-1
US3	Rabbit	1:500	N/A	Dr Thomas Mettenleiter and Dr Barbara Klup
UL34	Rabbit	1:1000	1:500	Dr Richard Roller
SUN1	Rabbit	1:100	1:200	HPA 008346
H3K9me3	Rabbit	1:200	N/A	Upstate (07-523)

2.1.4. Secondary antibodies

Table 7 summarised all the antigen targets, sources, and dilutions of secondary antibodies used in this study. Secondary antibodies used for immunofluorescence (IF) were raised in donkey against rabbit, mouse or chicken IgG and conjugated with a variety of Alexa Fluor® dyes (Molecular Probes, Invitrogen). By contrast, for ECL based Western blotting, horseradish peroxidase conjugated to highly cross-absorbed goat anti-rabbit or anti-mouse antibodies were used. For fluorescence based Licor Western blotting, IRDye®-conjugated anti-mouse or anti-rabbit antibodies were used.

Table 7. Secondary antibodies used in this study

Antibody	Dye	Application/Dilution	Source
Anti-mouse	Alexa 568	IF 1:1000	Invitrogen (A11031)
Anti-Rabbit	Alexa 568	IF 1:1000	Invitrogen (A10042)
Anti-chicken	Alexa 488	IF 1:500	Invitrogen (A11039)
Anti-chicken	Alexa 568	IF 1:500	Invitrogen (A11041)
Anti-mouse	Alexa 647	IF 1:1000	Invitrogen (A31571)
Anti-rabbit	Alexa 647	IF 1:1000	Invitrogen (A31573)
Anti-mouse	Alexa 488	IF 1:1000	Invitrogen (A21202)
Anti-rabbit	Alexa 488	IF 1:1000	Invitrogen (A21206)
Anti-mouse	HRP	WB 1:3000	Promega (W4021)
Anti-rabbit	HRP	WB 1:5000	GE Healthcare (NA9340-1ML)
Anti-rabbit	IRDye® 800CW	IF 1:1000	Licor (926-32213)
Anti-mouse	IRDye® 800CW	IF 1:1000	Licor (926-32212)
Anti-rabbit	IRDye® 680CW	IF 1:1000	Licor (926-68073)
Anti-mouse	IRDye® 680CW	IF 1:1000	Licor (926-68070)

2.1.5. Virus stocks

The strain of wild-type HSV-1 used in this study was “herpes simplex virus type 2 strain 17+ (HSV-1 17+ WT)”. HSV-1 strain expressing RFP fused to VP26 was kindly provided by Frazer Rixon, MRC Virology Unit, University of Glasgow, Glasgow, UK and it has been used previously used (Pasdeloup, Beilstein et al. 2010). The HSV-1 strain vBSGFP27 expressing GFP fused to WT ICP27 under its own promoter was published in (Soliman, Sandri-Goldin et al. 1997). HSV-1 reporter virus expressing the enhanced green fluorescent protein (eGFP;HSV-1 strain C12) was used in one single experiment and it has been previously used (Griffiths, Koegl et al. 2013).

2.1.6. Lentiviral plasmids

The lentiviral packaging plasmids psPAX2 and pMD2.G used to generate self-inactivating lentiviral particles were a kind gift from Justina Cholewa-Waclaw (Adrian Bird Lab, Welcome Trust Centre for Cell Biology (WTCCB), Edinburgh) and were used as described previously with a variety of transfer plasmids (Zufferey, Dull et al. 1998)

2.1.7. Mammalian cells

HeLa, HT1080, U2OS, BKH-21 cells were obtained from ATCC. 293FT cells were a gift from Justina Cholewa-Waclaw (Adrian Bird Lab, WTCCB, Edinburgh). These cells are derived from the 293FT fast growing clone of 293 embryonic kidney cells which have been made to stably express the SV40 large T antigen from the pCMVSPORT6TAg.neo plasmid.

2.1.8. Commercial kits

Table 8. Commercial Kits used in this study

Kit	Provider
QIAprep Spin Miniprep Kit (27106)	Qiagen
QIAfilter Plasmid Midi Kit (12243) QIAquick	Qiagen
QIAquick Gel Extraction Kit (28704)	Qiagen
QIA DNeasy Blood&Tissue (69504)	Qiagen
StrataClone Blunt PCR Cloning Kit (240207)	Stratagene

2.2. Tissue culture methods

2.2.1. Cell maintenance and counting of cells

HeLa, HT1080, U20S and 293FT cells were grown in 1 X Growth Media (Dulbecco's modified Eagle's medium (DMEM) supplemented with 20% fetal calf serum (FBS), 100 units/ml penicillin (Invitrogen, UK) and 100 µg/ml streptomycin (Invitrogen, UK) and passaged every 2 days in a 1:5 dilution by trypsinization. 293FT cells were treated with G418 final concentration 0.5 mg/ml to maintain drug selection.
BHK-21 cells were maintained in Glasgow Modified Eagle's Medium (GMEM, Invitrogen, UK), supplemented with 2 mM L-glutamine (Invitrogen, UK), 100 units/ml penicillin (Invitrogen, UK) and 100 µg/ml streptomycin (Invitrogen, UK), 10% (v/v) new born calf serum and 10% (v/v) tryptose phosphate broth (TPB, Invitrogen, UK). For quantification of the cell number, cells were 1:1 diluted (50 µl of cells were mixed with 50 µl 0.1% trypan blue (w/v)) or 1: 9 diluted (10 µl of cells were mixed with 90 µl trypan blue) and the number of un-stained viable cells was counted using a haemocytometer under a microscope. The cell number was calculated by the following calculation:

Cell number per ml= unstained cell count x the dilution factor ×10

2.2.2. Transient plasmid transfection of Hela cells

For the NETs screen, 50,000 Hela cells were plated onto 13 mm coverslips (VWR International) in 24-well plates the day before transfection. Cells were transfected with 0.5 µg of plasmid DNA in 50 µl of JetPRIME buffer using 1 ul of JetPRIME reagent (Polyplus transfection) per well as per manufacturer's instructions. After 48 h, cells were infected during 8 h with HSV-1 17+ WT strain, fixed in 4% paraformaldehyde (PFA) PBS for 10 min following a stringent wash in PBS and subsequently stained with 4,6-diamidino-2 phenylindole, dihydrochloride (DAPI).

Coverslips were extensively washed three times with PBS before mounting them in Vectashield (Vecta Labs).

2.2.3. siRNA transient transfection in Hela and HT1080 cells

siRNA for Rab11b, Rab18, Rab1A and Rab24 were obtained from Dharmacon as SmartPools. siRNA for VAPB was ordered from SIGMA and it was used previously (De Vos, Morotz et al. 2012), sequence 5´ GCUCUUGGCUCUGGUGGUU 3´. The control siRNA was a random scrambled sequence (sense strand: 5'-CGUACGCGGAAUACUUCGA-3'; antisense strand 5'-UCGAAGUAUUCCGCGUACG-3') which lacks homology to the human or mouse exome.

Table 9. siRNA used in this study

siRNA	Product / Company
Rab11B	L-004727-00-0005 (Dharmacon)
NET23	SIGMA
Rab1A	L-008283-00-0005 (Dharmacon)
Rab24	L-010824-00-0005 (Dharmacon)
Rab18	L-008828-00-0005 (Dharmacon)
VAPB	SIGMA

55,000 Hela cells were plated in 12 well plates the day before the assay. 50 µM of each siRNA was transfected using 100 µl JetPRIME buffer and 3 µl of Jetprime reagent following manufacture´s introductions. At 48 h after transfection, the total final protein was extracted for Western blot analysis or cells were infected with HSV-1 17+ WT virus strain for the described experiments.

siRNA for NET23/STING was obtained from SIGMA. 1.5 x 10^6 HT1080 cells were plated in 6 well plates the day before transfection. In this case 100 µM of siRNA was

transfected using 200 µl JetPRIME buffer and 4 µl of Jetprime reagent for Western blot analysis or immunofluorescence experiments.

2.2.4. Establishment of STING/NET23-GFP stable cell line

To generate the inducible stable NET23/STING expressing cell line, lentiviruses encoding a doxycycline inducible NET23/STING fused to GFP at the C-terminus were prepared and transduced onto HT1080 cells. Transduced cells were selected with geneticin at 500 mg/ml. Inducible stable lines were induced with 1µg/ml doxycycline during 48 h.

Non-replicating lentiviruses carrying the NET23/STING-GFP construct were generated in 293FT cells by joint transfection of the pMD2.G plasmid, expressing the vesicular stomatitis virus glycoprotein (VSV-G) coat protein, the psPAX2 plasmid, expressing the viral proteins required to package, reverse transcribe and integrate the viral genome, and the transfer plasmid, containing the expression construct of interest, NET23/STING-GFP. Transfections were performed using lipofectamine 2000. Briefly, for the viral preparation, 4.6 µg psPAX2, 2.8 µg pMD2.G and 7.5 µg of the construct-specific transfer vector were mixed in 1.5 ml Opti-mEM. 36 µl lipofectamine 2000 was then added to an additional 1.5 ml Opti-mEM in a separate tube. Both DNA and lipofectamine containing solutions were mixed briefly by vortexing and then left at room temperature for 5 min. Following this incubation, DNA-containing Opti-mEM and Lipofectamine 2000-containing Opti-mEM were combined, mixed briefly by vortexing and incubated at room temperature for 20 min. During this time, 6 million 293FT cells - approximately one confluent 8.5 cm diameter plate – were trypsinised, pelleted, resuspended in 6 ml 1X Growth Medium and plated onto a fresh 8.5 cm diameter plate. Following the incubation, DNA-lipofectamine mixtures of Opti-MEM were added to the freshly plated 293FT cells. After 16 h 293FT media was replaced very gently with 10 ml 2X Growth Medium7. 48 h later the virus containing supernatant was aspirated, cleared of cellular debris by centrifugation for 10 min at 3,500 rpm and further clarified by filtration through a 0.45 μm^2 low protein binding PES syringe filter (Millipore, SLHP003RS). The clarified supernatant was then loaded into a 30 ml Oak Ridge round bottomed tube,

topped up with PBS if necessary to adjust the total tube volume to 25 ml and spun at 55,000 x g for 75 min at 4ºC. Lentiviral particles appeared as a small semi-transparent pellet on the side of the tube. The supernatant was then aspirated and the lentiviral particle pellet resuspended in the centrifuge tube by the addition of the desired volume of Opti-MEM or the required culture media followed by gentle shaking for 10 min at room temperature. If not used immediately aliquots were frozen at -80°C. Transduction was performed in a 6 well culture plates with 1 million HT1080 cells in the presence of 10 µg/ml protoamine sulphate (Sigma) for 16 h.

2.2.4. Innate Immune Response Induction

For FRAP experiments, a HT1080 cell line stably transfected with a doxycycline-inducible NET23/STING construct was first induced 48 h prior to IIR induction with 1µg/ml doxycycline. For immunofluorescence microscope experiments, HT1080 cells were plated and transfected with either siRNA control or NET23/STING siRNA as previously described.

IIR was induced by HSV-1 infection, poly I:C and plasmid DNA. Viral infection was performed with a MOI of 10 using HSV-1 17+ WT. Subsequently medium was added and the cells were incubated for additional 2 h before cell fixation for antibody staining or FRAP imaging.

HT1080 cells were transfected either with 20 µg/ml polyI:C or 5µg pcDNA3.1 using Lipofectamine 2000 (Invitrogen) for 2 h before cell fixation and antibody staining.

2.3. Virology methods

2.3.1. Preparation of virus stocks

Stocks of HSV-1 were generated in BHK-21 cells. 1.5 x 10^6 cells were plated in a 60 mm plate. The next day cells were infected with HSV-1 at a multiplicity of infection (MOI) of 0.001. Virus was adsorbed onto cells for 1h and incubated at 37 °C during 2 or 3 days until medium turned yellow and there was extensive cytopathic effect (cpe) (Figure 12). CPE produced by HSV-1 infection could be recognised due to morphological changes in the infected cells that become rounded and detach from the monolayer.

The cells were dislodged by scraping or gently tapping the plate and sonicated in a sonibath for 20-30 sec, centrifuged in 5,000 ×g at 4°C for 12 min and then the supernatant was transferred to 0.5 ml tubes. Samples were aliquoted, and stored at -80ºC before titration.

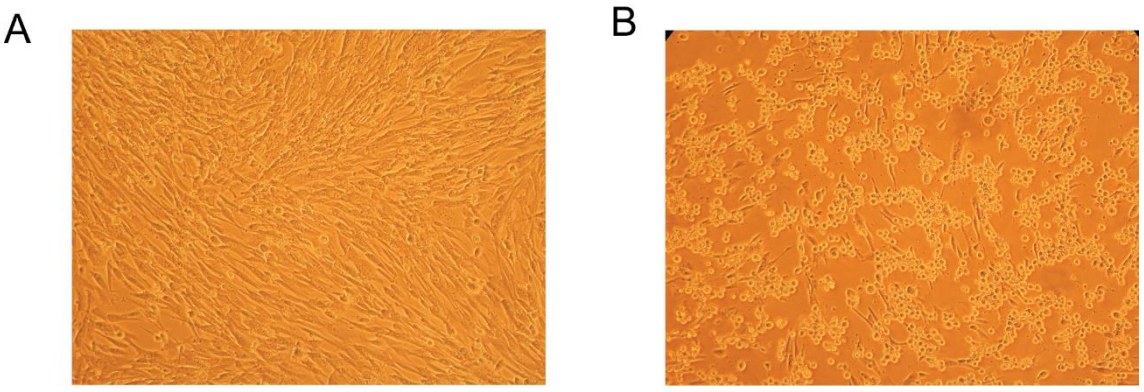

Figure 12. Cytopathic effect produced by HSV-1 infection in BHK21 cells. (A) *mock BHK21 cells* ***(B)*** *BGK21 cells infected with MOI 0.01 during 3 days. CPE could be observed as cells become rounded and they are detached from the monolayer.*

2.3.2. Titration of virus

Plaque assays were used to measure the concentration of virus in a sample i.e. virus titre. Cellular culture supernatant was harvested after 16 hpi. The samples were frozen at -80°C, thawed, and sonicated 3 times for 30 s each on a Branson 450 sonifier at 40% of maximum output level and constant duty cycle. $2x10^5$ U2OS cells were plated in 12 well plates the day before the infection. On the day of the assay, 10-fold serial dilutions usually (10^{-1} to 10^{-6}) were made from these viral supernatants and 100µl of each dilution for each viral prep was added to duplicate wells and incubated on confluent U2OS cells for 1h at 37°C. After 1h the virus was aspirated, cells were wash three times in PBS and overlaid with a 1:1 mixture of 1% (wt/vol) avicel (RC-591 NF) in sterile water–FBS-DMEM. The overlaid samples were cultured for 3 days before the avicel/medium overlay was removed. The cells then were fixed with methanol and stained with crystal violet solution (2% [wt/vol] crystal violet in 40% [vol/vol] methanol) in order to quantify viral plaque formation. Viral plaques were clearly observed under the microscope (Figure 13), counted and virus titre was calculated as plaque forming units (pfu/ml).

Titre = number of plaques × dilution/ final volume of virus plus cells added to the plate.

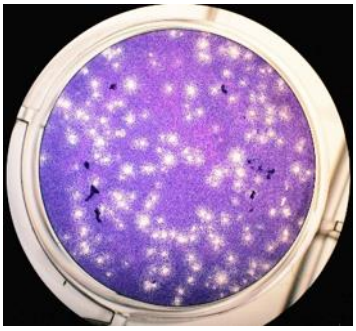

Figure 13. Example image of viral plaques stained with crystal violet. *Image of viral plaques produced by HSV-1 after three days of infection on a monolayer of Hela cells. Viral plaques were counted to calculate viral titres.*

2.3.3. Infection of cells

Once the titre of a given viral stock was known, the amount of virus from a viral stock with a desired MOI was calculated. The MOI corresponds to the number of PFUs delivered per cell. To infect cells, viral inoculum was prepared by mixing the required amount of viral stock with 3% serum supplemented media. Cells were incubated with the viral inoculum for an absorption period of 1 h at 5% CO2 atmosphere, 37°C. After 1h of adsorption either normal growth media was added without removing inoculum or monolayers were washed three times with PBS and replenished with normal growth media. Time zero (T0) or zero h post infection (0 hpi) corresponds to the end of the viral adsorption period. For mock infections the same medium used for preparation of viral inoculum was used only with no virus added.

2.3.4. Rescue experiment

Hela cells expressing the rescue constructs were plated in 12 well plates and transfected the next day with 50 nM of Rab1A, VAPB or Rab11b siRNA; 0.5 µg of pCDNA3.1 and 0.5 µg pCDNA3.1-GFP plasmid to check the efficiency of the transfection. After 48 h, cells were infected with HSV-1 WT at MOI 10. After 16 hpi, supernatants were collected for plaque assays.

2.3.5. Viral growth kinetics in NET29 knockdown Hela cells

100,000 Hela cells were plate in 24 well plates the day before transfection. Cells were transfected with either 20 µM of NET29 siRNA or control siRNA using Lipofectamine (2000) following manufacturer instructions. After two days postransfection, Hela cells were infected with eGFP; HSV-1 strain C12 during 1 h at 37ºC. After 1 h, cells were extensively washed with PBS and fresh medium was added to monitor virus growth kinetics as a measure of GFP-fluorescence. Replication was monitored at the indicated times post-infection using the POLARstar OPTIMA plate reader (BMG Labtech).

2.4. Nucleic acid methods

2.4.1. Plasmid construction

NETs expression plasmids used in the screen were cloned from IMAGE collection cDNAs as previously described (Schirmer, Florens et al. 2003, Malik, Korfali et al. 2010). NETs were fused to monomeric red fluorescent protein (mRFP) or to enhanced green fluorescent protein (EGFP) either at their C-terminus or N-terminus. All those used in the screen were under regulation of the CMV promoter.
NET23/STING was additionally cloned into both the pEGFP-N2 and pEGFP-C2 vectors for C- and N-terminal GFP fusions. The pEGFP-N2 fusion was further subcloned into pLVX- TRE3G using NheI and NotI as restriction sites for subsequent generation of lentiviruses for transduction to make stable inducible cell lines.

2.4.2. Cloning of VAPB, RAB11b and Rab1A

This experiment was performed by Andrew Stevensons at the University of Glasgow.
Primers for PCR amplifying VAPB, RAB11B and RAB1A were designed for in Fusion cloning (Clontech) into pCDNA3.1 using the following software: (http://www.clontech.com/US/Products/Cloning_and_Competent_Cells/Cloning_R es ources/Online_In-Fusion_Tools). The primers were designed to retain the *Eco*RI and *Bam*HI sites in the multiple cloning site of pCDNA3.1. For initial cloning of VAPB, RAB11B and RAB1A PCR was carried out using the appropriate primer set (Eurofins) and CloneAmp HiFi PCR Premix (Clontech). The template was cDNA that had been synthesized (Maxima kit with dsDNAse -Thermofisher) from RNA that had been extracted from differentiated NIKS16 cells. PCR products were treated with cloning enhancer (Clontech) and mixed with pCDNA3.1 (which had been previously digested with *Eco*RI and *Bam*HI (NEB) to linearize the vector) and cloned using the In-Fusion HD Cloning Kit (Clontech). Reactions were transformed into *E. coli* Stellar Competent Cells and selected on 100 µg/ml Ampicillin (Sigma). Plasmid DNA was

prepared (Qiagen QIAprep Spin Miniprep Kit) and plasmids digested *Eco*RI and *Bam*HI to confirm insert. Clones were then verified by DNA sequencing (Eurofins).

2.4.3. Mutagenesis of VAPB

This experiment was performed with the assistance of Andrew Stevensons at the University of Glasgow. For site directed mutagenesis of VAPB ((DNA sequence CTTGGCTCTGGTGGTT change to GTTTGCACTTGTCGTG) an inverse PCR was carried out on pCDNA3.1VAPB using primer set VAPB SDMfw1 and VAPBSDMrv1 with CloneAmp HiFi PCR Premix (Clontech). The PCR product was treated with cloning enhancer (Clontech) and the In-Fusion HD Cloning Kit (Clontech). Reactions were transformed into *E. coli* Stellar Competent Cells and selected on 100 µg/ml Ampicillin (Sigma). Plasmid DNA was prepared (Qiagen QIAprep Spin Mindiprep Kit) and the clone and mutation were verified by DNA sequencing (Eurofins). Note that mutagenesis was not required for Rab1A and Rab11b rescue constructs because their siRNAs targeted the 3' untranslated region.

2.4.4. Sequencing of plasmid DNA

The entire sequence of the cDNAs cloned into the expression vector was verified by sequencing. Sequencing was performed by the GenePool sequencing facility (University of Edinburgh). Provided chromatograms were analysed using the freeware program Gentle.

2.4.5. Isolation of genomic DNA

In order to isolate genomic DNA from HSV-1 infected Hela cells, the cells were trypsinised and centrifuged for 10 min at 200 X g. The supernatant was discarded and the pellet resuspended in 1ml of 1x PBS. After the pellet had been washed, DNA was isolated using the Qiagen DNeasy kit following the manufacter´s instructions. DNA was resuspended in 50µl of DNase/RNase free water.

2.4.6. qPCR

Cells transfected with siRNA against Rab1a, Rab24, Rab11b, VAPB and Rab18 as described above were infected with HSV-1 WT at an MOI of 10. Supernatants or pellets were collected at 16 hpi. DNA was purified from scraped pellet using the DNeasy Blood&Tissue Kit from Qiagen according to the manufacturer´s instructions. Viral DNA presence was analyzed by qPCR (Applied Biosystem 7500) with TakyonTM Low Rox Probe MasterMix dTTP Blue (Eurogentec) using primers detecting gD HSV-1 sequence (Weidmann, Meyer-Konig et al. 2003) (Forward: 5'-CGGCCGTGTGACACTATCG-3', Reverse:5'- CTCGTAAAATGGCCCCTCC-3', Probe: FAMCCATACCGACCACACCGACGAACC- TAMRA) and primer pair specific for GAPDH (Forward: 5'-CGCTCTCTGCTCCTCCTGTT-3', Reverse:5'-CCATGGTGTCTGAGCGATGT-3', Probe: 5'-CAAGCTTCCCGTTCTCAGCC-3'). qPCR was performed using as template the supernatant media collected from infected plates and boiled for 5 min at 95°C. Serial dilutions of known-titre HSV-1 solution were used as a standard curve to extrapolate the genomes/ml in the samples. Dilutions series of known standards were analysed in each plate. Standard curve was created comparing the known copies/reaction value with the mean of the Crossing threshold value (Ct value). Trendline was extrapolated by software, used to interpolate the genomes/ml of the analysed sample and data were compared with the control. When DNA extracted from pellet was analysed, both sets of primers where used in order to assess the cellularity of the sample. Values were calculated with ΔΔCT analysis and data are expressed in relative genome copy compare to the control.

PCR conditions were: 50°C for 2 minutes, 95°C for 2 minute, 45 cycles of 95°C for 15 seconds 55°C for 30 seconds and 72°C for 30 seconds.

2.5. Protein methods

2.5.1. Protein Extraction and Western blotting

Cell lysates were resuspended in 2X Loading sample buffer (1M Tris-HCl pH 6.8, 10% SDS, Glycerol, β-mercaptoethanol, 1% Bromophonol blue) and separated on 8-12% Tris-glycine-SDS. Subsequently the gels were transferred onto nitrocellulose membranes (Odyssey 926-31092) by means of semidry transfer (BIO-RAD). After transfer the membrane was blocked in blocking buffer (5% milk powder in TBS with 0.05% Tween-20) for 60 min. Subsequently, the membrane was incubated with the primary antibody diluted in blocking buffer at the dilutions indicated in Table 6 for 60 min at room temperature or overnight at 4°C. Six washes in TBS, 0.05% Tween-20 were then followed by incubation with the secondary antibody conjugated to horseradish peroxidase (HRP) or an IRDye® for 60 min at room temperature. After 6 washes in PBS, 0.05% Tween20, the membrane was incubated with the ECL reagent (Amersham) to allow the HRP to react with hydrogen peroxide and luminol to generate a fluorescent signal that was measured on an X-Ray film (CP-BU NEW, Agfa). Alternatively, for Li-Cor visualisation of blots, membranes IRdye®-conjugated antibodies were detected on a Li-Cor Odyssey Quantitative Fluorescence Imager.

2.5.2. Proteomics methods

2.5.2.1. NE and MMs fractions extraction

NEs and MMs were isolated using well-established procedures previously established and described in the lab (Korfali, Wilkie et al. 2010, Wilkie, Korfali et al. 2011). In brief, nuclei were first isolated from HeLa cells by hypotonic lysis in 10 mM HEPES pH 7.4, 1.5 mM $MgCl_2$, 10 mM KCl, 2 mM DTT and protease inhibitors (1 μM PMSF, 1 μg/ml aprotinin, 1 μM pepstatin A and 10 μM leupeptin hemisulphate) using a ‘tight’ dounce homogenizer (Wheaton, clearance between 0.1 and 0.15

mm). Cells were allowed to swell for 5-10 min and then nuclei were released by dounce homogenization with 20 vigorous strokes. Next, 1/10 volume of 1 M KCl was added to prevent nuclei themselves from lysing.

Nuclei were then pelleted at 1,000 x g in a swinging bucket rotor (e.g. 4,000 rpm in a Beckman Coulter J6-MC floor model centrifuge) for 20 min at 4°C to separate them from small vesicles and mitochondria that require higher speeds to pellet. To float/remove contaminating membranes, nuclei were resuspended in SHKM (50 mM HEPES pH 7.4, 25 mM KCl, 5 mM $MgCl_2$, 1 mM DTT and 1.8 M sucrose) and pelleted through a 5 ml 2.1 M sucrose cushion in a SW28 swinging bucket rotor (Beckman) at 4°C for 2 h at 82,000 x g. NEs were then prepared from isolated nuclei by two rounds of digestion with DNase and RNase in 0.3 M sucrose, 10 mM HEPES pH7.4, 2 mM $MgCl_2$, 0.5 mM $CaCl_2$, 2 mM DTT for 20 min followed by layering onto the same buffer with 0.9 M sucrose and centrifugation at 6,000 x g for 10 min at 4°C. MMs were isolated following similar established procedures. In brief, after removing nuclei as for NE preparations, 0.5 mM EDTA was added to inhibit metalloproteinases and mitochondria and other debris from post-nuclear supernatants were also removed by pelleting at 10,000 x g for 15 min. The supernatant was made to 2 M sucrose with SHKM and then overlaid with 1.86 M and 0.25 M sucrose layers. This was then subjected to centrifugation in a SW28 swinging bucket rotor (Beckman) at 4°C for 4 h at 57,000 x g to float MMs. The material between the 1.86 and 0.25 M layers was then diluted 4-fold with 0.25 M SHKM and pelleted at 152,000 x g in a type 45 Ti rotor (Beckman) for 1h.

NEs were extracted with 0.1 N NaOH, 10 mM DTT and pelleted by centrifugation at 150,000 x g for 30 min and washed 3X in sterile H_2O. MMs samples were washed in sterile H_2O without NaOH extraction. Samples were used for mass spectrometry analysis. HSV-1 infected MMs pellets were prepared and used for EM imaging.

2.5.2.2. Mass Spectrometry

Mass spectrometry analysis was performed by our collaborators Selene K. Swanson and Laurence Florens. Membrane pellets were resuspended in 30 µl of 100 mM Tris-HCl pH 8.5, 8 M Urea, then brought to 5 mM Tris(2-Carboxylethyl)-Phosphine

Hydrochloride (TCEP) and incubated 30 min at room temperature. Next this was reduced and alkylated with 10 mM chloroacetamide (CAM; Sigma) and incubated in the dark for 30 min followed by addition of Endoproteinase Lys-C (Roche) at 0.1 mg/ml and incubated 6 h at 37°C. The solution was diluted for 2 M Urea with 100 mM Tris-HCL pH 8.5 and 2 mM CaCl2 and 0.1 mg/ml Trypsin added and incubated at 37°C overnight. Formic acid was then added to 5% to quench reactions and samples were centrifuged to remove large undigested material (Florens, Korfali et al. 2008). Samples were then individually analysed by Multidimensional Protein Identification Technology (MudPIT) (Washburn, Wolters et al. 2001, Florens and Washburn 2006). Peptide mixtures were pressureloaded onto 250 µm fused silica microcapillary columns packed first with 3 cm of 5-µm Strong Cation Exchange material (Luna; Phenomenex), followed by 1 cm of 5-µm C18 reverse phase (Aqua; Phenomenex). Loaded 250 µm columns were connected using a filtered union (UpChurch) to 100 µm fused-silica columns pulled to a 5 µm tip using a P 2000 CO2 laser puller (Sutter Instruments) and packed with 9 cm of reverse phase material. The loaded microcapillary columns were placed in-line with a Quaternary Agilent 1100 series HPLC using a 10-step chromatography run over 20 h using a flow rate of 200–300 nl/min. The application of a 2.5 kV distal voltage electrosprayed the eluting peptides directly into a LTQ linear ion trap mass spectrometer (Thermo Scientific) equipped with a custom-made nano-LC electrospray ionization source and full MS spectra were recorded on the peptides over a 400 to 1,600 m/z range, followed by five tandem mass (MS/MS) events sequentially generated in a data-dependent manner on the first to fifth most intense ions selected from the full MS spectrum (at 35% collision energy). Dynamic exclusion was enabled for 120sec. RAW files were extracted into ms2 file format (McDonald, Tabb et al. 2004) using RawDistiller v. 1.0 (Zhang, Wen et al. 2011) MS/MS spectra were queried for peptide sequence information using SEQUEST v.27 (rev.9) (Eng, McCormack et al. 1994) against 55,691 human proteins (non-redundant NCBI 2014-02-04 release), plus 162 sequences from usual contaminants (e.g. human keratins…) and 77 NCBI RefSeq HSV1 proteins. To estimate false discovery rates, each non-redundant protein entry was randomized and added to the database bringing the total search space to 111,524 sequences. MS/MS spectra were searched without specifying

differential modifications, but +57 Da were added statically to cysteine residues to account for carboxamidomethylation. No enzyme specificity was imposed during searches, setting a mass tolerance of 3 amu for precursor ions and of ±0.5 amu for fragment ions.

Results from different runs were compared using DTASelect and CONTRAST (Tabb, McDonald et al. 2002)with criterion of DeltCn ≥ 0.08, XCorr ≥ 1.8 for singly, 2.5 for doubly-, and 3.5 for triply-charged spectra, and a maximum Sp rank of 10. Peptide hits from all analyses were merged to establish a master list of proteins (Appendix). Identifications mapping to shuffled peptides were used to estimate false discovery rates. Under these criteria the final FDRs at the protein and peptide levels were on average 0.72% and 0.24%, respectively.

To estimate relative protein levels, distributed normalized spectral abundance factors (dNSAFs) were calculated for each non-redundant protein (Appendix), as described in (Rice 1997). The complete MudPIT mass spectrometry dataset (raw files, peak files, search files, as well as DTASelect result files) can be obtained from the MassIVE database via ftp://MSV000079886@massive.ucsd.edu with a password NSR7095. The ProteomeXchange accession number for this dataset is PXD004519.

2.6. Microscopy methods

2.6.1. Indirect Immunofluorescence

Adherent cells were grown on coverslips and washed in PBS to remove cellular debris and remaining serum prior to fixation with either 4% para-formaldehyde (PFA) 1X PBS or methanol, for 10 min at room temperature. If cells were fixed in 4% PFA, they were then permeabilised for 6 min with 0.2% Triton-X-100 in PBS and then washed 3 times in PBS.

Coverslips were blocked in 3% bovine serum albumin (BSA), 10% human serum and 10% FBS, 1X PBS for 45 min at RT and subsequently incubated with the appropriate primary antibody (dilutions listed in Table 6). Following 3 washes in

PBS, coverslips were incubated with goat secondary antibodies conjugated with Alexa Fluor® dyes (summarised in Table 7) and DAPI at a final concentration of 2 µg/ml (1: 2,000). Coverslips were then extensively washed in PBS multiple times over the course of 15 min and then mounted on cover slips with VectaShield (Vector Labs) and used for microscopy.

For indirect immunofluorescence, images were acquired on a Nikon TE-2000 microscope using a 1.45 NA 100x objective, Sedat quad filter set, PIFOC Z-axis focus drive (Physik Instruments) and a CoolSnapHQ High Speed Monochrome CCD camera (Photometrics) run by Metamorph image acquisition software. For deconvolution analysis, Z-stacks were acquired at intervals of 0.2 µm from the 1 µm above to 1 µm below the imaged nucleus. For super resolution microscopy, cells were prepared and stained similarly except that images were taken using a Zeiss 880 confocal microscope with Airyscan and prepared for figures using Photoshop 8.0.

2.6.2. Fluorescence recovery after photobleaching (FRAP)

All fluorescence recovery after photobleaching (FRAP) experiments for regular STING/NET23-GFP and NET55-GFP constructs were performed on a Leica SP5 microscope equipped with an Argon laser using the 488 nm laser line and a 60x HCX PLAPO NA 1.4 oil objective. Temperature was maintained at 37°C in an environmental chamber (Life Imaging Services, Switzerland), cells were gassed using 5% CO_2 in air using a gas mixer (Life Imaging Services). Stably transfected inducible STING/NET23-GFP or NET55-GFP HT1080 cells were grown on 25 mm round coverslips mounted in an Attofluor incubation chamber (Life Technologies) were first induced for expression of the fusion protein during 48h with doxycycline. Coverslips were clamped into the chamber with 2 ml of preheated (37°C), phenol-free complete DMEM containing 25 mM Hepes-KOH. Five pre-bleach images were taken followed by bleaching an area in either the NE or ER for 1 s at full laser intensity. Subsequent images were taken in 2 phases. The first rapid phase consisted of 25 frames every 0.65secs to observe the rapid initial recovery. The

second slow phase consisted of 75 frames every 2 s. Image data was processed using Image-Pro Premier (Media Cybernetics Inc., MD, USA). Background and photobleach corrections were engaged using an algorithm written by David Kelly according to (Phair and Misteli 2001). A macro was written in VB.Net within Image Pro Premier whereby a region of interest (ROI) was applied to the bleach spot, background and non-bleached area of a nearby cell and corrected for movement automatically compared to the 5 pre-bleach images. If the imaged cell moved, the measured region of the bleached area was adapted manually in XY position for each frame. Recovery halftimes were calculated from normalized fluorescence values, while the immediate post-bleach value was set to 0% and the average of the ten last points of recovery curve to 100%.

For FRAP experiments, images were acquired on a Leica SP5 microscope.

TIF files were generated using Metamorph (Molecular Devices) or SP5 application suite (Leica) and exported into ImageProPlus at 12 bit for further analysis. Images were also directly imported into Adobe Photoshop CS6 for figure preparation, reducing them to 8 bit. To determine differences and compared datasets the Kolmogorov-Smirnov test (KS-test) was applied.

2.6.3. Electron Microscopy

MMs pellets were washed in sterile H_2O. VAPB, Rab18, Rab11b, Rab1A or Rab24 was depleted as previously described. Samples were fixed with 2.5% glutaraldehyde and 1% osmium tetroxide, then dehydrated through a graded alcohol series and embedded in Epon 812 resin. Thin sections were cut and examined in a JEOL 1200 EX II electron microscope.

To test the localization of viral particles in cells with knockdowns of vesicle fusion proteins, monolayer cultures of HeLa cells were seeded in a 60 mm dish and transfected with siRNAs against VFPs as above. 48 hours later cells were infected with HSV for 16 hpi at an MOI of 10, and subsequently fixed with 2.5% glutaraldehyde in 2% sucrose, 0.05M Cacodylate buffer, pH 7.2 overnight at 4°C. Cells were thoroughly washed with PBS, scraped and pelleted by centrifugation

followed by fixation with 1% osmium tetroxide (TAAB Labs, UK) and staining with 2% aqueous uranyl acetate for 1 h at room temperature. Cells were then harvested into PBS and pelleted through 3% low gelling temp agarose (Geneflow) at 45°C. The agarose was set at 4°C and cell pellets were cut into ~1 mm cubes, which were dehydrated through a graded alcohol series (30-100%) and embedded in Epon 812 resin (TAAB Labs, UK) followed by polymerization for 3 days at 65°C. Thin sections of 120 nm were cut with a UC6 ultramicrotome (Leica Microsystems, Germany) and examined with a JEOL 1200 EX II electron microscope and images were recorded on a Gatan Orius CCD camera.

2.6.4. Immunoelectron Microscopy

This experiment was performed at the University of Durham by our collaborators Christine A. Richardson and Martin W. Goldberg. Immuno-EM was performed on mock Hela and HSV-1 infected Hela for 16 h using the Tokuyasu (1973) method (Tokuyasu 1973). Cells were fixed *in situ* with 2% paraformaldehyde, 0.2% glutaraldehyde in PHEM buffer (60 mM Pipes, 25 mM Hepes, 2 mM MgCl2, 10 mM EGTA, pH 6.9) for 1 h, washed with PHEM buffer, then scraped off the culture dish. They were pelleted at 200 X g for 2 min and resuspended 0.1% glycine in PBS, pelleted at 400 x *g* for 2 min, resuspended 0.1% glycine in PBS for 15 min, pelleted at 400 x *g* for 2 min, resuspended in 1% gelatin (Dr Oetker) at 37°C for 10 min, pelleted at 400 x *g* for 2 min, resuspended in 10% gelatin for 10 min at 37°C, then replaced on ice. Gelatin embedded pellets were cut into ~5 mm cubes and immersed in 15% PVP (polyvinylpyrrolidone 10K molecular weight, Sigma), 0.17 M sucrose in PBS overnight. Samples were mounted and frozen in liquid nitrogen then sectioned on a cryo-ultramicrotome (UC6 with FC6 cryo-attachment; Leica). Cryosections were thawed, and the gelatin melted at 37°C, washed in 0.1% bovine serum albumin (BSA, Sigma) in PBS, then 1% BSA in PBS for 3 min, followed by overnight incubation with undiluted primary antibody, washed in PBS, incubated with secondary anti– mouse antibody conjugated to 10 nm colloidal gold (BBI solutions). Grids were then washed in PBS, transferred to 1% glutaraldehyde in PBS (5 min),

washed in water, and embedded in 2% methyl cellulose containing 0.4% uranyl acetate (Agar Scientific). A Hitachi H7600 TEM was used at 100 kV.

2.6.5. Fluorescence in situ hybridization

For FISH experiments HeLa cells were cultured on coverslips that were washed in PBS prior to fixation in 4% para-formaldehyde in 1X PBS for 10 min at room temperature. Cells were permeabilized for 6 min with 0.2% Triton-X-100 in PBS, followed by 3 washes in PBS.

(Next steps were developed and performed by Dr Rafal Czapiewski). Cells were next pre-equilibrated in 2X SCC and treated with RNase A (100µg/ml) at 37ºC for 1 h. Following washing in 2X SCC, cells were dehydrated with a 70%, 85% and 100% ethanol series. Coverslips were then air dried, heated to 70ºC and submerged into 85ºC preheated 70% formamide, 2X SSC (pH 7.0) for 18 min. A second ethanol dehydration series was then performed using -20ºC 70% ethanol for the first step. Coverslips were air dried and 150-300 ng biotin-labelled probe was added in hybridization buffer (50% formamide, 2X SSC, 1% Tween20, 10% Dextran Sulphate) containing 6 µg human Cot1 DNA (Invitrogen) and sheared salmon sperm DNA and incubated at 37°C for 24 h in a humidified chamber. Probes were generated from a plasmid encoding HSV-1 gene ICP27 by end labelling. After incubation, the coverslips were washed four times for 5 min each in 4X SSC at 50ºC followed by four times for 5 min each in 0.1X SSC at 65ºC. Coverslips were then preequilibrated in 4X SSC, 0.1% Tween-20 and blocked with 4% BSA before incubating for 30 min at room temperature with Alexa Fluor®conjugated-Steptavidin antibodies and DAPI at 2 µg/ml. Coverslips were subsequently washed 3 times in 4X SSC, 0.1% Tween-20 at 37ºC and mounted on slides in Vectashield (Vector Labs). Images from the midplane of the nucleus were acquired on a Nikon TE-2000 microscope using a 1.45 NA 100x objective, Sedat quad filter set, and a CoolSnapHQ High Speed Monochrome CCD camera (Photometrics) run by Metamorph image acquisition software. Images were analysed using ImageJ, using the DAPI stained image as a mask to determine nuclear area and the total

fluorescence intensity in the nucleus and in the whole cell were determined for over 100 cells for each condition.

2.6.6. Image quantification of chromatin compaction

Chromatin compaction images were captured using Metamorph acquisition software with identical settings after identical staining and fixing conditions. At least 50 nuclei were analysed per condition. To distinguish individual nuclei in a field, nuclei were either thresholded or manually identified and segmented with individual masks. Pixel intensities were extracted from raw 16-bit images in TIFF format as a numerical matrix in Image J 1.33, and subsequent analysis performed in R (http://www.R-project.org). Raw pixel intensities were normalized to the sum of total number of pixel intensities in each nucleus, to account for possible differences in overall intensity between nuclei, and localized peaks of higher signal, corresponding to denser chromatin, were identified by taking the 15th percentile of the normalized pixel signals as a lower threshold. The resulting signal peaks were then filtered so that peaks smaller than 20 pixels were discarded, and peaks closer than 3 pixels were joined together. Images taken with the microscope configuration described in the Immunofluorescence microscopy section above correspond to 1 pixel equalling 0.0645 mm. The distribution of numbers and areas of each individual peaks were then calculated and compared between samples using Kolmogorov-Smirnov tests for statistical significance (developed by Dr de las Heras).

2.6.7. Image quantification of vesicle fusion proteins NE versus ER

To validate NE translocation of vesicle fusion proteins, the relative pixel intensities in ER and NE were quantified compared to ER controls. Pixel intensity was measured at a point in the nuclear rim (based on DAPI staining) and at a point approximately 2 µm distant into the ER, and the NE/ER ratio was calculated. Four such measurements were taken from each cell for VAPB and the control calnexin

and 20 different cells were analysed. Tukey's boxplots for the ratios (NE/ER) for each protein in each cell line are shown in (*Figure 47*) with highlighting the median (central line), two quartiles above and below (box) and third quartile (error bars). We compared each sample to each control (mock infected) with the null hypothesis that control to sample differences are by random chance.

2.7. Bioinformatics

To detect enriched proteins in HSV-1 infected MMs, the ratio of HSV-1 infected MMs versus mock-infected MMs was calculated according to relative abundance determined by dNSAF values. To choose only proteins present in the NE before infection, the ratio of mock-infected NE versus mock-infected MMs was similarly calculated. Only proteins with a HSV-1 infected MMs: mock-infected MMs ratio higher than 1.3 and detected in the mock infected NE were selected.

Gene ontology (GO) analysis was performed in Ensembl BioMart and biologically interesting categories were represented either as a piechart or shown as bar plots in %. Biologically interesting GO-terms and their corresponding child terms were retrieved from the mySQL database http://amigo.geneontology.org (Carbon, Ireland et al. 2009). We used the following GO terms: "vesicle-mediated transport" (GO:0016192) "nucleocytoplasmic transport" (GO:0006913), "membrane organization" (GO:0061024), "regulation of protein phosphorylation" (GO:0001932) plus the one indicated in each table. To plot MS data pie charts, the relative proportions of the various classes were calculated from the relative abundances of the genes identified from each GO category, and this was compared to a pie chart compiled from all the genes in the human genome considering the same categories.

Chapter 3

Novel roles for NET23/STING within the Nuclear Envelope

3.1. Introduction

In the last few years, recent proteomic studies have identified tissue-specific NETs involved in multiple specific biological and cellular processes. (Schirmer, Florens et al. 2003, Korfali, Wilkie et al. 2010, Wilkie, Korfali et al. 2011). Interestingly, several of these proteins are linked to human diseases such as neuropathy and dystrophies (Ognibene, Sabatelli et al. 1999) (Fidzianska, Toniolo et al. 1998).

NETs have been also linked to the regulation of specific spatial genome organization within the nucleus (Gordon, Pope et al. 2015, Czapiewski, Robson et al. 2016). Heterochromatin is dynamically associated with the NE and recently it has become increasingly apparent that the genome follows a non-random organisation of chromatin (Lanctot, Cheutin et al. 2007, Zuleger, Kelly et al. 2011, Bickmore and van Steensel 2013). Moreover, enrichment of heterochromatin at the NE varies significantly between different cell types (Fawcett, Doxsey et al. 1981).

It is conceivable that mutations affecting lamin A, emerin and other NETs binding directly or indirectly with chromatin results in defective interactions of the NE with heterochromatin, impairing its correct localization at the nuclear periphery (Ognibene, Sabatelli et al. 1999). Thus, it is likely that other NETs might mediate heterochromatin changes observed in these NE-linked diseases

As an example, Emery-Dreifuss muscular dystrophy (EDMD) is linked to mutations in emerin and it presents alterations in the organization of chromatin with respect to the nuclear periphery (Bione, Maestrini et al. 1994, Bonne, Di Barletta et al. 1999). These defects in chromatin distribution were also observed in a mouse model presenting NE-linked cardiomyopathy (Wang, Herron et al. 2006). In addition to these alterations, modifications in the distribution of epigenetic silencing marks leading to changes in gene expression have been linked with patients presenting NE diseases. Indeed, alterations in gene expression patterns were found in NE-linked muscular dystrophy patients and in a mouse model for this disease (Melcon, Kozlov et al. 2006).

Altered patterns of heterochromatin distribution have been identified in several NE-linked diseases in which lamin A is mutated (Goldman, Shumaker et al. 2004, Columbaro, Capanni et al. 2005, Shumaker, Dechat et al. 2006, Lattanzi, Columbaro et al. 2007). These diseases are also linked to mutations in several NETs such as emerin and LBR.

Interestingly, a proteomic screen ran by Korfali et al. in NEs isolated from leukocytes, identified a NET named IAG2 which showed a strong chromatin compaction phenotype (Korfali, Wilkie et al. 2010). Additionally, the lab ran a screen for NETs identified in liver for potential roles in promoting chromatin compaction; NET23/STING was observed to promote a very strong increase in the amount of chromatin compaction compared with other tested NETs (Malik, Zuleger et al. 2014). This observation indicated the possibility of a previously uncharacterized nuclear role for NET23/STING in general chromatin architecture.

Multiple reports have linked NET23/STING with a role in IIR within the ER and mitochondria (Ishikawa and Barber 2008, Ishikawa, Ma et al. 2009, Chen, Sun et al. 2011). This protein has been shown to be translocated from the ER to perinuclear vesicles in the presence of dsDNA (Ishikawa, Ma et al. 2009, Holm, Jensen et al. 2012, Tanaka and Chen 2012). Whether this population of NET23/STING is functional at the NE remains unclear. Despite the translocation of this protein into perinuclear vesicles after IIR activation, and its identification as a NET in a proteomics screen carried out in Schirmer's lab a few years ago, its role at the NE has been largely neglected.

Recent experiments carried out in our lab have identified multiple NET23/STING NE-binding proteins that link this protein with IIR cascades. These observations, together with the potential role of NET23/STING in the regulation of the compacted state of chromatin, led us to hypothesize that NET23/STING might have a separate role within the NE.

This chapter aimed to test the hypothesis of NET23/STING being involved in chromatin compaction events. Furthermore, I aimed to investigate the contribution of this protein to IIR signalling within the NE.

3.2. NETs screen to identify proteins involved in chromatin compaction

In order to identify NE proteins that might be involved in chromatin compaction, a screen of multiple proteins previously identified in a NE proteomic analysis was performed in my supervisor´s lab to analyse the ability of these proteins to induce chromatin compaction when exogenously expressed. This study identified NET23/STING as a strong promoter for chromatin compaction.

Different NETs identified in proteomic studies in our lab were cloned as mRFP and/or HA tag fusions and transfected into stable Hela cells expressing H2B-GFP. Results showed little compacted chromatin in untransfected cells, as well as in most of the cells in which different NETs were transfected. However, expression of NET23/STING after 72 h post-transfection seemed to induce a high compaction of H2B-GFP labelled chromatin in NET23/STING transfected cells (*Figure 14*). The increase of density observed in this experiment suggested that overexpression of NET23/STING might be affecting chromatin compaction.

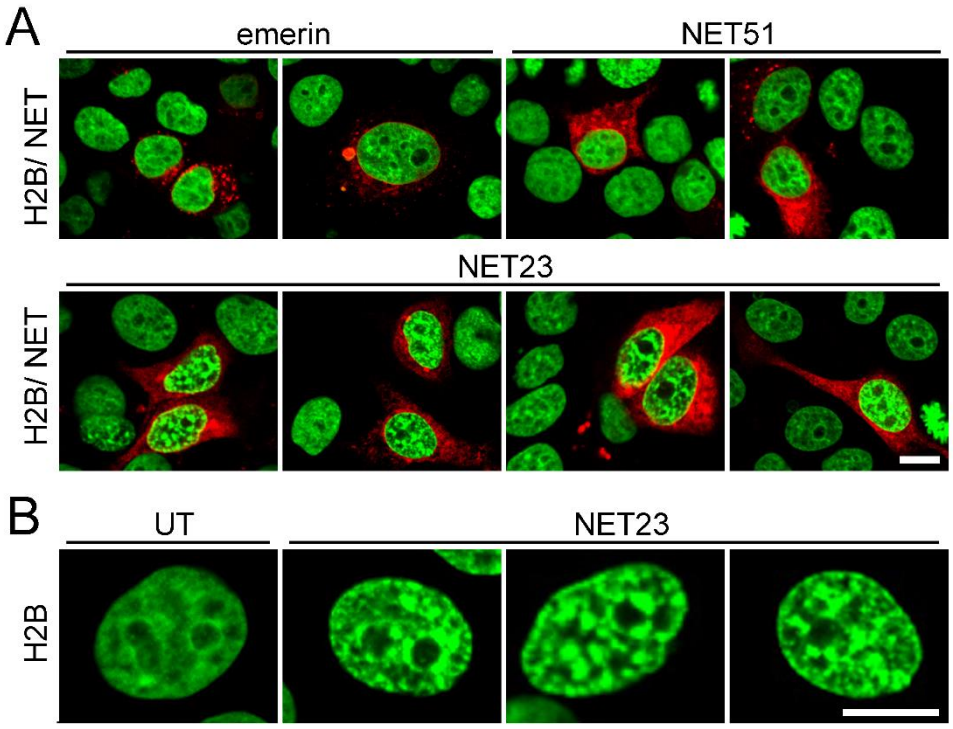

Figure 14. NETs screening for alterations in chromatin compaction. (A) *72 h post-transfection Hela cells stably expressing H2B-GFP did not show changes in the distribution of H2B (green) when emerin-RFP or NET51-mRFP are transiently expressed (upper panel). However, cells overexpressing NET23/STING-mRFP (lower panel) exhibited a dramatic alteration in chromatin compaction****. (B)*** *Zoom images of chromatin in untransfected cells and cells overexpressing NET23. Scale bars 10 µm. Taken from Malik et al. 2014. Experiment performed by Nikolaj Zuleger and Vassiliki Lazou.*

Moreover, Nikolaj Zuleger observed an increased in the chromatin compaction levels in the DAPI staining of multiple cells overexpressing NET23/STING tagged with mRFP, but lacking the expression of H2B tagged with GFP. This experiment supported that the chromatin compaction phenotype observed in cells transfected with NET23/STING was not due to a potential artificial interaction with the GFP labelled H2B molecules. In this case, the compaction was visualized using DAPI to stain the DNA. These results indicated that the observed chromatin compaction indeed was produced by the expression of NET23/STING (Figure 15A).

Moreover, he confirmed that the NET23/STING chromatin compaction phenotype was not cell-type dependent as it could be observed in multiple cell lines (Figure 15B). Interestingly, it is known that some of the cell lines tested in this experiment presented different visual levels of chromatin compaction. For instance, lymphocytes and mouse cells presented a higher level of chromatin compaction than the rest of the cell lines tested. Furthermore, NET23/STING is known to be highly expressed in these two cell lines. This observation raised the question whether there was a link between endogenous expression levels of NET23/STING and alterations in the state of chromatin compaction.

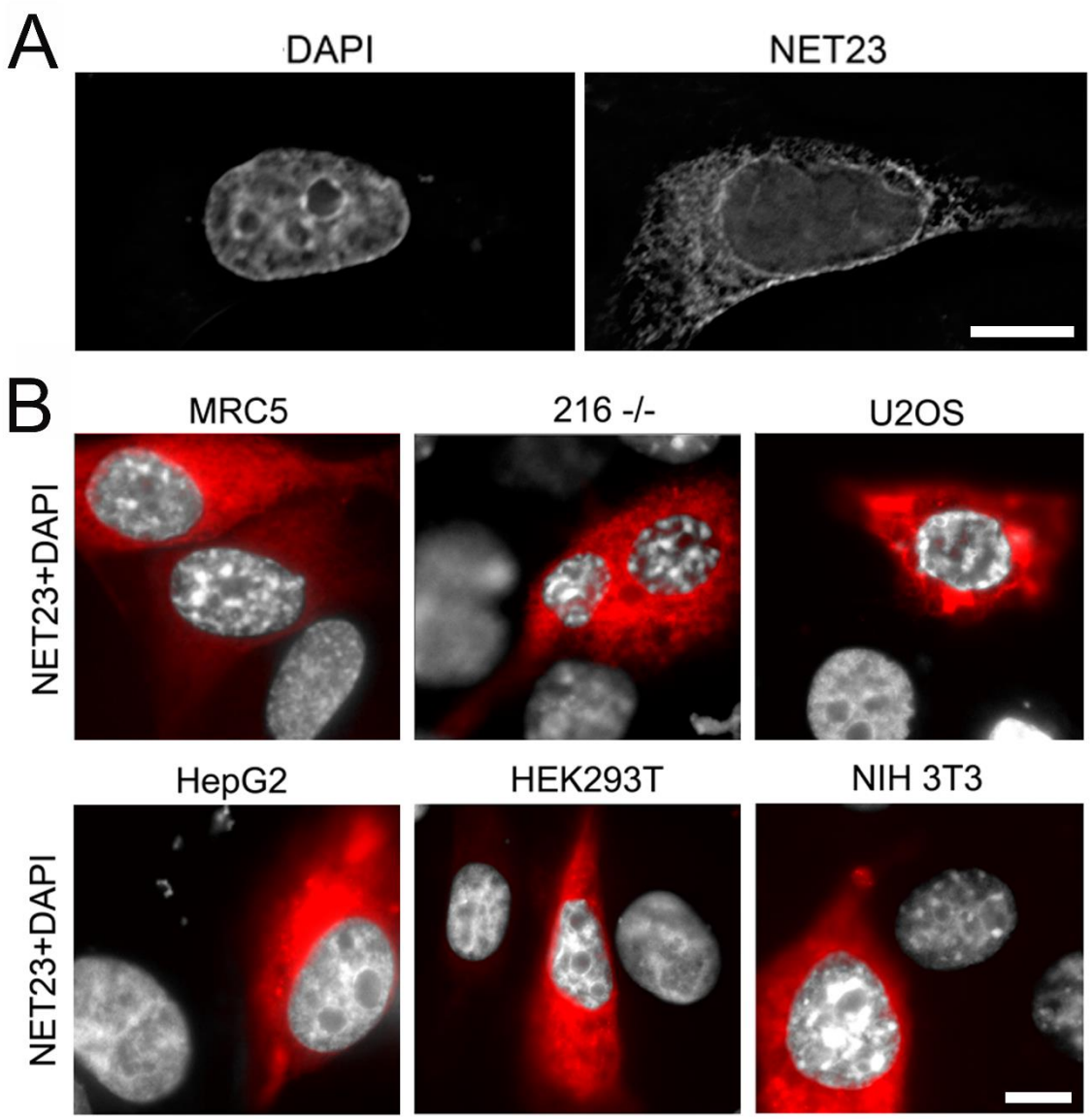

Figure 15. The NET23/STING chromatin compaction effect is independent of H2B-GFP construct or the epitope tag used and occurs in different cell types. ***(A)*** *Chromatin compaction was observed at the nuclear periphery of cells transfected with NET23/STING-mRFP but without the H2B-GFP transfected. The compaction was visualized using DAPI to stain the DNA.* ***(B)*** *Chromatin compaction was not cell dependent as it was observed in multiple cell lines not expressing H2B-GFP. MRC5 primary human lung fibroblasts, 216 -/- lamin A knockout mouse embryonic fibroblasts, U2OS human osteocarcinoma cells, HepG2 human liver cancer cells, HEK/293T human embryonic kidney cells, and NIH3T3 mouse fibroblasts. NIH3T3 showed higher levels of chromatin compaction. NET23/STING was shown in red and the DAPI staining for DNA in grey. Scale bars, 10 µm. Taken from Malik et al. 2014. Experiment performed by Nikolaj Zuleger.*

3.3. NET23 expression correlates with levels of chromatin compaction in different cell types

To be able to objectively measure the level of chromatin compaction observed in different cell lines, an algorithm was developed by Dr de las Heras to quantify this phenotype.

HT1080 cells were used to set up this experiment as they present lower basal level of epigenetic silencing marks and chromatin compaction (Ohzeki, Bergmann et al. 2012). DAPI was used to visualize nuclear DNA and imaging was done using an identical microscope and camera settings. High-density clusters were observed and multiple parameters such as number of clusters and size were calculated for these clusters (Figure 16, A).

Generally, the presence of a higher number of clusters in the nuclei of certain cells indicates a more heterogeneous nucleus due to the presence of chromatin clusters distributed within it. On the other hand, the observation of less number of clusters represents a more uniform and homogenous nucleus. Larger number of smaller individual clusters of dense chromatin could be observed in the nuclei of NET23/STING transfected cells based on the intensity of the DAPI signal compared with untransfected cells (Figure 16, B).

The algorithm used three basic parameters to detect chromatin compaction clusters. The main parameter was a *signal threshold* based on the DAPI staining to select pixels above a certain level with respect to the normalised DAPI pixel signal intensity. M*inimum cluster size parameter was used* to avoid the selection of spurious isolated specks and a *merge parameter* to control how close two separate clusters are before they are merged into one.

Multiple thresholds assigned to these parameters were tested to confirm that the algorithm was able to distinguish between the two conditions; NET23/STING overexpression and untransfected cells (Figure 16, C). Some of the tested thresholds included values between 5 to 20% of the normalised pixel DAPI signals (pixel intensities were normalized to the sum of total number of pixel intensities in

each nucleus), and a huge range of merge and minimum cluster size parameters (Figure 16, C).

Across the entire range of tested values, strong differences and confidence p-values could be observed for 15% DAPI signal intensity, 20-pixel minimum cluster size and 3 connecting pixels required for merging. Thus, to localize higher intensity peaks corresponding to denser chromatin regions, the 15% DAPI signal intensity of the normalised pixel signal was assigned as the lower threshold. Pixel peaks smaller than 20 pixels were discarded and those peaks that were closer than 3 pixels were merged together and quantified as one single peak rather than as single peaks.

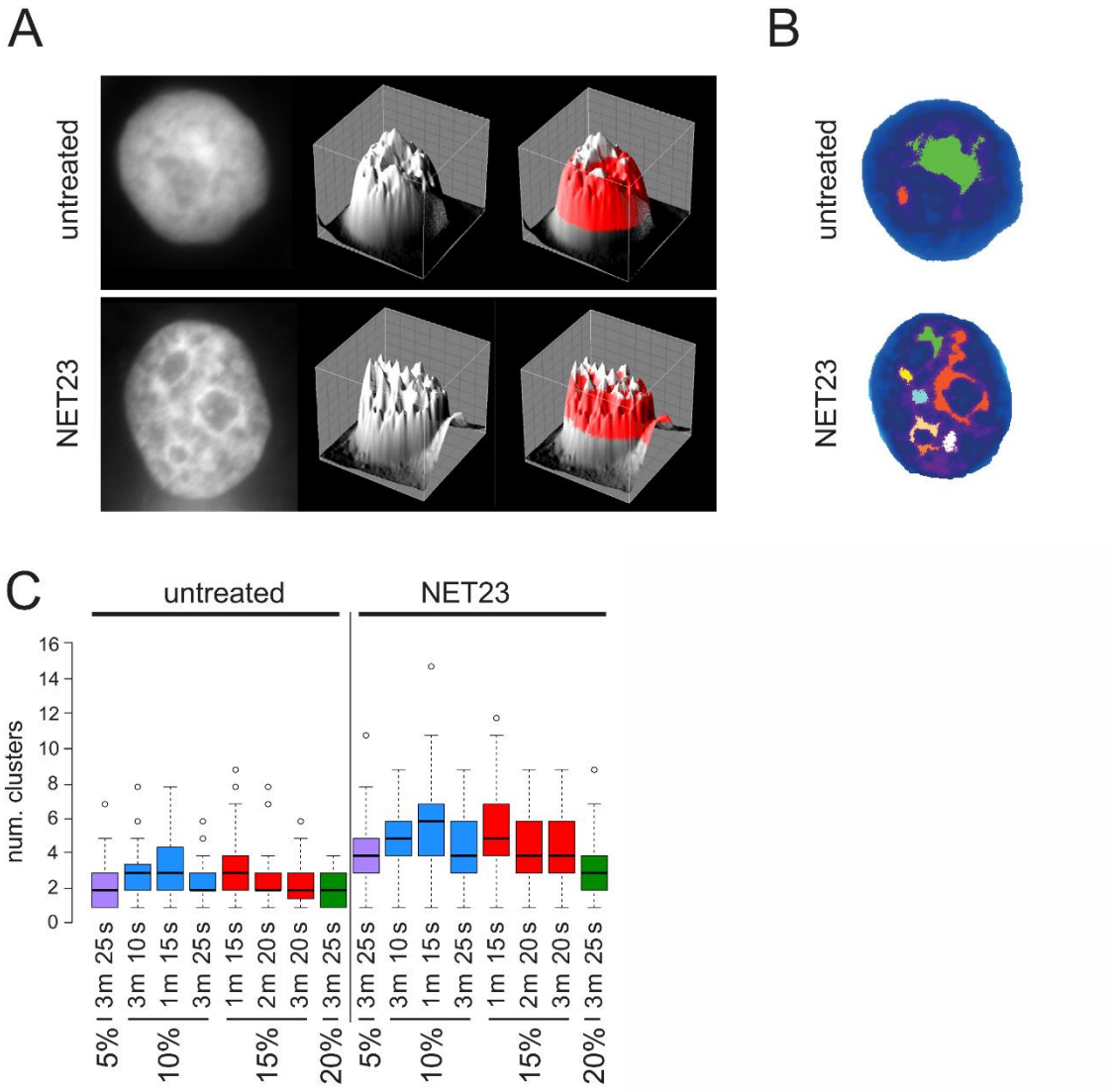

Figure 16. Different parameters tested to validate the algorithm used for measuring chromatin compaction*. **(A)** Topographic representation of pixel intensities from DAPI images from NET23/STING transfected and untransfected cells obtained using identical microscope and camera settings. The presence of high intensity pixel clusters can be observed in NET23/STING transfected cells compared with only a small number of high intensity pixel clusters detected in untransfected cells. **(B)** Colour representation of each high intensity pixel cluster for a particular plane in the cells shown in A. This indicates how accurately the algorithm distinguishes individual cluster in different planes. (C) Multiple thresholds assigned to different parameters to distinguish between untransfected and NET23/STING transfected cells. Pixel intensity cutoffs were tested from 5% to 20% total DAPI pixel intensity of the normalised pixel signal. Additionally, the number of pixels connecting clusters before merging them (m) and the minimum cluster size in pixels (s) were varied. This experiment confirmed that the algorithm is robust as significant differences for mostly all parameters tested were observed between untransfected and NET23/STING. Taken from Malik et al. 2014. (A, B and C were performed by Dr. de las Heras)*

To further test that the method was able to distinguish the chromatin clusters observed by microscopy, NET23/STING was overexpressed in HT1080 cells, and among other parameters, the distribution of the number of chromatin clusters in DAPI images was analysed and compared with images from control cells (Figure 17, A). The differences in the number of chromatin clusters between the two conditions could be clearly observed (Figure 17, B). Size of these chromatin clusters also showed a significance difference between control and cells overexpressing NET23/STING (Figure 17, C). In summary, cells overexpressing NET23/STING presented a higher number of clusters with smaller size compared with smaller numbers of clusters with a bigger individual area observed in control cells.

The chromatin compaction induced by NET23/STING could be due to a decrease in the nuclear area of the cells that were analysed. Thus, to be sure that the observed differences in chromatin compaction were produced by the presence of NET23/STING and they were not an artefact, the nuclear size was calculated showing no differences between the NET23/STING-transfected and control cells.

Indeed, no differences in nuclear area were observed between cells overexpressing NET23/STING and control cells (Figure 17, D).

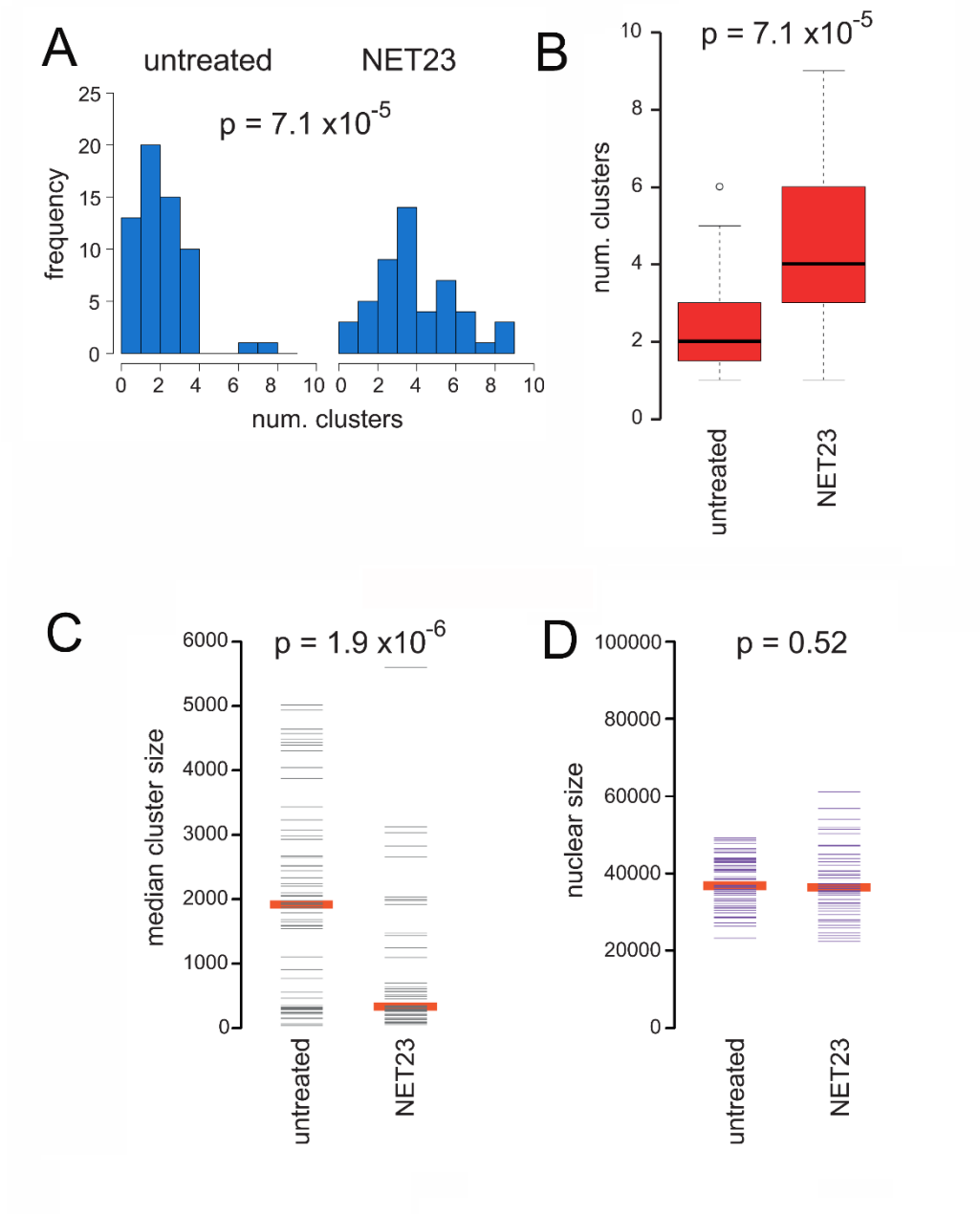

Figure 17. Characterization of the algorithm for measuring chromatin compaction. ***(A)*** *Histogram representation showing the distribution of the number of clusters in untransfected and NET23/STING transfected cells following the final parameters chosen as referred above* ***(B)*** *Box plots showing the number of clusters presented in DAPI images from cells exogenously expressing NET23/STING and control cells. The distributions were compared using a Kolmogorov-Smirnov (KS) test.* ***(C)*** *Box plot showing the distribution of data representing cluster size. Red bars represent the median of the distribution. The median cluster size of cells expressing NET23/STING is significantly smaller compared with control cells indicating a higher degree of chromatin compaction.* ***(D)*** *Nuclear size was also quantified for the cells analysed showing no changes between control and NET23/STING transfected cells. More than 100 cells were analysed per condition. Taken from Malik et al. 2014. (All measurements performed by myself).*

To test the hypothesis that chromatin compaction differences observed in multiple cell types were due to the endogenous NET23/STING function, and to further test that the chromatin compaction phenotype reflects the function of the endogenous NET23/STING rather than being an overexpression artefact, I measured the protein levels of NET23/STING and the degree of chromatin compaction based on the DAPI staining in a variety of cell lines.

NET23/STING endogenous levels were quantified by Western blot in five different immortalised cancer cell lines: HT1080, fibrosarcoma cells; Jurkat, human immortalized T-lymphocytes; EL4, mouse lymphoma cells; LNCaP, human prostate adenocarcinoma cells; and HEK293, human embryonic kidney cells. The levels of NET23/STING were normalised against alpha-tubulin levels (Figure 18, A). Results indicate that there is a clear correlation between endogenous levels of NET23/STING and number of clusters measured in each cell type using the cluster algorithm as a readout for chromatin compaction. Jurkat cells as well as EL4 cells presented high NET23/STING endogenous levels (22,000 and 14,000 arbitrary protein units respectively) correlating with a high number of clusters measured (5 and 4 respectively) (Figure 18, B, C).

Significant p-values showed the correlation between the higher level of chromatin condensation and the increase of NET23/STING endogenous levels (Figure 18, D).

Also, the nuclear size measurement of each cell line indicated similar values between all of them, arguing that the differences observed in chromatin compaction are not being affected by changes in the size of the nucleus (Figure 18, E).

Therefore, these results, together with the previous data, indicated that higher levels of chromatin condensation are linked with high endogenous expression levels of NET23/STING.

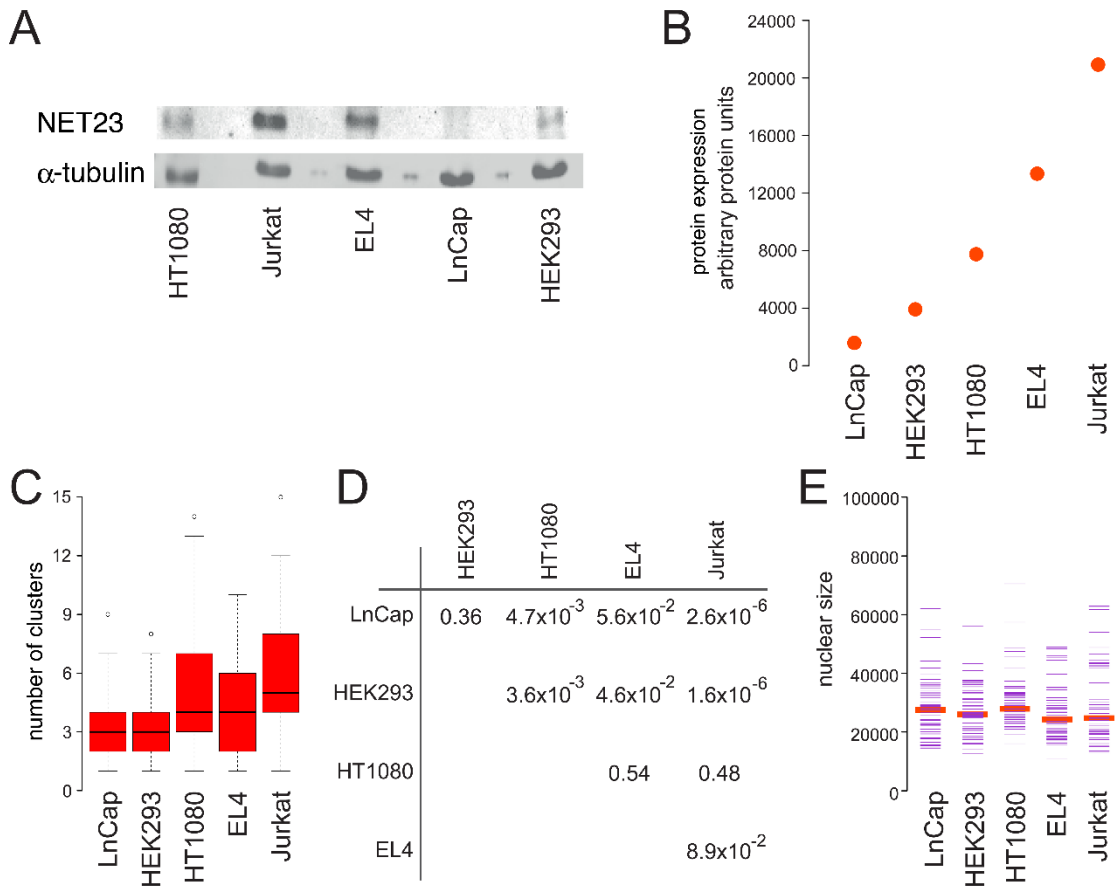

Figure 18. NET23/STING endogenous levels correlates with the degree of chromatin compaction in different observed cell lines. (A) *Western blot comparing endogenous expression levels of NET23/STING in five different cell lines using α-tubulin as a loading control. Jurkat cells presented the highest levels of endogenous NET23/STING expression.* ***(B)*** *NET23/STING quantification from 3 independent blots. Protein expression values are*

represented as arbitrary protein units and are normalised for α-tubulin. ***(C)*** *Using the algorithm described above, the number of clusters was measured in these five cell lines. Values are represented in box plots and the black bar represents the median of the number of clusters of each cell line. Results reveal a general trend that cells presenting a higher number of clusters have higher endogenous expression levels of NET23/STING.* ***(D)*** *Table showing the p-values (calculated using KS test) for all possible combinations from data represented in panel C.* ***(E)*** *Nuclear size measurements of each cell line showing no significant differences. P-values were calculated using the KS test and all of them were > 0.05 with the exception of HT1080 and EL-4 (p=0.039) and HT1080 and Jurkat cells (p=0.003). Taken from Malik et al. 2014. (All measurements performed by myself).*

To determine if the relationship between NET23/STING expression levels and chromatin compaction also pertains to primary cells (all cells tested in Figure 18 above were immortalised cancer lines), I analysed several primary human cells. Similarly, the amount of endogenous NET23/STING levels was quantified by Western blot in three primary cell lines presenting similar nuclear size; MRC5 lung fibroblasts, BJ foreskin fibroblasts, and AG dermal fibroblasts and the number of clusters representing chromatin compaction was measured (Figure 19).

This data showed a rough correlation between the degree of chromatin compaction measured using the cluster algorithm on DAPI-stained chromatin, and the endogenous levels of NET23/STING expressed in these three primary cell lines. MRC5 lung fibroblasts presented the smallest NET23/STING expression levels compared with AG and BJ cell lines, correlating with the smallest number of clusters among the three cell lines. Thus, NET23/STING appears to be playing a role in the regulation of endogenous levels of chromatin compaction.

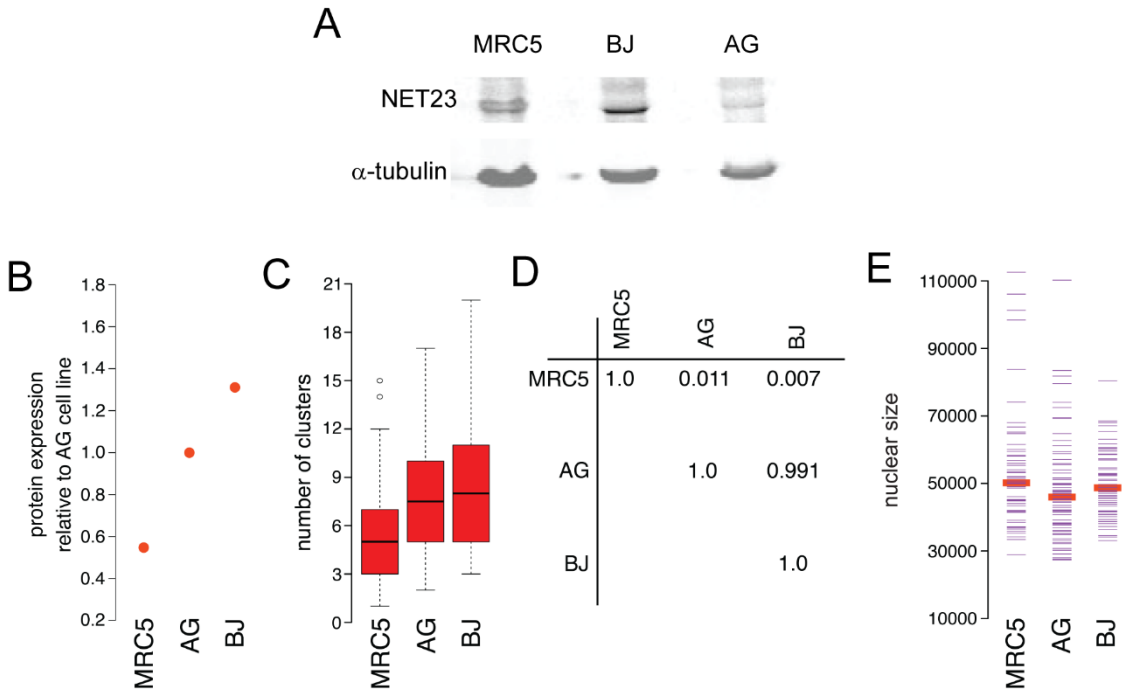

Figure 19. Endogenous NET23/STING expression correlates with chromatin compaction levels in three primary cell lines confirming the relationship between NET23/STING levels and the degree of chromatin compaction. (A) *Western blot showing endogenous NET23/STING expression in three primary cell lines with α-tubulin as a loading control. BJ cells reveal the highest levels of NET23/STING protein expression* ***(B)*** *NET23/STING quantification from three independent blots.* ***(C)*** *Number of clusters from MRC5, AG and BJ cells quantified with the algorithm. A clear correlation between NET23 expression and the number of chromatin clusters was observed.* ***(D)*** *P-values for comparing cluster number between the different primary cell lines. P-values were calculated with the KS test.* ***(E)*** *Nuclear size was quantified to exclude that this parameter could be affecting the quantification of chromatin compaction. Results show no notable difference in nuclear size among the three analysed primary cell lines. Taken from Malik et al. 2014. (All measurements performed by myself).*

To test that the readout of the algorithm reflects the classically defined denser chromatin observed in some cell types by EM studies, EM was performed on wild type HT1080 cells and cells expressing NET23/STING to visualize chromatin compaction levels. To regulate the expression levels of NET23/STING and avoid the induction of apoptosis produced by transient transfection of NET23/STING in cells analysed by EM, I made an inducible stable cell line expressing NET23/STING-GFP upon the addition of doxycycline.

EM analyses enabled visualization of the degree of chromatin compaction as denser stained areas of the nucleus using osmium tetroxide. This analysis revealed that wild type HT1080 and uninduced NET23/STING stable cells (no doxycycline) presented similar levels of chromatin compaction observed by density staining in the nucleus. However, HT1080 cells in which NET23/STING was stably induced upon the addition of doxycycline presented a higher denser stained areas of chromatin in the nuclear periphery and also in the nuclear interior (Figure 20). This data further supports a potential role for NET23/STING in inducing chromatin compaction.

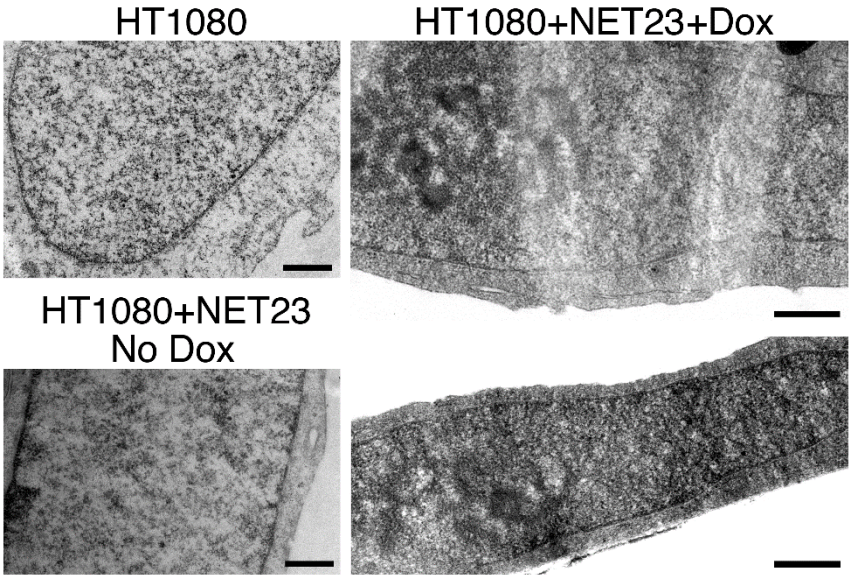

Figure 20. Electron microscopy reveals an increase in chromatin compaction in NET23/STING overexpressing cells as measured by electron densities. *The panel on the right shows EM images from HT1080 cells stably expressing NET23/STING upon the addition of doxycycline. They presented higher electron density staining areas in the nucleus using osmium tetroxide, suggesting higher degree of chromatin compaction. Panels on the left are the HT1080 parent cell line and the uninduced HT1080 stable cell line carrying the NET23/STING-GFP construct showing less electron dense staining in the nucleus. Scale bar 0.5 µm. Taken from Malik et al. 2014. (Experiment performed by myself with assistance from Alexander Makarov).*

3.5. NET23/STING alters levels of H3K9Me3 epigenetic mark

Giving the involvement of NET23/STING in IIR and that immune signalling cascades are often accompanied by epigenetic modifications, the observed chromatin compaction induced by NET23/STING might be mediated by epigenetic silencing mechanisms.

It is known that epigenetic marks such as histone acetylation and methylation regulate the expression of genes involved in inflammation and other innate immunity processes (De Santa, Totaro et al. 2007, De Santa, Narang et al. 2009). Multiple inflammatory genes suffer epigenetic modifications including DNA methylation and covalent histone modifications in order to regulate their expression. For example, Toll-like receptors (TLRs), that are key factors involved in the activation of the innate immunity via the recognition of pathogen-associated molecular patterns (PAMPs), activates signalling cascades leading to the modification of histones to regulate genes involved in innate immunity as NF-KB or IRF (Stender and Glass 2013).

To test if NET23/STING could promote chromatin compaction by the modification of epigenetic marks, Dr Malik tested if there was a correlation between the histone mark H3K9me3 and the expression of NET23/STING by immunofluorescence. HT1080 cells were transfected with NET23/STING-mRFP plasmid and stained with specific antibodies to epigenetic marks at 21 and 85 h post-transfection. Antibodies were against H3K18ac, a standard histone mark for activation of gene expression,

and H3K9me3, a classical histone mark for repressing and silencing gene expression. At 21 h post-transfection no change in the H3K18ac mark was observed while there was a small increase in H3K9me3 (Figure 21, A, B).

At 85 h post-transfection a strong decrease in acetylation at K18 along with another mark of active chromatin H3K4me2 was observed (Figure 21, C). The epigenetic mark H3K9me3 and S10 phosphorylation associated with polycomb repressed genes was also tested. This epigenetic mark is quite interesting as it adds a higher level of repression at polycomb marked genes. Polycomb proteins are involved in gene silencing through the regulation of histone methylation profiles of multiple genes involved in various cellular pathways (Sabbattini, Sjoberg et al. 2014). Cells expressing NET23/STING showed a reduction of this epigenetic mark indicating a loss of repression at polycomb marked genes (Figure 21, C).

Thus, the expression of NET23/STING is associated with changes in epigenetic marks, specifically a general increase in H3K9me3 mark linked with silencing genes and a decrease in the active histone marks H3K18Ac and H3K4me3 associated with gene activation. Interestingly, some genes are being loosened from particularly strong repression (polycomb marked genes).

This experiment was performed in transiently transfected cells in which the transfection of foreign DNA could induce IIR and complicate distinguishing a real effect produced by NET23/STING-induced chromatin compaction from downstream effects of the IIR signalling.

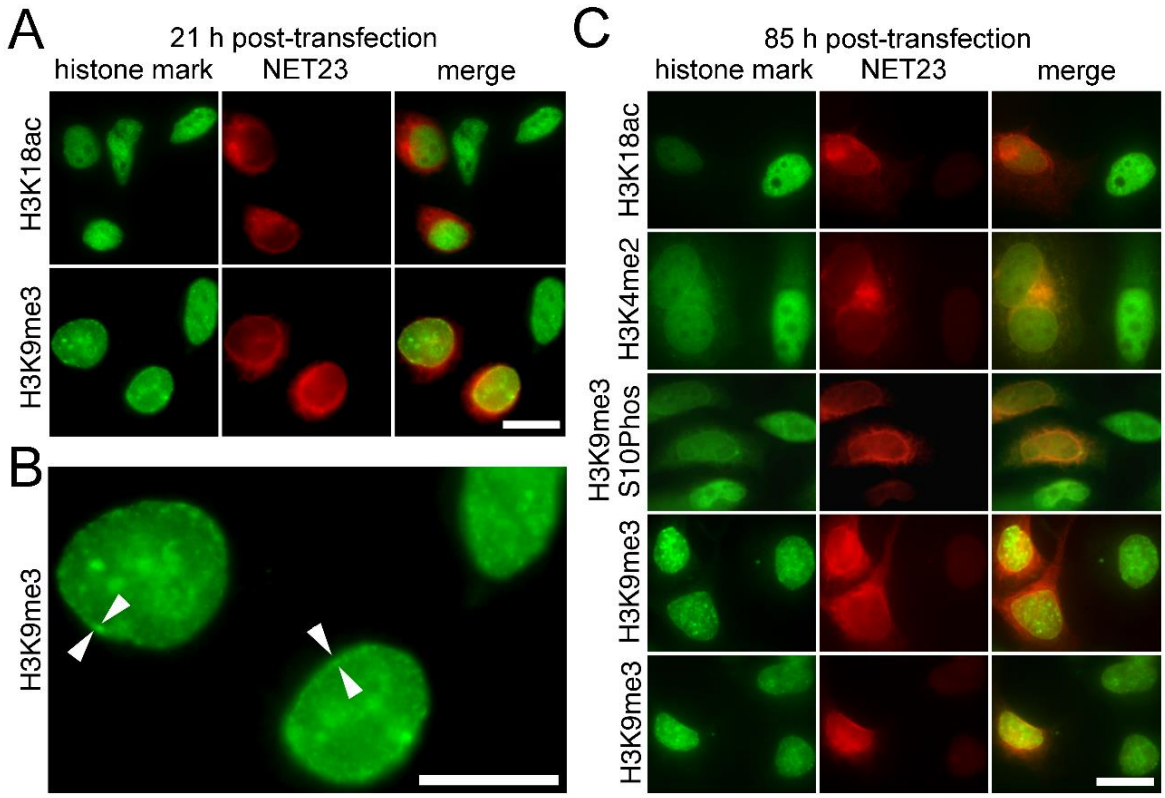

Figure 21. Epigenetic marks are associated with compacted chromatin induced by NET23/STING. *Cells were transfected with NET23/STING-mRFP and stained for epigenetic marks H3K9me3, H3K9m2, and H3K18ac* ***(A)*** *H3K9me3 was slightly increased after 21 h post-transfection however no change was observed in the H3K18ac mark.* ***(B)*** *Chromatin compaction induced by NET23/STING at this early timepoint is observed in the nuclear periphery correlating with an increase in HSK9me3 (white arrows). Higher magnification image from panel A.* ***(C)*** *At 85 h post-transfection a decrease of H3K18ac and H3K4me2 was observed indicating a general loss of active marks. At the same time, a strong increase in H3K9me3 was observed consistent with an increase in silencing marks. However, the stronger repression mark H3K9me3 combined with S10ph was reduced in cells transfected with NET23/STING. Scale bars 10 µm. Taken from Malik et al,2014. Experiment performed by Dr Malik.*

To determine if the increase in H3K9me3 silencing mark observed by immunofluorescence reflects absolute levels of this mark or is limited by epitope accessibility issues in the fixed cells, I performed a Western blot analysis in control cells and cells overexpressing NET23/STING tagged with GFP under the addition to quantify the protein expression levels in H3K9me3. To avoid the potential problems of IIR activation that could be generated by the transient transfection of a DNA plasmid due to a cell response to foreign DNA, I performed this experiment using the previously mentioned stable doxycycline-inducible cell line expressing NET23/STING fused with GFP that I generated. H3K9me3 levels were quantified by Western blot in lysates from this stable cell line and also, from the parent cell line with a NET23/STING knockdown and a control siRNA. Interestingly, protein levels of H3K9me3 were 4-fold increased in the stable cell lines overexpressing NET23/STING and slightly reduced in the siRNA NET23/STING parental line compared with the siRNA control (Figure 22). Thus, this indicates there is a general increase in the H3K9me3 repression mark associated with NET23/STING expression confirming the microscopy results described above.

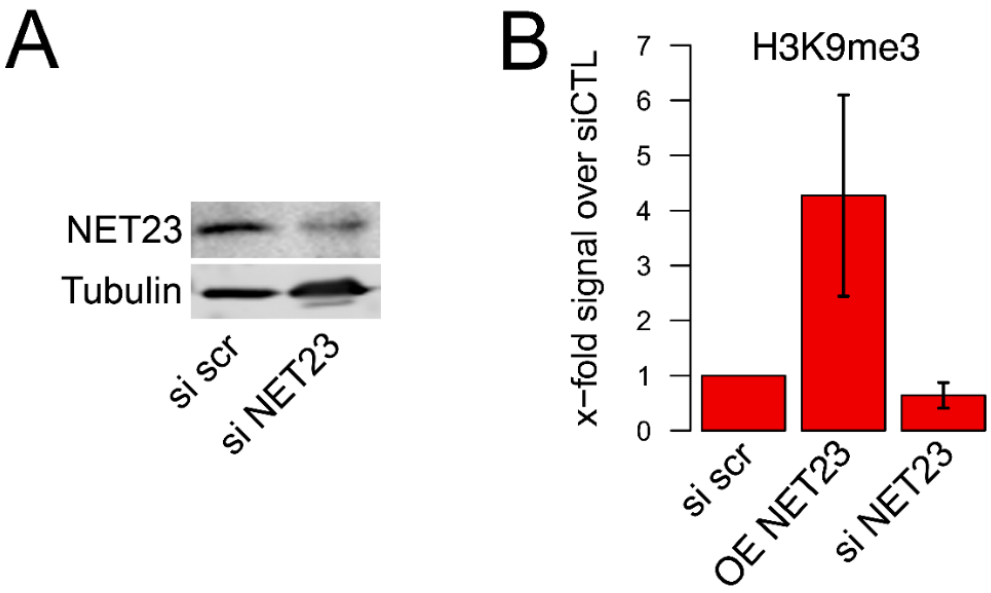

Figure 22. Levels of H3K9Me3 epigenetic mark correlates with NET23/STING protein expression. (A) *HT1080 cells were transfected with either siRNA oligos for siRNA control or for NET23/STING for 3 days. Lysate cells were analysed by Western blot showing a 30% reduction of NET23 levels compared with initial levels. Values were normalized against α-tubulin.* ***(B)*** *Cell lysates from HT1080 cells either treated with siRNA control or NET23/STING or the stably NET23/STING HT1080 cell line were analysed by western blot for H3K9me3 histone mark. Box plot representing H3K9me3 quantification from three independent blots with standard deviation. Staining and quantification revealed that H3K9me3 levels were increased by 4-fold in cells overexpressing NET23/STING upon the addition of doxycycline. However, H3K9me3 levels were slightly reduced when NET23/STING was depleted in HT1080 cells compared with siRNA control cells. Taken from Malik et al,.2014 Experiment performed by myself.*

3.6. Chromatin compaction is affected by NET23/STING depletion in HSV-1 infected cells

As previously mentioned, different studies have identified NET23/STING as a critical signalling molecule in the innate response to many bacterial, viral and eukaryotic pathogens (Ishikawa and Barber 2008, Ishikawa, Ma et al. 2009, Chen, Sun et al. 2011).

Cells infected with HSV-1 undergo a variety of changes in nuclear architecture (Bosse, Hogue et al. 2015). Herpesviruses, as well as many other DNA viruses, disturb the spatial organization of the host cell chromatin due to the formation of viral DNA replication compartments (VRC), which are the sites of replication, transcription and encapsidation of HSV-1 genomes (Placek and Berger 2010, Conn and Schang 2013). Nuclei of infected cells start to be expanded at early times post-infection during viral replication and host chromatin is marginalized to a thin intact layer at the nuclear boundary due to the expansion of the VRC. Drastic modification of the nucleolar morphology is also observed within the nucleus of infected cells. HSV-1 leads to a nucleoli increase in size that soon after infection localize close to

the NE and finally becomes fragmented into small pieces (Calle, Ugrinova et al. 2008, Sagou, Uema et al. 2010).

The host chromatin regulation of herpesvirus is a key regulatory step involving the suppression and the activation of different types of viral genes to ensure a successful viral infection. Immediately after infection, the genome of host cells exhibits an increase of repressive histone marks (H3K9me3) and a compacted heterochromatin as a rapid antiviral defence strategy (Conn and Schang 2013). The assembly of heterochromatin in a high compacted state limits the viral genome access for transcription and DNA viral replication and it appears as a cellular defence to infection. The increase of repressive histone signatures observed in the genome of host infected cells at early times post-infection initially suppresses the expression of the viral immediate early genes and the progression of the infection (Arbuckle and Kristie 2014).

To test whether the chromatin compaction associated with the initial stages of viral infection depends on the function of NET23/STING, I depleted this protein in HSV-1 infected cells to check if chromatin compaction fails to occur upon viral infection. To do so, HT1080 cells were treated with either siNET23/STING or scramble siRNA prior to HSV-1 infection. As previously reported, chromatin compaction was expected to increase at early times post-infection as a mechanism to avoid the access of binding factors and coactivators that ultimately activate viral gene expression. Unexpectedly, the levels of chromatin compaction in scramble siRNA infected cells were showing a reduction rather than an increase in the number of clusters measured by the cluster algorithm (Figure 23A). However, there was a clear difference in the amount of chromatin compaction observed in NET23/STING knockdown cells infected with HSV-1 for 2 hours. These cells showed the same level of chromatin compaction as non-infected cells (scramble and siNET23). This result suggested that the depletion of NET23/STING prevented the increase of the compaction state of chromatin that generally occurs at early stages upon HSV-1 infection (Figure 23, A).

It is important to mention, that the output of the algorithm might be affected by the differences observed in the nuclear size of infected and uninfected cells. As it is known that HSV-1 infection alters nuclear size, this parameter was analysed in the

same population of cells. Results showed a slightly difference in the nuclear size of infected and uninfected cells (Figure 23, B). Although the observed change in nuclear size might alter the final output of the algorithm, there is a clear effect in HSV-1 infected cells no longer expressing NET23/STING, in which levels of chromatin compaction that normally occur upon infection are mitigated.

Taken together these results and the alteration in the nuclear size observed between infected and non-infected cells, I can not unequivocally state that the changes in chromatin compaction observed in infected cells no longer expressing NET23/STING are an effect directly produced by NET23/STING. It also remains unclear why the number of clusters (used as a measure of chromatin compaction) were reduced in HSV-1 infected scramble siRNA control HT1080 cells.

Observation of chromatin by EM in wild type HSV-1 infected cells will allow us to determine whether chromatin compaction is increased in these cells compared with infected cells no longer expressing NET23/STING. Although the effect of the virus appeared to be mitigated by NET23/STING knockdown, future experiments will need to support this observation. For instance, reduced viral titers in cells no longer expressing NET23/STING might confirm this hypothesis.

It is important to point out that as I previously showed, the parental cell line HT1080 presented low NET23/STING expression levels compared with other cell lines. Therefore, it is not surprising that the levels of chromatin compaction upon NET23/STING silencing in non-infected HT1080 cells were not showing large differences compared with the siRNA control cells (Figure 23A).

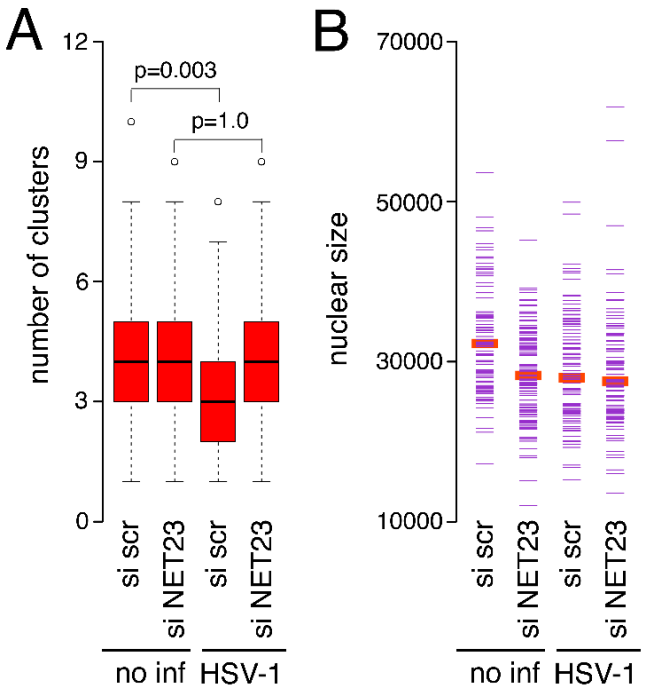

Figure 23. Effect of NET23/STING on chromatin compaction in HSV1 infected cells. ***(A)*** *HT1080 cells were transfected with either siRNA for control or NET23/STING during 3 days. After this cells were infected with HSV-1 during 2h with a MOI 5 to induce the IIR. Cells were fixed and stained with DAPI to quantify chromatin compaction using the cluster algorithm previously described. P-values were calculated using the KS-test to compare the HSV-1 infected cells between the different NET23/sting conditions* ***(B)*** *Nuclear size was analysed in the same population of cells indicating a notable difference when cells were infected with HSV-1. More than 100 cells were analysed per condition. Taken from Malik et al,.2014 Experiment performed by myself*

3.7. NET23/STING drives nucleo-cytoplasmatic shuttling of Syncrip and MEN1, potential innate immunity regulators

We have shown that NET23/STING is a nuclear protein capable of mediating chromatin distribution patterns associated with histone mark changes. Although this protein was first discovered in a proteomic study for nuclear proteins by Dr Schirmer in his post-doctoral work at Gerace's lab (Schirmer, Florens et al. 2003), different studies have shown the importance of NET23/STING in intracellular DNA-mediated and HSV-1-activated type I IFN production (Ishikawa and Barber 2011, Burdette and Vance 2013, Shu and Wang 2014). Additional studies have reported a role of NET23/STING in response to RNA, but its function is much less clear (Chen, Sun et al. 2011). All previous studies have ignored a potential additional or related NE role for NET23/STING in mediating the activation of IIR.

As mentioned in chapter 1, the lab found a striking number of indirect relationships between NET23/STING-NE binding partners and the transcription factors IRF3/7. 17 of these partners identified by co-IP interacted with six known IRF3/7 binding partners, some of which were RNA-binding partners among others, suggesting a highly redundant network by which NET23/STING could influence IIR signalling pathways. Additionally, NET23/STING was observed to be present in the INM in some cells and restricted to the INM in others, suggesting the potential redistribution of this protein into different nuclear locations under certain cell-specific conditions *(refer to chapter 1, 1.4 for further details).*

We postulated that these NET23/STING-NE binding partners might be novel IIR mediators because of their indirect relationship with IRF3/7 transcription factors and as NET23/STING is found in both the ONM and INM, it might be able to carry these binding partners between the two compartments for a function in activating IRF3/7 leading to type I-IFN production.

Syncrip and MEN1 were two of the 17 NET23/STING NE-binding partners identified that have been reported to interact with six IRF3/7 binding partners we propose to effect IIR activation.

Syncrip (synaptotagmin-binding, cytoplasmic RNA-interacting protein) is a member of the cellular heterogeneous nuclear ribonucleoprotein (hnRNP) family, known for their ability to interact with cellular proteins and RNAs facilitating many biological processes such as mRNA processing mechanisms (Mizutani, Fukuda et al. 2000, Bannai, Fukatsu et al. 2004). Interestingly, in addition to cellular functions, Syncrip was shown to be involved in viral RNA synthesis (Choi, Mizutani et al. 2004). Different studies have observed an interaction between Syncrip and RNA from different viruses. Syncrip binds to Hepatitis C Virus (HCV) RNA (Liu, Aizaki et al. 2009, Wang, Jeng et al. 2011) and to the Transmissible Gastroenteritis Coronavirus (TGEV) RNA, affecting the RNA replication of these viruses (Sola, Galan et al. 2011). Additionally, Syncrip has been associated with the GO term for "cellular response to type II IFN", linking this protein with downstream cascade signals. Despite the role of Syncrip in viral replication processes and its downstream activity, nobody has shown a specific mechanism of this protein within the activation of the IIR.

On the other hand, MEN1 (Multiple endocrine neoplasia type 1) is a tumour suppressor gene that encodes a protein called menin. This protein contains two nuclear localization signals and localizes predominantly to the nucleus (Gracanin, Dreijerink et al. 2009) (Sato, Matsubara et al. 1998). Previous studies observed a direct interaction between MEN1 and JunD, an AP-1 transcription factor involved in the regulation of a range of cellular processes including cell proliferation, death and differentiation (Agarwal, Guru et al. 1999, Ikeo, Yumita et al. 2004). This interaction results in the inhibiting of JunD´s activation of transcription. Also, MEN1 was shown to interact with NF-κB and repress NF-κB mediated transactivation (Heppner, Bilimoria et al. 2001).

To test if there was a NET23/STING-dependent redistribution of some of the identified NET23/STING-NE binding partners upon the induction of the IIR, and to test the potential involvement of NET23/STING in carrying IIR proteins between the nucleus and the cytoplasm, I analysed the redistribution pattern of Syncrip and MEN1 in cells treated with a control siRNA or NET23/STING siRNA.

Silencing of NET23/STING was confirmed by Western blot analysis of protein lysates from HT1080 cells treated with siRNA against NET23/STING for three days.

NET23/STING levels were clearly reduced in siNET23/STING treated cells compared with control cells (Figure 24, A).

HT1080 cells treated with NET23/STING siRNA or control siRNA were transfected with either plasmid DNA or poly I:C (synthetic RNA analogue to dsRNA) or infected with HSV-1 in order to induce the IIR.

Once STING is activated by an external stimuli, TBK1 is recruited producing the phosphorylation of IRF3 that results in its translocation into the nucleus for type I IFN production. IRF3 is a protein that has an active nuclear localization signal (NLS) which is recognized by importin-α receptors and transported to the nucleus through the NPC central channel (Kumar, McBride et al. 2000, Zhu, Fang et al. 2015).

On the other hand, poly I:C, a mimetic form of dsRNA is recognized by RIG-I or MDA5, specific sensor for RNA. This recognition allows MAVS aggregation in the mitochondria leading to the phosphorylation of IRF3 by the activation of TBK1 (Burdette and Vance 2013). Thus, IRF3 staining was used as a control to confirm that IIR was activated. As expected, accumulation of IRF3 was observed in the nucleus of control siRNA cells treated with poly I:C or plasmid DNA confirming the activation of the IIR. (Figure 24, B left panels). Same effect was observed in HSV-1 infected cells (Figure 26). It is important to mention that the phosphorylation of IRF3 and its translocation into the nucleus might be promoted by some of the identified NE-NET23/STING binding partners rather than by TBK1, something that will need to be studied.

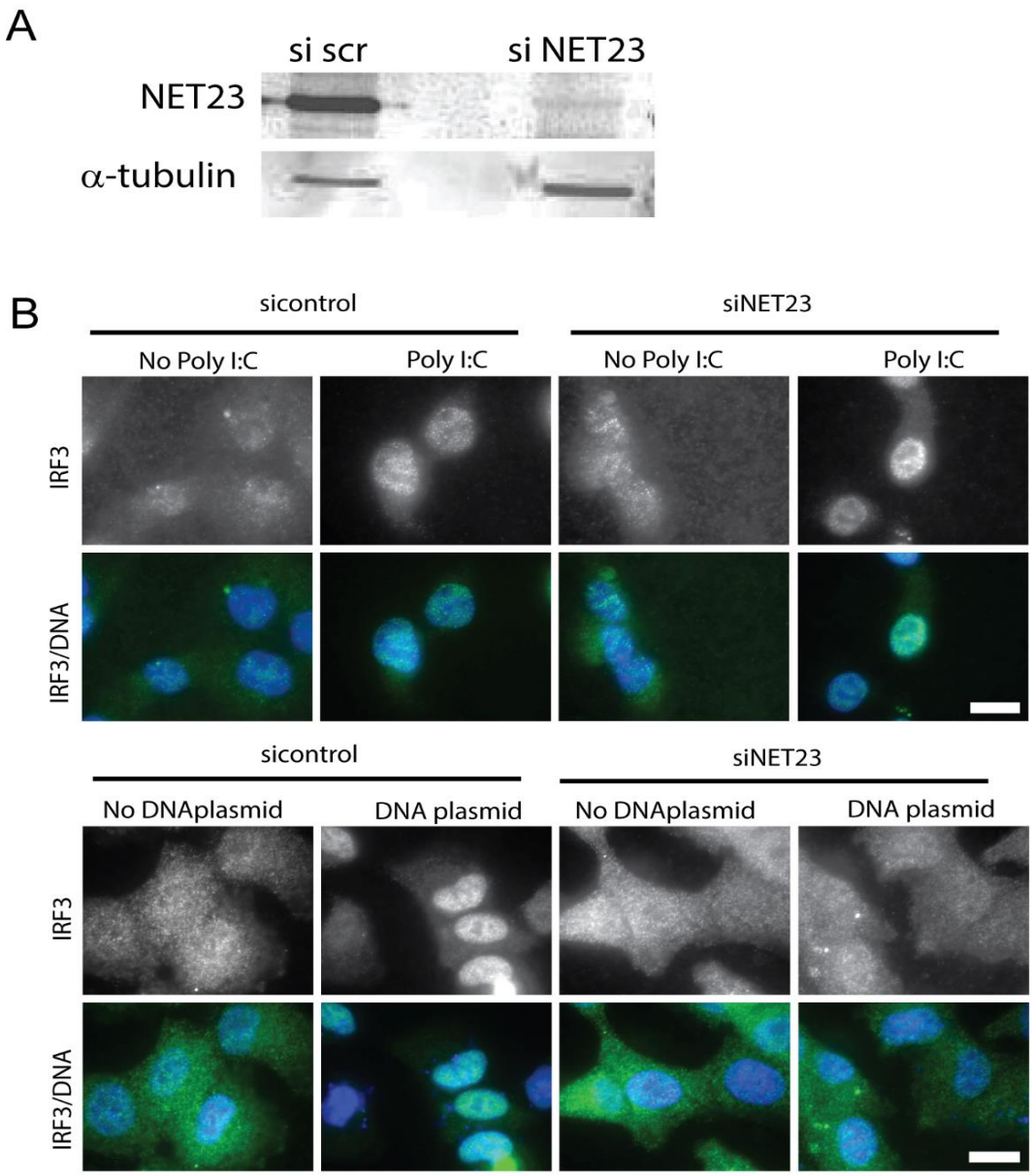

Figure 24. IRF3 translocates into the nucleus upon IIR activation by either poly I:C or DNA plasmid. ***(A)*** *NET23/STING knockdown. HT1080 cells were transfected with siRNA for either control or NET23/STING. Protein lysates from control and NET23/STING depleted cells were analysed by western blot for NET23/STING and α-tubulin.* ***(B)*** *HT1080 cells were transfected with siRNA for either control or NET23/STING for 3 days. After this, the IIR was activated by either poly I:C (top panel) or DNA plasmid (bottom panel) during 2 h. IRF3 is being translocated into the nucleus in either control or NET23/STING depleted cells upon IIR induction by poly I:C. However, IRF3 fails to redistribute when the IIR is activated by DNA plasmid in cells no longer expressing NET23/STING. Scale bar= 10 μm*

In siRNA control cells which the IIR was induced by either poly I:C or plasmid DNA, Syncrip and MEN1 proteins showed a clear redistribution from the nucleus to the cytoplasm (Figure 25, left panel) (Figure 26). However, in cells where NET23/STING was depleted, Syncrip and MEN1 redistribution failed to occur (Figure 25, right panel) (Figure 26). The amount of IRF3, Syncrip and MEN1 was quantified in the nucleus and in the cytoplasm of 100 siRNA control cells and 100 NET23/STING knocked down cells with and without the activation of the IIR by poly I:C, plasmid DNA or HSV-1 (Figure 26). Interestingly, when the IIR was induced by HSV-1 infection, the directionality of Syncrip and MEN1 translocation in control cells is the opposite than the one observed with plasmid DNA or poly I:C, but again, the redistribution of Syncrip is mitigated when NET23/STING is knocked down while MEN1 seemed not be affected (Figure 26).

This quantification confirmed the redistribution of MEN1 and Syncrip upon IIR activation by either poly I:C or plasmid DNA in the siRNA control (p-value<0.001). However, in cells where NET23/STING was depleted there was no significant difference observed in the MEN1 and Syncrip redistribution.

In addition, as previously was described, I observed that IRF3 failed to redistribute normally in NET23/STING knockdown cells upon IIR activation with plasmid DNA (Figure 24, B) (Ishikawa, Ma et al. 2009). This result suggested that NET23/STING probably functions in mediating intracellular DNA-triggered IFN production upstream of TBK1 as IRF3 is not phosphorylated and therefore translocated into the nucleus. However, IIR activation by HSV-1 or poly I:C upon NET23/STING knockdown did not produce any defect in IRF3 redistribution leading to a normal translocation of this protein into the nucleus (Figure 24, B).

Thus, the unaffected redistribution of IRF3 in NET23/STING knock down cells where the IIR has been activated upon HSV-1 infection or poly I:C argues that the Syncrip and MEN1 effects are not a downstream effect of NET23/STING IIR signalling defect produced by its depletion, suggesting the possibility of NET23/STING being involved in transport pathways of these proteins.

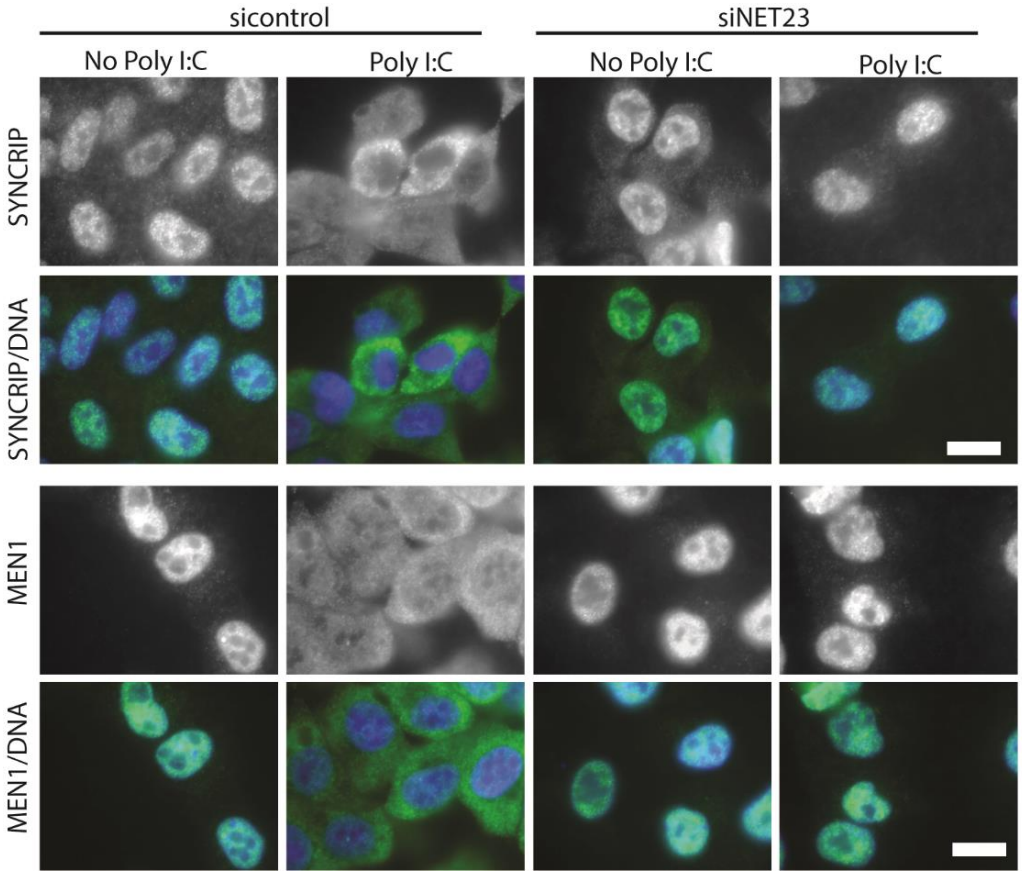

Figure 25. NET23/STING binding partners SYNCRIP and MEN1 normally redistribute during IIR and fail to redistribute in NET23/STING knockdown cells. *SYNCRIP and MEN1 are translocated from the nucleus to the cytoplasm after IIR by poly I:C in siRNA control cells (left panel). This translocation fails to occur when NET23/STING is depleted from cells (right panel). Scale bar= 10 µm*

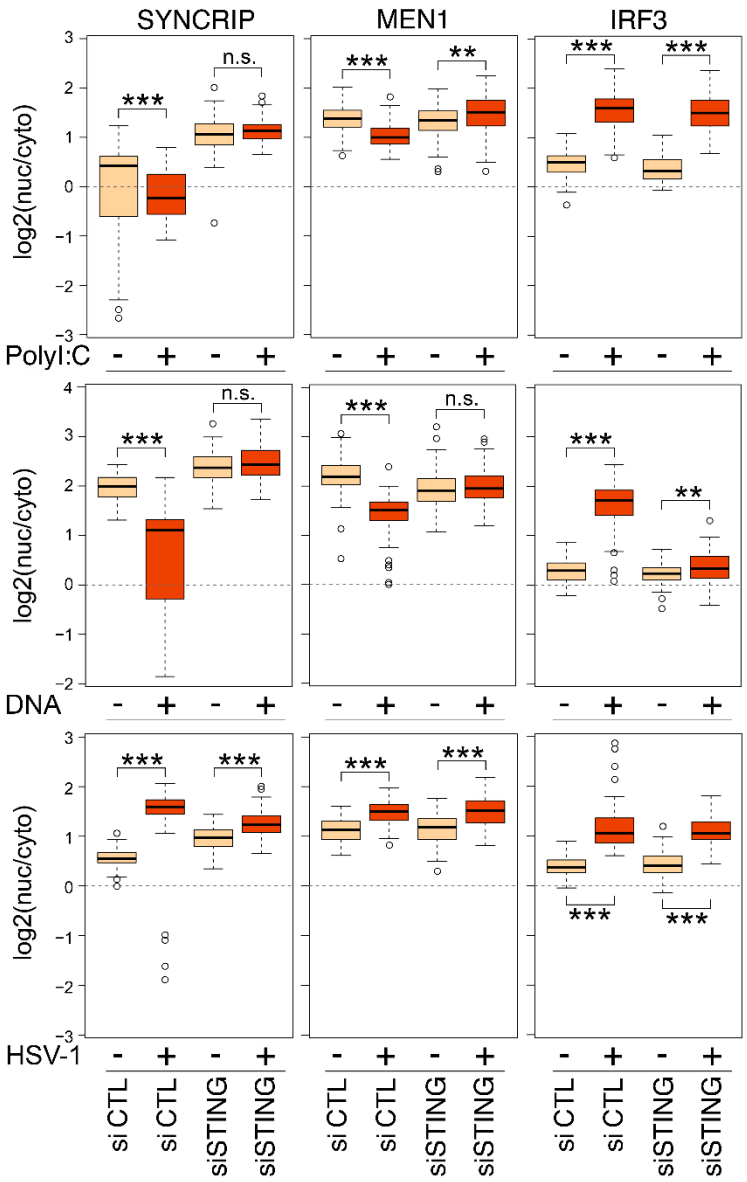

Figure 26. SYNCRIP and MEN1 shuttling upon IIR activation is dependent on NET23/STING. *Quantification of nucleo-cytoplasmic redistribution of NET23 binding partners with or without NET23/STING knockout upon activation of IIR with poly I:C, plasmid DNA (dsDNA) or HSV1 infection. P-values were calculated with KS test (* p < 0.05, ** p<0.01, *** p < 0.001)*

3.8. NET23/STING shuttling is increased upon IIR activation in the ER and in the NE

To further investigate the hypothesis of NET23/STING acting as a transporter for proteins involved in IIR, I used FRAP to quantify the mobility of this protein within the NE and the ER after the induction of the IIR. I postulated that NET23/STING might promote the shuttling of factors involved in IIR between the nucleus and cytoplasm, thus its mobility could change upon IIR activation.

It has been shown that FRAP in the NE predominantly measures NETs translocation from the ER to the NE rather than movement of NETs within the NE. NETs, as the rest of membrane proteins, are synthetized in the ER and need to reach their final destination, the INM. To do so, NETs need to travel from the ER to the ONM to finally translocate into the INM via the peripheral channels of the NPCs.

PA and FRAP studies performed by Nikolaj Zuleger showed the presence of different NET pools due to an exchange of these proteins between ER, ONM and INM. FRAP studies in NETs showed that the recovery of fluorescence within the NE was not due to protein movement within the NE but rather translocation from the ER to the NE. Generally, NETs in the NE present interactions with nuclear components resulting in NETs tethered to the NE after their translocation from the ER. Thus, the mobility of NETs within the NE was observed to be slower when compared with the mobility of NETs within the ER, in where proteins are completely mobile and present free membrane diffusion, resulting in a faster mobility.

This was further confirmed by PA-GFP studies which allow to detect the movement of a particular pool of proteins in living cells. This experiment showed that NET binding in the NE is really tight as photoactivated NETs in the NE were relatively immobile, confirming that the NE fluorescence recovery of FRAP experiments depended on the exchange of NETs between the ER and the INM rather than on the movement of NETs within the NE. Additionally, PA studies performed in the ER showed that photoactivated NETs were quickly accumulated in the NE rather than stay in the ER, confirming the previous observations. Furthermore, FRAP experiments of NETs in the ER showed higher mobility than those proteins bleached

in the NE. In conclusion, these observations clearly support that FRAP in the NE is predominantly measuring ER- INM translocation (Zuleger, Kelly et al. 2011).

Based on these studies, the term "translocation" will be used in this thesis for movement of NETs from the ER into the INM of the NE

If NET23/STING was acting as a transport receptor for IIR proteins in and out of the nucleus to activate transcription factors IRF3/7, we expected its translocation from the ER to the NE to be increased upon the activation of the IIR. For this propose, NET23/STING mobility within the NE and ER was quantified by FRAP upon the activation of the IIR by HSV-1 (Figure 27).

To avoid the activation of the IIR due to the transfection of plasmid DNA, I used the NET23/STING-GFP inducible cell line previously generated in which the expression of this protein was controlled by the addition of doxycycline to the medium. As a control, a stable cell line expressing the nuclear protein NET55 fused with GFP was used to test whether other NETs lose NE tethering connections and thus, might shuttle in and out of the nucleus upon the HSV-1 induced IIR activation. FRAP was performed in these two stable cell lines under normal conditions and upon the activation of the IIR by HSV-1 infection.

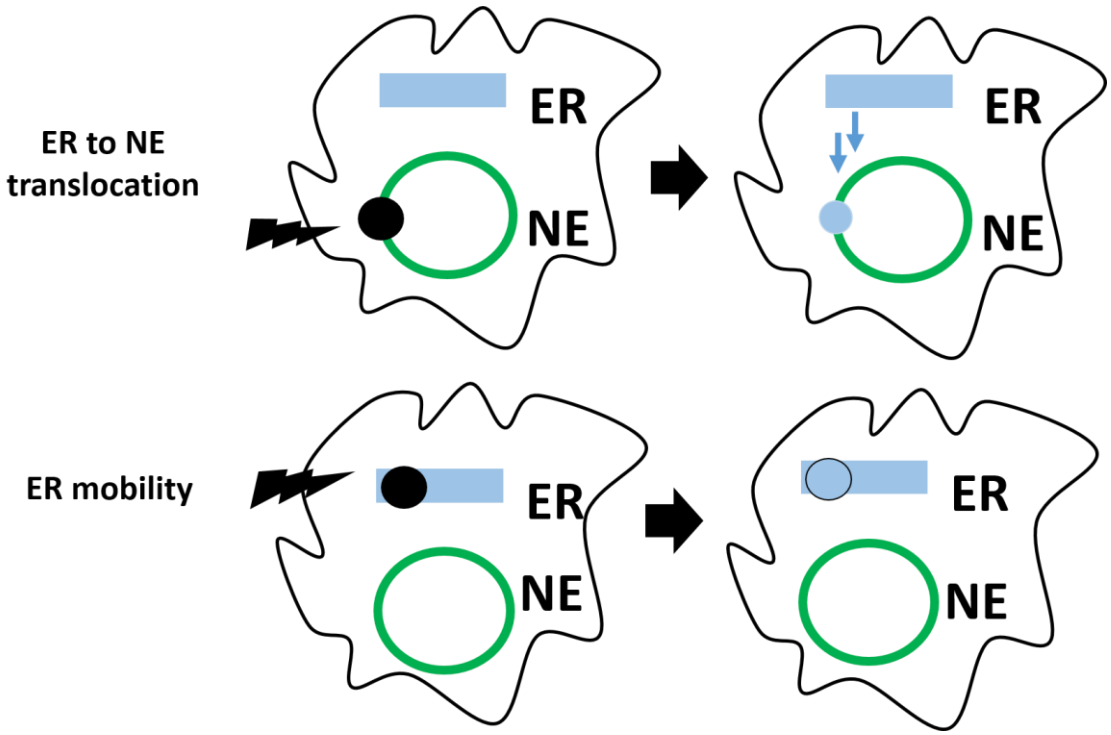

Figure 27. Schematic of the FRAP experiment to study NET23/STING dynamics upon IIR activation. *After NE photobleaching, fluorescence recovery of NET23/STING within the NE is mainly due to translocation of this protein from the ER into the NE (blue) rather than from diffusion of unbleached NET23/STING protein in the NE (green). After ER photobleaching, fluorescence recovery of NET23/STING in the ER is due to the diffusion of NET23/STING within the ER (blue).*

The t½ is the parameter that indicates the time in which 50% of the maximal recovery achievable from the bleached fluorescence has been recovered and in this case it is used as a relative measure for protein translocation; the lower the t½ is, the faster the translocation of the studied protein occurs.

For FRAP experiments, five pre-bleach images were taken followed by bleaching a spot of 1µm in the ER and NE for 1 s at full laser intensity. The fluorescence recovery was measured before, during and after the bleach in either the NE or the ER to generate fluorescence recovery curves. The t½ was calculated from normalized fluorescence values while the immediate post-bleach value was set to 20-30% of the starting fluorescence signal (0.2-0.3 normalized values in the graphic) and the

average of the ten last points of the recovery curve to 100% (1 normalized value in the graphic) *(for further details refer to Materials and Methods chapter).*

To circumvent variability due to imaging and to objectively optimize the best experimental parameters to perform FRAP, different validations were done. Various parameterizations were tested such as laser intensity and post-bleach time recovery.

Photobleaching of NET23/STING tagged with GFP was performed in the NE and ER of mock and HSV-1 infected inducible stable cell lines. I conducted three independent experiments in each of which FRAP was performed within the NE and ER on 5-6 individual cells per condition; mock and HSV-1 infected cells. Fluorescence recovery was measured at the indicated times. As observed in Figure 15, for experiments performed in the NE, the fluorescence recovery of each individual experiment was roughly similar between them. The mean of the t½ and the SD from the means of each experiment showed robust values, confirming the reproducibility and accuracy of this technique (Table 10).

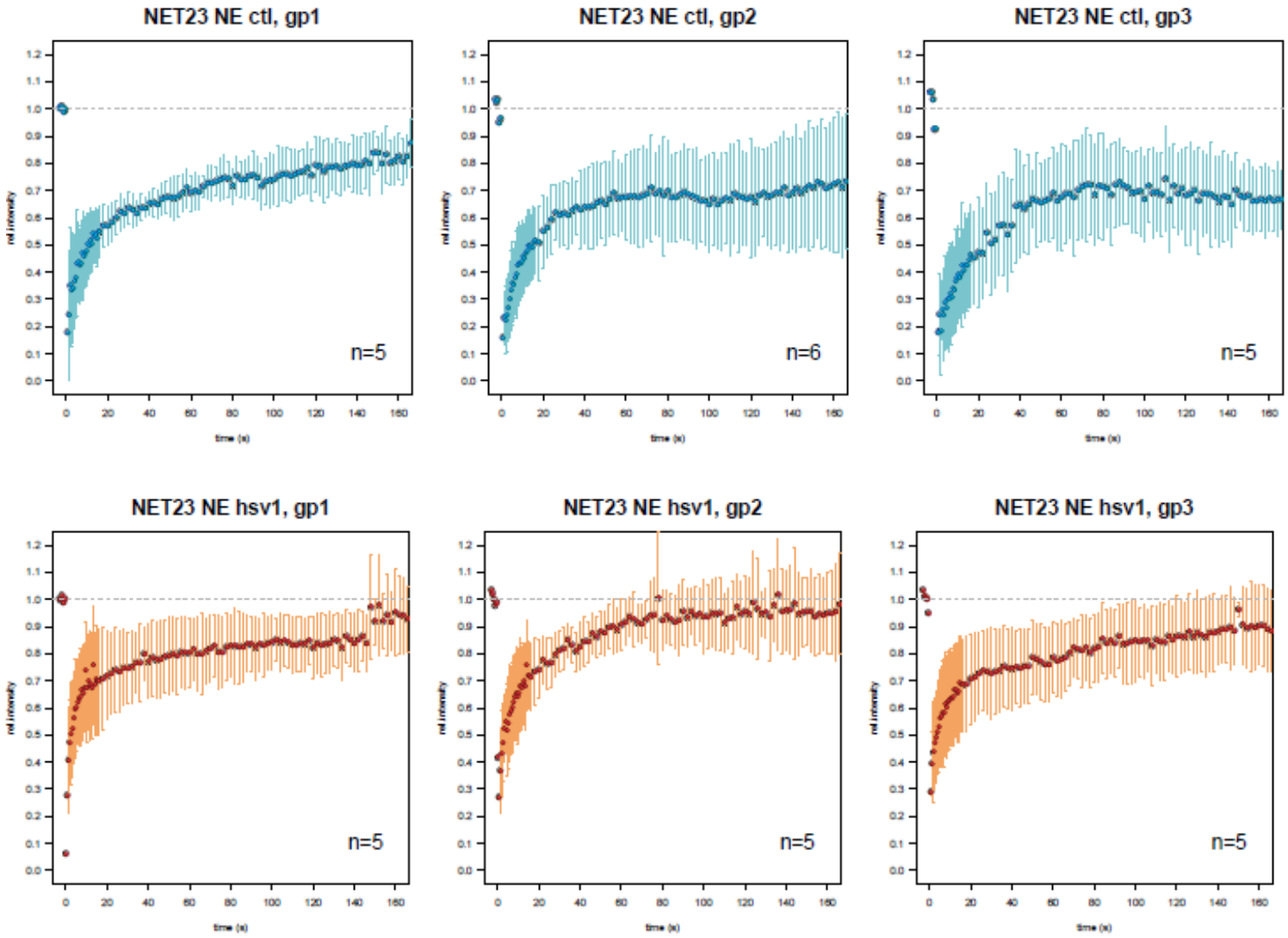

Figure 28. Fluorescence recovery curves from three independent experiments to calculate t½. *NET23/STING translocation within the NE was quantified in three independent experiments for mock and HSV-1 infected cells to validate the reproducibility of the technique. Representation of three fluorescence recovery curves from three independent experiments in which NET23/STING translocation was measured in 5 or 6 mock or HSV-1 infected cells, showed a clear reproducibility of NET23/STING translocation in the NE for each condition.*

Induction of the IIR with HSV-1 infection increased the mobility of NET23/STING in the NE compared with mock infected cells. The t½ of NET23/STING in the NE is significantly decreased by 1/3 from 11.1 s to 6.7 s. In contrast for the control NET55 the t½ was unaffected (Figure 29).

In addition, I also assessed the fluorescence recovery of NET23/STING and NET55 after IIR induction in the ER. NET23/STING mobility was significantly increased by 8 s in HSV-1 infected cells compared with uninfected cells while NET55 was unaffected upon IIR activation (Figure 29) (Figure 30). A faster mobility of NET23/STING in the ER is consistent with a redistribution of NET23/STING from the ER to the Golgi in where it assembles into punctuate structures containing TBK1, a kinase needed for the phosphorylation of IRF3.

Table 10 summarizes the mean of the recovery times ($t^{1/2}$) for NET23/STING and NET55 within the NE and ER in control and HSV-1 infected cells. It also includes SD from the means of each experiment and the p-values calculated with one-way Anova test.

In addition, as previously shown for other NETs by Nikolaj Zuleger, the faster mobility of NET23/STING observed in the ER of HSV-1 infected cells, is reflecting a faster translocation of this protein from the ER to the NE, possibly acting as a transport receptor for different proteins involved in IIR that provide directionality to NET23/STING forcing the movement within the ER towards the NE.

Based on previous PA studies performed for other NETs in which photoactivated NETs within the ER were quickly accumulated in the NE rather than stay in the ER, together with the faster ER mobility that NET23/STING showed upon IIR activation, it is extremely likely that NET23/STING shuttling is being increased upon IIR activation from the ER to the NE. These results suggested that the increase in NET23/STING mobility upon IIR is associate with the redistribution of NET23/STING-NE binding partners in and out the nucleus that ultimately will lead to the activation of transcription factors involved in IIR.

Altogether, this data supports that NET23/STING is not just acting as an upstream activator of the IIR. But it also shuttles between the nucleus and the cytoplasm likely acting as a carrier for proteins involved in IIR in either direction. NET23/STING binding partners, as Syncrip and MEN1, can redistribute and might be activating IIR

factors by its translocation, probably, through the peripheral channels. Further experiments will need to confirm the use of peripheral channels by NET23/STING and its NE-binding partners.

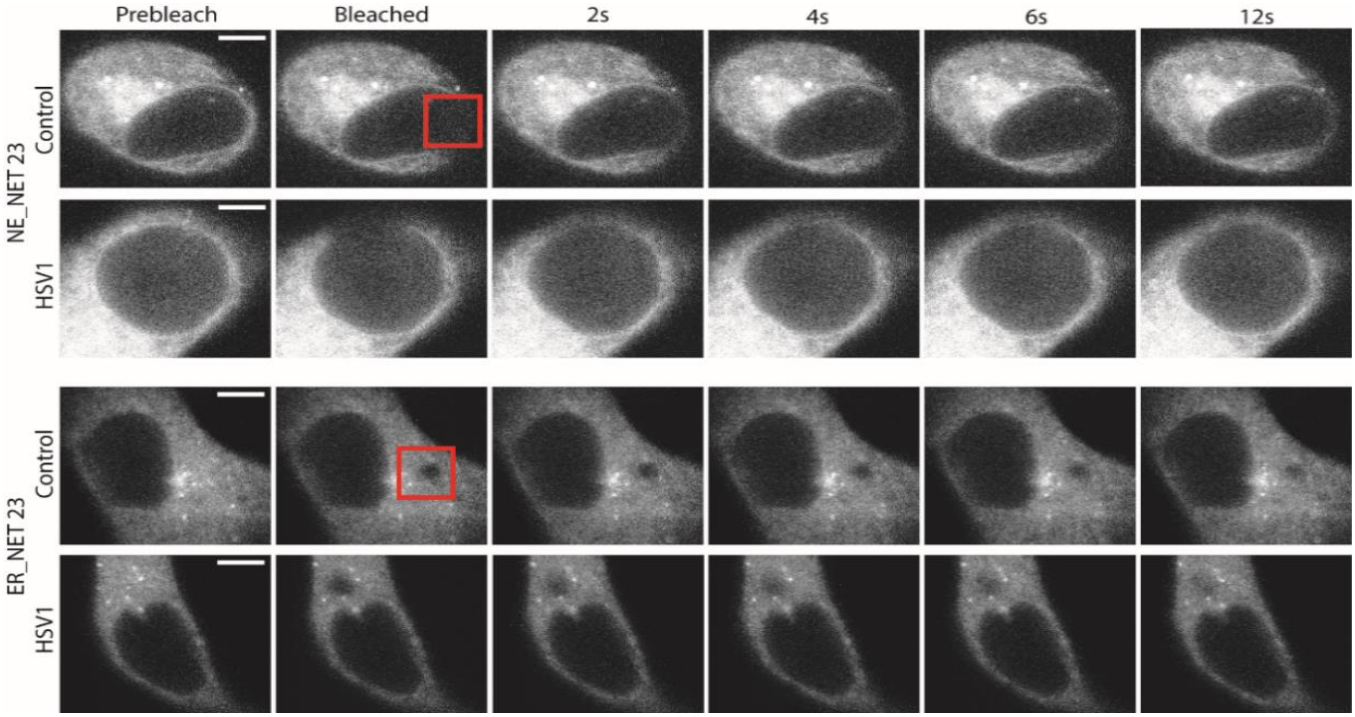
Prebleach
Bleached
2s
4s
6s
12s
NE_NET 23
Control
HSV1
ER_NET 23
Control
HSV1

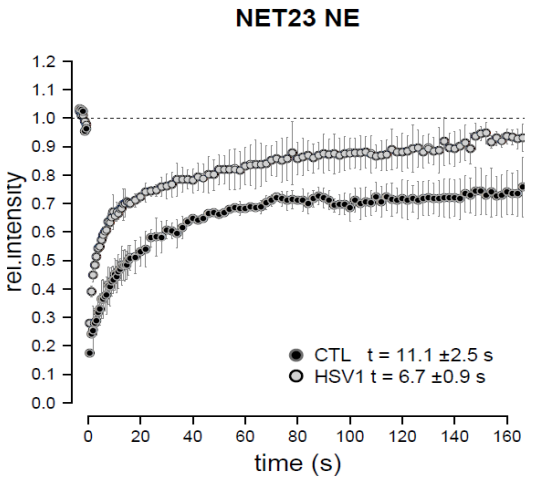
NET23 NE
rel.intensity
time (s)
CTL t = 11.1 ±2.5 s
HSV1 t = 6.7 ±0.9 s

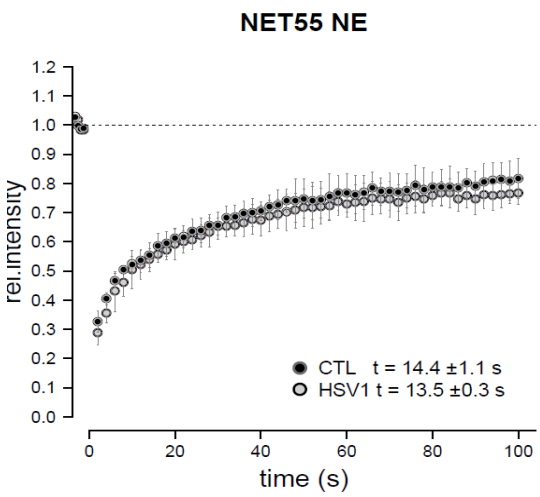
NET55 NE
rel.intensity
time (s)
CTL t = 14.4 ±1.1 s
HSV1 t = 13.5 ±0.3 s

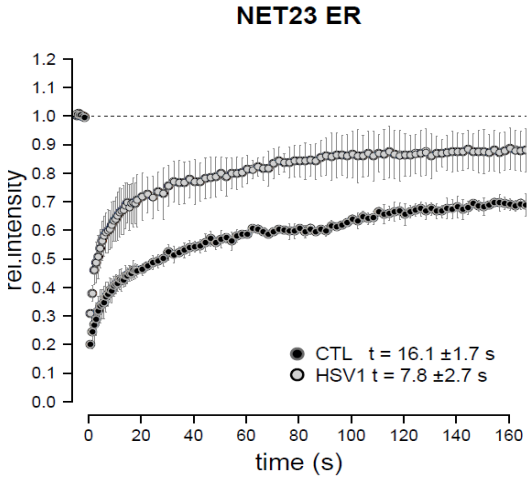
NET23 ER
rel.intensity
time (s)
CTL t = 16.1 ±1.7 s
HSV1 t = 7.8 ±2.7 s

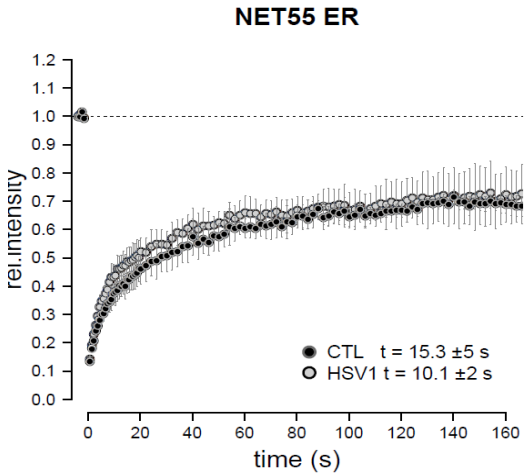
NET55 ER
rel.intensity
time (s)
CTL t = 15.3 ±5 s
HSV1 t = 10.1 ±2 s

Figure 29. NET23/STING mobility in the NE and ER increases upon IIR activation. *Stably-transfected HT1080 cells expressing NET23/STING-GFP were bleached in the NE (top panel) and in the ER (lower panel). Fluorescence recovery in the bleached area is monitored (red box represent the beached area). NET23/STING recovery within the NE or ER was very slow in control cells compared with HSV-1 infected cells. The recovery curves for ER and NE FRAP for NET23/STING and the control NET55 are displayed below. Scale bar = 5 µm*

Table 10. NE and ER FRAP recovery times (t½) s for NET23/STING and NET55 mobility in control and HSV1 infected cells.

			[a] t ½	t½-sd	t½+sd	sd	One-way Anova p-value
NET23	NE	CTL	12.9	11.3	14.5	*1.59*	0.002
		HSV1	5.1	4.2	5.9	*0.87*	
	ER	CTL	16.1	14.4	17.8	*1.71*	0.011
		HSV1	7.8	5.1	10.5	*2.70*	
NET55	NE	CTL	14.4	13.3	15.5	*1.11*	0.261
		HSV1	13.5	13.3	13.8	*0.27*	
	ER	CTL	15.3	10.3	20.2	*4.95*	0.168
		HSV1	10.1	8.1	12.1	*2.01*	

[a] NET23/STING and NET55 t½ recovery times within the NE and ER are presented together with the standard deviation (sd). P-values were calculated with one-way Anova test. Comparison of the recovery times (t½) between the control and HSV-1 infected cells presented p-values ≤ 0.05.

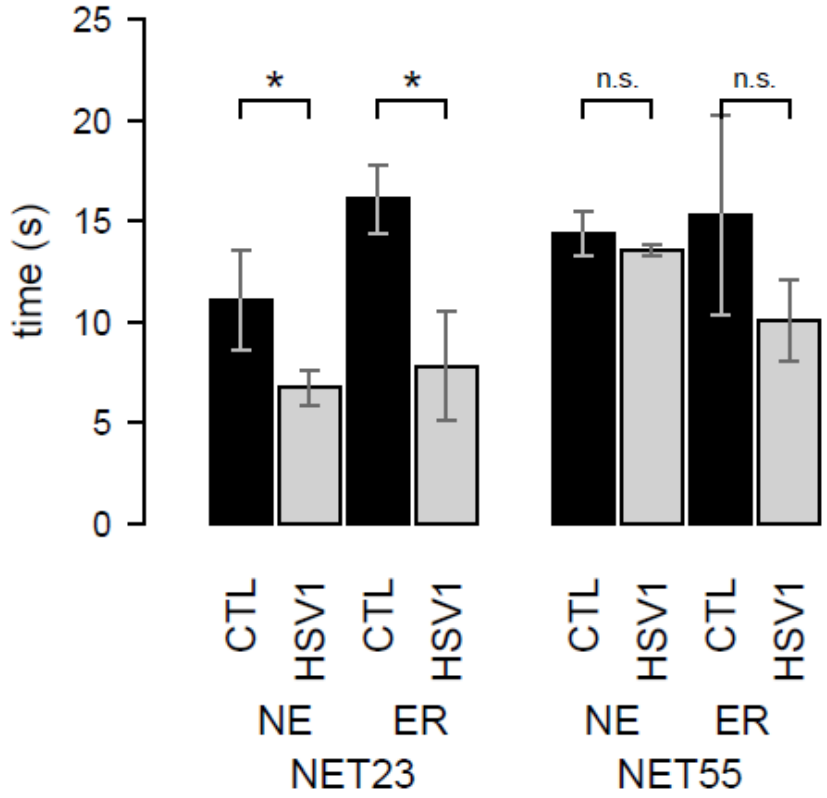

Figure 30. NET23/STING mobility is significantly increased upon HSV-1 infection in HSV-1 infected cells *Comparison of the recovery half times (t½) for NET23/STING and NET55 in either NE or ER from control and HSV-1 infected cells. P-values * < 0.05 / ns: difference non significance.*

3.9. Summary of Chapter 3

In this chapter, two novel nuclear functions for NET23/STING have been identified; its role in chromatin remodelling together with its ability of acting as a transport receptor directing the nucleo-cytoplasmic redistribution of proteins contributing to IIR.

STING was originally introduced as NET23 from a proteomic study of NETs in my supervisor´s lab (Schirmer, Florens et al. 2003). Since then, this protein has been shown to be localized also at the ER and mitochondria playing a role in the activation of IIR signalling cascades that stimulate IRF3/7 transcription factors (Ishikawa and Barber 2008, Ishikawa, Ma et al. 2009, Barber 2011, Chen, Sun et al. 2011, Ishikawa and Barber 2011). However, its function within the NE has been completely ignored. This chapter has been focused on the experiments I performed to test the hypothesis of NET23 being involved in chromatin compaction and in IIR signalling within the NE.

Firstly, I confirmed the correlation between NET23/STING and the chromatin compaction phenotype observed in cells overexpressing this protein. Moreover, I showed that the chromatin compaction phenotype dependant on NET23/STING expression is linked with an increase in certain epigenetic marks. I demonstrated that the chromatin compaction levels of eight cell lines correlated with their endogenous NET23/STING expression levels confirming the involvement of this protein in regulating levels of chromatin compaction.

Furthermore, I showed by EM that cells overexpressing NET23/STING presented higher levels of chromatin compaction when compared with control cells. In addition, I showed that HSV-1 infection is mitigated by the depletion of NET23/STING and how the silencing of this protein is preventing the chromatin compaction phenotype that is generally observed in host cells at early times post infection.

Additionally, I used FRAP as a method to study the behaviour of NET23/STING within the NE and ER upon the induction of the IIR. I clearly confirmed an increase in the translocation of NET23 from the ER to the NE in HSV-1 infected cells. This result, together with immunofluorescent microscopy studies in which I showed that Syncrip and MEN1, two NET23/STING NE-binding partners, failed to redistribute in

NET23/STING knockdown cells, strongly argues for NET23/STING acting as a transporter for IIR proteins. Thus, this supports our hypothesis in which NET23/STING might be involved in the shuttling of proteins between the nucleus and cytoplasm in order to activate the IIR. Although future experiments need to confirm this hypothesis, I can clearly state that in this chapter I confirmed a novel and unknown NET23/STING role within the NE.

Chapter 4

NETs redistribution during HSV-1 nuclear egress

4.1. Introduction

Viruses are experts at remodelling cellular membranes, breaching them during cell entry or deforming them during the course of infections for budding. Herpesviruses represent an unusual case of viral budding. This family of virus starts in the nucleus by the assembly of new DNA viral capsids that leave the nucleus to reach the cytoplasm in which they acquire the tegument proteins and the final envelope. The viral nucleocapsids are around 125 nm of diameter, too large to pass through the NPCs. It is for this reason that herpesviruses have developed different strategies to break through the NE and reach the cytoplasm to complete its lifecycle.

During budding at the NE, capsids become enveloped at the INM (primary envelopment), which results in the formation of PEP inside the perinuclear space. These particles then fuse with the ONM (de-envelopment) releasing naked capsids into the cytosol. However, the viral capsids do not have unimpeded access to the INM (Bigalke and Heldwein 2016).

The NE presents a unique set of NETs that theoretically should hamper the ability of nucleocapsids to get access to this membrane (Florens, Korfali et al. 2008, Korfali, Wilkie et al. 2010, Malik, Korfali et al. 2010). The majority of these proteins are thought to localize to the INM by a diffusion and retention mechanism. As the ER is continuous with the ONM, NETs diffuse in these two membrane systems after

synthesis using their transmembrane domains. They can subsequently diffuse from the ONM laterally through the peripheral channels of the NPC to reach the INM where they are retained by interactions with the lamina and / or chromatin (Zuleger, Kerr et al. 2012, Zuleger, Boyle et al. 2013, Laba, Steen et al. 2014, Ungricht, Klann et al. 2015).

The nuclear lamina, a dense meshwork of filaments and lamin binding proteins is underlying the INM also hampering the budding of nucleocapsids at this membrane. The lamina meshwork is made up of intermediate filaments proteins that polymerize to form 10 nm diameter filaments of sufficient density to block the large viral capsids. The binding between lamins, chromatin and NETs form a complex web of links resulting in a tightly entwined protein meshwork for nucleocapsids to bypass (Gruenbaum, Margalit et al. 2005).

Herpesviruses have developed different strategies to locally disassemble the nuclear lamina that are critical for the viral capsids to gain access to the INM to achieve primary envelopment. Total dismantling of the NE takes place during processes normally involved in cellular dynamics such as in mitosis.

During mitosis, the lamina meshwork disassembles between prophase and metaphase and reassembles during interphase (Gerace and Blobel 1980). Lamins and NETs like emerin are phosphorylated by cellular kinases to break down the nuclear lamina and dissociate lamina components. Nuclear lamina is completely disassembled by site-specific, reversible phosphorylation of lamins by multiple cellular kinases such as PKA, PKC, MAPK and Cdc2 (Peter, Sanghera et al. 1992, Fields and Thompson 1995, Likhacheva and Bogachev 2001). During herpesvirus infection nuclear lamina is only partially dissolved in areas with high concentrations of the NEC (Reynolds, Liang et al. 2004, Bjerke and Roller 2006, Leach and Roller 2010). It is thought that herpesviruses partially mimic some of these cellular processes by the activation of viral and cellular kinases in these sites, resulting in the phosphorylation of lamins and the disruption of the lamin polymer and lamin interactions with other proteins and DNA facilitating access of nucleocapsids to the INM (Simpson-Holley, Colgrove et al. 2005, Leach and Roller 2010). However, there is much about the interactions of herpesviruses with the NE that remains poorly understood.

It seems likely that in order to achieve budding at the INM for the formation of PEP, herpesviruses must disrupt not only the lamin polymer, but also the many NETs that interact with both lamins and chromatin. Recent studies have shown that the localization of emerin and LBR is altered during viral nuclear egress resulting in an increase of the mobility of these proteins and their redistribution into a cytoplasmic compartment (Scott and O'Hare 2001, Leach, Bjerke et al. 2007, Morris, Hofemeister et al. 2007). These observations suggested that with lamin dissociation the tethering of these proteins is disrupted resulting in their release from the INM. However, both proteins bind not only to lamins, but also to chromatin. Thus, these proteins could also be direct targets of the virus and be phosphorylated similarly to lamins by viral and cellular kinases to break their interactions with chromatin.

As the INM has hundred of NETs, it is a formidable barrier for viruses to bypass beyond just the lamins, emerin and LBR and thus, it is reasonable to postulate that HSV-1 is targeting some other NETs to facilitate its access to the NE. NETs present at the INM could be targeted for degradation or could lose their interaction with the nuclear lamina and / or with chromatin to allow their redistribution so that the membrane becomes accessible for primary envelopment of nucleocapsids. At the same time, it is also possible that some NETs might interact with capsid or primary tegument proteins to actually facilitate nuclear egress.

I hypothesized that INM proteins could be targeted and redistributed during viral infection into cytoplasmic compartments to allow an efficient access of HSV-1 nucleocapsids to the INM and thereby facilitating nuclear egress.

In this chapter I will describe a screening for NETs that I performed in order to study by immunofluorescence microscopy the involvement of some NETs during HSV egress at the NE.

4.2. Screening of NETs during HSV-1 infection

In order to determine whether the localization of NETs changes in response to HSV-1 infection, 13 NETs were screened to analyse their distribution patterns within the NE.

Hela cells were infected with HSV-1 for 8 h after being transiently transfected with different NETs tagged with either RFP or GFP. The infected cells were fixed and subcellular distribution of NETs was then studied by immunofluorescence microscopy. I made use of HSV-1 strains in which a viral protein was fused with either RFP or GFP (complementing the fluorophore of the transfected NET) to identify infected cells. In the case of transfecting NETs fused with GFP I used a viral strain in where the capsid protein VP26 was tagged with RFP. On the other hand, if the NET was tagged to RFP the viral strain used contained ICP27 fused with GFP (Figure 31).

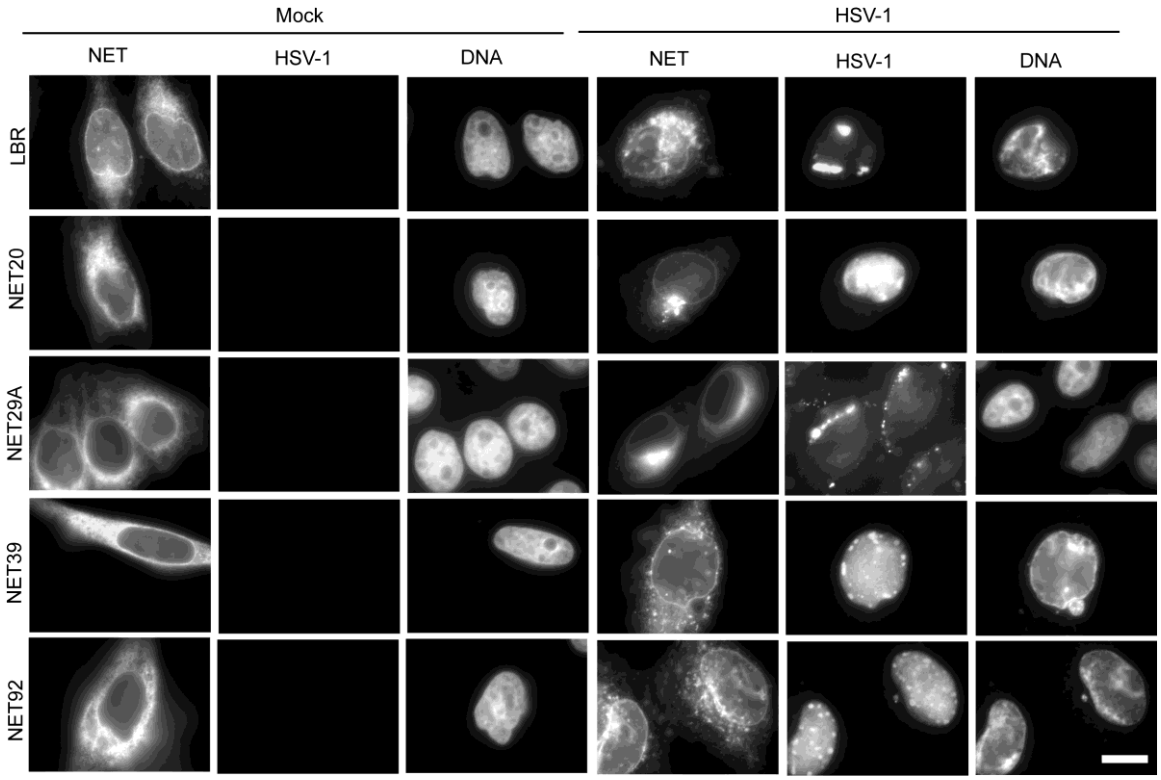

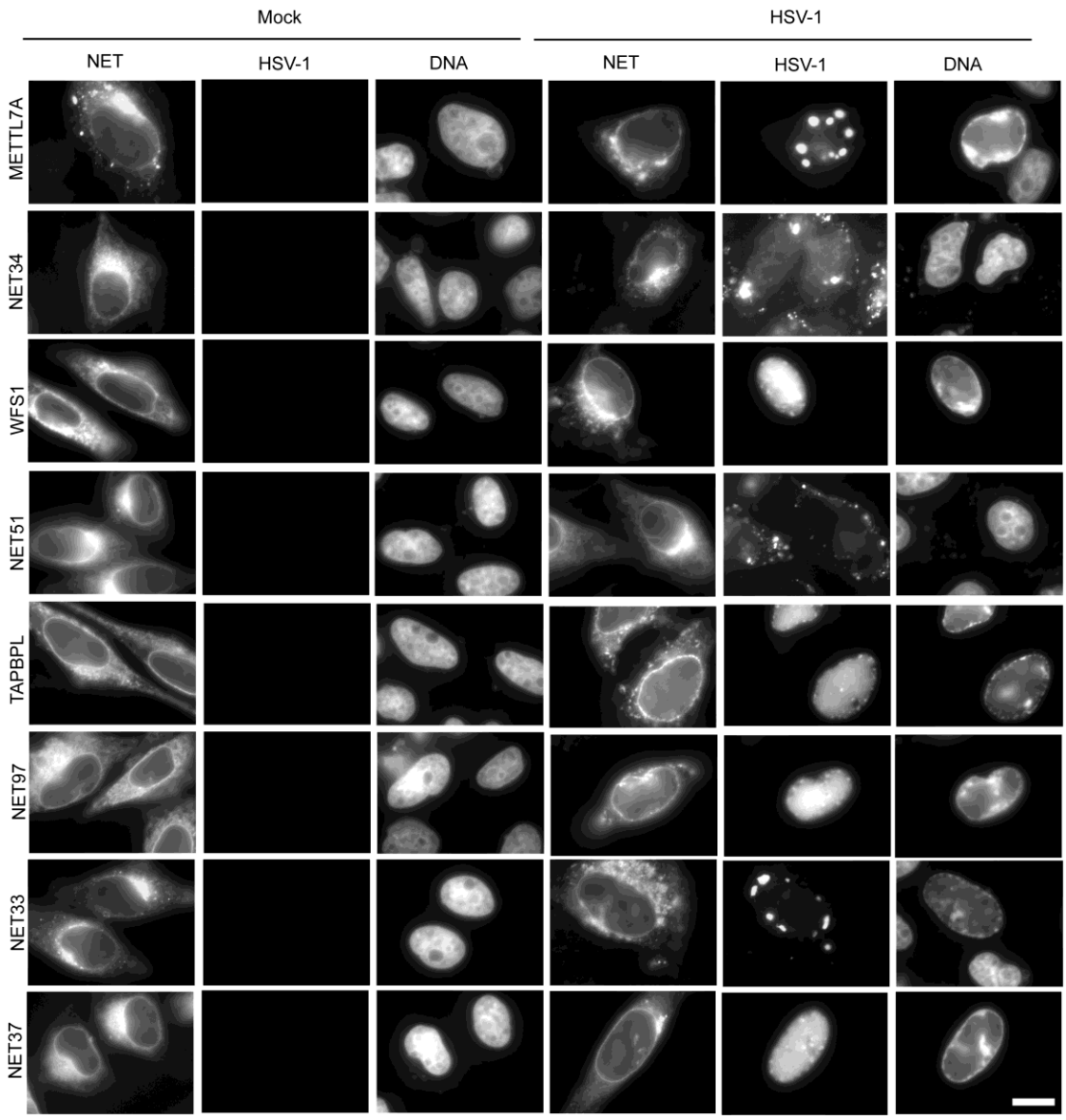

Figure 31. NETs redistribution upon HSV-1 infection. *Hela cells were transfected with different NETs tagged with either RFP or GFP. HSV-1 strain containing either ICP27-GFP or VP26-RFP was used to infect the transfected cells depending on the tag fused with each NET. After 8 hpi cells were fixed and observed by immunofluorescence microscopy. Three phenotypes in the localization of NETs can be observed:* ***(1)*** *NETs showing a redistribution to the ER upon viral infection including LBR, NET20 and NET29A proteins.* ***(2)*** *NETs changing from a smooth NE distribution to a punctuate pattern around the NE and ER including NET39 and NET92, and* ***(3****) NETs that are not notably different in distribution upon viral infection compared with mock cells including NET34, WFS1, NET51, TAPBPL, NET97, NET33, NET37 NET34 and METTL7A. Scale bars: 10 µm*

As expected, in mock cells NETs localized at the nuclear rim with a roughly uniform distribution on the membrane. NETs are also detected in the ER in a homogenous distribution pattern. Note that absent available antibodies it remains uncertain for most NETs whether the ER pool is normal or an overexpression artefact due to saturation of binding sites at the NE. Infection with wild-type virus altered the localization of some NETs resulting in three different scenarios: NETs translocated into the ER, NETs becoming punctuate within the NE, and NETs showing no changes (Figure 31).

As has been previously shown, in cells infected with HSV-1 the nuclear-rim signal of LBR became distorted and redistributed to a membranous cytoplasmic compartment (Scott and O'Hare 2001). In addition, small intranuclear domains could be observed. Previous studies identified the cytoplasmic compartment to which LBR translocated upon infection as the ER. Interestingly, *NET20 and NET29A* showed a similar phenotype to that of LBR upon viral infection. In cells infected with HSV-1, the signal of these two NETs within the NE strongly decreases while starting to accumulate at the ER at 8 hpi.

Two other tested NETs, *NET39 and NET92* presented a different phenotype to that described for LBR, NET20 and NET29A. After infection, NET39 and NET92 still accumulated at the NE of infected cells but showing a patchier distribution. In addition, punctuate structures around the NE and ER could be observed. Notably, the presence of intranuclear granular structures with the appearance of protein conglomerations could be detected in some cases (Figure 31)

The rest of the NETs screened in this analysis including NET34, WFS1, NET51, TAPBPL, NET97, NET33, NET37 NET34 and METTL7A did not show any clear alteration in distribution after infection with HSV-1. All NETs tested are listed in Table 11. The two redistribution phenotypes observed for some of the tested NETs suggest a potential direct or indirect involvement of these proteins during viral egress as their localization is being affected during viral infection. Interestingly, LBR, NET29A and NET39 have been previously described as playing a role in chromosome organization. Therefore, the virus might be targeting these proteins to release their tethering at the INM of chromatin creating a more flexible environment for nucleocapsids to reach the NE for viral egress.

Table 11. Phenotype of screened NETs upon HSV-1 infection
TM: number of transmembrane domains

Gene Name	Alternative Name	TM	Chrom. Organization	Phenotype upon HSV1
LBR	LBR	8	YES	ER accumulation
METTL7A	NKP2	1	NO	N/E
FAM105A	NET20	1	NO	ER accumulation
TMEM120A	NET29	5	YES	ER accumulation
SLC39A14	NET34	7	NO	N/E
WFS1	mNET2	9	YES	N/E
PPAPDC3	NET39	3	YES	Punctuate struct.
ATLA3	NET92	2	?	Punctuate struct.
C14orf1	NET51	4	NO	N/E
TAPBPL	NKP39	1	YES	N/E
AADACL1	NET97	1	?	N/E
SCARA5	NET33	1	NO	N/E
KIAA1161	NET37	1	NO	N/E

Based on the results obtained by immunofluorescence microscopy I could conclude that certain types of NETs are being affected by HSV-1 infection. If a NET is localised to the NE by only its interaction with lamin, the redistribution observed upon viral infection could be an indirect effect of lamin disassembly. However, if a NET in addition is interacting with chromatin, either the chromatin or the NET has to be directly targeted by the virus in order to break the tethering of the NET to the NE and produce its redistribution. Thus, it still remains unclear whether the redistribution observed for some upon viral infection is a direct or indirect aid for the virus.

Additionally, based on the availability of antibodies present in the lab, I decided to test whether some NETs are being degraded during viral infection. For this, Western blot analyses were performed in HSV-1 infected Hela cells. Cells were either mock infected or infected for 8 h with a MOI of 10 with 17+ wt strain of HSV-1. The cell

lysate was extracted and analysed by Western blot for different NETs including NET5, LAP2B, WFS1, Tmem214 and emerin. I observed that multiple lower molecular weight bands resulting from protein degradation were not present in any of the tested NETs indicating that NET degradation by HSV-1 infection is unlikely to occur at least on these tested proteins (Figure 32).

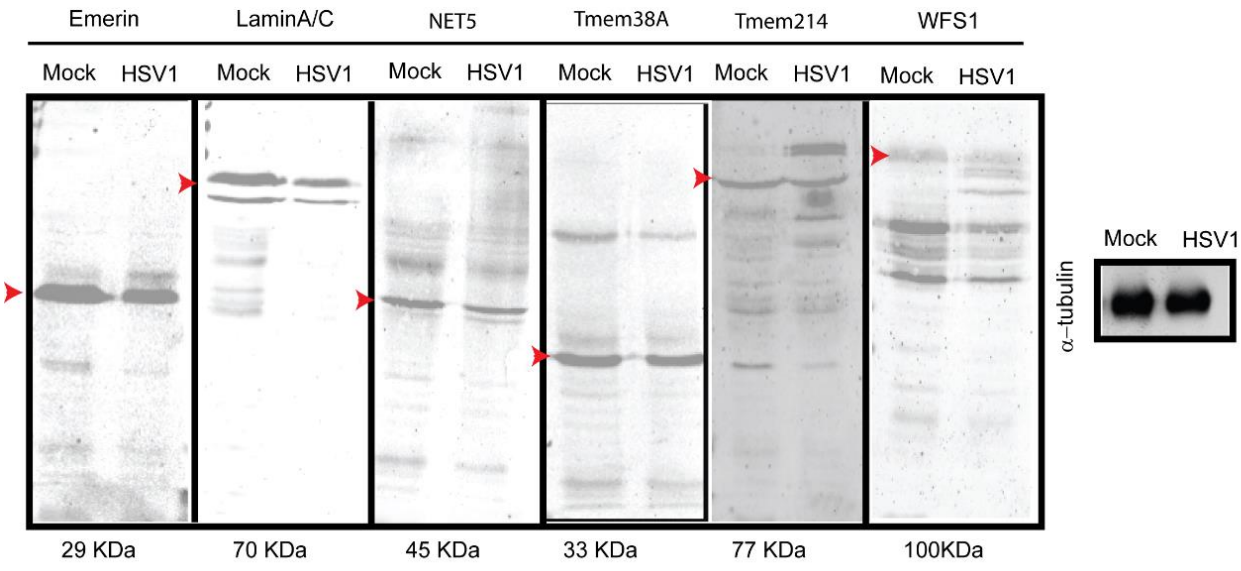

Figure 32. NETs are not being degraded upon HSV-1 infection. *Lysates from Hela cells infected for 8 h with w+ HSV-1 were analysed by Western blot for NETs degradation. Emerin Lamin A/C, NET5, Tmem38A, Tmem214 and WFS1 are not suffering degradation upon HSV-1 infection. α-tubulin was used as an internal control.*

4.3. HSV-1 production is decreased in NET29 depleted cells

In the previous section I have shown that NET29, a INM protein known to affect chromosome organization, accumulates in the ER after HSV-1 infection. A single preliminary study was performed in order to investigate if NET29 is implicated in HSV-1 growth. This experiment was done in Dr Finn Gray´s lab as part of one

collaboration aimed to identify potential host proteins that could affect HSV-1 viral growth (this data is not shown in this thesis).

To do so, I used a single-step viral growth assay and directly compared WT and NET29 knockdown cells. Hela cells were transfected with siRNA against NET29 during three days before being infected with a HSV-1 strain that expressed a GFP protein to monitor virus growth kinetics as a measure of GFP fluorescence. I found that viral production already was decreased in NET29 knockdown cells at 10 hpi and a more than 2-fold difference was observed at 30 hpi compared with siRNA control cells (Figure 33).

Importantly, the defect in viral infectivity resulting from NET29 depletion suggested the potential role of this NET during HSV-1 viral growth. However, further experiments will be required in order to confirm this observation.

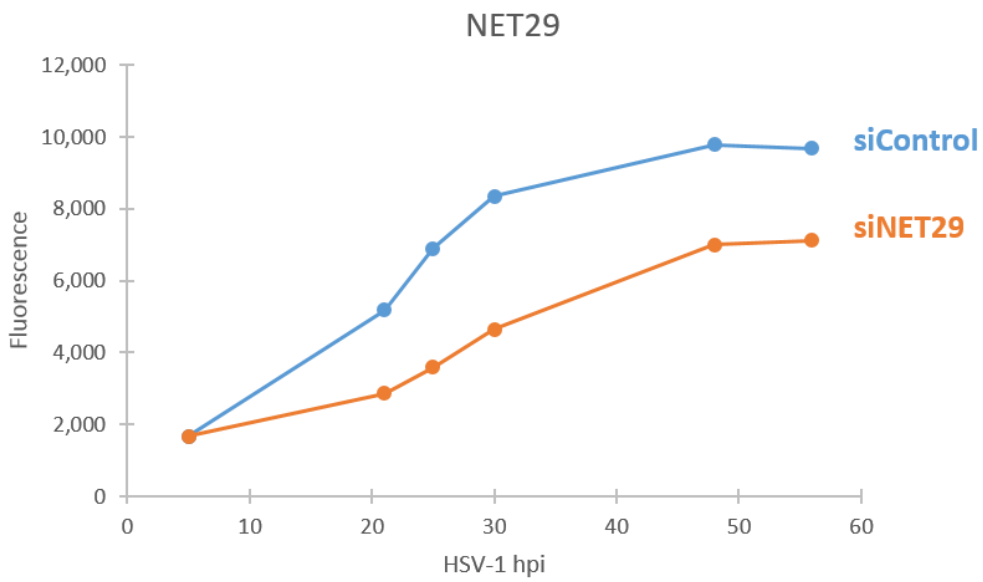

Figure 33. NET29 depletion inhibits HSV-1 production by 2-fold*. Hela cells were transfected with either siRNA against NET29 or siRNA control. After 3 days, the siRNA transfected cells were tested for the capacity to influence replication of the HSV-1 GFP reporter virus from 5 to 60 h post-infection. Virus replication slopes during the linear phase were calculated and normalized to mock-transfected cells. Replication slopes were then compared to replication upon knockdown of NET29 and control siRNA cells.*

4.4. Summary of chapter 4

In this chapter I conducted a screen for NETs that can be redistributed during HSV-1 infection. For this, I initially transfected Hela cells with multiple NETs tagged with either RFP or GFP. After, cells were infected with HSV-1 and the position of the NETs was analysed by fluorescence microscopy. This identified three categories: NETs redistributing to the ER, NETs that become punctate at the NE, and NETs that are unchanged. Further study may identify the contributions of these different groups to infection.

NET20 and NET29 with the already described protein LBR underwent a partial redistribution from INM to a significant accumulation observed in the ER of infected cells at 8 hpi. In addition, the localization of other NETs is changing from a uniform pattern lining the nuclear membrane to an uneven distribution with concentrations of dots that appear to be in the outer surface of the ER and nuclear membrane

The redistribution of some NETs during HSV-1 infection suggests a potential direct or indirect involvement of these proteins during viral egress. Furthermore, I observed that some of these NETs seem not to be degraded after HSV-1 infection, suggesting that the observed phenotype is not a consequence of the degradation of the NET that could lead into the partial redistribution of the protein within the ER but rather of a total redistribution of the protein during viral egress at the NE.

Together with the finding that the depletion of NET29 in HSV-1 infected cells produced a reduction in HSV-1 viral growth, these observations open the possibility of the involvement of NETs during HSV-1 infection in addition to the already described protein LBR and emerin.

Chapter 5

Identification of host cellular proteins involved in HSV-1 nuclear egress

5.1. Introduction

Both, the NETs that became punctate at the NE and those that remained distributed throughout the NE in the previous chapter are physically poised such that they could in theory functionally participate in the mechanism of egress. As an example, they could potentially interact with capsid or tegument proteins increasing the affinity of viral particles for the NE or help wrap the INM around the new virus particles synthesized within the nucleus facilitating nuclear egress. Alternatively, just by not being redistributed away from sites of egress, those that remained unchanged might be captured in primary envelopes even if they have no functional role. More steps of the herpesvirus lifecycle are known to involve the commandeering of host cell proteins (Li, Zhang et al. 2006, Ni, Wang et al. 2012, Christensen, Jensen et al. 2016); thus it is not surprising that HSV-1 might co-opt host machinery during nuclear egress.

Nuclear membrane proteins enter the nucleus after synthesis in the ER by lateral diffusion through the peripheral channels of the NPC. According to the lateral diffusion hypothesis, described in the introduction, once NETs are inside the nucleus, interactions with the nuclear lamina largely immobilize proteins in the INM.

However, if these interactions are broken, proteins become free to diffuse laterally and are able to diffuse back into the ONM and throughout the ER (Ohba, Schirmer et al. 2004, Zuleger, Korfali et al. 2008, Zuleger, Kelly et al. 2011, Ungricht and Kutay 2015). Thus, it might be expected that during the process of de-envelopment in which the PEP fuse with the ONM, the host proteins facilitating the budding at the INM presented in the primary envelope would release and diffuse into the ER.

With this idea in mind and with the purpose of capturing host proteins involved in HSV-1 primary envelopment, I used a well characterised method originally developed by Peter Walter for isolating microsomes (MMs), lipid vesicles coming principally from the ER. Based on the hypothesis that proteins involved or captured in PEP would partially distribute to the ER, I applied this already developed method to isolate MMs from mock and HSV-1 infected cells and searched for proteins that changed abundance in the ER after infection. Important to note that a potential caveat to this method is the capture of later proteins already synthesized in the ER.

In this chapter I will describe the optimization and development of the isolation of MMs from HSV-1 infected cells for the identification of cellular proteins involved in herpesvirus egress at the NE. Subsequently, this chapter will show the mass spectrometry analysis of the HSV-1 MMs compared with the mock MMs and the identification of a group of vesicle fusion host proteins that might be co-opt HSV-1 machinery during egress at the NE.

5.2. Isolation of MMs from HSV-1 infected cells: a novel approach to identify host proteins involved in viral egress at the NE.

In order to identify potential host proteins involved in the process of primary envelopment, I considered the possibility of performing mass spectrometry analysis on NEs from HSV-1 infected cells and comparing the protein content with mock NEs. However, during infection HSV-1 weakens the lamin polymer making the NE weak and prone to rupture. Since NE isolation procedures depend on a strong intact NE

isolating, isolation of NEs from infected cells will necessarily result in fragmentation and high contamination. To get around this problem and detect host proteins involved in HSV-1 egress, I performed the isolation of MMs from HSV-1 infected cells.

MMs are *in vitro* spherical lipid vesicles derived principally from the ER that were firstly obtained by Claude in 1943. To study the functions and biochemistry of the ER, it was necessary to isolate the ER membrane and separate it from other components of the cytoplasm. When cells or tissues are disrupted, the ER breaks into small fragments and creates many small closed vesicles called MMs (˜200-400 nm in diameter). The general structure of the membranous compartment of the ER is transformed from a tubular to vesicle structure while the protein content remains consistent through the fractionation.

I postulated that host proteins on the INM that either participate in the process of primary envelopment or get captured in the envelope of PEP, will become part of the ONM when egress yields their fusion with the ONM for release of non-enveloped particles into the cytoplasm.

Although the PEP are large (125 nm) they are still much smaller than the MMs (200-400 nm) and so, PEP that had moved to the lumen of the ER or from fragmented weak nuclei during the isolation procedure could be encapsulated and isolated inside the MMs. Furthermore, host proteins involved in primary envelopment at the INM would be released in the ONM or ER. As such we expected to have a significant enrichment of host proteins participating in primary envelopment in the MMs fraction of HSV-1 infected cells compared to mock cells (Figure 34).

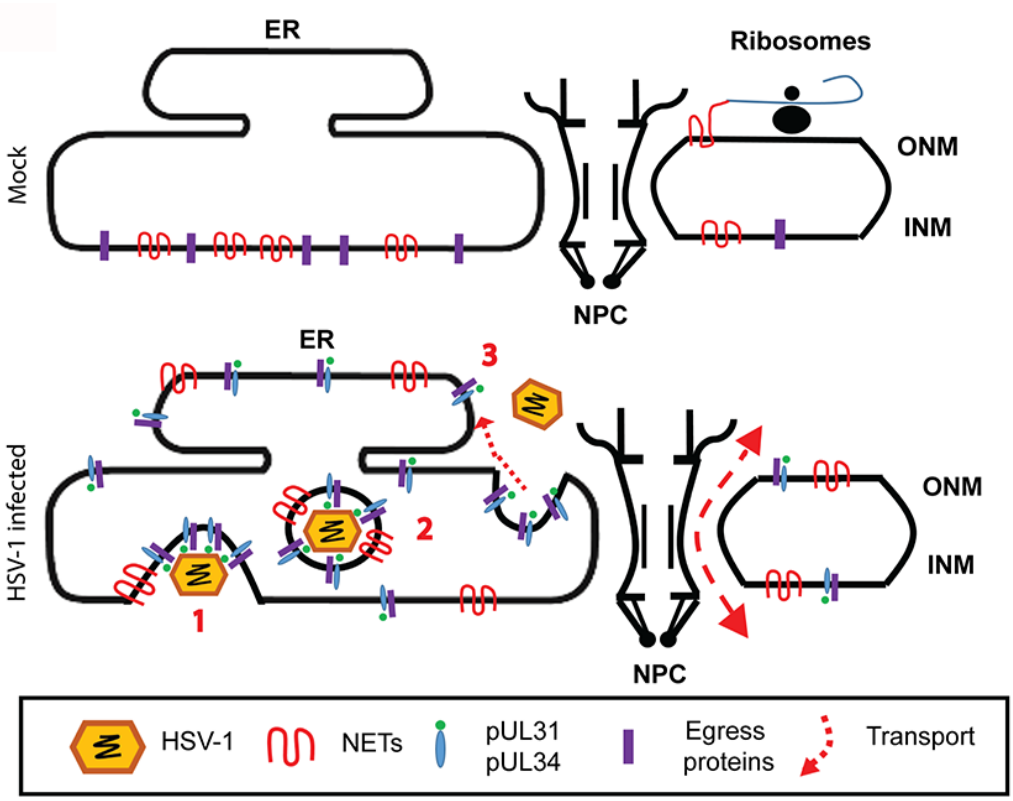

Figure 34. Schematic representation of the main hypothesis to detect host proteins involved in primary envelopment. *NE in mock* ***(top panel)*** *and HSV-1 infected cells* ***(bottom panel).*** *NETs and potentially as yet unidentified egress proteins are only transiently in the ER and ONM after synthesis (top panel). These proteins laterally diffuse through the peripheral channels of the NPC to reach the INM where they are retained by interactions with other lamina components. In HSV-1 infected cells, some of these interactions are broken so that nucleocapsids bud at the INM* ***(1)*** *into the lumen of the NE followed by scission of the INM to form primary enveloped particles that include INM lipids and potentially any INM proteins either involved or captured in the process* ***(2)****. During de-envelopment the INM-derived primary envelope lipids and proteins fuse with the ONM releasing proteins involved or captured in primary envelopment* ***(3)****. Due to continuity of the ONM with the ER these proteins can diffuse into the ER or re-translocate back to the INM. UL31 and UL34 are two known viral proteins involved in primary envelopment at the NE. We postulated that host cell proteins of the INM that are either captured during the process of primary envelopment/de-envelopment or actively participating in this process would be released into the ONM and diffuse into the ER.*

MMs extraction protocols have been well established in our lab to use proteins identified in MMs as an in silico subtractive fraction to compare with proteins isolated in proteomic analysis of the NE of muscle nuclei and leukocytes (Korfali, Fairley et al. 2009, Korfali, Florens et al. 2016). Taking advantage of the optimised protocols set up in our lab for many years and with the purpose to determine potential host proteins involved during herpesvirus nuclear egress, a proteomic analysis on isolated ER-enriched MMs from HSV-1 and mock infected cells was performed, searching for NE proteins that increased their abundance in the ER during viral infection (Figure 35).

In addition, NEs from mock-infected cells were isolated to establish the composition of the NE specifically in Hela cells prior to infection. If proteins are involved in primary envelopment, I expect to have an enrichment of these proteins in HSV-1 infected MMs compared with mock-infected MMs. Furthermore, these proteins will be less abundant in mock-infected NEs compared with HSV-1 MMs as a result of translocation from the NE into the ER.

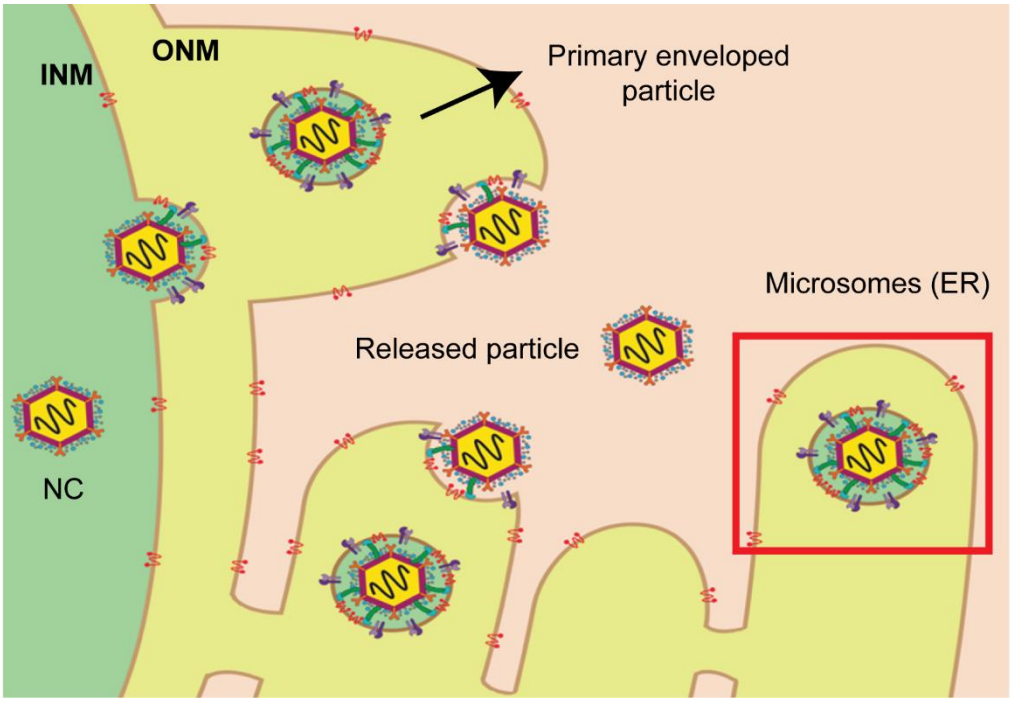

Figure 35. Schematic representation of the isolation of MMs to detect host proteins involved in HSV-1 egress and potential primary enveloped particles (PEP) trapped in the ER. *Nucleocapsids (NC) synthesized in the nucleus bud at the INM forming PEP that subsequently fuse with the ONM. In some cases, due to the continuity of the NE and ER lumen, they can also fuse with the ER. In both cases naked capsids are released into the cytoplasm while the primary envelope derived from the INM and containing host proteins remains in these structures (ER and ONM). Host proteins involved in primary envelopment and released into the ER and ONM during de-envelopment might be detected by the isolation of MMs (membranous structures from the ER). In addition, PEP might be captured inside MMs because as 200-400 nm structures they are large enough to accommodate the ~125 nm PEP.*

As at least a portion of the total protein pool for proteins involved in secondary envelopment might diffuse into the ER, such changes might be measured as an increase in the MMs fraction. Thus, it was necessary to harvest cells for fractionation at a time when nuclear egress is heavily engaged, but before secondary envelopment proteins are being heavily produced. These proteins will flood the ER in preparation for secondary envelopment, so that harvesting too late in infection might confuse the identification of nuclear egress proteins. Therefore, it was

important to first determine the optimal time during infection where nuclear egress has started but before secondary envelopment. To do this, the expression of two viral proteins, US3 and gC was tracked during the course of the infection in Hela cells. US3 is a kinase expressed at early time points before primary envelopment. On the other hand, gC is a component of the final envelope that is acquired in the Golgi during secondary envelopment when viral particles have accumulated in the cytoplasm after their release from the nucleus. Thus, the expression of gC will indicate the prevalence of virus particles already in the cytoplasm. US3 expression in HSV-1 infected Hela cells was detectable at 3 hpi, but it began to be highly expressed at 9 hpi, reaching maximal levels by 12 hpi (Figure 36, A). At this time, gC started to be detectable, increasing expression levels by 24 hpi. These results suggested that the best time to increase the possibility of having viral particles in the process of nuclear egress and minimize capturing changes in the ER and Golgi associated with secondary envelopment was before 12 hpi (Figure 36, A).

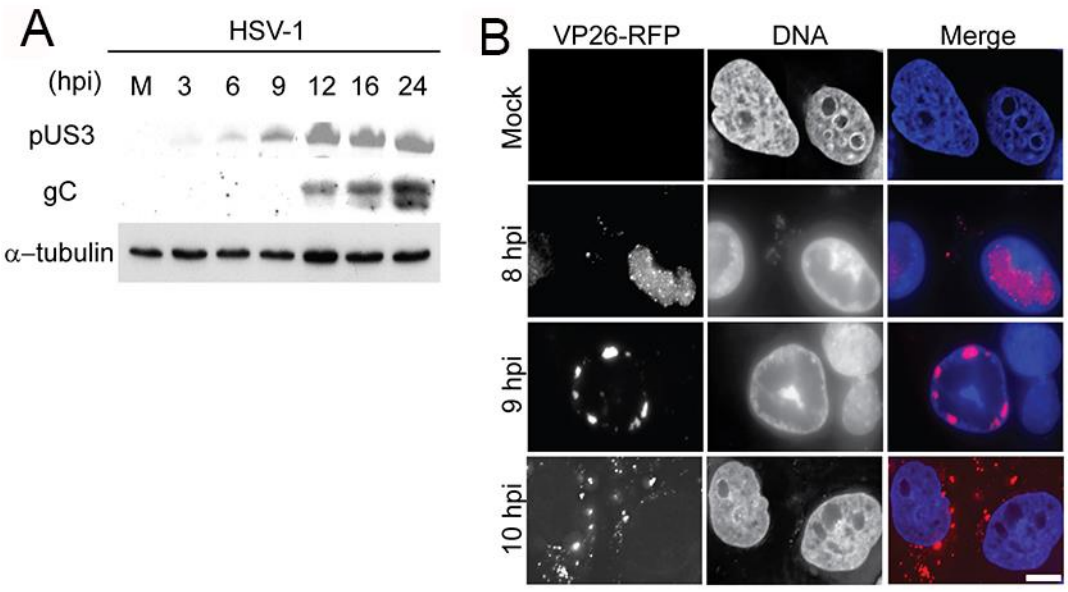

Figure 36. Optimized conditions for HSV-1 MMs isolation. (A) *An expression time course of US3 and gC viral proteins was analyzed by Western blot isolate HSV-1 infected MMs before significant secondary envelopment has occurred. Cell lysates from Hela cells infected at MOI 10 were prepared at indicated times post-infection. α-tubulin was used as a loading control.* ***(B)*** *Fluorescence microscopy images of an HSV-1 strain with VP26 capsid*

protein fused with RFP in Hela cells after 8, 9 and 10 hpi. At 8 hpi most of VP26 signal was located inside the nuclei of infected cells. At 9 hpi cells started to show perinuclear localization of VP26. At 10hpi some viral particles were detected in the cytoplasm of infected cells. Scale bar, 10 µm

As an independent measure, a parallel experiment was run to determine the cellular localization of HSV-1 at different times post infection. An HSV-1 strain containing the VP26 capsid protein tagged with RFP was followed in a time course experiment by fluorescence microscopy. VP26 is a basic 12 KDa protein encoded by the UL35 gene that decorates the outer surface of the capsid shell forming a layer between the capsid and the tegument and it is acquired by the viral particle inside the nucleus of the infected cells. Fluorescence microscopy revealed that at 8 hpi most of infected cells contained viral particles inside the nuclei. However, at 9 hpi viral particles are visible in the periphery of the nucleus close to the NE while at 10 hpi some viral particles are already presented in the cytoplasm of infected cells (Figure 36, B). Based on this observation, together with the presence of gC at 12 hpi, ER-enriched MMs were isolated between 8 and 9 hpi in order to increase the probability of having viral particles in the process of nuclear egress

Once the optimal time frame in which most of viral particles will be in the process of nuclear egress at the NE was established, I proceeded with the protocol to isolate MMs. For this, 30 L of Hela cells were grown in roller bottles and infected with HSV-1 at a MOI of 10 in order to ensure a rapid and even infection throughout the cell population. After 8 hpi, cells were collected by trypsinization and collected by centrifugation.

MMs and NEs were prepared following previous published protocols from the lab (Figure 37, A). To isolate NEs, nuclei were first isolated from Hela cells treated with hypotonic lyses buffer using a tight dounce homogenization (Figure 37, B). Nuclei were pelleted to separate them from small vesicles and other cytosolic components such as mitochondria, which will be present in the supernatant of the prep (post nuclear supernatant), also containing the ER (MMs). To float/remove contaminating membranes, nuclei were resuspended in a solution containing 1.8M sucrose and pelleted through a 2.1M sucrose cushion. NEs were then prepared from isolated

nuclei by multiple rounds of digestion in order to remove nucleoplasmic content. To break chromatin up into small pieces, enzymatic digestion of DNA and RNA was performed. To ensure efficient chromatin removal during NE preparation, DAPI staining was used to check under the fluorescent microscope that chromatin has been removed. The fluorescence intensity of NE digested samples is much fainter after chromatin digestion compared with control, with only the presence of chromatin in a few areas around the nuclear rim and little fluorescence signal remaining in the nucleoplasm (Figure ***38***, A).

MMs from HSV-1 and mock infected cells were isolated following similar established procedures. Post-nuclear supernatant containing cytosolic components such as the ER (MMs) was first subjected to centrifugation to pellet and remove mitochondria and other debris. After this, MMs were resuspended in a 2M sucrose solution and overlaid with 1.86 M and 0.25 M sucrose layers. This was then subjected to centrifugation allowing MMs to float upward into the less dense sucrose layer. MMs were found at the interphase between the 1.8 M sucrose layer and the uppermost 0.25 M sucrose layer, giving rise to a fluffy transparent-white fraction (Figure ***38***, B). The microsomal bands were recovered by aspiration and sucrose present in the fractions was diluted before pelleting the membranes by ultracentrifugation.

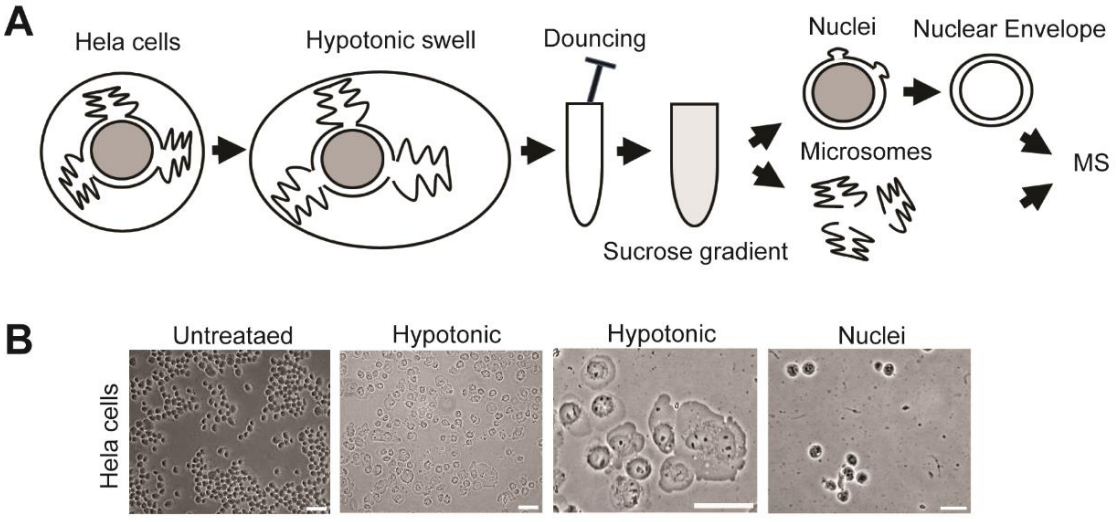

Figure 37. Isolation of MMs and NEs for proteomic analysis. (A) *Method schematic. Cells were disrupted and lysed using a dounce homogenizer after hypotonic swelling. Nuclei were subsequently cleaned of contaminating membranes by pelleting through sucrose gradients. NEs were prepared by subsequently digesting and removing DNA and RNA. Separately, MMs were prepared from the crude cellular membrane fraction by floating (after pelleting mitochondria) through sucrose gradients and collecting the microsome-enriched fraction. Cellular fractions from mock and HSV-1 infected cells were analysed by mass spectrometry to identify host proteins released into the ONM during HSV-1 egress, that once in the ONM can diffuse to the ER and INM. (**B)** Cell fractions. Mock and HSV-1 infected Hela cells were swollen hypotonically (middle panels) and dounce homogenized (right panel) to release nuclei. Phase-contrast light microscope images are shown. Scale bars, 10 µm.*

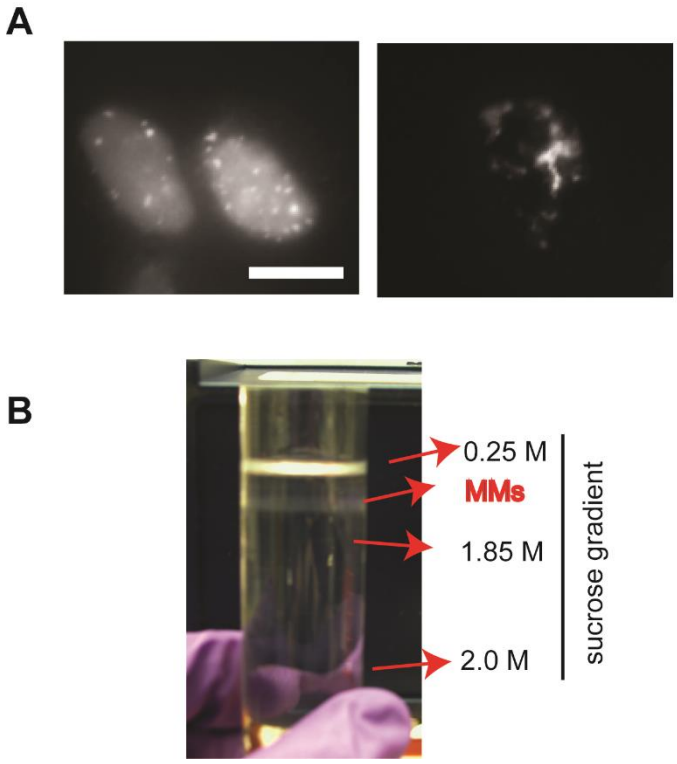

Figure 38. MM and NE isolation. *(**A)** Removal of chromatin from purified nuclei, nuclei stained with DAPI and imaged with fluorescence microscope. Purified nuclei without chromatin digestion (left image) compared with purified nuclei after digestion with DNase I and RNase (right image). The majority of chromatin has been removed except areas in where it is tightly associated with NE. (**B)** Isolation of MMs in a sucrose gradient. MMs are found at the interphase between the 1.85 M and 0.25 sucrose layer. They present a fluffy-white appearance. Scale bar 10 µm.*

In order to analyse the purity of the NE and MM fractions, Western blot analyses were performed to detect the expression of specific NE and MM markers (Figure 39, A). In addition, a Golgi marker in both fractions was tested to assess contamination with Golgi membranes. In the case of the NE fractions, nuclear lamins and NETs should become significantly enriched after the isolation. NE markers Lap2β and Lamin A/C were only found in NE fractions while they were absent from ER fractions. On the other hand, the ER marker calnexin was predominantly expressed in the MM fraction with a small amount in the NE fraction (Figure 39, A). This result was expected since the ONM is continuous with the ER so many proteins are shared between these two structures. Importantly, both NE and MM fractions were free of contamination with the Golgi membranes that function in secondary envelopment as the Golgi marker GM-130 was absent from the fractions (Figure 39, B). In addition, Coomassie staining from MMs and NEs fractions showed that there was a clear distinction in the composition of these two fractions (Figure 39, C).

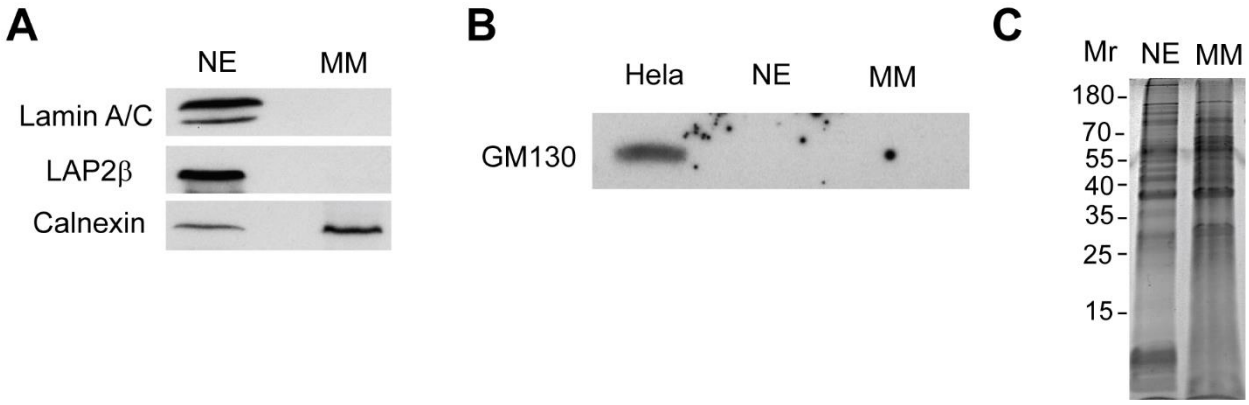

Figure 39. Cell fraction purity. (A) *Western blot of NE and MM fractions stained with ER and NE markers to determine fraction purity. The ER marker calnexin was present in both NE and MM fractions as expected because the ONM is continuous with the ER and many proteins are shared. In contrast, the NE markers lamin A/C and Lap2β were absent from MMs. Similar amounts of total protein were loaded as in (C). (**B)** Western blot of total protein lysates Hela, NE and MMs fractions stained with GM130, a Golgi marker to show the*

absence of Golgi membranes in both fractions ***(C)*** *Coomassie-stained gel of NE and MMs fractions showed a clear difference in protein composition.*

To further confirm the isolation of MMs, EM was performed on HSV-1 infected MMs with the assistance of Alexander Makarov. The electron micrographs clearly showed the presence of the expected single membrane vesicles corresponding to MMs. These microsomal structures are around 200-400 nm of diameter and in some cases they are presented as perfect spherical vesicles. However, some MMs seem to be open as a result of the processing of the sample for EM (Figure 40, A). In addition to this, some electron micrographs showed the presence of electron dense symmetrical structures of around 100 nm diameter inside these microsomal vesicles with the appearance of virus particles (Figure 40, B). These particles might have been produced during douncing due to the weakened NE or they might be PEP that have escaped from the NE lumen and diffused into the ER lumen. Based on only EM images alone I could not confirm the identification of these particles as primary enveloped virions. However, due to the MMs isolation time frame and the appearance of these structures under EM, it is likely that they are PEP that have been either trapped during the isolation procedure or released into the ER during primary envelopment at the NE. These particles observed in EM micrographs presented a smooth envelope and were characterised by a clear halo between the bordered rim of the nucleocapsid and primary tegument, thus further arguing they are PEP because no surface projections characteristic of secondary enveloped particles could be detected in the particle membranes.

Although further experiments such as immunogold EM will be needed to confirm the identity of these particles trapped inside MMs by the identification of proteins already known to be part of the PEP, such as UL31 and UL34, this approach could potentially be used with future modifications to obtain a pure population of PEP.

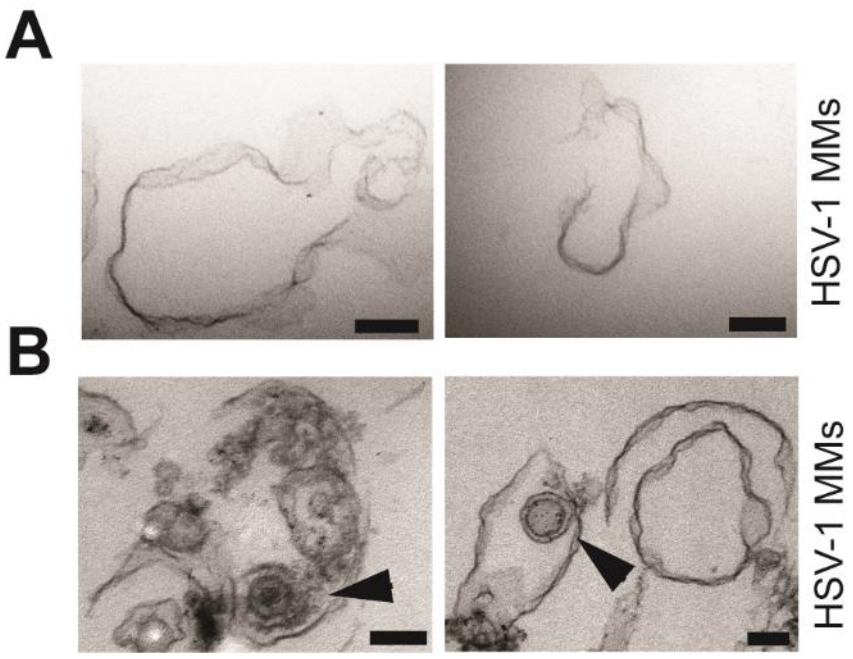

Figure 40. Ultrastructure of isolated MMs from HSV-1 infected cells. *Electron micrographs showed the characteristic single-membrane structure of the MMs. (**A)** MMs without presence of viral particles in its interior. (**B)** MMs containing electron dense symmetrical structures of around 100 nm diameter (arrows) that probably represent primary enveloped particles trapped in the ER during primary envelopment. Scale bars, 100 nm. Experiment performed with the assistance of Alexander Makarov.*

5.3. Identification of potential viral proteins present in primary enveloped virions

The composition of primary enveloped virions is only partially known due to difficulties in isolating this intermediate viral form for proteomic analysis. Mass spectrometry analysis was performed by our collaborators Selene K. Swanson and Laurence Florens using Multi-Dimension Protein Identification Technology (MudPIT) LC/LC/MS/MS approach on each of the fractions. As expected from the EM structures with the appearance of viral particles, HSV-1 proteins were detected in the HSV-1 infected MMs. Particularly, 35 HSV-1 proteins were identified and interestingly, 7 of these 35 identified proteins were previously found in a study that

attempted to isolate and identify the protein composition of primary enveloped virions (Padula, Sydnor et al. 2009). The 7 proteins (out of 8) that were found in this earlier study as well as in our proteomic data sets included different known tegument proteins such as VP22, the UL34 protein, already known for its role during herpesvirus egress at the NE and its unique presence in PEP and the gD protein, previously suggested to be associated with HSV-1 primary virions. Surprisingly, the viral protein UL31, which is known to be associated with UL34 forming the NEC complex during primary envelopment, failed to be identified in Padula´s study. However, both proteins were found in our datasets (Table 12).

In addition to the proteins previously identified in Padula´s study, we managed to find several other tegument proteins and glycoproteins. It is important to note that the relative abundance of the glycoproteins identified in our study can be broken down into two groups based on their dNSAF scores, a measure of the percentage of the total mass of the mass spectrometry run accounted for by a particular protein based on spectral abundance and its molecular weight. The first group including gD, gB and gC were all based on abundance estimated from spectral counts present at roughly 6X greater abundance than the others detected in the second group of glycoproteins that included gE, gM, gH and gI (Table 12).

This data is consistent with previous studies in which gD, gB and gC were associated with primary virions (Torrisi, Di Lazzaro et al. 1992, Jensen and Norrild 1998). Moreover, gB has been shown to be implicated in fusion with the ONM during egress (Wisner, Wright et al. 2009). Hence, the glycoproteins presenting a higher spectral abundance are likely to be present in primary envelopes and participate in primary envelopment while the less abundant glycoproteins are simply beginning to be expressed in the ER and in the process of moving from the ER to the Golgi in where they will support secondary envelopment. Nonetheless, though the trend may be real, it is likely an oversimplification as gH was also implicated in ONM fusion (Farnsworth, Wisner et al. 2007, Wright, Wisner et al. 2009) despite that our data place it in the less abundant set.

I postulate that the additional tegument proteins identified in our proteomic analyses are likely to belong to PEP. As these tegument proteins are not transmembrane proteins, they would have been lost during the purification of MMs unless they

belong to primary envelopes captured in the MMs as part of the de-envelopment process or as part of primary enveloped virions captured within the MMs (Figure 40, B). All viral proteins identified in HSV-1 MMs are listed in Table 12 with the unique peptides (P), spectral counts (S) and dNSAF values associated to them.

Table 12. Abundance of viral proteins identified in HSV-1 MMs.

Rank based on dNSAF values

Viral Protein	P	S	dNSAF
US6 Glycoprotein D	7	38	0.00303
UL27 Glycoprotein B	14	62	0.00216
UL44 Glycoprotein C	6	30	0.00185
Nuclear egress membrane protein pUL34	4	15	0.00171
Virion protein US2	4	14	0.00151
Membrane protein UL45	2	7	0.00128
UL49 Tegument protein VP22	4	11	0.00115
UL19/VP5 Major capsid protein	18	46	0.00105
UL48 Tegument protein VP16	6	16	0.00103
UL50 Deoxyuridine triphosphatase	3	12	0.00102
US8 Glycoprotein E	8	16	0.00091
UL18/VP23 Capsid triplex subunit 2	4	9	0.00089
UL46 Tegument protein VP11/12	7	19	0.00083
UL47 Tegument protein VP13/14	7	14	0.00063
UL10 Glycoprotein M	1	8	0.00053
UL42 DNA pol processivity subunit	4	8	0.00052
US7 Glycoprotein I	3	6	0.00048
UL40 Ribonucleotide reductase subunit 2	3	5	0.00046
Tegument protein UL7	3	4	0.00042
UL22 Glycoprotein H	5	11	0.00041
pUL31 Nuclear egress lamina protein	2	4	0.00041
UL29/ICP8 Single-stranded DNA binding protein	7	15	0.00039
UL39 Ribonucleotide reductase subunit 1	8	14	0.00039
Tegument protein UL51	2	3	0.00039

ICP4	10	15	0.00036
US10	2	3	0.0003
UL12 Deoxyribonuclease	4	6	0.0003
UL54 Multifunctional expression regulator	3	4	0.00025
UL24	1	2	0.00023
US1/ICP22	2	3	0.00023
UL41 Tegument host shutoff protein	2	3	0.00019
Tegument protein UL21	1	3	0.00018
UL26/VP24/VP21 Capsid maturation protease	2	3	0.00015
UL39/VP19C Capsid triplex subunit 1	1	2	0.00014
Tegument protein UL25	2	2	0.00011

5.4. Mass Spectrometry analysis for the identification of host proteins involved in HSV-1 nuclear egress

It is reasonable to expect that proteins present in the INM recruited during primary envelopment and de-envelopment should be more abundant in the MMs fraction from HSV-1 infected cells compared with mock-infected cells as they would be released into the ONM during de-envelopment and diffuse into the ER. Thus, I expected the proteins of greatest interest to occur in the NE fraction before infection and later be increased in the HSV-1 infected MMs fraction.

I calculated the relative enrichment ratio for each protein based in their dNSAF score in the HSV-1 MMs versus mock MMs. The Distributed Normalized Spectral Abundance Factor (dNSAF) is a value used to measure protein abundance based on spectral counts that are distributed to each protein based on the amount of unique peptides/spectral counts found for each protein and as a reflection of their mass out of the total mass for a particular mass spectrometry run. I extracted all proteins in the HSV-1 infected MMs that were at least 30% increased over the mock MMs based on their dNSAF values (all proteins with a ratio smaller than 1.3 were discarded from the analysis focusing only on those proteins presenting a HSV-1 MMs/mock MMs ≥ 1.3). Only the 8.8% (146 host proteins) of the total proteins

detected in the dataset presented an increase of 30% or higher in HSV-1 MMs while around the 26.5% of proteins of the total proteins detected in the dataset were unchanging in dNSAF score**.**

The 146 host proteins presenting a 30% increase were selected and are listed in Table 13.

Table 13. Abundance and relative ratios of host proteins with a 30% enrichment in HSV-1 infected MMs.
Rank based on HSV1-MMs:Mock-MMs dNSAF ratio

Gene	***HSV1MMs dNSAF***	***MockMMs dNSAF***	***MockNE dNSAF***	***HSV1MMs:Mock-MMsjh***	**MockNE:Mock-MMs**
NOP10	0.000491	X	0.001925	INF	INF
ARF4	0.000349	X	0.000076	INF	INF
SELT	0.000322	X	0.000211	INF	INF
AGPAT5	0.000173	X	0.001128	INF	INF
APMAP	0.000151	X	0.000197	INF	INF
RAB38	0.000149	X	0.000778	INF	INF
SNRNP70	0.000144	X	0.000470	INF	INF
CHTOP	0.000127	X	0.000828	INF	INF
ZFPL1	0.000101	X	0.000662	INF	INF
RAB6B	0.000101	X	0.000632	INF	INF
ABHD12	0.000079	X	0.000206	INF	INF
MOSPD2	0.000069	X	0.000361	INF	INF
WLS	0.000058	X	0.000378	INF	INF
AATF	0.000056	X	0.000147	INF	INF
ATP8B2	0.000051	X	0.000067	INF	INF
SLC39A6	0.000042	X	0.000054	INF	INF
DDX27	0.000039	X	0.000103	INF	INF
ATP9B	0.000027	X	0.000107	INF	INF
IGF2R	0.000013	X	0.000016	INF	INF
NOP2	0.000149	0.000015	0.000049	9.933333	3.266667
HNRNPC	0.000411	0.000042	0.000134	9.785714	3.190476

TUBA1C	0.006650	0.000718	0.000079	9.261838	0.110028
PAF1	0.000194	0.000026	0.000169	7.461538	6.500000
TUBA8	0.000164	0.000022	0.000021	7.454545	0.954545
AFG3L2	0.000237	0.000032	0.002009	7.406250	62.781250
ITPR3	0.000035	0.000005	0.000323	7.000000	64.600000
VAPB	0.002286	0.000363	0.003261	6.297521	8.983471
SLC4A7	0.000333	0.000056	0.000218	5.946429	3.892857
NOLC1	0.000090	0.000018	0.000478	5.000000	26.555556
RAB34	0.000204	0.000041	0.000267	4.975610	6.512195
PTGS2	0.000104	0.000021	0.000408	4.952381	19.428571
VAMP7	0.000702	0.000142	0.002523	4.943662	17.767606
HNRNPA2B1	0.001290	0.000261	0.000241	4.942529	0.923372
STEAP2	0.000138	0.000028	0.000090	4.928571	3.214286
LMNB1	0.000167	0.000034	0.000109	4.911765	3.205882
EPHB4	0.000229	0.000047	0.000233	4.872340	4.957447
GOLGA5	0.000129	0.000035	0.001236	3.685714	35.314286
ATP11B	0.000080	0.000022	0.000314	3.636364	14.272727
RPN1	0.002952	0.000817	0.001218	3.613219	1.490820
HNRNPR	0.000297	0.000090	0.000194	3.300000	2.155556
TMEM30A	0.000348	0.000106	0.000227	3.283019	2.141509
STOM	0.000546	0.000177	0.000428	3.084746	2.418079
PRPH	0.005996	0.001976	0.003582	3.034413	1.812753
SPCS3	0.001048	0.000353	0.000912	2.968839	2.583569
ALYREF	0.000714	0.000241	0.000467	2.962656	1.937759
DES	0.001290	0.000460	0.000262	2.804348	0.569565
TRPM4	0.000026	0.000010	0.000101	2.600000	10.100000
ADAM17	0.000038	0.000015	0.000199	2.533333	13.266667
PTGS1	0.000105	0.000042	0.000411	2.500000	9.785714
PIGK	0.000080	0.000032	0.003742	2.500000	116.937500
LUC7L	0.000085	0.000034	0.000569	2.500000	16.735294
TM9SF3	0.000107	0.000043	0.001185	2.488372	27.558140
PTPN1	0.000072	0.000029	0.000189	2.482759	6.517241
PCDH19	0.000057	0.000023	0.000112	2.478261	4.869565
PPIC	0.000297	0.000120	0.000387	2.475000	3.225000

RPS25	0.000754	0.000305	0.000328	2.472131	1.075410
NDUFA4	0.000388	0.000157	0.001521	2.471338	9.687898
DPM1	0.000242	0.000098	0.000158	2.469388	1.612245
ARL6IP5	0.000669	0.000271	0.001092	2.468635	4.029520
EBAG9	0.000148	0.000060	0.000771	2.466667	12.850000
MYO1F	0.000086	0.000035	0.000037	2.457143	1.057143
SORCS2	0.000054	0.000022	0.000283	2.454545	12.863636
PTPRK	0.000044	0.000018	0.000029	2.444444	1.611111
CLCN7	0.000078	0.000032	0.000102	2.437500	3.187500
LRRC8C	0.000078	0.000032	0.000256	2.437500	8.000000
SLC23A2	0.000048	0.000020	0.000126	2.400000	6.300000
PPIB	0.002619	0.001178	0.001331	2.223260	1.129881
LAMP1	0.000678	0.000305	0.000295	2.222951	0.967213
HNRNPH2	0.000756	0.000351	0.000183	2.153846	0.521368
P4HB	0.002289	0.001077	0.000242	2.125348	0.224698
ARL8B	0.004056	0.001915	0.000662	2.118016	0.345692
DDX21	0.000264	0.000125	0.000230	2.112000	1.840000
ANKH	0.001980	0.000957	0.000083	2.068966	0.086729
LMNA	0.000994	0.000498	0.002535	1.995984	5.090361
RAB11B	0.007065	0.003560	0.012242	1.984551	3.438764
MTDH	0.000216	0.000109	0.000494	1.981651	4.532110
RPS19	0.001734	0.000877	0.000566	1.977195	0.645382
HNRNPU	0.000624	0.000316	0.000204	1.974684	0.645570
SRSF3	0.001078	0.000559	0.001051	1.928444	1.880143
CD34	0.000571	0.000297	0.000107	1.922559	0.360269
TMED10	0.002727	0.001452	0.001125	1.878099	0.774793
RAB9A	0.000469	0.000253	0.001226	1.853755	4.845850
EFNB2	0.000354	0.000191	0.000493	1.853403	2.581152
ADAM10	0.000252	0.000136	0.000329	1.852941	2.419118
KIDINS220	0.000053	0.000029	0.000672	1.827586	23.172414
EPHB2	0.000423	0.000232	0.000525	1.823276	2.262931
CSPG4	0.000068	0.000038	0.000088	1.789474	2.315789
TARDBP	0.000380	0.000215	0.000099	1.767442	0.460465
SPCS2	0.001391	0.000788	0.001635	1.765228	2.074873

ITGAV	0.000314	0.000178	0.000779	1.764045	4.376404
PI4K2A	0.000328	0.000186	0.000429	1.763441	2.306452
RPL3	0.001326	0.000758	0.000509	1.749340	0.671504
SRSF7	0.000469	0.000270	0.000509	1.737037	1.885185
HNRNPF	0.000617	0.000356	0.000198	1.733146	0.556180
RAB1A	0.005357	0.003093	0.036801	1.731975	11.898157
LMAN2	0.000618	0.000357	0.002537	1.731092	7.106443
RAB18	0.003509	0.002038	0.045044	1.721786	22.102061
TUBB	0.005893	0.003463	0.000555	1.701704	0.160266
MET	0.000045	0.000027	0.000029	1.666667	1.074074
HNRNPM	0.000431	0.000261	0.000112	1.651341	0.429119
EMC3	0.000482	0.000292	0.001888	1.650685	6.465753
STX7	0.000241	0.000146	0.001888	1.650685	12.931507
FLNC	0.000652	0.000395	0.000060	1.650633	0.151899
SEC61A1	0.000132	0.000080	0.000759	1.650000	9.487500
SFXN3	0.000193	0.000117	0.000505	1.649573	4.316239
NCAM1	0.000659	0.000400	0.000144	1.647500	0.360000
SCAMP2	0.000382	0.000232	0.001248	1.646552	5.379310
RAB23	0.000265	0.000161	0.000346	1.645963	2.149068
FADS1	0.000125	0.000076	0.000492	1.644737	6.473684
VCAM1	0.000291	0.000177	0.000254	1.644068	1.435028
SLC25A1	0.000202	0.000123	0.000264	1.642276	2.146341
MLEC	0.000215	0.000131	0.001406	1.641221	10.732824
RNF121	0.000192	0.000117	0.000377	1.641026	3.222222
DKC1	0.000124	0.000075	0.000081	1.640000	1.080000
NPC1	0.000049	0.000030	0.000096	1.633333	3.200000
FLOT2	0.001248	0.000773	0.001343	1.614489	1.737387
HIST3H2A	0.004352	0.002733	0.002030	1.592389	0.742774
ANXA2	0.046451	0.029388	0.003270	1.580611	0.111270
NCL	0.001151	0.000735	0.000636	1.565986	0.865306
GNAQ	0.001537	0.000995	0.000114	1.544724	0.114573
ITGA6	0.000288	0.000187	0.000263	1.540107	1.406417
GNAO1	0.001171	0.000771	0.000145	1.518807	0.188067
KRAS	0.002006	0.001340	0.000109	1.497015	0.081343

SPTLC2	0.000168	0.000113	0.000146	1.486726	1.292035
TMX3	0.000208	0.000140	0.000814	1.485714	5.814286
SGCD	0.000653	0.000440	0.000852	1.484091	1.936364
SLC1A5	0.000174	0.000118	0.000228	1.474576	1.932203
H2AFV	0.000827	0.000567	0.000926	1.458554	1.633157
PCBP1	0.000820	0.000570	0.000231	1.438596	0.405263
CLPTM1	0.000376	0.000266	0.002025	1.413534	7.612782
RPL36	0.001197	0.000848	0.003519	1.411557	4.149764
SLC25A11	0.000400	0.000284	0.000523	1.408451	1.841549
RAB2A	0.002520	0.001800	0.011039	1.400000	6.132778
RAB35	0.002658	0.001899	0.002655	1.399684	1.398104
MYO1B	0.001487	0.001074	0.000381	1.384544	0.354749
RAP2C	0.001088	0.000787	0.000897	1.382465	1.139771
SLC12A4	0.000146	0.000106	0.000908	1.377358	8.566038
ECE1	0.000415	0.000302	0.000542	1.374172	1.794702
SSR3	0.000849	0.000619	0.001775	1.371567	2.867528
PTPRA	0.000396	0.000289	0.000518	1.370242	1.792388
SACM1L	0.000321	0.000238	0.000769	1.348739	3.231092
DDX17	0.000762	0.000571	0.000056	1.334501	0.098074
MRC2	0.000149	0.000112	0.000861	1.330357	7.687500
RHOA	0.002438	0.001841	0.000878	1.324280	0.476915
NOLC1	0.000405	0.000309	0.002752	1.310680	8.906149
NPM1	0.004811	0.003679	0.000559	1.307692	0.151943

These proteins were analysed for specific gene ontology (GO) terms in order to determine if there were any functionally interesting categories of proteins that might be involved during HSV-1 egress at the NE. The relative proportions of the various GO-terms were calculated from the relative abundances of the genes identified from each GO category and they were plotted as pie charts. This was later compared to a pie chart compiled from all the genes in the human genome considering the same categories (Figure 41, A).

Several GO-terms were strongly enriched in the select HSV-1-infected MMs including vesicle organization (GO:0016050), vesicle mediated transport proteins

(GO:0016192), nuclear transport (GO:0051169) and membrane fusion proteins (GO:0061025) (Figure 41A). The vesicle organization, the vesicle mediated transport and membrane fusion category presented a 6, 3 and 4-fold enrichment respectively in HSV-1 MMs (Figure 41, B). The presence of proteins involved in membrane organization and vesicle fusion events captured my attention, not only for the big increase they presented compared with the total human genome, but also for their potential relevance to herpesvirus nuclear egress as they might be mediating vesicle fusion events assisting viral budding during egress at the NE.

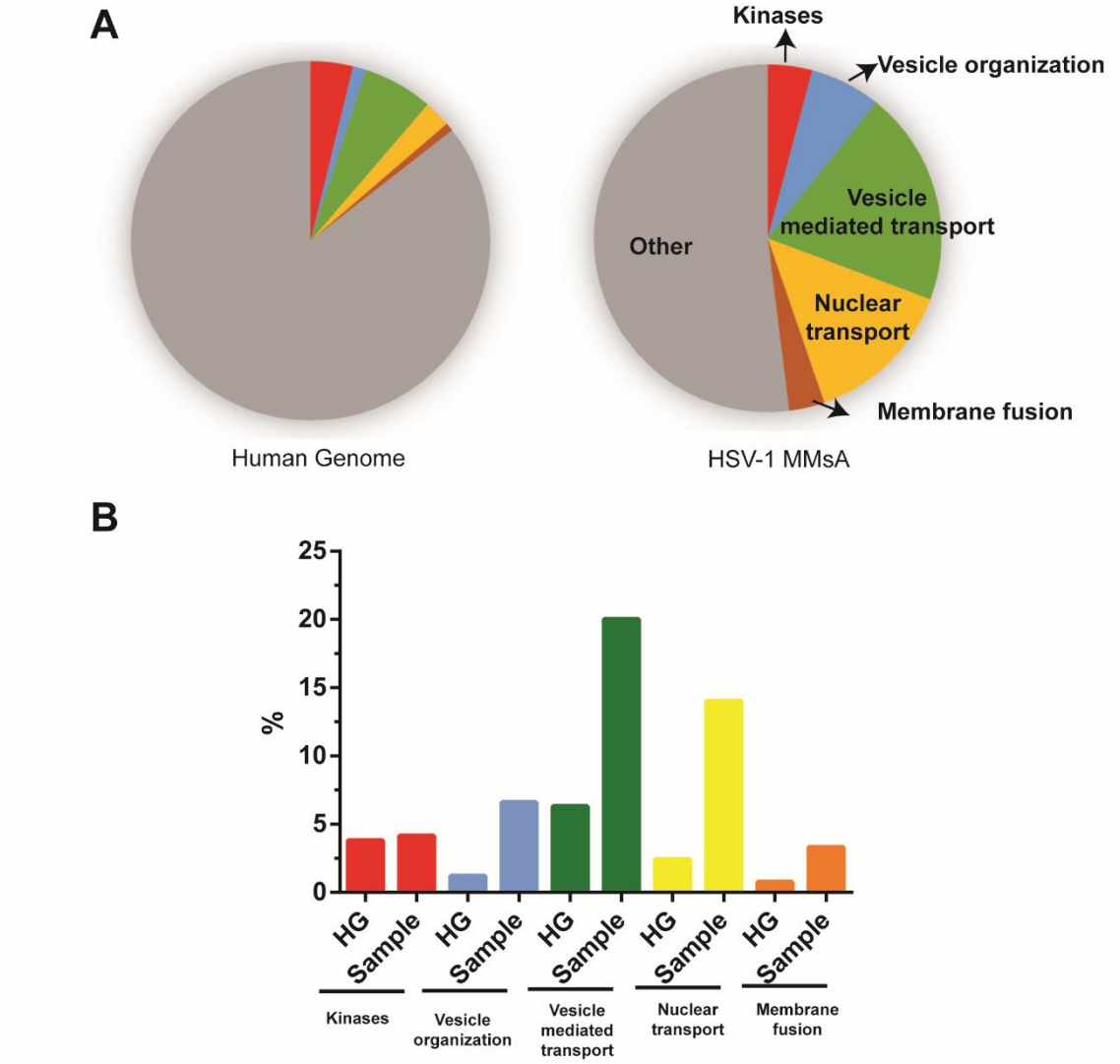

Figure 41. Gen Ontology (GO) classification for enriched proteins from HSV-1 infected MMs. (A) *Proteins increased at least 30% in HSV-1 MMs versus mock MMs were analysed for specific GO terms and compared with their representation in the total human genome. (**B)** Representation of the relative abundance of specific GO terms for enriched proteins presented HSV-1 MMs (sample) versus the total human genome (HG). Vesicle mediated transport proteins represents 20% in HSV-1 MMs versus 6.6 % in the total human genome.*

These 146 selected proteins were then sorted based on their presence in the NE, considering only those that were at least 40% enriched in the NE versus the MMs control to suggest that they were reasonably abundant in the NE to begin with (all proteins with a ratio smaller than 1.4 were discarded from the analysis focusing only on those proteins presenting a Mock-infected NEs/Mock-infected MMs ≥ 1.4). 107 of the 146 proteins followed these selection criteria based on their relative enrichment ratio Mock-infected NEs/Mock-infected MMs. Proteins involved in vesicle fusion events were still enriched in this
group of selected proteins (23.25%) compared with the number of vesicle fusion proteins present in the total human genome (6.3%) (Figure 42).

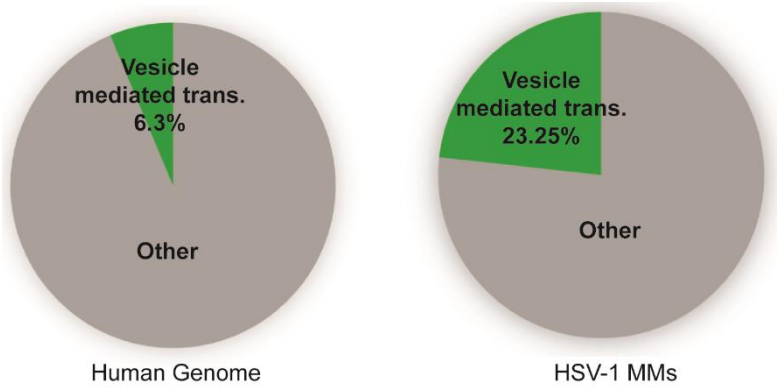

Figure 42. Vesicle mediated transport Gen Ontology (GO) term. *Proteins with a 30% enrichment in HSV-1 MMs versus control and enriched at least 40% in NE versus MMs of mock cells were analysed for the GO term vesicle mediate transport (GO:0016192). Vesicle mediated transport proteins represent 23.25% of the enriched proteins detected in HSV-1 MMs compared with 6.3% of all genes encoded in the human genome.*

Next, the 107 selected proteins were individually analysed for specific GO-terms that are represented in a table in which GO term categories such as vesicle organization (GO:0016050), small GTPase mediated signal transduction (GO:0007264), or endomembrane system organization (GO: 0010256) were highly overrepresented in some of the HSV-1 enriched proteins (Table 14).

The rest of GO categories analysed were: single-organism membrane organization (GO:0044802), nucleocytoplasmic transport (GO:0006913), vesicle fusion (GO: 0006906), intracellular protein transport (GO:0006886), membrane fusion (GO:0061025), kinase activity (GO:0016301), lipid transport (GO:0006869), cell adhesion (GO:0007155) and endocytosis (GO:0006897).

Some proteins of this list did not present any of the GO terms mentioned above. However, they showed other GO terms and functions that were not considered on this analysis as for example HNRNPC, a protein involved in RNA splicing and gene expression (GO:0008380) or ARL6IP5, a protein involved in apoptotic signalling pathways in response to oxidative stress (GO:0097193).

Table 14. Gen Ontology (GO) terms for the 107 proteins enriched in HSV-1 MMs

Gene	membrane fusion	vesicle fusion	vesicle Organization	cell adhesion	lipid transport	kinase activity	single-organism membrane organization	nucleocytoplasmic transport	small GTPase mediated signal transduction	intracellular protein transport	endocytosis	endomembrane system organization
AATF				■								
ABHD12												
ADAM10												
ADAM17				■								
AFG3L2	■						■			■		
AGPAT5												
ALYREF												
APMAP												
ARF4									■			
ARL6IP5												
ATP11B					■		■					
ATP8B2					■		■					
ATP9B					■		■				■	■
CHTOP								■				
CLCN7												
CLPTM1				■								
CSPG4												
DDX21												
DDX27												
DPM1												
EBAG9												
ECE1												
EFNB2				■								
EMC3												

EPHB2												
EPHB4												
FADS1												
FLOT2												
GOLGA5												
H2AFV												
HNRNPC												
HNRNPR												
IGF2R												
ITGA6												
ITGAV												
ITPR3												
KIDINS220												
LMAN2												
LMNA												
LMNB1												
LRRC8C												
LUC7L												
MLEC												
MOSPD2												
MRC2												
MTDH												
NDUFA4												
NOLC1												
NOLC1												
NOP10												
NOP2												
NPC1												
PAF1												
PCDH19												
PI4K2A												
PIGK												
PPIC												
PRPH												

PTGS1												
PTGS2												
PTPN1												
PTPRA												
PTPRK												
RAB11B												
RAB18												
RAB1A												
RAB23												
RAB2A												
RAB34												
RAB38												
RAB6B												
RAB9A												
RNF121												
RPL36												
RPN1												
SACM1L												
SCAMP2												
SEC61A1												
SELT												
SFXN3												
SGCD												
SLC12A4												
SLC1A5												
SLC23A2												
SLC25A1												
SLC25A11												
SLC39A6												
SLC4A7												
SNRNP70												
SORCS2												
SPCS2												
SPCS3												

SRSF3												
SRSF7												
SSR3												
STEAP2												
STOM												
STX7												
TM9SF3												
TMEM30A												
TMX3												
TRPM4												
VAMP7												
VAPB												
VCAM1												
WLS												
ZFPL1												

5.5. Summary of chapter 5

In this chapter I used a well characterised method, the isolation of microsomes, within the context of HSV-1 nuclear egress as a novel approach to identify cellular proteins that might be playing a role during herpesvirus egress at the NE. EM studies of MMs isolated from HSV-1 infected cells revealed the presence of viral particles that are likely PEP captured within these structures. If so, this technique could provide the opportunity to isolate PEP and study their composition by mass spectrometry analysis.

Mass spectrometry analysis on HSV-1 infected MMs revealed the enrichment of a certain type of host proteins, vesicle membrane fusion proteins, that could be potentially driving nuclear egress of herpesvirus particles. Three of these vesicle membrane fusion proteins that were identified on this study were analysed in detail in the next chapter, which will show their functional relevance during HSV-1 nuclear egress.

Chapter 6

VAPB, Rab11b and Rab18 Contribute to HSV-1 Infectivity by Facilitating Egress through the Nuclear Membrane

6.1. Introduction

As previously described in chapter 5, we postulated that host membrane proteins involved in virus nuclear egress would move from the INM to ONM due to membrane fusion events in primary envelopment and de-envelopment and then diffuse into the ER. For this, MMs and NEs from mock or HSV-1 infected cells were isolated to identify proteins that changed abundance in the ER with infection and might be involved in nuclear egress. One of the more abundant groups of proteins detected in HSV-1 MMs was the one falling under the “vesicle fusion” category.

Herpesviruses frequently co-op host cell proteins to support different steps of their life cycle. Cellular vesicle fusion proteins have been previously described to be involved in EBV egress by the induction of vesicle formation. However, this was not observed for HSV-1 egress (Lee, Liu et al. 2012). The vesicle fusion protein

enrichment observed in HSV-1 MMs led us to hypothesize the potential role of these proteins during nuclear egress.

In this chapter, I will describe the identification and functional characterisation of three vesicle fusion proteins identified in our mass spectrometry datasets, VAPB, Rab11b and Rab18 and their involvement during HSV-1 nuclear egress.

6.2. Vesicle fusion proteins identified in HSV-1 infected MMs

As mentioned before, several Gene Ontology (GO) terms for proteins enriched in HSV-1 infected MMs were strongly linked with vesicle fusion events. Thus, some of the proteins categorized under biological processes for vesicle mediated transport (GO:0016192), vesicle organization (GO:0016050), membrane fusion (GO:0061025) and endomembrane system organization (GO: 0010256) were selected from the list of proteins that were previously ranked based on their 1.3-fold and 1.4-fold enrichment in HSV-1 MMs and mock NE respectively. The stringency of the selection criteria was then increased for this set of vesicle fusion proteins, only considering those candidates that had at least 5 spectra in the NE fraction suggesting their abundance in the sample. The relative enrichment in each of the fractions for these selected proteins was plotted (Figure 43) and their peptides, spectral counts and dNSAF values are given in Table 15.

Table 15. Abundance of vesicle fusion proteins enriched in HSV-1 infected MMs

	HSV-1 infected MMs			Mock infected MMs			Mock infected NEs			Ratios	
Gene	P	S	dNSAF	P	S	dNSAF	P	S	dNSAF	1	2
VAPB	2	7	0.0023	1	3	0.0004	2	8	0.0033	6.3	9.0
VAMP 7	2	4	0.0007	1	2	0.0001	3	11	0.0025	4.9	17.8
RAB1 1B	7	49	0.0071	6	61	0.0036	7	65	0.0122	2.0	3.4
RAB9 A	2	3	0.0005	1	4	0.0003	3	6	0.0012	1.9	4.8
RAB1 A	4	35	0.0054	5	50	0.0031	5	184	0.0368	1.7	11.9
RAB1 8	8	23	0.0035	7	33	0.0020	8	226	0.0450	1.7	22.1
STX7	1	2	0.0002	1	3	0.0001	4	12	0.0019	1.7	12.9
RAB2 A	4	17	0.0025	6	30	0.0018	9	57	0.0110	1.4	6.1
RAB3 5	3	17	0.0027	4	30	0.0019	3	13	0.0027	1.4	1.4

1: Ratio HSV-1 MMs/Mock MMs 2 Ratio Mock NE: Mock MMs

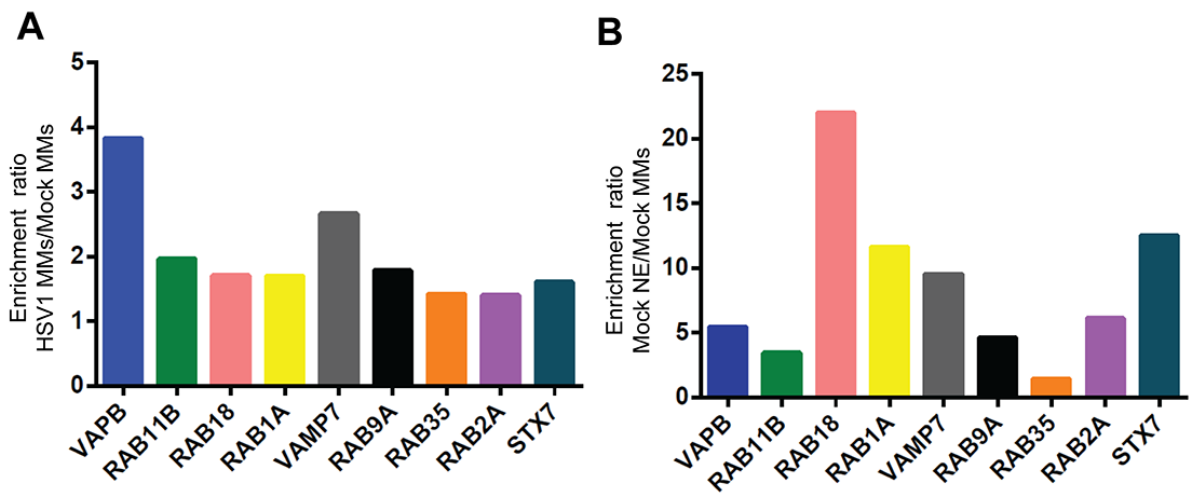

Figure 43. Enrichment of vesicle fusion proteins in HSV-1 infected MMs identified by mass spectrometry. (A) *Protein abundance estimates based on spectral counts and protein molecular weight as a percentage of the total mass of spectra identified per mass spectrometry run (dNSAF) were used to calculate the relative enrichment between the three mass spectrometry datasets (HSV-1 MMs, Mock-infected MMs and Mock NEs). The ratio of dNSAF values for different vesicle fusion proteins between HSV-1 infected MMs and mock-infected MMs* ***(A)*** *and between NEs and mock-infected MMs* ***(B)*** *are shown.*

Three proteins were chosen for detailed analysis upon HSV-1 infection, VAPB, Rab11b and Rab18. VAPB is a member of the Vesicle-associated membrane protein (VAMP)-Associated Protein family of ER C-tail anchored proteins. It functions as an adaptor protein to recruit target proteins to the ER and execute various cellular functions. It has been also suggested to be implicated in ER stress and the unfolded protein response (UPR), ER to Golgi transport and microtubule organization (Peretti, Dahan et al. 2008, Prosser, Tran et al. 2008, Ratnaparkhi, Lawless et al. 2008, Fasana, Fossati et al. 2010). Rab11b and Rab18 are membrane-associated proteins belonging to the Ras-related small GTPases. Rab11b is reported in the recycling and early endosomes (Ullrich, Reinsch et al. 1996, Mammoto, Ohtsuka et al. 1999) while Rab18 is reported also in the ER, endosome and lipid droplets (Lutcke, Parton et al. 1994, Brasaemle, Dolios et al. 2004).

6.3. Knockdown of vesicle fusion proteins results in nuclear accumulation of virus particles and significant reduction of HSV-1 viral titers

The proteins redistributed upon HSV-1 infection according to the mass spectrometry data could directly benefit the virus or reflect a general perturbation of vesicle trafficking during infection.

To determine if they play a role during the life cycle of the virus, siRNA was used to knock down VAPB, Rab18 and Rab11b and the effect on viral titers tested. Rab24 and Rab1a were also knocked down as controls. Rab24 was used as a negative control as it did not increase in the HSV-1 infected MMs compared to mock-infected MMs and it has been previously described as a non-target protein through HSV-1 life cycle. Rab1a was used as a positive control because this protein required for ER-to Golgi complex transport has been shown to be involved in HSV-1 mature particle assembly (secondary envelopment) and there are studies showing that its knockdown reduces viral growth by 60% (Zenner, Yoshimura et al. 2011, Soo, Halloran et al. 2015).

HeLa cells were transfected with siRNA oligos and after 48 h the cells were lysed and analyzed by Western blot (Figure 44, A). VAPB was knocked down to nearly undetectable levels (95%) while the Rab11b and Rab18 protein showed at least 85% of protein silencing. The controls Rab1a and Rab24 were knocked down similarly to roughly 80%. Another set of siRNA transfections was undertaken and at 48 h transfected cells were subsequently infected with HSV-1 at a MOI of 10. At 16 hpi supernatant from these cells was collected and tested by virus titration assay. As expected by previous studies, very little effect of Rab24 knockdown could be observed, while Rab1a knock down reduced viral titers by 62% (Figure 44, B). Interestingly, VAPB, Rab11b and Rab18 vesicle fusion proteins identified by our proteomic approach exhibited a stronger reduction in virus titers than the Rab1a knockdown (Figure 44, B). As an average of three separate experiments, Rab18 knockdown yielded ~70% reduction in virus titers. Rab11b knockdown had an even stronger effect with ~85% reduction in virus titers. Finally, VAPB knockdown showed

the highest effect on viral titres with an over 90% reduction in viral growth (Figure 44, B).

To further confirm these observations and exclude an off-target knockdown, siRNA resistant for VAPB, Rab11b and Rab1a were generated. As expected, the effect on viral titres previously observed was not off-target effect of the siRNAs as the rescue experiments yielded full recovery of virus titres (Figure 44, C).

To determine if the reduction on viral titres is produced by a defect on viral release rather than in viral replication, the effect of VAPB, Rab11b and Rab18 on viral genomes produced was also tested. Supernatants and cell pellets were collected and analyzed by qPCR. As expected from the virus titer experiments, the knockdowns resulted in a very significant reduction in virion (as measured by viral DNA copy number) release from the cell with the control being unaffected, similar to what was found in the titration data (Figure 44, D, left graph). However, qPCR for viral genomes in the infected whole cell pellets revealed that virus production was not significantly altered between the control and VAPB, Rab11b or Rab18 knockdowns (Figure 44, D, right graph). Interestingly, viral genome numbers in the siRNA treated infected cells were all slightly higher than the control, presumably because of their accumulation within the nucleus when the egress pathways are disrupted.

This result suggests that viral replication is not affected when these three vesicle fusion proteins are depleted in HSV-1 infected cells. Thus, the reduction in excreted HSV-1 genomes and the effective viral production in the nucleus is consistent with a role of VAPB, Rab18 and Rab11b in steps for egress as opposed to replication. However, these analyses do not distinguish whether the loss in titers reflects a function in nuclear egress or secondary envelopment. The reduction of viral release could be affected in either the exit of the virus from the nucleus during primary envelopment or the exit of the virus from the ER/Golgi during secondary envelopment. To distinguish between these possibilities, EM of control and siRNA HSV-1 infected cells was performed with the assistance of our collaborators Swetha Vijayakrishnan and Marion McElwee the University of Glasgow. If these vesicle fusion proteins were involved in nuclear egress, viral particles would be observed to accumulate in the nucleus of HSV-1 infected cells.

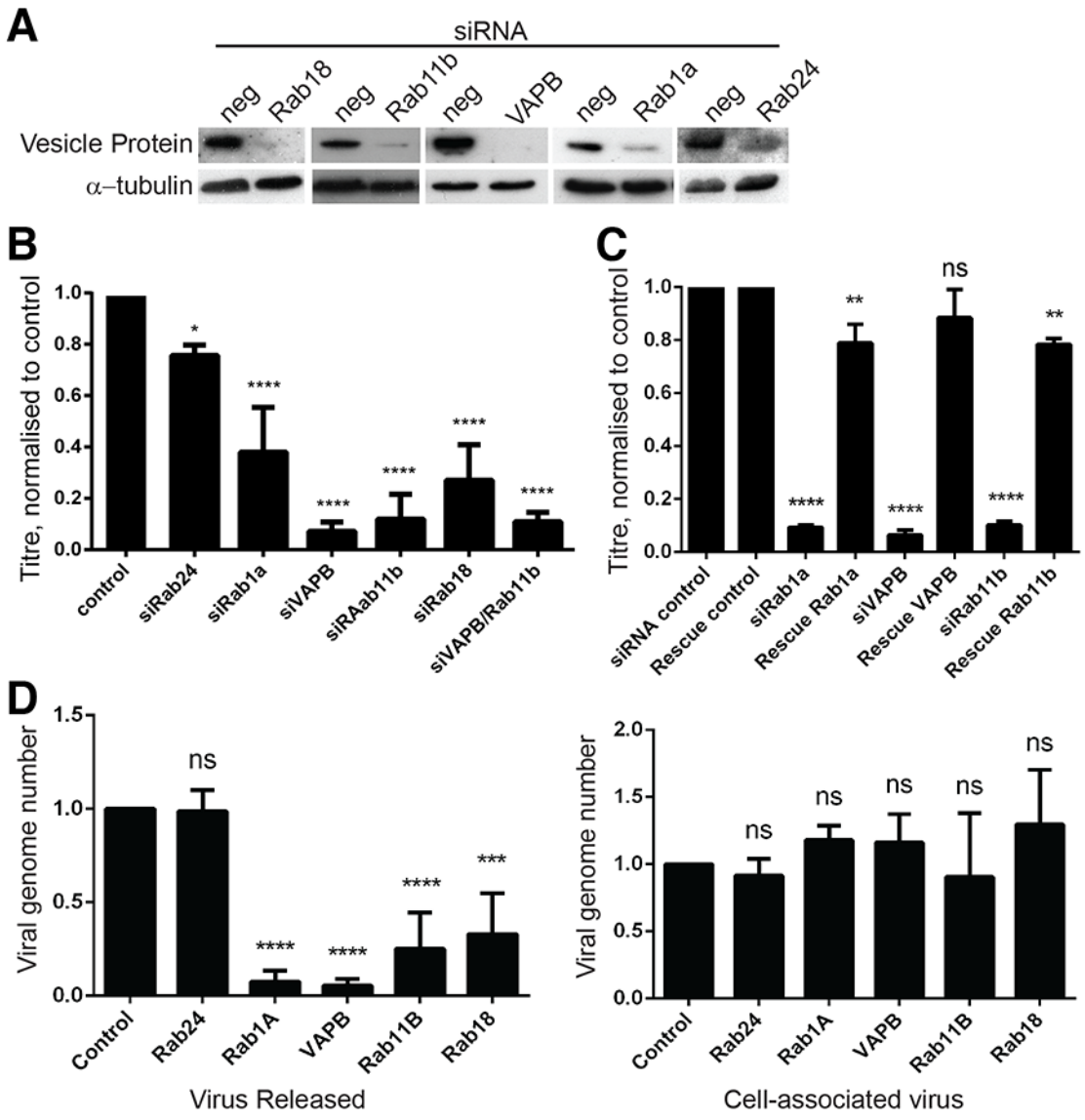

Figure 44. VAPB, Rab11b and Rab18 knockout inhibits HSV-1 infection*. **(A)** HeLa cells were transfected with siRNA oligos for the indicated proteins and after 48 h the cells were lysed and analyzed by Western blot with the indicated antibodies to check protein knockdown**. (B)** Hela cells were transfected with the control, Rab24, Rab1a, VAPB, Rab11b, Rab18, or a combined VAPB and Rab11b siRNA. After 48 h, cells were infected with HSV-1 (MOI, 10) and supernatant virions were collected at 16 hpi. Titers were established on U2OS cells and bars represent the average of three independent experiments, normalized to the control siRNA. Error bars are to the standard deviation and the p-values for comparing each condition with the control are shown (****p ≤ 0.0001; **

*p≤0.005**). (C)** Rescue experiments with cells expressing wild-type protein resistant to the siRNAs were performed. In all cases the cells carrying both the rescue plasmid and the siRNAs recovered to roughly 80-90% of the control virus titers. **(D)** HSV-1 genome copy numbers were determined from released viral particles and from cell pellets by qPCR. HSV-1 genome copy number from viral particles released from infected cells is reduced by 87% in siRab11b, 80% in siRab18 HSV-1 and 90% in siVAPB. However, HSV-1 genome copy* number is unaffected in cell-associated virus compared with control. The p-values for comparing each condition with the control indicate a statistical significance in released virus while there is no significant difference in cell-associated virus (ns). All statistical tests were performed by one-way ANOVA and multiple comparisons were done by Dunnett´s test.

EM of control cells infected with virus yielded the expected distribution with some nuclear particles undergoing assembly and many virus particles accumulating in the cytoplasm at 16 hpi (Figure 45, upper left panel). The same phenotype was observed for the Rab24 knockdown infected cells (Figure 45, upper right panel). However, at 16 hpi, accumulation of a large amount of viral particles was observed in the nucleus of HSV-1 infected cells in where Rab11b, Rab18 and VAPB was depleted (Figure 45, other image panels). Interestingly for VAPB knockdown, some images revealed enveloped particles trapped in lumenal extensions of the NE (Figure 45,B). Quantification of nuclear and cytoplasmic particles in several EM images was consistent with the visually observed tendency to accumulate particles in the nucleus. VAPB knockdown cells showed around 6 times more viral particles accumulated in the nucleus while the number of cytoplasmic particles significantly decreased when compared with control cells (Figure 45, C).

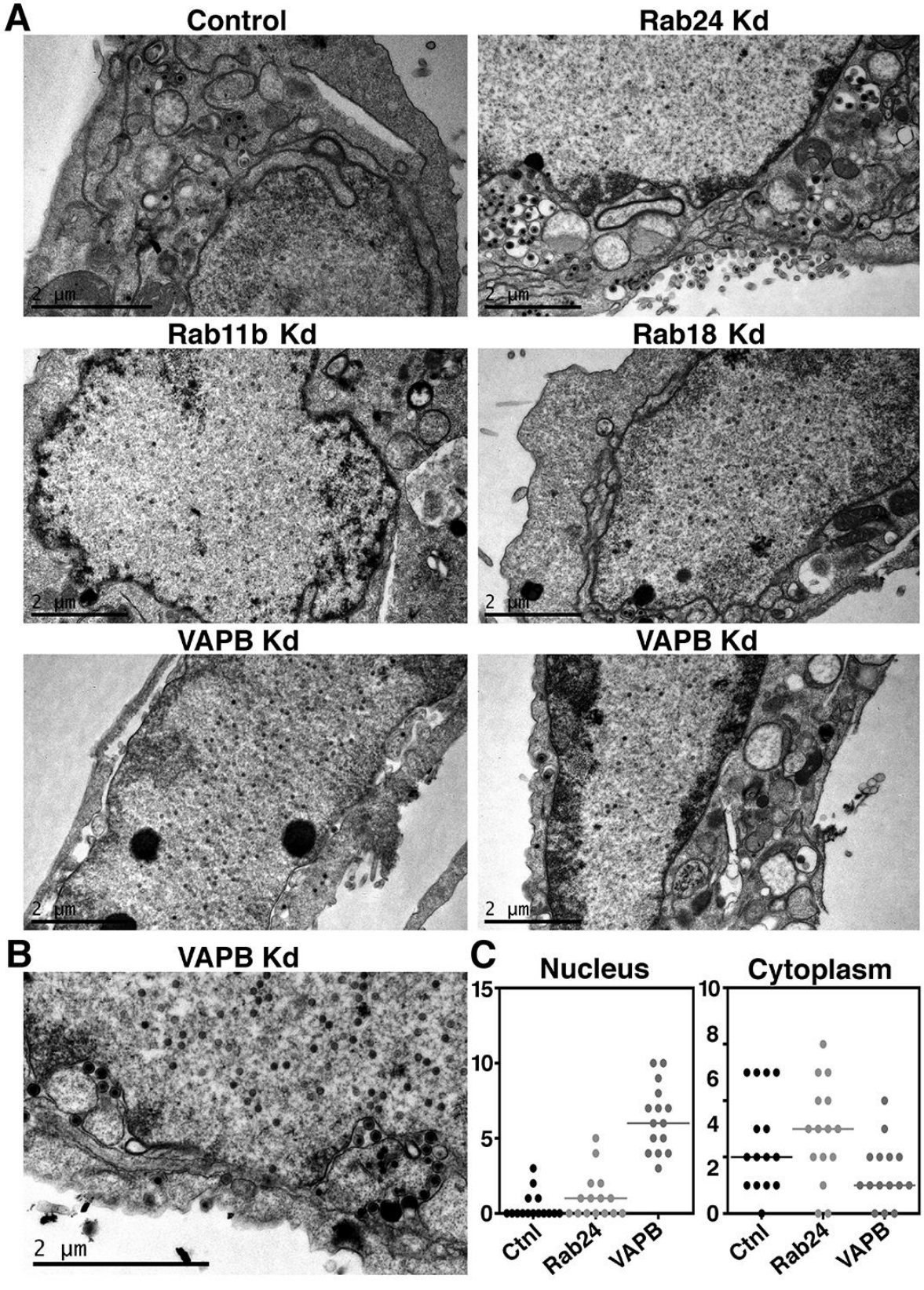
A
Control
Rab24 Kd
Rab11b Kd
Rab18 Kd
VAPB Kd
VAPB Kd
2 µm
B
VAPB Kd
2 µm
C
Nucleus
Cytoplasm
15
10
5
0
10
8
6
4
2
0
Ctnl
Rab24
VAPB
Ctnl
Rab24
VAPB

Figure 45. Electron microscopy reveals accumulation of virus particles in the nucleus with vesicle protein knockdowns. *In control and Rab24 knockdown cells some non-enveloped virus particles could be observed in the nucleoplasm, but many both enveloped and non-enveloped particles could also be observed in the cytoplasm as well as released mature particles just outside the cell. In contrast many more nucleoplasmic non-enveloped particles were observed in the Rab11b, Rab18 and VAPB knockdowns. Very few enveloped particles were observed for these three knockdowns in either the cytoplasm or nucleus, but some seemingly enveloped particles could be seen for Rab11b and VAPB knockdowns in association with the nuclear envelope and non-enveloped particles for the Rab18 knockdown. Bottom right panel. Quantification of particles for the control and Rab24 knockdowns revealed relatively few particles in the nucleus compared to the cytoplasm whereas for the VAPB knockdown there were mostly particles in the nucleus and few in the cytoplasm. Further quantification was not engaged because this was done more accurately by fluorescence in situ hybridization (see next figure). Experiment performed with the assistance of Swetha Vijayakrishnan and Marion McElwee at the University of Glasgow.*

As EM only captures viral particles in a particular section of the nucleus, we sought to perform an improved analysis to better quantify the number of viral particles trapped in the nucleus by fluorescence in situ hybridization (FISH). This experiment was performed by Dr Rafal Czapiewski, member of Schirmer´s lab with high experience in FISH techniques.

For this, infected cells with control and vesicle fusion protein knockdowns were hybridized with a biotin-labelled probe for the gene encoding the HSV-1 ICP27 protein and subsequently visualized by incubation with streptavidin conjugated fluorophore. The cells were pre-treated with RNase so that ICP27 RNA transcripts would not be recognized, but only viral genomes. Co-staining with DAPI identified the nuclear boundaries and imaging revealed the presence of viral particles in the cytoplasm in the non-target siRNA control cells, the Rab24 knockdown that had not changed according to the mass spectrometry results, and the Rab1A knockdown that is known to affect secondary envelopment but not nuclear egress (Figure 46, A). In contrast, the FISH signal for viral genomes was visually restricted to the nucleus in the VAPB, Rab11b and Rab18 knockdowns (Figure 46, A). The intensity of total FISH signal in each cell and also that just in the nucleus using the DAPI

staining as a mask was determined. The total signal divided by the nuclear signal was then plotted so that the amount of signal outside the nucleus is reflected in values above 1 (Figure 46, B). All three controls exhibited a clear increase in cytoplasmic viral particles while VAPB, Rab11b and Rab18 knockdowns all remained around 1 showing a significant difference as compared with controls.
These results clearly show that these three vesicle fusion proteins act at the level of HSV-1 nuclear egress.

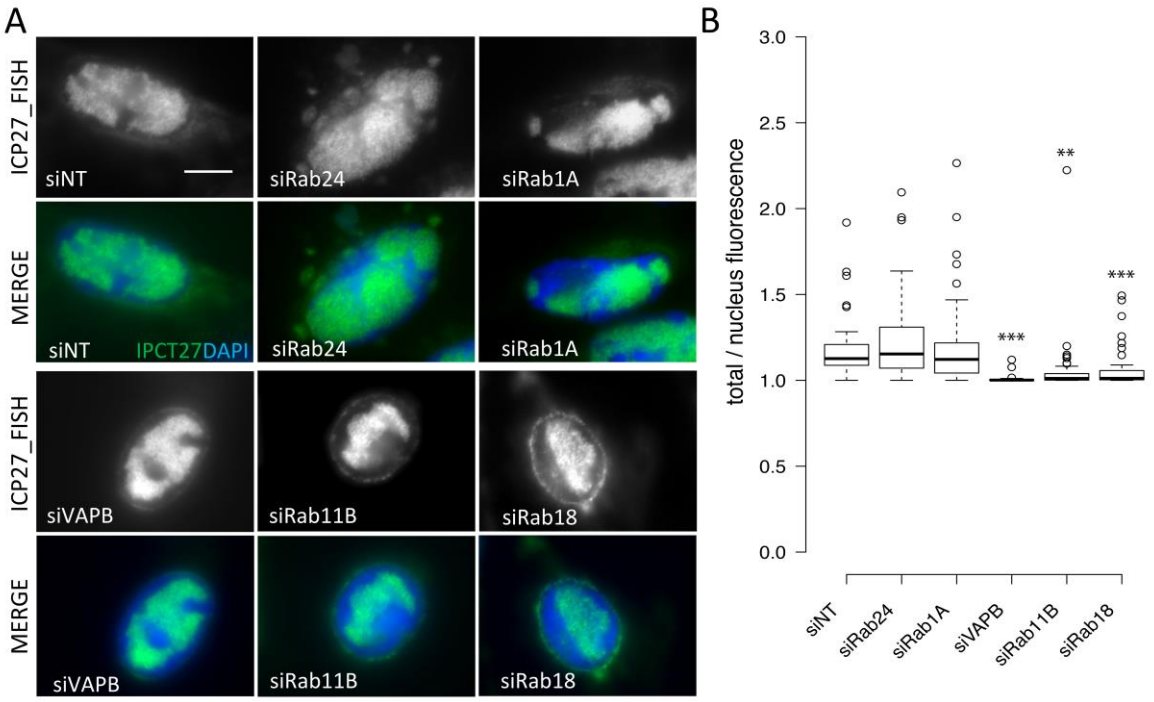

Figure 46. Fluorescence in situ hybridization (FISH) to quantify nuclear and cytoplasmic virus particles in vesicle fusion protein knockdown cells. (A) *The virus gene ICP27 was used as a probe and labelled with biotin. Cells were knocked down for vesicle fusion proteins as in Figures 4 and 5, infected with HSV-1 and at 16 hpi fixed and processed for FISH. The hybridized virus gene was visualized with streptavidin conjugated to Alexa488 dye and imaged by immunofluorescence microscopy. Cells were co-stained with DAPI to identify the nucleus. Scale bar, 10 µm.* ***(B)*** *Using the DAPI nuclear staining to generate a mask of the nuclear area the nuclear pools of hybridized virus ICP27 DNA were quantified. The total hybridized ICP27 DNA in the same cell was also quantified and plotted divided by the nuclear signal so that values above 1 reflect the cytoplasmic pool of viral*

*genomes. A clear increase in cytoplasmic viral genomes can be seen for the non-target siRNA control, the Rab24 and the Rab1A knockdowns while no notable increase in cytoplasmic viral genomes was observed for VAPB, Rab11b and Rab18 knockdowns. Statistical measurements were performed using a 2-tailed ANOVA analysis: ***p<0.001.*

6.4. VAPB is recruited to the NE during HSV-1 infection

To further analyse the role of these vesicle fusion proteins in HSV-1 infection, the intracellular distribution of VAPB was explored by indirect immunofluorescence in HSV-1 infected Hela cells. For this Hela cells were infected, fixed and stained at 8 and 16 hpi with HSV-1 MOI 10. Indirect immunofluorescence analysis was performed to confirm the VAPB NE localization indicated by the proteomics data (Figure 47, A). In order to select for analysis only those cells infected by HSV-1, the infection was performed using an HSV-1 strain in which ICP27 was tagged with GFP. Supporting the proteomics results, VAPB was visibly observed to accumulate at the NE over time in the infected cells compared to the mock-infected cells with the strength of the signal dissipating through the ER.

To support this visual readout, this re-localization pattern was observed in three independent experiments and image pixel intensities were measure in the NE and in the ER. Results clearly demonstrated a statistically significant increase in detection of VAPB at the NE early in HSV-1 infection that it is maintained at late points post infection. To quantify the relative signal for VAPB in the NE and ER, multiple lines were drawn through the middle of the nucleus of at least 40 cells and the signal intensity at the edge of the nucleus based on DAPI staining for the DNA was measured and also the signal in the ER along the same line but 2 µm away from the nucleus was also measured. The ratio of NE to ER signal intensity was plotted (Figure 47, A lower graph panel), revealing a strongly statistically significant near doubling of the NE:ER signal ratio between the mock-infected cells and the 16 hpi timepoint with the 8 hpi timepoint in between.

To make sure this was not a general effect produced during HSV-1 infection on membrane proteins, the distribution of calnexin, an ER protein also present in the ONM, was also sampled. Staining for calnexin yielded no notable visible increase

at the NE in infected cells and quantification confirmed that there was no increase in the NE:ER ratio (Figure 47, B).

To confirm that the VAPB increase observed at the NE during HSV-1 infection is not due to changes in the protein levels, total cell lysates were analysed by Western blot using LiCOR fluorescence intensity measurements in mock and HSV-1 infected cells. Results revealed that VAPB levels were unchanged throughout the infection suggesting that the NE accumulation observed in HSV-1 infected cells is due to a protein redistribution rather than an increment in total protein levels (Figure 47, C).

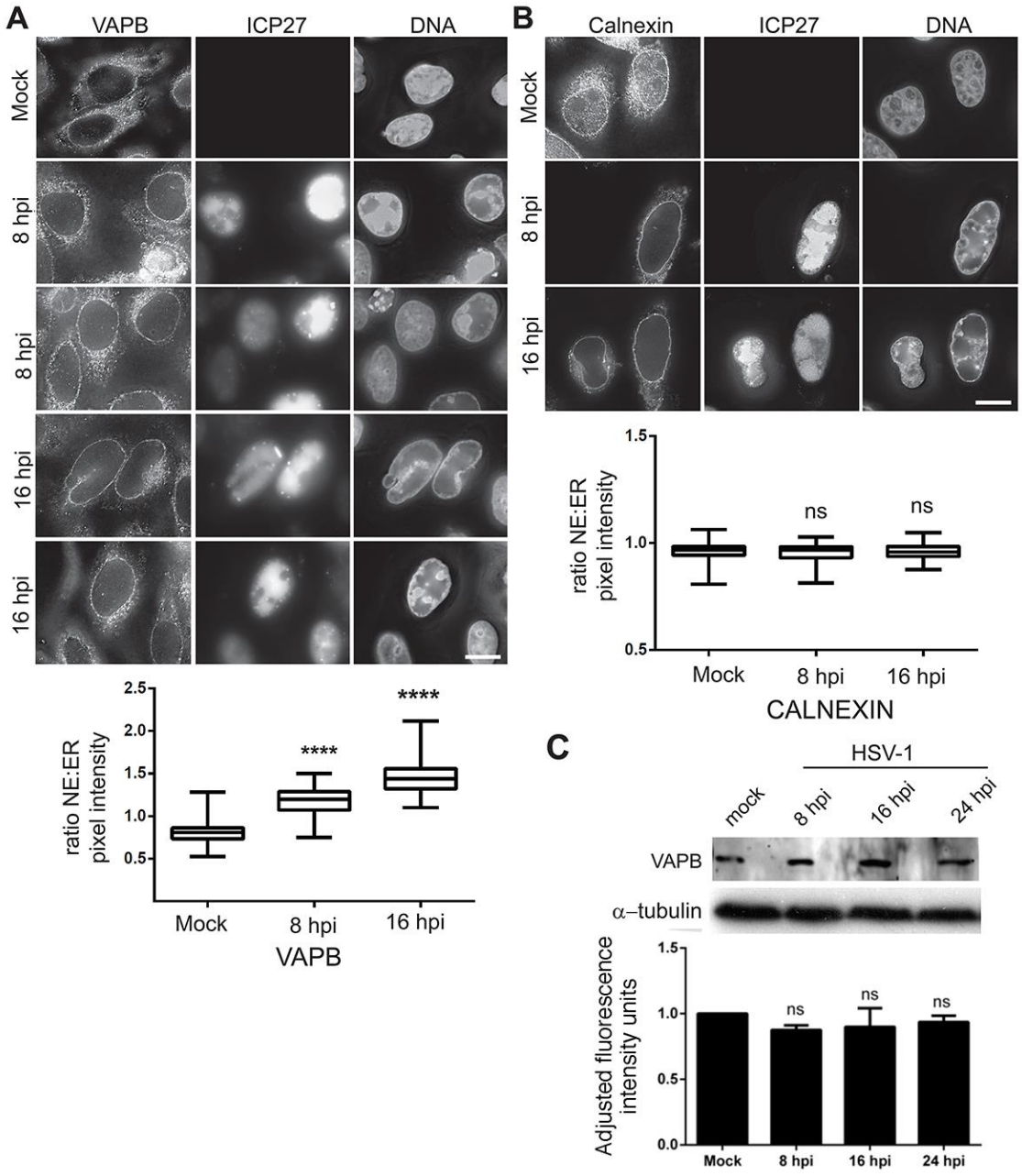

Figure 47. VAPB is recruited to the NE during HSV-1 infection. (A) *Hela cells were either mock infected or infected with MOI 10 HSV-1 vBSGFP27 (encoding WT ICP27 fused to GFP). At 8 and 16 hpi cells were fixed and processed for immunofluorescence microscopy with VAPB mouse monoclonal antibodies and DNA stained with DAPI. ICP27-GFP is shown to identify infected cells. Scale bar, 10 μm. The VAPB signal appeared visually to increase at the NE during infection. To quantify this putative NE redistribution, the relative pixel intensities in the ER and NE were quantified. For each cell five lines were*

drawn through the middle of the nucleus and pixel intensity was measured at a point in the nuclear rim (based on DAPI staining) and at a point 2 µm distant into the ER and the NE/ER ratio was calculated. Boxplots from 30 cells are shown in the graph below the images with the median (central line) and the error bars (grey) marked. Each sample was compared with its control (mock cells) by one-way ANOVA analysis followed by Dunnett´s test *multiple-comparison test. Significant p-values (****p ≤ 0.0001) illustrate the general trend of these vesicle fusion proteins to accumulate at the NE upon infection**. (B)** As a control the same analysis was performed staining for the ER and ONM marker Calnexin. In this case no significant change in the relative distribution was observed**. (C)** Analysis of total protein levels of VAPB in HSV-1 infected cells during infection. Lysates were prepared from mock-infected HeLa cells or HeLa cells infected with WT HSV-1 with MOI 10 after 8, 16 and 24 hpi in three separate experiments. Each lysate was analyzed by Western blots with the antibodies shown and using fluorophore-conjugated secondary antibodies for quantification by Li-COR. No obvious differences were observed in VAPB protein levels at any of the time points.*

6.5. VAPB co-localizes with HSV-1 nuclear egress protein UL34 at and around the NE

Previous studies have shown that HSV-1 nuclear egress is a highly regulated process driven by the heterodimeric viral complex of UL31 and UL34. This complex accumulates at the NE during infection where it recruits cellular kinases to phosphorylate lamins thus promoting their disassembly so that the virus has access to the inner nuclear membrane for fusion events. Moreover, this complex appears to also directly participate in primary envelopment since EM studies of infected cells showed no evidence of primary enveloped particles in the absence of this protein (Roller et al., 2000).

VAPB exhibited almost complete co-localization with UL34 at the NE (Figure 48, A). The specificity of the co-localization with UL34 was underscored using an HSV-1 strain in which ICP27 WT protein was tagged with GFP. ICP27 is both involved in nucleocytoplasmic trafficking of viral intronless mRNAs and targets host cell introncontaining RNAs for destruction (Sandri-Goldin 2008, Malik, Tabarraei et al.

2012). Accordingly, ICP27 accumulates partly at the NE and also in nucleoplasmic punctae; however, these are different from the sites of primary envelopment as ICP27 is also known not to be in the capsid or tegument of primary particles. No overlapping fluorescence signals were observed at all between ICP27 and VAPB (Figure 48, A most right panel).

As a transmembrane protein, VAPB should in theory only be in the NE and not in the nucleoplasm. Yet some of the staining signal appeared to be several microns away from the NE, appearing to occur in punta in the nucleoplasm. This type of staining pattern has previously been reported for UL34 as infection often induces extensive invaginations of the NE. To confirm that VAPB punta are from invaginations, 0.2 µm sections were taken in imaging for several cells. Continuity to the membrane was observed when following puncta through individual sections, revealing these internal punctae to be membrane invaginations of the NE as well as showing co-localization between VAPB and UL34 throughout (Figure 48, B).

To further confirm the colocalization between VAPB and pUL34, super resolution microscopy was performed using a Zeiss 880 confocal microscope with Airyscan by Charles Dixon. Results also showed a co-localization for both punta and at the membrane (Figure 48, C).

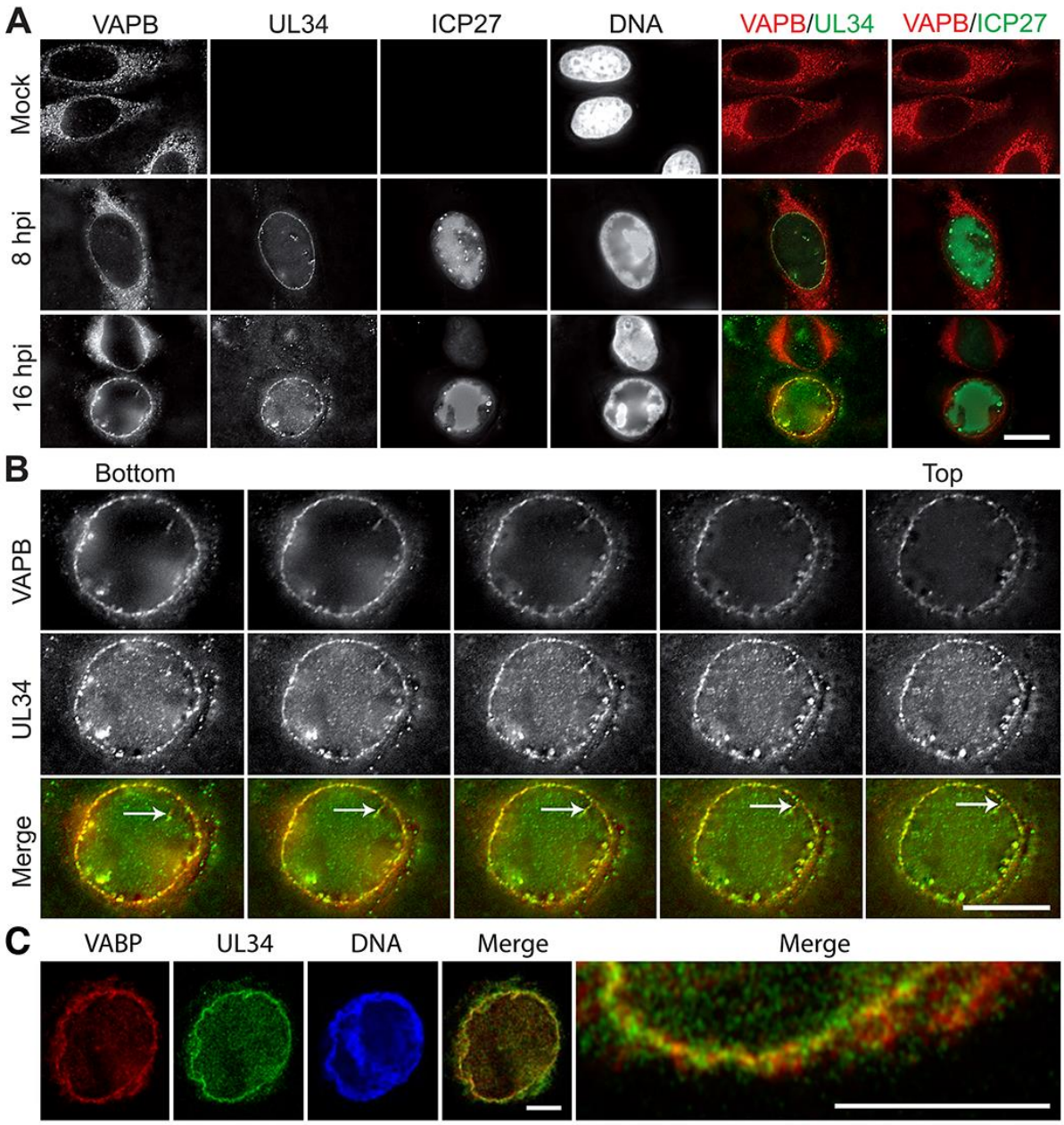

Figure 48. VAPB colocalizes with pUL34 at the nuclear membrane of HSV-1 infected cells. (A) *HeLa cells infected with HSV-1 vBSGFP27 (encoding WT ICP27 fused to GFP) at MOI 10 were fixed at 8 and 16 hpi, permeabilized, and stained with UL34 and VAPB antibodies. VAPB, but not control ICP27, co-localized with UL34. Scale bar, 10 μm.* ***(B)*** *As internal punctae were observed in addition to NE staining, z-series were also taken to determine whether VAPB punctae were from nuclear invaginations or other non-membrane associated structures. All images are deconvolved from stacks with individual sections shown. Sections (0.2 μm each step) clearly show that internal punctae (single arrows) are connected in different sections to the membrane. Scale bar, 10 μm.* ***(C)*** *HeLa cells infected*

with wild-type HSV-1 strain 17+ were fixed at 10 hpi and stained with VAPB mouse monoclonal antibodies, UL34 chicken antibodies and DAPI. Images were taken using a Zeiss 880 confocal Airyscan super resolution microscope. Considerable co-localization was observed between VAPB and UL34. Scale bars, 5 µm. C was performed by Charles Dixon.

6.6. VAPB participates in HSV-1 primary envelopment

VAPB showed to be translocated to the NE in HSV-1 infected cells in both, proteomic and immunofluorescence analysis. Viral particles accumulated in the nucleus were observed by FISH and EM after depletion of this protein in HSV-1 infected cells. Based on this results, it is clear that VAPB is playing a role during nuclear egress. However, HSV-1 nuclear egress is divided in primary envelopment, and de-envelopment.

In order to investigate if VAPB was involved in either envelopment or de-envelopment or both, immunogold labelling EM was performed by our collaborators Martin W. Goldberg and Christine A. Richardson at the University of Durham.

If just involved in de-envelopment, VAPB might be expected to only accumulate in the ONM and not translocate to the INM. Thus its distribution between the membranes was investigated in both, mock infected and HSV-1 infected cells, by immunogold labelling EM. Observations of imunogold results showed that nearly all images examined had VAPB protein in both INM and ONM in both the mock infected (Figure 49, A) and HSV-1 infected cells Figure 49, B). The finding of VAPB in the NE of mock-infected cells is consistent with its identification in NEs by the mass spectrometry data (Table 15). Gold particles at the NE were counted, considering separately those in the ONM, the INM, the NE lumen, and at the NPC (Figure 49, C). This indicated an increase in the INM pool during HSV-1 infection, consistent with the NE increase observed by immunofluorescence microscopy (Figure 49, A). Most surprisingly was the capturing in several images of virus particles inside the nucleus that contained gold particles labelling the VAPB Figure 49, D and E). This strongly argues that VAPB normally participates in the process of primary envelopment. Whether it has an additional separate role in de-envelopment has yet to be determined.

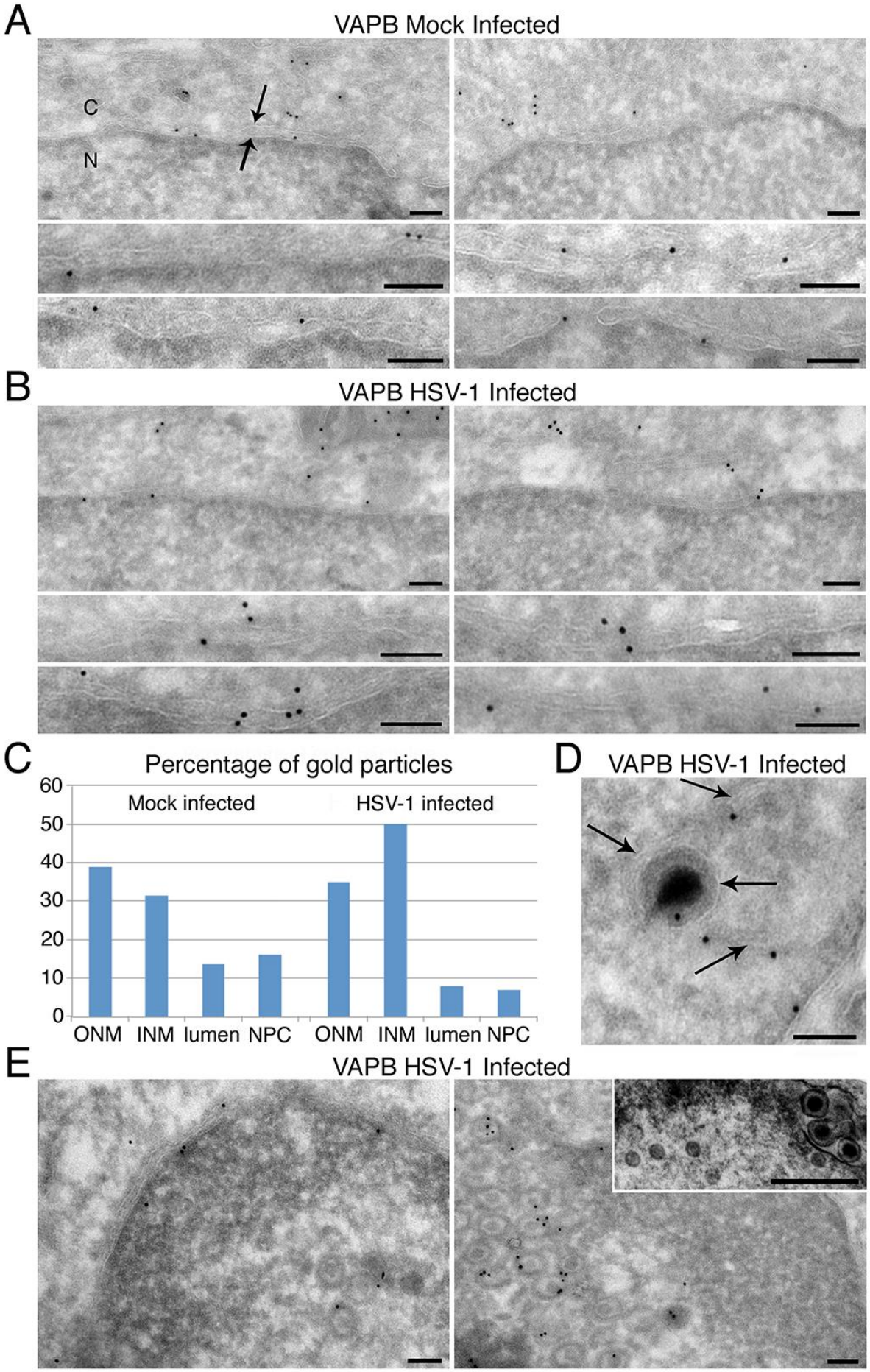
A
VAPB Mock Infected
C
N
B
VAPB HSV-1 Infected
C
Percentage of gold particles
Mock infected
HSV-1 infected
60
50
40
30
20
10
0
ONM
INM
lumen
NPC
ONM
INM
lumen
NPC
D
VAPB HSV-1 Infected
E
VAPB HSV-1 Infected

Figure 49. VAPB accumulates in both the ONM and INM. *Hela cells either mock infected or infected with WT HSV-1 MOI 10 for 16 h were fixed and cryosectioned prior to labelling with VAPB mouse monoclonal antibodies and anti-mouse conjugated gold particles for electron microscopy. In all panels the cytoplasm is on the top and the nucleoplasm is on the bottom with this labeled in the upper left panel by C and N respectively. This panel also contains two arrows with that facing down delineating the ONM and that facing up delineating the INM. All scale bars, 100 nm.* ***(A)*** *Mock infected cells. Note the lower right panel contains one gold particle in transit at the NPC and one in the INM.* ***(B)*** *HSV-1 infected cells.* ***(C)*** *Quantification of 206 and 163 gold particles at the NE from respectively the mock infected and HSV-1 infected populations. The percentage of total NE particles touching the ONM and the INM are given along with those in the NE lumen and those at the NPC are given.* ***(D)*** *High magnification image of a most likely HSV-1 primary enveloped particle with a gold particle indicating VAPB just under the primary envelope membrane. Note that this appears to be located in a membrane bound invagination, possibly from the NE lumen as a membrane can be distinguished within the nucleoplasm (rightward pointing arrows). This membrane also is associated with gold particles. The presumed primary envelope is indicated by the sole leftward pointing arrow.* ***(E)*** *Lower magnification images showing multiple nuclear associated virus particles labelling with the VAPB immunogold particles. Although it cannot be fully ascertained from these images if these particles have a primary envelope, comparison with the inset image from standard electron microscopy of the VAPB knockdown infected cells shows that they have more the appearance of the non-enveloped (left) than enveloped (right) particles.This experiment was performed by Martin W. Goldberg and Christine A. Richardson.*

6.7. Summary of chapter 6

In this chapter, we analysed the role of three vesicle fusion proteins, VAPB, Rab11b and Rab18 and found their unique contribution during HSV-1 nuclear egress. We found for the first time that HSV-1 utilizes a class of host proteins, the vesicle fusion proteins in viral nuclear egress.

The knockdown of these proteins yielded reduced titers of released virus, furthermore EM studies of cells in which either VAPB, Rab11b and Rab18 was depleted showed an accumulation of virus particles within the nucleus. Interestingly, VAPB showed a clear NE accumulation in HSV-1 infected cells in where it co-localizes with the UL34 viral protein. More strikingly, VAPB was observed by immunogold labelling electron microscopy on nucleus associated virus particles.

Chapter 7
General Discussion

Over the las years it has become evident that the NE is no longer considered as a simple barrier between the cytoplasm and components of the nucleus. Instead, lot of recent exciting new roles have been shown for this membrane that are vital for the cell. For instance, the NE participates in new ways of ribosome transport in which ribosomal proteins produced in the cytosol are imported into the nucleus, where they associate with newly synthesized ribosomal RNA (rRNA), and are then exported back to the cytoplasm to perform their function. Additionally, novel NE roles have been suggested in providing anchoring sites for chromosomes to the nuclear periphery in order to regulate gene expression regulation.

The results presented in this thesis argues in favour of a previously uncharacterized nuclear role for the multifunctional protein NET23/STING potentially in both innate immune signalling and general chromatin architecture. Moreover, I presented data that could explain the involvement of NET23/STING itself in mediating IIR against RNA despite that it does not bind to RNA.

This work additionally shed light on the nuclear egress of HSV-1, one of the less understood steps in herpesvirus life cycle. I identified a new group of host proteins, vesicle membrane fusion proteins that are involved in this step facilitating the exit of new HSV-1 viral capsid from the nucleus of infected cells to complete their maturation.

7.1. NET23/STING can mediate chromatin compaction from the NE

NET23/STING was firstly introduced in a proteomics' study as a NE integral protein (Schirmer, Florens et al. 2003). Since then, multiple studies have identified this protein in different compartments of the cell such as ER and mitochondria, linking its function to innate immune signaling pathways (Ishikawa and Barber 2008, Zhong, Yang et al. 2008, Ishikawa, Ma et al. 2009, Burdette and Vance 2013). However, the role of NET23/STING within the NE has been completely ignored.

Epigenetic is a stably heritable phenotype that results as an alteration or modification in the DNA function but without modifying its sequence. These changes are produced by chemical modifications on both DNA and DNA-associated histones. During my PhD, I have shown for the first time the involvement of NET23/STING in promoting a chromatin compaction state and epigenetic changes from the NE.

Quantification of clusters as a measure of chromatin compaction and EM observations of cells overexpressing NET23/STING clearly indicates that NET23/STING may contribute generally to chromatin compaction. The observed chromatin compaction phenotype identified in this study might also be produced by the recruitment of epigenetic factors or enzymes to the NE or by the direct effect of NET23/STING on chromatin as it is known this protein directly interacts with chromatin. This novel role is further supported by the identification of bromodomain proteins and chromatin-associated complexes as NET23/STING-NE binding partners that might mediate the previously mentioned involvement of NET23/STING in chromatin remodeling and other epigenetic alterations associated with its role in IIR.

Upon a pathogen attack, host cells undergo enormous changes in their transcriptional program, resulting in the activation and repression of multiple genes involved in key processes (e.g., immunity, apoptosis, cell survival) to trigger an appropriate response (Bierne, Hamon et al. 2012). The principal goal of a cell infected with an external pathogen is to avoid the propagation of the infection within the host organism. For this propose, the cell activates innate immune signal

cascades for the release of interferons and cytokines in order to target the immune system to the infected cell. Multiple epigenetic changes related with the regulation of the IIR to face infections have been observed (Vanden Berghe, Ndlovu et al. 2006, Kugelberg 2015). Thus, the process in which the IIR is activated by a pathogen infection can be influenced by epigenetic modifications within the infected cell. For example, the activation of TLRs by pathogens, results in the downstream activation of IIR genes involved in the production of proinflammatory factors and it is known that TLR gene expression is regulated by several alterations to the epigenetic signature such as histone modifications (Hennessy and McKernan 2016).

Acetylation of histone promotes a relaxed chromatin structure promoting gene transcription as transcription factors have access to the DNA resulting in gene expression. On the other hand, deacetylation of histone compacts the chromatin structure favoring gene silencing. Silencing epigenetic marks play a pivotal role in the global IIR (Stender and Glass 2013). It has been shown that the inhibition of histone deacetylases (HDACs) impairs essential biologic functions of the IIR of infected cells, as their ability to induce a proinflammatory response and kill pathogens is being reduced increasing the susceptibility to infection (Roger, Lugrin et al. 2011).

Epigenetic modifications regulate the expression of the genome to produce multiple innate immune response signals as a cellular response to external stimuli. Recent studies have highlighted the possibility of certain pathogens such as virus and bacteria to directly target and influence diverse epigenetic factors like histone modifications and chromatin-associated complexes to either promote host defense or to allow pathogen persistence. For instance, histone deacetylase expression is found to increase upon infection of plants with pathogens and transgenic plants overexpressing the deacetylase are more susceptible to infection (Ding, Bellizzi Mdel et al. 2012). Also, Listeria monocytogenes, bacteria that is the main causative agent of listeriosis, has been shown to rapidly increase acetylation of histones (H3S10p, H3K14ac, and H4K8ac) resulting in the activation of the proinflammatory gene *IL-8* (Schmeck et al. 2005; Opitz et al. 2006). Thus, there is likely a ‘‘tug-of-war’’ effect going on in the infected cell between the pathogen efforts to block the

activation of the IIR within the host cell and the host cell to find the right balance in its response to block the spread of the infection within the rest of organism.

An increase in the histone marks H3K9me3 has been shown at early times post infection in HSV-1 infected cells resulting in an increase in chromatin compaction that might suggest a defense mechanism of the host cell. This repression is known to be countered by the virus through the recruitment of the required enzymes to remove the repressive histone marks while installing the activating marks for the advantage of the virus (Arbuckle and Kristie 2014). This is consistent with the results presented in this thesis in which the depletion of NET23/STING prevented the increase of chromatin compaction that normally occurs early upon HSV-1 infection. Furthermore, these results showed the attenuation of HSV-1 in cells no longer expressing NET23/STING. Although it remains unclear why the effect of HSV-1 infection in HT1080 cells was to reduce instead of increase chromatin compaction, though the nuclear size changes in this experiment could affect the output of the algorithm, the effect of the virus was mitigated by NET23/STING depletion. Furthermore, in order to confirm the role of NET23/STING in the alteration of the chromatin compaction state of HSV-1 infected cells, EM studies could be performed in order to analyze the state of chromatin on HSV-1 infected cells no longer expressing NET23/STING.

Previous experiments performed in my lab showed that the distribution of NET23/STING at the NE was lost in lamin A knockout mouse embryonic fibroblasts (Malik, Korfali et al. 2010) suggesting a potential link of NET23/STING to lamin A. Thus, considering the interrelation between these two proteins, it follows logically that NET23/STING may be involved in some of the chromatin changes observed in NE-diseases in which lamin A is involved.

Several NE diseases caused by defects in NETs, lamins and epigenetic marks presented an aberrant distribution of chromatin (Ognibene, Sabatelli et al. 1999, Sewry, Brown et al. 2001, Goldman, Shumaker et al. 2004). Considering the role of NET23/STING in promoting endogenous chromatin compaction from the NE, it is likely that this protein could also contribute to mediate chromatin epigenetic patterns in certain NE diseases. This is supported by observations that both the NET23/STING compaction phenotype and the observed EM changes in chromatin

in some NE diseases have been linked to epigenetic modifications. For example, in fibroblast from Hutchison-Gilford Progeria patients, in which lamin A protein is mutated, there is a reduction of epigenetic marks associated with silenced chromatin such as H3K9me3 and H3K27me3 while there is an increase of H4K20me, epigenetic mark associated with active chromatin (De Sandre-Giovannoli, Bernard et al. 2003, Eriksson, Brown et al. 2003).

7.2. Identification of RNA binding proteins as NET23/STING NE partners

The data presented in this thesis points out a new potential role for this extremely multifunctional protein in acting as a transporter for NE-specific NET23/STING binding partners involved in innate immunity.

This protein was firstly identified as an important cytoplasmic sensor by recognizing pathogen DNA, but not RNA, in the ER and triggering the activation of signaling cascades to promote the induction of IRF3/7 transcription factors. The role of this protein in response to RNA is much less clear (Zhong, Yang et al. 2008, Sun, Li et al. 2009, Chen, Sun et al. 2011). Several studies have shown a function of NET23/STING in host innate immunity against certain positive sense single strand RNA viruses with no DNA intermediaries. Of note, a study with NET23/STING knockout mice showed higher susceptibility to RNA virus infection such as Sendai virus (SeV) and vesicular stomatitis virus (VSV) (Ishikawa and Barber 2008). Furthermore, the initial characterization of mouse embryonic fibroblasts with depletion of NET23/STING presented a defect in the induction of the interferon response to RNA viruses. Additional studies have shown that although NET23/STING interacts with key elements of the RNA-sensing pathways like RIG-I and MAVS (Zhong, Yang et al. 2008, Sun, Li et al. 2009, Zhong, Zhang et al. 2009) and it may be essential for the induction of certain STAT6 target genes, it is not an absolute requirement for the activation of the interferon response to RNA, presumably because there are redundant pathways that can activate IRF3/7 transcription factors for the production of interferons (Ishikawa and Barber 2008,

Chen, Sun et al. 2011, Sauer, Sotelo-Troha et al. 2011). The many disparate roles of NET23/STING make it difficult to distinguish details of NET23/STING signaling pathways and how this protein might mediate IIR against RNA viruses without binding RNA. However, our finding that multiple NET23/STING NE-binding partners were RNA binding factors could explain the greater sensitivity to RNA virus infection in NET23/STING knockout mice, indicating the involvement of this protein in mediating IIR against RNA virus.

7.3. Partner protein distribution changes

Additionally, I found that NET23/STING mediates shuttling of NE binding proteins in and out the nucleus in response to an external signal such as HSV-1 infection or Poly I:C treatment. Two STING-NE co-IP partners, Syncrip and MEN1 that normally shuttle between the nucleus and cytoplasm during IIR, failed to redistributed in NET23/STING depleted cells. This means that the distribution of these partners is NET23/STING dependent upon IIR activation arguing that this transmembrane protein can carry proteins in either direction as a response to external stimuli.

To our knowledge, no IIR roles have been reported for Syncrip or MEN1. Thus, their contribution to IIR has been lately tested in my lab. For this, a luciferase assay was performed in which NFκB, ISRE, ISG56 and IFNß-luciferase reporters (IIR reporters used to quantify IIR activity) were activated upon co/transfection of STING and cyclic GMP-AMP synthase (cGAS). As previously stated, cGAS produces a second messenger (cGAMP) that is bound by STING/NET23 during IIR. This assay allowed to determine whether a binding partner protein was important for the IIR activation based on a loss of luciferase activity compared to controls. The luciferase signal from some of the reporters was mitigated when Syncrip and MEN1 were depleted from cells in which the IIR was activated by poly I:C. This data supported that the NET23/STING NE-binding proteins could mediate STING functions in polyI:C induced IIR.

It is known that RNA viruses often activate IIR through NFκB mediated signaling pathways (Schmitz, Kracht et al. 2014). Interestingly cells no longer expressing Syncrip showed a reduction in the activation of the NFκB -reporter known to be activated by RNA viruses (Zhong, Yang et al. 2008), indicating the potential involvement of Syncrip in NET23/STING-mediated IIR. These data argued that Syncrip RNA-binding function could mediate NET23/STING functions in RNA induced IIR.

7.4. NET23/STING shuttling in the NE

The NE FRAP experiments performed in this thesis, showed that the translocation of NET23/STING in HSV-1 infected cells is significantly increase compared with mock-infected cells. As NE FRAP experiments predominantly quantifies the translocation of NE transmembrane proteins from the ER to the NE through the NPC peripheral channels and the observation that some NE-binding partners such as Syncrip and MEN1 failed to redistributed in cells no longer expressing NET23/STING, we could speculate that NET23/STING is acting as a shuttling protein carrying signals upon IIR activation. Although further studies such as PA experiments will need to shed light on the dynamics of NET23/STING, this could provide a multiply redundant backup mechanism for activating IIR through peripheral channel transport of the NET23/STING-NE binding partners previously identified that can interact with IRF3/7 partners activating immune cascade signals.

7.5. NET23/STING provides an alternative transport pathway via the NPC peripheral channels

Data presented in this thesis indicates that NET23/STING is not just an upstream activator of the IIR, but presents a previously uncharacterized nuclear role for this multifunctional protein in both general chromatin architecture acting as a chromatin regulator and in innate immune signaling as a nucleo-cytoplasmic driver for NE-specific NET23/STING binding partners involved in IIR.

These new roles may also reflect an alternative and creative mechanisms for the host cell to get around the efforts of the pathogen to block the IIR. Numerous pathogens have evolved different mechanisms to hijack and block the central channels of the NPC to inhibit host nucleocytoplasmic transport pathways facilitating viral infection (Le Sage and Mouland 2013). For example, ICP27 herpesvirus protein and HIV-1 viral ribonucleoproteins (vRNP) have been shown to interact with Nup62, a nucleoporin present in the NPC central channel (Chang, Lee et al. 2012, Malik, Tabarraei et al. 2012). But NETs can still travel through the peripheral channels of the NPC (Zuleger, Kerr et al. 2012). Thus, in cases in which transport through the NPC central channels is blocked due to the infection of the host cell by certain pathogens, NET23/ STING is likely to still be able to target to the INM where it could engage its nuclear functions such as promoting chromatin compaction.

NETs, like all membrane proteins are synthesized in the ER and to reach the INM they have to move within the ER towards the ONM in where they finally translocate into the INM via the NPCs. NETs targeting to the INM bind to nuclear components in the nucleoplasm like lamins and chromatin. Some of these NETs can recruit heterochromatin by either direct interaction with it or by the recruitment of specific epigenetic marks such as silencing factors, adding new epigenetic signatures to chromatin once it is at the periphery (Stancheva and Schirmer 2014).

The transmission of epigenetic changes in response to signaling through the peripheral channels is a relatively novel concept, however, some NETs have been shown to promote epigenetic marks by binding to silencing factors and recruiting them to the NE. For example, the NET LBR can bind DNA methylation enzyme MeCP2 and the NETs LAP2b and emerin can bind the histone deacetylase HDAC3 (Somech, Shaklai et al. 2005, Guarda, Bolognese et al. 2009, Demmerle, Koch et al. 2012). Thus, epigenetic marks could be transmitted in response to IIR signals through the peripheral channels by the recruitment of some of these enzymes by transmembrane proteins present in the NE. The significant increase in H3K9me3 of cells overexpressing NET23/STING by Western blot and its first appearance at the nuclear periphery by immunofluorescence microscopy in the cells exogenously expressing NET23/STING suggests that this NET may directly recruit histone modifying enzymes to the NE in addition to other epigenetic marks as an extra

defense mechanism for the host cell. Furthermore, upon IIR activation, NET23/STING might be carrying some of the identified NE binding partners such as bromodomain proteins involved in chromatin remodeling through the peripheral channels in order to regulate chromatin architecture. Future work will need to test whether the depletion of some of these proteins identified by co-IP block the effects on chromatin marks associated with NET23/STING overexpression.

The increase in translocation observed for NET23/STING in the NE after HSV-1 infection together with the failed redistribution of some NE binding partners identified to be involved in IIR (Syncrip and MEN1), let me to propose a model in which NET23/STING, in response to pathogen infection, might be activated and redistributed from the ER to the NE while carrying NE-binding partners involved in immune cascade signaling through the peripheral channels. In addition, NET23/STING could promote epigenetic changes from the INM resulting in modifications in chromatin architecture that could activate or repress epigenetic marks in order to aid the cell to overcome infection (Figure 50).

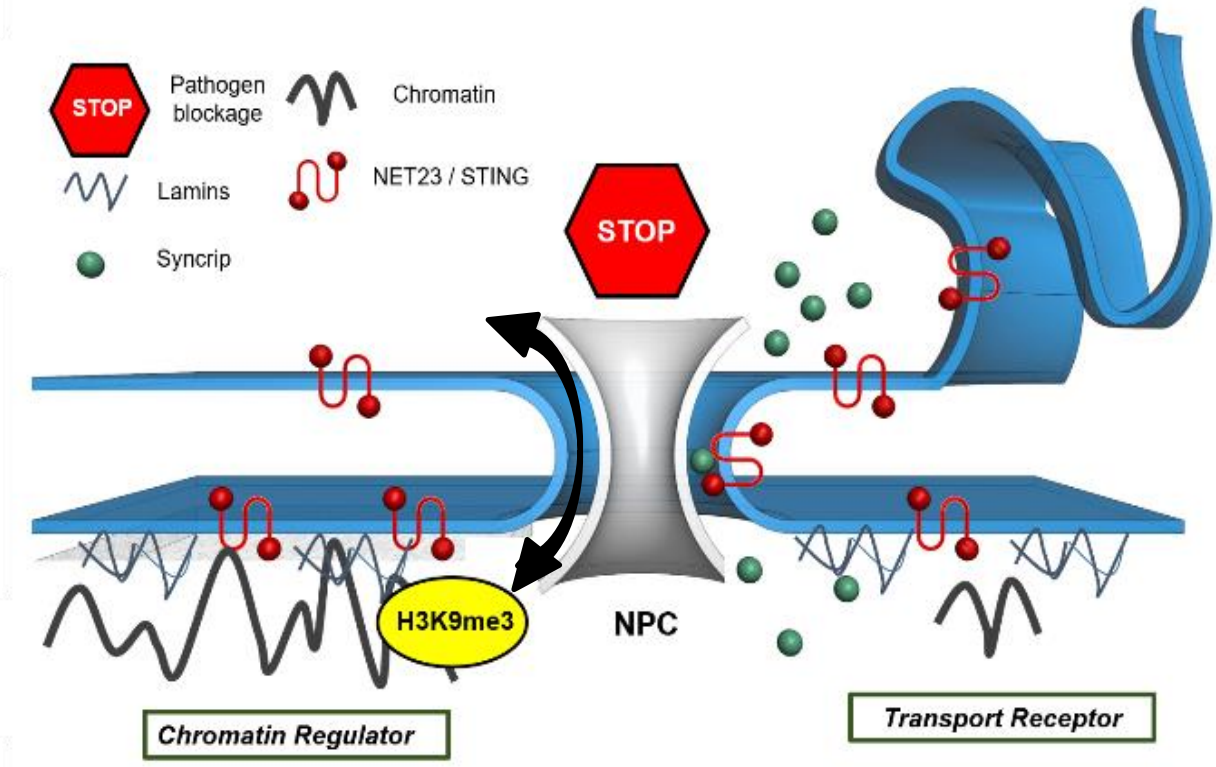

Figure 50. Model for NET23/STING acting as a chromatin regulator and serving as a transport receptor. NET23/STING promotes epigenetic marks such as H3K9me3 that may compact chromatin in response to infection. Also, NET23/STING might act as a carrier for proteins involved in IIR such as Syncrip and MEN1 facilitating their translocation through the peripheral channels. When the central channel of NPC is disrupted by pathogen infections, NET23/STING could use the peripheral channels to carry binding partners between the nucleus and cytoplasm or activate epigenetic enzymes to activate the IIR.

7.6. Future Experimental Directions

7.6.1 Distinguishing central from peripheral channel transport

In order to get more insights into the role of NET23/STING within the NE, it will be necessary to capture the translocation of Syncrip and MEN1 at the peripheral channels of the NPC to confirm that both proteins translocate together with NET23/STING through these channels in response to external stimuli. It is important to mention that, as Syncrip and MEN1 are soluble cargoes, they could use both, central and peripheral channels to translocate and that the NET23/STING effects are only a backup mechanism for cases where central channel transport has been blocked by pathogens.

Thus, to study if the transit of NET23/STING NE-binding partners such as Syncrip and MEN1 are restricted to the peripheral channels, the IIR could be activated in +/- NET23/STING depleted cells after microinjections with WGA antibody to block the central channel transport or gp210 antibody to block peripheral channel transport (Ohba, Schirmer et al. 2004) in order to analyze the localization of NET23/STING binding partners.

To attempt to capture NET23/STING binding partners in the peripheral channels, FRB-FKBP rapamycin trap system could be used (Chen, Zheng et al. 1995, Klemm, Beals et al. 1997). For this purpose, stable cell lines expressing FRB fused with either Nup62 (nucleoporin from the central channel) or Nup35 (nucleoporin from the peripheral channel) could be used to trap FKBP-Syncrip or FKBP-MEN1 fusions upon addition of rapamycin. Thus, if the NET23/STING binding partners translocate through the peripheral channel, it should be captured just with Nup35; if it goes just through the central channels, it should be captured just with Nup62 and if it uses both, central and peripheral channels, then both Nups will capture these NET23/STING binding partners (Figure 51).

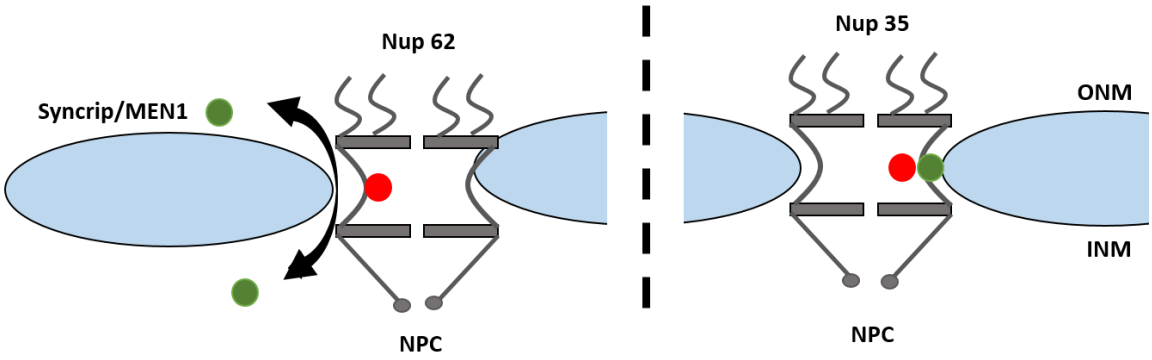

Figure 51. Schematic representation of FRB/FKBP rapamycin capture experiment. Upon the addition of the drug rapamycin, FKBP-GFP fusion proteins (Syncrip or MEN1) are expected to be captured in the NPC peripheral channels in cells expressing Nup35-mRFP-FRB, a peripheral channel trap protein, while be able to pass freely through peripheral channels in cells expressing FRB-mRFP-Nup62, a central channel trap protein.

Separately, I could use SPEED (Single-Point Edge-Excitation subDiffraction) microscopy, a super resolution approach developed by Weidong Yang which allows the study of 3D transport routes at the NPC, being able to distinguish transport through the peripheral NPC channels (Ma, Kelich et al. 2016). GFP-labelled NET23/STING, Syncrip and MEN1 could be analyzed for peripheral channel transport upon IIR activation using polyI:C and infection by viruses known to interfere with central channel transport such as HSV-1 and HIV.

7.6.2 Regulation of NET23/ STING activity at the NE

Additionally, it has been shown that NET23/STING is phosphorylated by TBK1 at the C-terminus upon the activation of the IIR. This phosphorylation is essential to later recruit and activate IRF3, resulting in the stimulation of interferons and cytokines (Tanaka and Chen 2012, Liu, Cai et al. 2015). It is logical to suggest that the phosphorylation of NET23/STING might disrupt its connection with other NE proteins such as the previously mentioned interaction with lamin A, so that,

NET23/STING would become more mobile facilitating its increased shuttling. Thus, the study of the mobility of NET23/STING by FRAP and PA techniques using a phoshonull and phosphomimic NET23/STING mutant could confirm an increased translocation of this protein confirming its role as a transmembrane peripheral channel transport receptor.

7.6.3 Mediation of RNA IIR

It has been suggested that NET23/STING mediates IIR to RNA viruses but does not bind to RNA. However, the identification of ss and dsRNA NET23/STING binding partners may have a functional relevance for this protein that could be involved in sensing a wider variety of pathogen nucleic acids and carry these binding partners to the nucleus. The identification of the RNA-binding protein Syncrip as a novel IIR mediator suggests that the NET23/STING shuttling of RNA-binding partners could explain how NET23/STING activates the IIR in response to RNA viruses without binding RNA.

Other NET23/STING NE-binding partners identified by co-IP, such as ZRANBP2, PRPF40A, SNRNP70, RPS27A and DDX5, are also reported as RNA-binding proteins. Of these, only DDX5 has a known IIR link, being targeted by hepatitis C and several other viruses to shut down IRF3 transcription factor (Li, Ge et al. 2013, Moy, Cole et al. 2014, Upadya, Aweya et al. 2014, Zhao, Ge et al. 2015).

An interesting direction would be to test the effects that the knockdown of these NET23/STING NE binding proteins could have in the IIR using a IIR luciferase reporter assay. Once several partners would be identified as having an effect on the IIR, CRAC techniques could be performance during viral infection in order to identify actual viral RNAs bound to these NET23/STING NE binding partners and get insights into their role during IIR signaling.

In order to confirm the involvement of several novel IIR mediators that likely function redundantly to provide, through NET23/STING, a backup mechanism for the cell to activate the IIR when central channel of NPC is blocked and further support the results from the luciferase assay, it would be interesting to study whether some of

these NET23/STING RNA-binding partners hamper viral growth. For this, viral titers could be performed in individual and combinatorial depleted cells.

7.7. Herpesvirus nuclear egress

In the last few years it has become clear that herpesvirus capsids leave the nucleus following a membrane envelopment process at the NE by a vesicle-mediated process that enables budding of nucleocapsids at the INM resulting in the formation of PEP in the NE lumen. Then, these particles fuse with the ONM releasing naked capsids into the cytoplasm where a second envelopment process takes place. There are two well-known viral proteins that play a role in this process and that are conserved among the herpesviridae family, UL31 and UL34 (Bigalke and Heldwein 2015, Bosse and Enquist 2016, Hellberg, Passvogel et al. 2016). Before reaching the INM, nucleocapsids need to face the nuclear lamina, a dense meshwork of filaments, nuclear lamin binding proteins and NETs that maintain the structure of the nucleus. The involvement of cellular kinases, such as Cdk1 and PKC has been previously suggested in order to phosphorylate and soften the nuclear lamina facilitating the access of the viral nucleocapsids to the INM (Morrison and DeLassus 2011).

In the work presented in this thesis I aimed to shed light on the nuclear egress of HSV-1 by the identification of host cellular proteins that might be co-operating with UL31 and UL34 or be involved in alternative pathways helping viral nucleocapsids to cross the NE. Furthermore, as the NE contains hundreds of transmembrane proteins interacting with lamins and chromatin, it is likely to hypothesize that in order to achieve a successful nuclear egress, HSV-1 must target and disrupt some of these connections prior envelopment at the NE.

7.7.1. Potential identification of multiple viral proteins as part of primary enveloped particles

One of the hypotheses we pursued in order to identify host cellular proteins involved in herpesvirus nuclear egress was that proteins from the INM captured during the process of primary envelopment/de-envelopment or actively participating in the primary envelope are released into the ONM and diffuse into the ER. With this idea in mind, MMs from HSV-1 infected cells were isolated and subjected to MS analyses. Although the core purpose of this study was not the isolation of PEP, the EM observation of viral particles inside isolated MMs that presented similar characteristics and appearance to PEP suggested that this approach in combination with immunogold labeling could be used in the future to obtain a pure fraction of PEP trapped in the NE lumen. The isolation of PEP could be subjected to an in-depth proteome analysis that will provide new insights into HSV-1 biology. Sucrose gradients could be used to concentrate and purify PEP from HSV-1 infected MMs. Immunogold labelling using already known viral proteins present in PEP should confirm the isolation of these particles.

The composition of PEP is only partially known due to difficulties in isolating this assembly intermediate viral form for complete proteomic analysis. Until the moment, only a limited study performed by Padula and colleagues attempted to isolate primary virions and identified 8 viral proteins as part of the primary envelope (Padula, Sydnor et al. 2009). Although only gD of the viral coat glycoproteins was identified in this study as being part of the primary enveloped, other studies have indicated the presence of gB and gC (Torrisi, Di Lazzaro et al. 1992, Jensen and Norrild 1998) that we found of similar abundance to gD in our mass spectrometry analysis. Thus, it is reasonable to suggest that our MS datasets contain most or all of the proteins, both viral and host cell-encoded, that are in PEP. Even though I performed different experiments to determine the optimal time during infection where nuclear egress has started but before secondary envelopment, I cannot clearly distinguish which proteins were present due to synthesis in the ER and which are in captured PEP. Nevertheless, the grouping of higher abundance glycoproteins

that were all previously reported in PEP suggests that other virion proteins may be identified by similar abundance groupings.

While capsid and some tegument proteins are expected in the PEP, the functional significance and role, if any, for glycoproteins in nuclear egress is unclear. During secondary envelopment viral glycoproteins located in the TGN interact with tegument proteins presented in the surface of capsids helping to pull the host membranes around viral particles. Thus, it is possible that during primary envelopment viral glycoproteins play a part in anchoring the INM onto the capsid in a similar way as during secondary envelopment. Evidence supporting this hypothesis came from the colocalisation of gB, gH, UL31 and UL34 at the NE together with cellular proteins CD98hc and β1-intergrin. This study argues that these cellular proteins probably interact directly and/or indirectly with viral proteins gB, gH, UL31 and UL34 regulating HSV-1 nuclear egress (Hirohata, Arii et al. 2015). Thus, it is likely that these viral protein complexes may recruit other host proteins needed for both primary and secondary envelopment such as vesicle fusion proteins that could drive membrane fusion events at the NE.

7.7.2. Vesicle fusion membrane proteins involved in nuclear egress

Recent studies have shown that the process of nuclear egress is not exclusive to herpesviruses as it has also been observed during the export of RNPs, large synaptic ribonucleoparticles in Drosophila (Speese, Ashley et al. 2012, Fradkin and Budnik 2016). These particles are too large to cross the NPC, therefore as in the case of herpesviruses, RNPs need to develop new mechanisms to cross through the NE. The existence of nuclear egress events in non-infected cells argues that herpesviruses might usurp or mimic this cellular pathway during infection. Although different studies suggested common biological mechanism between the nuclear egress of RNPs and herpesvirus PEP, no cellular proteins have been yet identified to be involved in HSV-1 nuclear egress.

Recently EM-tomography studies have argued that only electron density for UL31 and UL34 is observed at sites of fusion with the INM, suggesting that the presence of only these two viral proteins is sufficient to push the INM around the nucleocapsids (Hagen, Dent et al. 2015). But this process is likely much more complex as UL31 is a phosphoprotein that does not present transmembrane domains and it localizes to the INM through interaction with UL34, a protein which is still uncertain whether is a full transmembrane protein or it is ectopically associated to the NE. To our knowledge no study has ever directly tested whether UL34 is a transmembrane protein or ectopically associated with the membrane. In Shiba paper, the topology of UL34 is investigated in order to study in which cellular compartment the N-terminal region of the protein was inserted (Shiba, Daikoku et al. 2000). However, this study did not perform any experiment to test whether the C-terminus extended into the opposing cellular compartment. Although this study stated that this C-terminus is likely a type II transmembrane protein based on the use of a hydrophobic stretch of 22 to 37 residues near the C-terminus, this could also be observed for an ectopically associated protein. Moreover, they did not directly test its membrane insertion. The digitonin permeabilization experiment, previously used to distinguish between antigens on the nuclear and cytoplasmic side of the NE, could be used to directly test the membrane insertion of UL34. However, this could be a difficult experiment to perform in the case of this viral protein. If UL34 is a transmembrane protein, there would be only three aminoacids in the NE lumen making difficult the production of a specific antibody for only these three amino acids and adding a tag would be likely to alter normal topology.

Thus, as UL34 seems to be presenting a weak association to the membrane as compared to other proteins presenting multiple transmembrane domains within the NE and taking into account that herpesviruses frequently co-op host cell machinery to support various aspects of their life cycle, it is likely that other cellular proteins are being used for a more efficient nuclear egress by being involved in membrane curvature for budding at the NE or by co-operating with UL31 and UL34 pulling the INM around the new viral particles. This argument is further supported by the need of proteins to be strongly associated to membrane through the interaction with other

protein complexes in order to effect membrane curvature and be able to pull the surrounding membrane around a specific cargo (Jarsch, Daste et al. 2016).

Accordingly, the involvement of host proteins such as ESCRT proteins has recently been shown for Epstein-Barr virus EBV. In this case, the Chmp4b protein important for scission complex assembly largely co-localized in perinuclear aggregates with EBV protein BFRF1 and inhibition of the Alix bridging protein resulted in accumulation of capsid proteins in the nucleus. However, they also reported that the ability to induce vesicle formation was not found for HSV-1 UL34 protein (Lee, Liu et al. 2012). The identification of VAPB, Rab11b and Rab18 as vesicle fusion proteins contributing to virus egress points out the possibility of other host proteins contributing to herpesvirus egress

VAPB is a member of the Vesicle-associated membrane protein (VAMP) Associated Protein family of ER C-tail anchored proteins. It functions as an adaptor protein to recruit target proteins to the ER and execute various cellular functions such as lipid transport, membrane trafficking and membrane fusion (Lev, Ben Halevy et al. 2008). A nuclear link has also previously been found for VAPB where its knockdown resulted in a failure of NPC proteins gp210 and Nup214 and the nuclear membrane protein emerin to accumulate at the nuclear envelope (Tran, Chalhoub et al. 2012). However, as VAPB was predominantly found in the ER in this study, this could as easily reflect general disruption of protein synthesis, post-translational modifications and trafficking caused by VAPB knockdown which is known to induce Golgi fragmentation and disrupted ER to ERGIC (ER-Golgi Intermediate Compartment) to Golgi trafficking (Peretti, Dahan et al. 2008, Kuijpers, Yu et al. 2013). In contrast we found clear accumulation of VAPB in the nuclear membrane during HSV-1 infection and its considerable co-localization with UL34 suggesting a direct function in nuclear egress. This does not discount the possibility that VAPB has both direct and indirect effects on HSV-1 processing and trafficking or a possible additional role in secondary envelopment.

A potential additional role for the two Rab proteins tested in secondary envelopment is also a possibility, especially as a previous study reported Rab11b involvement in secondary envelopment (Hollinshead, Johns et al. 2012). Rab proteins are membrane-associated proteins belonging to the Ras-related small GTPases. There

are over 50 Rab proteins encoded by mammalian genomes with only 19 of them having functions in the Golgi and only 6 of these functioning exclusively in the Golgi (Liu and Storrie 2012). Moreover, Rab11b is reported also in the recycling and early endosomes (Ullrich, Reinsch et al. 1996) and Rab18 is reported also in the ER, endosome and lipid droplets (Lutcke, Parton et al. 1994, Brasaemle, Dolios et al. 2004). Functionally, Rab proteins have been shown to be crucial regulators for many aspects of membrane trafficking including vesicle formation, budding, docking and fusion so that they could contribute to multiple aspects of both envelopment and de-envelopment, as well as secondary envelopment.

The only previously known functional links between Rab11b and viruses are a study showing its involvement in herpes secondary envelopment in the Golgi (Hollinshead, Johns et al. 2012) and a report of its involvement in hantavirus release from cells (Rowe, Suszko et al. 2008). Rab18, in contrast, is linked to multiple RNA viruses for their assembly around lipid droplets in the cytoplasm, including hepatitis C and Dengue virus (Salloum, Wang et al. 2013, Dansako, Hiramoto et al. 2014); however, such functions are clearly distinct from its contribution to herpesvirus nuclear egress. Nonetheless, due to the wide range of functions linked to Rab proteins it remains possible that some of their effects on the virus could be indirect. For example, Rab11b was recently shown to be involved in proper sorting of the protease-activated receptor-1 protein (Grimsey, Coronel et al. 2016), thus raising the possibility that Rab protein recruitment of as yet unknown proteins to the NE could contribute to post-translational processing of herpesvirus proteins.

Although only the depletion of VAPB, Rab11b and Rab18 were tested for viral titers, additional vesicle membrane fusion proteins such as VAMP7, Rab9a, Rab2A and STX7 were identified to have similar NE localization and an increase in HSV-1 infected MMs compared to mock-infected MMs. These finding indicated the potential interplay of other host cell vesicle fusion proteins during viral nuclear egress suggesting the potential redundancy in the use of vesicle membrane fusion proteins that can readily explain why combined knockdowns did not yield a greater reduction in viral titers.

Thus, based on my results and previous studies for other herpesviruses, vesicle membrane fusion proteins might be involved in HSV-1 nuclear egress perhaps

affecting the curvature of the INM or ONM or co-operate with UL31, UL34 or other viral proteins facilitating viral budding into the NE lumen. Further experiments will need to confirm the specific mechanisms by which these vesicle fusion proteins are being involved in HSV-1 nuclear egress. For instance, an interesting direction would be to determine whether the vesicle fusion proteins identified in this thesis physically interact with UL31 and/or UL34 by the performance of pulldown assays.

7.7.3. Vesicle fusion proteins involved in envelopment or de-envelopment?

One of the main questions that remains about the role of these vesicle membrane fusion proteins is whether they contribute to primary envelopment, de-envelopment or both during herpesvirus nuclear egress. The immunogold labelling EM data showed VAPB associating with nucleoplasmic virus particles, making a role in primary envelopment almost certain. However, the immunogold EM data also clearly shows VAPB localizes both to the ONM and the INM during HSV-1 infection, which indicates that its potential contribution could affect either or both steps. It is important to note that while the appearance in either membrane could reflect functionality, if these transmembrane proteins translocate by lateral diffusion in the membrane through the peripheral NPC channels similarly to other NETs, then the presence in both membranes could also simply reflect this diffusion process due to the many NPCs in the membrane. In considering a possible dual function, it is important to note that previous studies of gB and gH depletion or mutants revealed an accumulation of PEP in both the nucleoplasm and in the NE lumen (Farnsworth, Wisner et al. 2007, Wright, Wisner et al. 2009). In contrast, knockdown of VAPB, Rab11b and Rab18 all resulted principally in accumulation of non-enveloped encapsidated virus particles in the nucleoplasm with very few observed in the NE lumen. This observation is more what would be expected for a role in primary envelopment at the INM as the depletion of these proteins are hampering the ability of these particles to become wrapped by the INM reaching the NE lumen and, accordingly, is consistent with the observation of VAPB in both the INM and ONM

during normal infection, as any protein in the INM that got into PEP would be redistributed to the ONM upon de-envelopment. It is important to note that this does not contradict any of the previous studies in which UL31 and UL34 depletion showed reduced HSV-1 titers when compared with wild type infection as HSV-1 has been shown to still get out of the nucleus in the absence of these two viral proteins (Miller, Hill et al. 1976, Wagenaar, Pol et al. 1995, Klupp, Granzow et al. 2001, Haugo, Szpara et al. 2011) suggesting the presence of multiple mechanisms by which herpesvirus is able to cross the NE.

7.7.4. NETs might be playing a role in herpesvirus nuclear egress

The presence of hundreds of different NETs within the NE and the numerous interactions with the nuclear lamina likely suggest that these transmembrane proteins might be either targeted by herpesvirus capsids prior to envelopment at the INM or they might be assisting viral fusion events with capsid and/or tegument protein, like glycoproteins do in secondary envelopment, facilitating a proximal access of viral particles to the INM that will result in membrane deformation.

Previously, some NETs such as LBR have been shown to undergo a partial redistribution from a predominantly INM localization to a significant proportion accumulating in the ER upon HSV-1 infection (Scott and O'Hare 2001). Thus, it is not surprising the relocalization suffered by some other NETs observed by immunofluorescence microscopy in this thesis. Interestingly, NET29 and NET39 are known to have a direct role in chromosome organization and their observed accumulation at cytoplasmic or ER compartment during HSV-1 infection could implicate the break of connections between NETs and chromatin in order to facilitate viral access to the INM arguing the possibility of other NETs being removed from the NE in order to facilitate primary envelopment.

This is just preliminary data; so further experiments are needed to confirm these observations. There is still the question of whether these NETs are being targeted directly by the virus or the observed redistribution is an indirect consequence of a

disruption between chromatin, lamins and NETs. One direction that would be interesting to pursue is if the absence of some of these NETs is affecting viral growth. To address this question, viral titers could be performed in infected cells in which the knockdown of multiple rather than individual NETs would be tested as it is likely that the silencing of a single NET would not yield a greater reduction in viral titers due to the complex interplay of these proteins during viral nuclear egress.

It is also important to have in mind that some of these NETs, as shown for emerin, might be suffering post-translational modifications such as phosphorylation (Leach, Bjerke et al. 2007, Morris, Hofemeister et al. 2007). The identification of new cellular kinases in our MS dataset suggesting their potential involvement in nuclear egress clearly supports this idea.

These post-translational modifications might be induced during viral infection in order to alter the tethering of NETs with chromatin at the NE facilitating the access of nucleocapsids to the membrane. Thus, another approach will be to test if some of the screened NETs present phosphorylation as a consequence of HSV-1 infection. For this, MS analysis should be performed on HSV-1 MMs previously isolated using phosphatase inhibitors buffers in order to block dephosphorylation of proteins.

7.7.5. Herpesvirus nuclear egress final remarks

This work provides an advance in the field of herpesvirus nuclear egress in which I have found for the first time for HSV-1 the involvement of multiple vesicle fusion proteins in this viral step.

Despite recent studies arguing that UL31/34 is sufficient to allow membrane invaginations at the NE (Bigalke, Heuser et al. 2014) (Hagen, Dent et al. 2015) and pointing out that neither of these studies measured the efficiency of membrane budding compared to a normal infection, it seems likely that the discovery of vesicle fusion proteins in this thesis might provide an alternative pathway for herpesvirus nuclear egress besides the already known UL31 and UL34 proteins. However, there are many questions still to be answered. What is the relative contribution of UL31/34

and these vesicle fusion proteins to primary envelopment? What viral proteins recruit the vesicle fusion proteins and do they directly interact?

Additionally, the novel approach presented in this thesis in which MMs from HSV-1 infected cells are isolated in order to find potential host proteins involved in nuclear egress could be modified in the future to isolate a pure fraction of PEP in order to gain a deep understanding of the protein composition of these particles.

The study presented in this thesis presents novel insights into one of the least understood steps in HSV-1 life cycle through the identification of vesicle fusion host proteins that are being involved in viral egress and could possibility represent novel targets for therapeutic interventions.

Referencees

Agarwal, S. K., S. C. Guru, C. Heppner, M. R. Erdos, R. M. Collins, S. Y. Park, S. Saggar, S. C. Chandrasekharappa, F. S. Collins, A. M. Spiegel, S. J. Marx and A. L. Burns (1999). "Menin interacts with the AP1 transcription factor JunD and represses JunD-activated transcription." Cell **96**(1): 143-152.

Akhtar, J. and D. Shukla (2009). "Viral entry mechanisms: cellular and viral mediators of herpes simplex virus entry." FEBS J **276**(24): 7228-7236.

Akira, S., S. Uematsu and O. Takeuchi (2006). "Pathogen recognition and innate immunity." Cell **124**(4): 783-801.

Arbuckle, J. H. and T. M. Kristie (2014). "Epigenetic repression of herpes simplex virus infection by the nucleosome remodeler CHD3." MBio **5**(1): e01027-01013.

Aydin, I., S. Weber, B. Snijder, P. Samperio Ventayol, A. Kuhbacher, M. Becker, P. M. Day, J. T. Schiller, M. Kann, L. Pelkmans, A. Helenius and M. Schelhaas (2014). "Large scale RNAi reveals the requirement of nuclear envelope breakdown for nuclear import of human papillomaviruses." PLoS Pathog **10**(5): e1004162.

Baines, J. D., E. Wills, R. J. Jacob, J. Pennington and B. Roizman (2007). "Glycoprotein M of herpes simplex virus 1 is incorporated into virions during budding at the inner nuclear membrane." J Virol **81**(2): 800-812.

Bannai, H., K. Fukatsu, A. Mizutani, T. Natsume, S. Iemura, T. Ikegami, T. Inoue and K. Mikoshiba (2004). "An RNA-interacting protein, SYNCRIP (heterogeneous nuclear ribonuclear protein Q1/NSAP1) is a component of mRNA granule transported with inositol 1,4,5-trisphosphate receptor type 1 mRNA in neuronal dendrites." J Biol Chem **279**(51): 53427-53434.

Barber, G. N. (2011). "Innate immune DNA sensing pathways: STING, AIMII and the regulation of interferon production and inflammatory responses." Curr Opin Immunol **23**(1): 10-20.

Baricheva, E. A., M. Berrios, S. S. Bogachev, I. V. Borisevich, E. R. Lapik, I. V. Sharakhov, N. Stuurman and P. A. Fisher (1996). "DNA from Drosophila melanogaster beta-heterochromatin binds specifically to nuclear lamins in vitro and the nuclear envelope in situ." Gene **171**(2): 171-176.

Berk, J. M., K. E. Tifft and K. L. Wilson (2013). "The nuclear envelope LEM-domain protein emerin." Nucleus **4**(4): 298-314.

Bhuin, T. and J. K. Roy (2014). "Rab proteins: the key regulators of intracellular vesicle transport." Exp Cell Res **328**(1): 1-19.

Bickmore, W. A. and B. van Steensel (2013). "Genome architecture: domain organization of interphase chromosomes." Cell **152**(6): 1270-1284.

Bierne, H., M. Hamon and P. Cossart (2012). "Epigenetics and bacterial infections." Cold Spring Harb Perspect Med **2**(12): a010272.

Bigalke, J. M. and E. E. Heldwein (2015). "The Great (Nuclear) Escape: New Insights into the Role of the Nuclear Egress Complex of Herpesviruses." J Virol **89**(18): 9150-9153.

Bigalke, J. M. and E. E. Heldwein (2016). "Nuclear Exodus: Herpesviruses Lead the Way." Annu Rev Virol **3**(1): 387-409.

Bigalke, J. M., T. Heuser, D. Nicastro and E. E. Heldwein (2014). "Membrane deformation and scission by the HSV-1 nuclear egress complex." Nat Commun **5**: 4131.

Bione, S., E. Maestrini, S. Rivella, M. Mancini, S. Regis, G. Romeo and D. Toniolo (1994). "Identification of a novel X-linked gene responsible for Emery-Dreifuss muscular dystrophy." Nat Genet **8**(4): 323-327.

Bjerke, S. L. and R. J. Roller (2006). "Roles for herpes simplex virus type 1 UL34 and US3 proteins in disrupting the nuclear lamina during herpes simplex virus type 1 egress." Virology **347**(2): 261-276.

Boehmer, P. E. and I. R. Lehman (1997). "Herpes simplex virus DNA replication." Annu Rev Biochem **66**: 347-384.

Bonifacino, J. S. and B. S. Glick (2004). "The mechanisms of vesicle budding and fusion." Cell **116**(2): 153-166.

Bonne, G., M. R. Di Barletta, S. Varnous, H. M. Becane, E. H. Hammouda, L. Merlini, F. Muntoni, C. R. Greenberg, F. Gary, J. A. Urtizberea, D. Duboc, M. Fardeau, D. Toniolo and K. Schwartz (1999). "Mutations in the gene encoding lamin A/C cause autosomal dominant Emery-Dreifuss muscular dystrophy." Nat Genet **21**(3): 285-288.

Bonne, G., F. Leturcq and R. Ben Yaou (1993). Emery-Dreifuss Muscular Dystrophy. GeneReviews(R). R. A. Pagon, M. P. Adam, H. H. Ardinger et al. Seattle (WA).

Bosse, J. B. and L. W. Enquist (2016). "The diffusive way out: Herpesviruses remodel the host nucleus, enabling capsids to access the inner nuclear membrane." Nucleus **7**(1): 13-19.

Bosse, J. B., I. B. Hogue, M. Feric, S. Y. Thiberge, B. Sodeik, C. P. Brangwynne and L. W. Enquist (2015). "Remodeling nuclear architecture allows efficient transport of herpesvirus capsids by diffusion." Proc Natl Acad Sci U S A **112**(42): E5725-5733.

Brack, A. R., J. M. Dijkstra, H. Granzow, B. G. Klupp and T. C. Mettenleiter (1999). "Inhibition of virion maturation by simultaneous deletion of glycoproteins E, I, and M of pseudorabies virus." J Virol **73**(7): 5364-5372.

Brack, A. R., B. G. Klupp, H. Granzow, R. Tirabassi, L. W. Enquist and T. C. Mettenleiter (2000). "Role of the cytoplasmic tail of pseudorabies virus glycoprotein E in virion formation." J Virol **74**(9): 4004-4016.

Brasaemle, D. L., G. Dolios, L. Shapiro and R. Wang (2004). "Proteomic analysis of proteins associated with lipid droplets of basal and lipolytically stimulated 3T3-L1 adipocytes." J Biol Chem **279**(45): 46835-46842.

Bruns, H. (1980). "Electron microscopic studies of herpes simplex virus type 1 infection of macrophages, T- and B-lymphocytes of mice." Arch Virol **64**(3): 257-268.

Burdette, D. L. and R. E. Vance (2013). "STING and the innate immune response to nucleic acids in the cytosol." Nat Immunol **14**(1): 19-26.

Cai, M., Y. Huang, R. Ghirlando, K. L. Wilson, R. Craigie and G. M. Clore (2001). "Solution structure of the constant region of nuclear envelope protein LAP2 reveals two LEM-domain structures: one binds BAF and the other binds DNA." EMBO J **20**(16): 4399-4407.

Caillet, M., K. Janvier, A. Pelchen-Matthews, D. Delcroix-Genete, G. Camus, M. Marsh and C. Berlioz-Torrent (2011). "Rab7A is required for efficient production of infectious HIV-1." PLoS Pathog **7**(11): e1002347.

Callan, H. G. and S. G. Tomlin (1950). "Experimental studies on amphibian oocyte nuclei. I. Investigation of the structure of the nuclear membrane by means of the electron microscope." Proc R Soc Lond B Biol Sci **137**(888): 367-378.

Calle, A., I. Ugrinova, A. L. Epstein, P. Bouvet, J. J. Diaz and A. Greco (2008). "Nucleolin is required for an efficient herpes simplex virus type 1 infection." J Virol **82**(10): 4762-4773.

Caputo, S., J. Couprie, I. Duband-Goulet, E. Konde, F. Lin, S. Braud, M. Gondry, B. Gilquin, H. J. Worman and S. Zinn-Justin (2006). "The carboxyl-terminal nucleoplasmic region of MAN1 exhibits a DNA binding winged helix domain." J Biol Chem **281**(26): 18208-18215.

Carbon, S., A. Ireland, C. J. Mungall, S. Shu, B. Marshall, S. Lewis, G. O. H. Ami and G. Web Presence Working (2009). "AmiGO: online access to ontology and annotation data." Bioinformatics **25**(2): 288-289.

Chang, C. W., C. P. Lee, Y. H. Huang, P. W. Yang, J. T. Wang and M. R. Chen (2012). "Epstein-Barr virus protein kinase BGLF4 targets the nucleus through interaction with nucleoporins." J Virol **86**(15): 8072-8085.

Chang, Y. E. and B. Roizman (1993). "The product of the UL31 gene of herpes simplex virus 1 is a nuclear phosphoprotein which partitions with the nuclear matrix." J Virol **67**(11): 6348-6356.

Chen, H., H. Sun, F. You, W. Sun, X. Zhou, L. Chen, J. Yang, Y. Wang, H. Tang, Y. Guan, W. Xia, J. Gu, H. Ishikawa, D. Gutman, G. Barber, Z. Qin and Z. Jiang (2011). "Activation of STAT6 by STING is critical for antiviral innate immunity." Cell **147**(2): 436-446.

Chen, J., X. F. Zheng, E. J. Brown and S. L. Schreiber (1995). "Identification of an 11-kDa FKBP12-rapamycin-binding domain within the 289-kDa FKBP12-rapamycin-associated protein and characterization of a critical serine residue." Proc Natl Acad Sci U S A **92**(11): 4947-4951.

Chiacchia, K. B. and K. Drickamer (1984). "Direct evidence for the transmembrane orientation of the hepatic glycoprotein receptors." J Biol Chem **259**(24): 15440-15446.

Choi, K. S., A. Mizutani and M. M. Lai (2004). "SYNCRIP, a member of the heterogeneous nuclear ribonucleoprotein family, is involved in mouse hepatitis virus RNA synthesis." J Virol **78**(23): 13153-13162.

Christensen, M. H., S. B. Jensen, J. J. Miettinen, S. Luecke, T. Prabakaran, L. S. Reinert, T. Mettenleiter, Z. J. Chen, D. M. Knipe, R. M. Sandri-Goldin, L. W. Enquist, R. Hartmann, T. H. Mogensen, S. A. Rice, T. A. Nyman, S. Matikainen and S. R. Paludan (2016). "HSV-1 ICP27 targets

the TBK1-activated STING signalsome to inhibit virus-induced type I IFN expression." EMBO J **35**(13): 1385-1399.

Christensen, M. H., S. B. Jensen, J. J. Miettinen, S. Luecke, T. Prabakaran, L. S. Reinert, T. Mettenleiter, Z. J. Chen, D. M. Knipe, R. M. Sandri-Goldin, L. W. Enquist, R. Hartmann, T. H. Mogensen, S. A. Rice, T. A. Nyman, S. Matikainen and S. R. Paludan (2016). "HSV-1 ICP27 targets the TBK1-activated STING signalsome to inhibit virus-induced type I IFN expression." EMBO J.

Cohen, S., S. Au and N. Pante (2011). "How viruses access the nucleus." Biochim Biophys Acta **1813**(9): 1634-1645.

Columbaro, M., C. Capanni, E. Mattioli, G. Novelli, V. K. Parnaik, S. Squarzoni, N. M. Maraldi and G. Lattanzi (2005). "Rescue of heterochromatin organization in Hutchinson-Gilford progeria by drug treatment." Cell Mol Life Sci **62**(22): 2669-2678.

Conn, K. L. and L. M. Schang (2013). "Chromatin dynamics during lytic infection with herpes simplex virus 1." Viruses **5**(7): 1758-1786.

Connolly, S. A., J. O. Jackson, T. S. Jardetzky and R. Longnecker (2011). "Fusing structure and function: a structural view of the herpesvirus entry machinery." Nat Rev Microbiol **9**(5): 369-381.

Cook, A., F. Bono, M. Jinek and E. Conti (2007). "Structural biology of nucleocytoplasmic transport." Annu Rev Biochem **76**: 647-671.

Copeland, A. M., W. W. Newcomb and J. C. Brown (2009). "Herpes simplex virus replication: roles of viral proteins and nucleoporins in capsid-nucleus attachment." J Virol **83**(4): 1660-1668.

Courvalin, J. C., N. Segil, G. Blobel and H. J. Worman (1992). "The lamin B receptor of the inner nuclear membrane undergoes mitosis-specific phosphorylation and is a substrate for p34cdc2-type protein kinase." J Biol Chem **267**(27): 19035-19038.

Czapiewski, R., M. I. Robson and E. C. Schirmer (2016). "Anchoring a Leviathan: How the Nuclear Membrane Tethers the Genome." Front Genet **7**: 82.

Dahl, K. N., S. M. Kahn, K. L. Wilson and D. E. Discher (2004). "The nuclear envelope lamina network has elasticity and a compressibility limit suggestive of a molecular shock absorber." J Cell Sci **117**(Pt 20): 4779-4786.

Dahl, K. N., A. J. Ribeiro and J. Lammerding (2008). "Nuclear shape, mechanics, and mechanotransduction." Circ Res **102**(11): 1307-1318.

Dansako, H., H. Hiramoto, M. Ikeda, T. Wakita and N. Kato (2014). "Rab18 is required for viral assembly of hepatitis C virus through trafficking of the core protein to lipid droplets." Virology **462-463**: 166-174.

Davison, A. J. (2010). "Herpesvirus systematics." Vet Microbiol **143**(1): 52-69.

De Sandre-Giovannoli, A., R. Bernard, P. Cau, C. Navarro, J. Amiel, I. Boccaccio, S. Lyonnet, C. L. Stewart, A. Munnich, M. Le Merrer and N. Levy (2003). "Lamin a truncation in Hutchinson-Gilford progeria." Science **300**(5628): 2055.

De Santa, F., V. Narang, Z. H. Yap, B. K. Tusi, T. Burgold, L. Austenaa, G. Bucci, M. Caganova, S. Notarbartolo, S. Casola, G. Testa, W. K. Sung, C. L. Wei and G. Natoli (2009). "Jmjd3 contributes to the control of gene expression in LPS-activated macrophages." EMBO J **28**(21): 3341-3352.

De Santa, F., M. G. Totaro, E. Prosperini, S. Notarbartolo, G. Testa and G. Natoli (2007). "The histone H3 lysine-27 demethylase Jmjd3 links inflammation to inhibition of polycomb-mediated gene silencing." Cell **130**(6): 1083-1094.

De Vos, K. J., G. M. Morotz, R. Stoica, E. L. Tudor, K. F. Lau, S. Ackerley, A. Warley, C. E. Shaw and C. C. Miller (2012). "VAPB interacts with the mitochondrial protein PTPIP51 to regulate calcium homeostasis." Hum Mol Genet **21**(6): 1299-1311.

Dechat, T., J. Gotzmann, A. Stockinger, C. A. Harris, M. A. Talle, J. J. Siekierka and R. Foisner (1998). "Detergent-salt resistance of LAP2alpha in interphase nuclei and phosphorylation-dependent association with chromosomes early in nuclear assembly implies functions in nuclear structure dynamics." EMBO J **17**(16): 4887-4902.

Demmerle, J., A. J. Koch and J. M. Holaska (2012). "The nuclear envelope protein emerin binds directly to histone deacetylase 3 (HDAC3) and activates HDAC3 activity." J Biol Chem **287**(26): 22080-22088.

Dempsey, A. and A. G. Bowie (2015). "Innate immune recognition of DNA: A recent history." Virology **479-480**: 146-152.

Diefenbach, R. J., M. Miranda-Saksena, M. W. Douglas and A. L. Cunningham (2008). "Transport and egress of herpes simplex virus in neurons." Rev Med Virol **18**(1): 35-51.

Ding, B., R. Bellizzi Mdel, Y. Ning, B. C. Meyers and G. L. Wang (2012). "HDT701, a histone H4 deacetylase, negatively regulates plant innate immunity by modulating histone H4 acetylation of defense-related genes in rice." Plant Cell **24**(9): 3783-3794.

Dreger, M., L. Bengtsson, T. Schoneberg, H. Otto and F. Hucho (2001). "Nuclear envelope proteomics: novel integral membrane proteins of the inner nuclear membrane." Proc Natl Acad Sci U S A **98**(21): 11943-11948.

Duffy, C., J. H. Lavail, A. N. Tauscher, E. G. Wills, J. A. Blaho and J. D. Baines (2006). "Characterization of a UL49-null mutant: VP22 of herpes simplex virus type 1 facilitates viral spread in cultured cells and the mouse cornea." J Virol **80**(17): 8664-8675.

Dwyer, D. E. and A. L. Cunningham (2002). "10: Herpes simplex and varicella-zoster virus infections." Med J Aust **177**(5): 267-273.

Eibauer, M., M. Pellanda, Y. Turgay, A. Dubrovsky, A. Wild and O. Medalia (2015). "Structure and gating of the nuclear pore complex." Nat Commun **6**: 7532.

Eisenberg, R. J., D. Atanasiu, T. M. Cairns, J. R. Gallagher, C. Krummenacher and G. H. Cohen (2012). "Herpes virus fusion and entry: a story with many characters." Viruses **4**(5): 800-832.

Elliott, G., G. Mouzakitis and P. O'Hare (1995). "VP16 interacts via its activation domain with VP22, a tegument protein of herpes simplex virus, and is relocated to a novel macromolecular assembly in coexpressing cells." J Virol **69**(12): 7932-7941.

Eng, J. K., A. L. McCormack and J. R. Yates (1994). "An approach to correlate tandem mass spectral data of peptides with amino acid sequences in a protein database." J Am Soc Mass Spectrom **5**(11): 976-989.

Eriksson, M., W. T. Brown, L. B. Gordon, M. W. Glynn, J. Singer, L. Scott, M. R. Erdos, C. M. Robbins, T. Y. Moses, P. Berglund, A. Dutra, E. Pak, S. Durkin, A. B. Csoka, M. Boehnke, T. W. Glover and F. S. Collins (2003). "Recurrent de novo point mutations in lamin A cause Hutchinson-Gilford progeria syndrome." Nature **423**(6937): 293-298.

Farnsworth, A., K. Goldsmith and D. C. Johnson (2003). "Herpes simplex virus glycoproteins gD and gE/gI serve essential but redundant functions during acquisition of the virion envelope in the cytoplasm." J Virol **77**(15): 8481-8494.

Farnsworth, A., T. W. Wisner, M. Webb, R. Roller, G. Cohen, R. Eisenberg and D. C. Johnson (2007). "Herpes simplex virus glycoproteins gB and gH function in fusion between the virion envelope and the outer nuclear membrane." Proc Natl Acad Sci U S A **104**(24): 10187-10192.

Fasana, E., M. Fossati, A. Ruggiano, S. Brambillasca, C. C. Hoogenraad, F. Navone, M. Francolini and N. Borgese (2010). "A VAPB mutant linked to amyotrophic lateral sclerosis generates a novel form of organized smooth endoplasmic reticulum." FASEB J **24**(5): 1419-1430.

Fatahzadeh, M. and R. A. Schwartz (2007). "Human herpes simplex virus infections: epidemiology, pathogenesis, symptomatology, diagnosis, and management." J Am Acad Dermatol **57**(5): 737-763; quiz 764-736.

Fawcett, D. W. (1966). "On the occurrence of a fibrous lamina on the inner aspect of the nuclear envelope in certain cells of vertebrates." Am J Anat **119**(1): 129-145.

Fawcett, D. W., S. Doxsey and G. Buscher (1981). "Salivary gland of the tick vector (R. appendiculatus) of East Coast fever. I. Ultrastructure of the type III acinus." Tissue Cell **13**(2): 209-230.

Fidzianska, A., D. Toniolo and I. Hausmanowa-Petrusewicz (1998). "Ultrastructural abnormality of sarcolemmal nuclei in Emery-Dreifuss muscular dystrophy (EDMD)." J Neurol Sci **159**(1): 88-93.

Fields, A. P. and L. J. Thompson (1995). "The regulation of mitotic nuclear envelope breakdown: a role for multiple lamin kinases." Prog Cell Cycle Res **1**: 271-286.

Florens, L., N. Korfali and E. C. Schirmer (2008). "Subcellular fractionation and proteomics of nuclear envelopes." Methods Mol Biol **432**: 117-137.

Florens, L. and M. P. Washburn (2006). "Proteomic analysis by multidimensional protein identification technology." Methods Mol Biol **328**: 159-175.

Foisner, R. and L. Gerace (1993). "Integral membrane proteins of the nuclear envelope interact with lamins and chromosomes, and binding is modulated by mitotic phosphorylation." Cell **73**(7): 1267-1279.

Fossum, E., C. C. Friedel, S. V. Rajagopala, B. Titz, A. Baiker, T. Schmidt, T. Kraus, T. Stellberger, C. Rutenberg, S. Suthram, S. Bandyopadhyay, D. Rose, A. von Brunn, M. Uhlmann, C. Zeretzke, Y. A. Dong, H. Boulet, M. Koegl, S. M. Bailer, U. Koszinowski, T. Ideker, P. Uetz, R. Zimmer and J. Haas (2009). "Evolutionarily conserved herpesviral protein interaction networks." PLoS Pathog **5**(9): e1000570.

Fradkin, L. G. and V. Budnik (2016). "This bud's for you: mechanisms of cellular nucleocytoplasmic trafficking via nuclear envelope budding." Curr Opin Cell Biol **41**: 125-131.

Franke, W. W., U. Scheer, G. Krohne and E. D. Jarasch (1981). "The nuclear envelope and the architecture of the nuclear periphery." J Cell Biol **91**(3 Pt 2): 39s-50s.

Fuchs, W., B. G. Klupp, H. Granzow, N. Osterrieder and T. C. Mettenleiter (2002). "The Interacting UL31 and UL34 Gene Products of Pseudorabies Virus Are Involved in Egress from the Host-Cell Nucleus and Represent Components of Primary Enveloped but Not Mature Virions." Journal of Virology **76**(1): 364-378.

Fuchs, W., B. G. Klupp, H. Granzow, N. Osterrieder and T. C. Mettenleiter (2002). "The interacting UL31 and UL34 gene products of pseudorabies virus are involved in egress from the host-cell nucleus and represent components of primary enveloped but not mature virions." J Virol **76**(1): 364-378.

Funk, C., M. Ott, V. Raschbichler, C. H. Nagel, A. Binz, B. Sodeik, R. Bauerfeind and S. M. Bailer (2015). "The Herpes Simplex Virus Protein pUL31 Escorts Nucleocapsids to Sites of Nuclear Egress, a Process Coordinated by Its N-Terminal Domain." PLoS Pathog **11**(6): e1004957.

Furukawa, K. (1999). "LAP2 binding protein 1 (L2BP1/BAF) is a candidate mediator of LAP2-chromatin interaction." J Cell Sci **112 (Pt 15)**: 2485-2492.

Galdiero, S., A. Falanga, M. Vitiello, H. Browne, C. Pedone and M. Galdiero (2005). "Fusogenic domains in herpes simplex virus type 1 glycoprotein H." J Biol Chem **280**(31): 28632-28643.

Gerace, L. and G. Blobel (1980). "The nuclear envelope lamina is reversibly depolymerized during mitosis." Cell **19**(1): 277-287.

Gerace, L. and B. Burke (1988). "Functional organization of the nuclear envelope." Annu Rev Cell Biol **4**: 335-374.

Geumann, U., S. V. Barysch, P. Hoopmann, R. Jahn and S. O. Rizzoli (2008). "SNARE function is not involved in early endosome docking." Mol Biol Cell **19**(12): 5327-5337.

Gillen, J., W. Li, Q. Liang, D. Avey, J. Wu, F. Wu, J. Myoung and F. Zhu (2015). "A survey of the interactome of Kaposi's sarcoma-associated herpesvirus ORF45 revealed its binding to viral ORF33 and cellular USP7, resulting in stabilization of ORF33 that is required for production of progeny viruses." J Virol **89**(9): 4918-4931.

Goldberg, M., A. Harel, M. Brandeis, T. Rechsteiner, T. J. Richmond, A. M. Weiss and Y. Gruenbaum (1999). "The tail domain of lamin Dm0 binds histones H2A and H2B." Proc Natl Acad Sci U S A **96**(6): 2852-2857.

Goldman, R. D., D. K. Shumaker, M. R. Erdos, M. Eriksson, A. E. Goldman, L. B. Gordon, Y. Gruenbaum, S. Khuon, M. Mendez, R. Varga and F. S. Collins (2004). "Accumulation of mutant lamin A causes progressive changes in nuclear architecture in Hutchinson-Gilford progeria syndrome." Proc Natl Acad Sci U S A **101**(24): 8963-8968.

Gordon, M. R., B. D. Pope, J. Sima and D. M. Gilbert (2015). "Many paths lead chromatin to the nuclear periphery." Bioessays **37**(8): 862-866.

Gorlich, D. and U. Kutay (1999). "Transport between the cell nucleus and the cytoplasm." Annu Rev Cell Dev Biol **15**: 607-660.

Gracanin, A., K. M. Dreijerink, R. B. van der Luijt, C. J. Lips and J. W. Hoppener (2009). "Tissue selectivity in multiple endocrine neoplasia type 1-associated tumorigenesis." Cancer Res **69**(16): 6371-6374.

Granzow, H., B. G. Klupp, W. Fuchs, J. Veits, N. Osterrieder and T. C. Mettenleiter (2001). "Egress of alphaherpesviruses: comparative ultrastructural study." J Virol **75**(8): 3675-3684.

Granzow, H., B. G. Klupp and T. C. Mettenleiter (2004). "The Pseudorabies Virus US3 Protein Is a Component of Primary and of Mature Virions." Journal of Virology **78**(3): 1314-1323.

Griffiths, S. J., M. Koegl, C. Boutell, H. L. Zenner, C. M. Crump, F. Pica, O. Gonzalez, C. C. Friedel, G. Barry, K. Martin, M. H. Craigon, R. Chen, L. N. Kaza, E. Fossum, J. K. Fazakerley, S. Efstathiou, A. Volpi, R. Zimmer, P. Ghazal and J. Haas (2013). "A systematic analysis of host factors reveals a Med23-interferon-lambda regulatory axis against herpes simplex virus type 1 replication." PLoS Pathog **9**(8): e1003514.

Grimsey, N. J., L. J. Coronel, I. C. Cordova and J. Trejo (2016). "Recycling and Endosomal Sorting of Protease-activated Receptor-1 Is Distinctly Regulated by Rab11A and Rab11B Proteins." J Biol Chem **291**(5): 2223-2236.

Gross, S. T., C. A. Harley and D. W. Wilson (2003). "The cytoplasmic tail of Herpes simplex virus glycoprotein H binds to the tegument protein VP16 in vitro and in vivo." Virology **317**(1): 1-12.

Gruenbaum, Y., A. Margalit, R. D. Goldman, D. K. Shumaker and K. L. Wilson (2005). "The nuclear lamina comes of age." Nat Rev Mol Cell Biol **6**(1): 21-31.

Guarda, A., F. Bolognese, I. M. Bonapace and G. Badaracco (2009). "Interaction between the inner nuclear membrane lamin B receptor and the heterochromatic methyl binding protein, MeCP2." Exp Cell Res **315**(11): 1895-1903.

Guttinger, S., E. Laurell and U. Kutay (2009). "Orchestrating nuclear envelope disassembly and reassembly during mitosis." Nat Rev Mol Cell Biol **10**(3): 178-191.

Hagen, C., K. C. Dent, T. Zeev-Ben-Mordehai, M. Grange, J. B. Bosse, C. Whittle, B. G. Klupp, C. A. Siebert, D. Vasishtan, F. J. Bauerlein, J. Cheleski, S. Werner, P. Guttmann, S. Rehbein, K. Henzler, J. Demmerle, B. Adler, U. Koszinowski, L. Schermelleh, G. Schneider, L. W. Enquist, J. M. Plitzko, T. C. Mettenleiter and K. Grunewald (2015). "Structural Basis of Vesicle Formation at the Inner Nuclear Membrane." Cell **163**(7): 1692-1701.

Haugo, A. C., M. L. Szpara, L. Parsons, L. W. Enquist and R. J. Roller (2011). "Herpes simplex virus 1 pUL34 plays a critical role in cell-to-cell spread of virus in addition to its role in virus replication." J Virol **85**(14): 7203-7215.

Heessen, S. and M. Fornerod (2007). "The inner nuclear envelope as a transcription factor resting place." EMBO Rep **8**(10): 914-919.

Hellberg, T., L. Passvogel, K. S. Schulz, B. G. Klupp and T. C. Mettenleiter (2016). "Nuclear Egress of Herpesviruses: The Prototypic Vesicular Nucleocytoplasmic Transport." Adv Virus Res **94**: 81-140.

Hennessy, C. and D. P. McKernan (2016). "Epigenetics and innate immunity: the 'unTolld' story." Immunol Cell Biol **94**(7): 631-639.

Heppner, C., K. Y. Bilimoria, S. K. Agarwal, M. Kester, L. J. Whitty, S. C. Guru, S. C. Chandrasekharappa, F. S. Collins, A. M. Spiegel, S. J. Marx and A. L. Burns (2001). "The tumor suppressor protein menin interacts with NF-kappaB proteins and inhibits NF-kappaB-mediated transactivation." Oncogene **20**(36): 4917-4925.

Hill, G. M., E. S. Ku and S. Dwarakanathan (2014). "Herpes simplex keratitis." Dis Mon **60**(6): 239-246.

Hinshaw, J. E., B. O. Carragher and R. A. Milligan (1992). "Architecture and design of the nuclear pore complex." Cell **69**(7): 1133-1141.

Hirohata, Y., J. Arii, Z. Liu, K. Shindo, M. Oyama, H. Kozuka-Hata, H. Sagara, A. Kato and Y. Kawaguchi (2015). "Herpes Simplex Virus 1 Recruits CD98 Heavy Chain and beta1 Integrin to the Nuclear Membrane for Viral De-Envelopment." J Virol **89**(15): 7799-7812.

Hoffmann, K., C. K. Dreger, A. L. Olins, D. E. Olins, L. D. Shultz, B. Lucke, H. Karl, R. Kaps, D. Muller, A. Vaya, J. Aznar, R. E. Ware, N. Sotelo Cruz, T. H. Lindner, H. Herrmann, A. Reis and K. Sperling (2002). "Mutations in the gene encoding the lamin B receptor produce an altered nuclear morphology in granulocytes (Pelger-Huet anomaly)." Nat Genet **31**(4): 410-414.

Hoger, T. H., G. Krohne and J. A. Kleinschmidt (1991). "Interaction of Xenopus lamins A and LII with chromatin in vitro mediated by a sequence element in the carboxyterminal domain." Exp Cell Res **197**(2): 280-289.

Hollinshead, M., H. L. Johns, C. L. Sayers, C. Gonzalez-Lopez, G. L. Smith and G. Elliott (2012). "Endocytic tubules regulated by Rab GTPases 5 and 11 are used for envelopment of herpes simplex virus." EMBO J **31**(21): 4204-4220.

Holm, C. K., S. B. Jensen, M. R. Jakobsen, N. Cheshenko, K. A. Horan, H. B. Moeller, R. Gonzalez-Dosal, S. B. Rasmussen, M. H. Christensen, T. O. Yarovinsky, F. J. Rixon, B. C. Herold, K. A. Fitzgerald and S. R. Paludan (2012). "Virus-cell fusion as a trigger of innate immunity dependent on the adaptor STING." Nat Immunol **13**(8): 737-743.

Holm, C. K., S. H. Rahbek, H. H. Gad, R. O. Bak, M. R. Jakobsen, Z. Jiang, A. L. Hansen, S. K. Jensen, C. Sun, M. K. Thomsen, A. Laustsen, C. G. Nielsen, K. Severinsen, Y. Xiong, D. L. Burdette, V. Hornung, R. J. Lebbink, M. Duch, K. A. Fitzgerald, S. Bahrami, J. G. Mikkelsen, R. Hartmann and S. R. Paludan (2016). "Influenza A virus targets a cGAS-independent STING pathway that controls enveloped RNA viruses." Nat Commun **7**: 10680.

Holmer, L. and H. J. Worman (2001). "Inner nuclear membrane proteins: functions and targeting." Cell Mol Life Sci **58**(12-13): 1741-1747.

Ikeo, Y., W. Yumita, A. Sakurai and K. Hashizume (2004). "JunD-menin interaction regulates c-Jun-mediated AP-1 transactivation." Endocr J **51**(3): 333-342.

Ishikawa, H. and G. N. Barber (2008). "STING is an endoplasmic reticulum adaptor that facilitates innate immune signalling." Nature **455**(7213): 674-678.

Ishikawa, H. and G. N. Barber (2011). "The STING pathway and regulation of innate immune signaling in response to DNA pathogens." Cell Mol Life Sci **68**(7): 1157-1165.

Ishikawa, H., Z. Ma and G. N. Barber (2009). "STING regulates intracellular DNA-mediated, type I interferon-dependent innate immunity." Nature **461**(7265): 788-792.

Jarsch, I. K., F. Daste and J. L. Gallop (2016). "Membrane curvature in cell biology: An integration of molecular mechanisms." J Cell Biol **214**(4): 375-387.

Jensen, H. L. and B. Norrild (1998). "Herpes simplex virus type 1-infected human embryonic lung cells studied by optimized immunogold cryosection electron microscopy." J Histochem Cytochem **46**(4): 487-496.

Johns, H. L., C. Gonzalez-Lopez, C. L. Sayers, M. Hollinshead and G. Elliott (2014). "Rab6 dependent post-Golgi trafficking of HSV1 envelope proteins to sites of virus envelopment." Traffic **15**(2): 157-178.

Johnson, D. C. and P. G. Spear (1982). "Monensin inhibits the processing of herpes simplex virus glycoproteins, their transport to the cell surface, and the egress of virions from infected cells." J Virol **43**(3): 1102-1112.

Johnson, D. C., T. W. Wisner and C. C. Wright (2011). "Herpes simplex virus glycoproteins gB and gD function in a redundant fashion to promote secondary envelopment." J Virol **85**(10): 4910-4926.

Jones, F. and C. Grose (1988). "Role of cytoplasmic vacuoles in varicella-zoster virus glycoprotein trafficking and virion envelopment." J Virol **62**(8): 2701-2711.

Kelly, B. J., C. Fraefel, A. L. Cunningham and R. J. Diefenbach (2009). "Functional roles of the tegument proteins of herpes simplex virus type 1." Virus Res **145**(2): 173-186.

Klemm, J. D., C. R. Beals and G. R. Crabtree (1997). "Rapid targeting of nuclear proteins to the cytoplasm." Curr Biol **7**(9): 638-644.

Klupp, B., J. Altenschmidt, H. Granzow, W. Fuchs and T. C. Mettenleiter (2008). "Glycoproteins required for entry are not necessary for egress of pseudorabies virus." J Virol **82**(13): 6299-6309.

Klupp, B. G., W. Fuchs, H. Granzow, R. Nixdorf and T. C. Mettenleiter (2002). "Pseudorabies virus UL36 tegument protein physically interacts with the UL37 protein." J Virol **76**(6): 3065-3071.

Klupp, B. G., H. Granzow, W. Fuchs, G. M. Keil, S. Finke and T. C. Mettenleiter (2007). "Vesicle formation from the nuclear membrane is induced by coexpression of two conserved herpesvirus proteins." Proc Natl Acad Sci U S A **104**(17): 7241-7246.

Klupp, B. G., H. Granzow and T. C. Mettenleiter (2000). "Primary envelopment of pseudorabies virus at the nuclear membrane requires the UL34 gene product." J Virol **74**(21): 10063-10073.

Klupp, B. G., H. Granzow and T. C. Mettenleiter (2001). "Effect of the pseudorabies virus US3 protein on nuclear membrane localization of the UL34 protein and virus egress from the nucleus." J Gen Virol **82**(Pt 10): 2363-2371.

Knipe, D. M. and A. Cliffe (2008). "Chromatin control of herpes simplex virus lytic and latent infection." Nat Rev Microbiol **6**(3): 211-221.

Kobiler, O., N. Drayman, V. Butin-Israeli and A. Oppenheim (2012). "Virus strategies for passing the nuclear envelope barrier." Nucleus **3**(6): 526-539.

Korfali, N., E. A. Fairley, S. K. Swanson, L. Florens and E. C. Schirmer (2009). "Use of sequential chemical extractions to purify nuclear membrane proteins for proteomics identification." Methods Mol Biol **528**: 201-225.

Korfali, N., L. Florens and E. C. Schirmer (2016). "Isolation, Proteomic Analysis, and Microscopy Confirmation of the Liver Nuclear Envelope Proteome." Methods Mol Biol **1411**: 3-44.

Korfali, N., G. S. Wilkie, S. K. Swanson, V. Srsen, D. G. Batrakou, E. A. Fairley, P. Malik, N. Zuleger, A. Goncharevich, J. de Las Heras, D. A. Kelly, A. R. Kerr, L. Florens and E. C. Schirmer (2010). "The leukocyte nuclear envelope proteome varies with cell activation and contains novel transmembrane proteins that affect genome architecture." Mol Cell Proteomics **9**(12): 2571-2585.

Kugelberg, E. (2015). "Macrophages: Controlling innate immune memory." Nat Rev Immunol **15**(10): 596.

Kuijpers, M., K. L. Yu, E. Teuling, A. Akhmanova, D. Jaarsma and C. C. Hoogenraad (2013). "The ALS8 protein VAPB interacts with the ER-Golgi recycling protein YIF1A and regulates membrane delivery into dendrites." EMBO J **32**(14): 2056-2072.

Kumar, K. P., K. M. McBride, B. K. Weaver, C. Dingwall and N. C. Reich (2000). "Regulated nuclear-cytoplasmic localization of interferon regulatory factor 3, a subunit of double-stranded RNA-activated factor 1." Mol Cell Biol **20**(11): 4159-4168.

Kupper, K., A. Kolbl, D. Biener, S. Dittrich, J. von Hase, T. Thormeyer, H. Fiegler, N. P. Carter, M. R. Speicher, T. Cremer and M. Cremer (2007). "Radial chromatin positioning is shaped by local gene density, not by gene expression." Chromosoma **116**(3): 285-306.

Laba, J. K., A. Steen and L. M. Veenhoff (2014). "Traffic to the inner membrane of the nuclear envelope." Curr Opin Cell Biol **28**: 36-45.

Lanctot, C., T. Cheutin, M. Cremer, G. Cavalli and T. Cremer (2007). "Dynamic genome architecture in the nuclear space: regulation of gene expression in three dimensions." Nat Rev Genet **8**(2): 104-115.

Lattanzi, G., M. Columbaro, E. Mattioli, V. Cenni, D. Camozzi, M. Wehnert, S. Santi, M. Riccio, R. Del Coco, N. M. Maraldi, S. Squarzoni, R. Foisner and C. Capanni (2007). "Pre-Lamin A processing is linked to heterochromatin organization." J Cell Biochem **102**(5): 1149-1159.

Lau, L., E. E. Gray, R. L. Brunette and D. B. Stetson (2015). "DNA tumor virus oncogenes antagonize the cGAS-STING DNA-sensing pathway." Science **350**(6260): 568-571.

Le Sage, V. and A. J. Mouland (2013). "Viral subversion of the nuclear pore complex." Viruses **5**(8): 2019-2042.

Leach, N., S. L. Bjerke, D. K. Christensen, J. M. Bouchard, F. Mou, R. Park, J. Baines, T. Haraguchi and R. J. Roller (2007). "Emerin is hyperphosphorylated and redistributed in herpes simplex virus type 1-infected cells in a manner dependent on both UL34 and US3." J Virol **81**(19): 10792-10803.

Leach, N. R. and R. J. Roller (2010). "Significance of host cell kinases in herpes simplex virus type 1 egress and lamin-associated protein disassembly from the nuclear lamina." Virology **406**(1): 127-137.

Lee, C. P., P. T. Liu, H. N. Kung, M. T. Su, H. H. Chua, Y. H. Chang, C. W. Chang, C. H. Tsai, F. T. Liu and M. R. Chen (2012). "The ESCRT machinery is recruited by the viral BFRF1 protein to the nucleus-associated membrane for the maturation of Epstein-Barr Virus." PLoS Pathog **8**(9): e1002904.

Lee, K. K., T. Haraguchi, R. S. Lee, T. Koujin, Y. Hiraoka and K. L. Wilson (2001). "Distinct functional domains in emerin bind lamin A and DNA-bridging protein BAF." J Cell Sci **114**(Pt 24): 4567-4573.

Leuzinger, H., U. Ziegler, E. M. Schraner, C. Fraefel, D. L. Glauser, I. Heid, M. Ackermann, M. Mueller and P. Wild (2005). "Herpes simplex virus 1 envelopment follows two diverse pathways." J Virol **79**(20): 13047-13059.

Lev, S., D. Ben Halevy, D. Peretti and N. Dahan (2008). "The VAP protein family: from cellular functions to motor neuron disease." Trends Cell Biol **18**(6): 282-290.

Li, C., L. L. Ge, P. P. Li, Y. Wang, M. X. Sun, L. Huang, H. Ishag, D. D. Di, Z. Q. Shen, W. X. Fan and X. Mao (2013). "The DEAD-box RNA helicase DDX5 acts as a positive regulator of Japanese encephalitis virus replication by binding to viral 3' UTR." Antiviral Res **100**(2): 487-499.

Li, H., J. Zhang, A. Kumar, M. Zheng, S. S. Atherton and F. S. Yu (2006). "Herpes simplex virus 1 infection induces the expression of proinflammatory cytokines, interferons and TLR7 in human corneal epithelial cells." Immunology **117**(2): 167-176.

Likhacheva, E. V. and S. S. Bogachev (2001). "Lamins and their functions in cell cycle." Membr Cell Biol **14**(5): 565-577.

Liu, H. M., H. Aizaki, K. S. Choi, K. Machida, J. J. Ou and M. M. Lai (2009). "SYNCRIP (synaptotagmin-binding, cytoplasmic RNA-interacting protein) is a host factor involved in hepatitis C virus RNA replication." Virology **386**(2): 249-256.

Liu, S., X. Cai, J. Wu, Q. Cong, X. Chen, T. Li, F. Du, J. Ren, Y. T. Wu, N. V. Grishin and Z. J. Chen (2015). "Phosphorylation of innate immune adaptor proteins MAVS, STING, and TRIF induces IRF3 activation." Science **347**(6227): aaa2630.

Liu, S. and B. Storrie (2012). "Are Rab proteins the link between Golgi organization and membrane trafficking?" Cell Mol Life Sci **69**(24): 4093-4106.

Liu, Y., J. Li, J. Chen, Y. Li, W. Wang, X. Du, W. Song, W. Zhang, L. Lin and Z. Yuan (2015). "Hepatitis B virus polymerase disrupts K63-linked ubiquitination of STING to block innate cytosolic DNA-sensing pathways." J Virol **89**(4): 2287-2300.

Loret, S., G. Guay and R. Lippe (2008). "Comprehensive characterization of extracellular herpes simplex virus type 1 virions." J Virol **82**(17): 8605-8618.

Lutcke, A., R. G. Parton, C. Murphy, V. M. Olkkonen, P. Dupree, A. Valencia, K. Simons and M. Zerial (1994). "Cloning and subcellular localization of novel rab proteins reveals polarized and cell type-specific expression." J Cell Sci **107 (Pt 12)**: 3437-3448.

Ma, J., J. M. Kelich and W. Yang (2016). "SPEED Microscopy and Its Application in Nucleocytoplasmic Transport." Methods Mol Biol **1411**: 503-518.

Maelfait, J., E. Seiradake and J. Rehwinkel (2014). "Keeping your armour intact: how HIV-1 evades detection by the innate immune system: HIV-1 capsid controls detection of reverse transcription products by the cytosolic DNA sensor cGAS." Bioessays **36**(7): 649-657.

Maison, C., A. Pyrpasopoulou, P. A. Theodoropoulos and S. D. Georgatos (1997). "The inner nuclear membrane protein LAP1 forms a native complex with B-type lamins and partitions with spindle-associated mitotic vesicles." EMBO J **16**(16): 4839-4850.

Malhas, A. N. and D. J. Vaux (2009). "Transcription factor sequestration by nuclear envelope components." Cell Cycle **8**(7): 959-960.

Malik, P., N. Korfali, V. Srsen, V. Lazou, D. G. Batrakou, N. Zuleger, D. M. Kavanagh, G. S. Wilkie, M. W. Goldberg and E. C. Schirmer (2010). "Cell-specific and lamin-dependent targeting of novel transmembrane proteins in the nuclear envelope." Cell Mol Life Sci **67**(8): 1353-1369.

Malik, P., A. Tabarraei, R. H. Kehlenbach, N. Korfali, R. Iwasawa, S. V. Graham and E. C. Schirmer (2012). "Herpes simplex virus ICP27 protein directly interacts with the nuclear pore complex through Nup62, inhibiting host nucleocytoplasmic transport pathways." J Biol Chem **287**(15): 12277-12292.

Malik, P., N. Zuleger, J. I. de las Heras, N. Saiz-Ros, A. A. Makarov, V. Lazou, P. Meinke, M. Waterfall, D. A. Kelly and E. C. Schirmer (2014). "NET23/STING promotes chromatin compaction from the nuclear envelope." PLoS One **9**(11): e111851.

Mammoto, A., T. Ohtsuka, I. Hotta, T. Sasaki and Y. Takai (1999). "Rab11BP/Rabphilin-11, a downstream target of rab11 small G protein implicated in vesicle recycling." J Biol Chem **274**(36): 25517-25524.

Manilal, S., T. M. Nguyen, C. A. Sewry and G. E. Morris (1996). "The Emery-Dreifuss muscular dystrophy protein, emerin, is a nuclear membrane protein." Hum Mol Genet **5**(6): 801-808.

Manna, D., J. Aligo, C. Xu, W. S. Park, H. Koc, W. D. Heo and K. V. Konan (2010). "Endocytic Rab proteins are required for hepatitis C virus replication complex formation." Virology **398**(1): 21-37.

Margalit, A., S. Vlcek, Y. Gruenbaum and R. Foisner (2005). "Breaking and making of the nuclear envelope." J Cell Biochem **95**(3): 454-465.

Maric, M., A. C. Haugo, W. Dauer, D. Johnson and R. J. Roller (2014). "Nuclear envelope breakdown induced by herpes simplex virus type 1 involves the activity of viral fusion proteins." Virology **460-461**: 128-137.

Martinez, V., E. Caumes and O. Chosidow (2008). "Treatment to prevent recurrent genital herpes." Curr Opin Infect Dis **21**(1): 42-48.

Mattout-Drubezki, A. and Y. Gruenbaum (2003). "Dynamic interactions of nuclear lamina proteins with chromatin and transcriptional machinery." Cell Mol Life Sci **60**(10): 2053-2063.

McDonald, W. H., D. L. Tabb, R. G. Sadygov, M. J. MacCoss, J. Venable, J. Graumann, J. R. Johnson, D. Cociorva and J. R. Yates, 3rd (2004). "MS1, MS2, and SQT-three unified, compact, and easily parsed file formats for the storage of shotgun proteomic spectra and identifications." Rapid Commun Mass Spectrom **18**(18): 2162-2168.

McGeoch, D. J., M. A. Dalrymple, A. J. Davison, A. Dolan, M. C. Frame, D. McNab, L. J. Perry, J. E. Scott and P. Taylor (1988). "The complete DNA sequence of the long unique region in the genome of herpes simplex virus type 1." J Gen Virol **69 (Pt 7)**: 1531-1574.

McGeoch, D. J., F. J. Rixon and A. J. Davison (2006). "Topics in herpesvirus genomics and evolution." Virus Res **117**(1): 90-104.

Melcon, G., S. Kozlov, D. A. Cutler, T. Sullivan, L. Hernandez, P. Zhao, S. Mitchell, G. Nader, M. Bakay, J. N. Rottman, E. P. Hoffman and C. L. Stewart (2006). "Loss of emerin at the nuclear envelope disrupts the Rb1/E2F and MyoD pathways during muscle regeneration." Hum Mol Genet **15**(4): 637-651.

Mellerick, D. M. and N. W. Fraser (1987). "Physical state of the latent herpes simplex virus genome in a mouse model system: evidence suggesting an episomal state." Virology **158**(2): 265-275.

Mettenleiter, T. C. (2002). "Herpesvirus Assembly and Egress." Journal of Virology **76**(4): 1537-1547.

Mettenleiter, T. C. (2004). "Budding events in herpesvirus morphogenesis." Virus Res **106**(2): 167-180.

Mettenleiter, T. C. (2016). "Breaching the Barrier-The Nuclear Envelope in Virus Infection." J Mol Biol **428**(10 Pt A): 1949-1961.

Mettenleiter, T. C., B. G. Klupp and H. Granzow (2009). "Herpesvirus assembly: an update." Virus Res **143**(2): 222-234.

Milbradt, J., R. Webel, S. Auerochs, H. Sticht and M. Marschall (2010). "Novel mode of phosphorylation-triggered reorganization of the nuclear lamina during nuclear egress of human cytomegalovirus." J Biol Chem **285**(18): 13979-13989.

Miller, N. G., M. W. Hill and M. W. Smith (1976). "Positional and species analysis of membrane phospholipids extracted from goldfish adapted to different environmental temperatures." Biochim Biophys Acta **455**(3): 644-654.

Miranda-Saksena, M., R. A. Boadle, P. Armati and A. L. Cunningham (2002). "In rat dorsal root ganglion neurons, herpes simplex virus type 1 tegument forms in the cytoplasm of the cell body." J Virol **76**(19): 9934-9951.

Mizutani, A., M. Fukuda, K. Ibata, Y. Shiraishi and K. Mikoshiba (2000). "SYNCRIP, a cytoplasmic counterpart of heterogeneous nuclear ribonucleoprotein R, interacts with ubiquitous synaptotagmin isoforms." J Biol Chem **275**(13): 9823-9831.

Monier, K., J. C. Armas, S. Etteldorf, P. Ghazal and K. F. Sullivan (2000). "Annexation of the interchromosomal space during viral infection." Nat Cell Biol **2**(9): 661-665.

Morris, J. B., H. Hofemeister and P. O'Hare (2007). "Herpes simplex virus infection induces phosphorylation and delocalization of emerin, a key inner nuclear membrane protein." J Virol **81**(9): 4429-4437.

Morrison, L. A. and G. S. DeLassus (2011). "Breach of the nuclear lamina during assembly of herpes simplex viruses." Nucleus **2**(4): 271-276.

Moses, M. J. (1956). "Studies on nuclei using correlated cytochemical, light, and electron microscope techniques." J Biophys Biochem Cytol **2**(4 Suppl): 397-406.

Mou, F., E. G. Wills, R. Park and J. D. Baines (2008). "Effects of lamin A/C, lamin B1, and viral US3 kinase activity on viral infectivity, virion egress, and the targeting of herpes simplex virus U(L)34-encoded protein to the inner nuclear membrane." J Virol **82**(16): 8094-8104.

Moy, R. H., B. S. Cole, A. Yasunaga, B. Gold, G. Shankarling, A. Varble, J. M. Molleston, B. R. tenOever, K. W. Lynch and S. Cherry (2014). "Stem-loop recognition by DDX17 facilitates miRNA processing and antiviral defense." Cell **158**(4): 764-777.

Muranyi, W., J. Haas, M. Wagner, G. Krohne and U. H. Koszinowski (2002). "Cytomegalovirus recruitment of cellular kinases to dissolve the nuclear lamina." Science **297**(5582): 854-857.

Naldinho-Souto, R., H. Browne and T. Minson (2006). "Herpes simplex virus tegument protein VP16 is a component of primary enveloped virions." J Virol **80**(5): 2582-2584.

Ni, L., S. Wang and C. Zheng (2012). "The nucleolus and herpesviral usurpation." J Med Microbiol **61**(Pt 12): 1637-1643.

Ognibene, A., P. Sabatelli, S. Petrini, S. Squarzoni, M. Riccio, S. Santi, M. Villanova, S. Palmeri, L. Merlini and N. M. Maraldi (1999). "Nuclear changes in a case of X-linked Emery-Dreifuss muscular dystrophy." Muscle Nerve **22**(7): 864-869.

Ohba, T., E. C. Schirmer, T. Nishimoto and L. Gerace (2004). "Energy- and temperature-dependent transport of integral proteins to the inner nuclear membrane via the nuclear pore." J Cell Biol **167**(6): 1051-1062.

Ohzeki, J., J. H. Bergmann, N. Kouprina, V. N. Noskov, M. Nakano, H. Kimura, W. C. Earnshaw, V. Larionov and H. Masumoto (2012). "Breaking the HAC Barrier: histone H3K9 acetyl/methyl balance regulates CENP-A assembly." EMBO J **31**(10): 2391-2402.

Ojala, P. M., B. Sodeik, M. W. Ebersold, U. Kutay and A. Helenius (2000). "Herpes simplex virus type 1 entry into host cells: reconstitution of capsid binding and uncoating at the nuclear pore complex in vitro." Mol Cell Biol **20**(13): 4922-4931.

Okada, Y., T. Suzuki, Y. Sunden, Y. Orba, S. Kose, N. Imamoto, H. Takahashi, S. Tanaka, W. W. Hall, K. Nagashima and H. Sawa (2005). "Dissociation of heterochromatin protein 1 from lamin B receptor induced by human polyomavirus agnoprotein: role in nuclear egress of viral particles." EMBO Rep **6**(5): 452-457.

Olins, A. L., G. Rhodes, D. B. Welch, M. Zwerger and D. E. Olins (2010). "Lamin B receptor: multi-tasking at the nuclear envelope." Nucleus **1**(1): 53-70.

Orzalli, M. H., N. A. DeLuca and D. M. Knipe (2012). "Nuclear IFI16 induction of IRF-3 signaling during herpesviral infection and degradation of IFI16 by the viral ICP0 protein." Proc Natl Acad Sci U S A **109**(44): E3008-3017.

Osada, S., S. Y. Ohmori and M. Taira (2003). "XMAN1, an inner nuclear membrane protein, antagonizes BMP signaling by interacting with Smad1 in Xenopus embryos." Development **130**(9): 1783-1794.

Ostlund, C., T. Sullivan, C. L. Stewart and H. J. Worman (2006). "Dependence of diffusional mobility of integral inner nuclear membrane proteins on A-type lamins." Biochemistry **45**(5): 1374-1382.

Owen, D. J., C. M. Crump and S. C. Graham (2015). "Tegument Assembly and Secondary Envelopment of Alphaherpesviruses." Viruses **7**(9): 5084-5114.

Padula, M. E., M. L. Sydnor and D. W. Wilson (2009). "Isolation and preliminary characterization of herpes simplex virus 1 primary enveloped virions from the perinuclear space." J Virol **83**(10): 4757-4765.

Paludan, S. R. and A. G. Bowie (2013). "Immune sensing of DNA." Immunity **38**(5): 870-880.

Park, R. and J. D. Baines (2006). "Herpes simplex virus type 1 infection induces activation and recruitment of protein kinase C to the nuclear membrane and increased phosphorylation of lamin B." J Virol **80**(1): 494-504.

Pasdeloup, D., F. Beilstein, A. P. Roberts, M. McElwee, D. McNab and F. J. Rixon (2010). "Inner tegument protein pUL37 of herpes simplex virus type 1 is involved in directing capsids to the trans-Golgi network for envelopment." J Gen Virol **91**(Pt 9): 2145-2151.

Pasdeloup, D., D. Blondel, A. L. Isidro and F. J. Rixon (2009). "Herpesvirus capsid association with the nuclear pore complex and viral DNA release involve the nucleoporin CAN/Nup214 and the capsid protein pUL25." J Virol **83**(13): 6610-6623.

Passvogel, L., B. G. Klupp, H. Granzow, W. Fuchs and T. C. Mettenleiter (2015). "Functional characterization of nuclear trafficking signals in pseudorabies virus pUL31." J Virol **89**(4): 2002-2012.

Penfold, M. E., P. Armati and A. L. Cunningham (1994). "Axonal transport of herpes simplex virions to epidermal cells: evidence for a specialized mode of virus transport and assembly." Proc Natl Acad Sci U S A **91**(14): 6529-6533.

Peretti, D., N. Dahan, E. Shimoni, K. Hirschberg and S. Lev (2008). "Coordinated lipid transfer between the endoplasmic reticulum and the Golgi complex requires the VAP proteins and is essential for Golgi-mediated transport." Mol Biol Cell **19**(9): 3871-3884.

Peter, M., J. S. Sanghera, S. L. Pelech and E. A. Nigg (1992). "Mitogen-activated protein kinases phosphorylate nuclear lamins and display sequence specificity overlapping that of mitotic protein kinase p34cdc2." Eur J Biochem **205**(1): 287-294.

Phair, R. D. and T. Misteli (2001). "Kinetic modelling approaches to in vivo imaging." Nat Rev Mol Cell Biol **2**(12): 898-907.

Pignatelli, S., P. Dal Monte, M. P. Landini, B. Severi, R. Nassiri, J. Gilloteaux, J. M. Papadimitriou, G. R. Shellam, T. Mertens, C. Buser, D. Michel and P. Walther (2007). "Cytomegalovirus primary envelopment at large nuclear membrane infoldings: what's new?" J Virol **81**(13): 7320-7321; author reply 7321-7322.

Placek, B. J. and S. L. Berger (2010). "Chromatin dynamics during herpes simplex virus-1 lytic infection." Biochim Biophys Acta **1799**(3-4): 223-227.

Polioudaki, H., N. Kourmouli, V. Drosou, A. Bakou, P. A. Theodoropoulos, P. B. Singh, T. Giannakouros and S. D. Georgatos (2001). "Histones H3/H4 form a tight complex with the inner nuclear membrane protein LBR and heterochromatin protein 1." EMBO Rep **2**(10): 920-925.

Prosser, D. C., D. Tran, P. Y. Gougeon, C. Verly and J. K. Ngsee (2008). "FFAT rescues VAPA-mediated inhibition of ER-to-Golgi transport and VAPB-mediated ER aggregation." J Cell Sci **121**(Pt 18): 3052-3061.

Prunuske, A. J. and K. S. Ullman (2006). "The nuclear envelope: form and reformation." Curr Opin Cell Biol **18**(1): 108-116.

Ratnaparkhi, A., G. M. Lawless, F. E. Schweizer, P. Golshani and G. R. Jackson (2008). "A Drosophila model of ALS: human ALS-associated mutation in VAP33A suggests a dominant negative mechanism." PLoS One **3**(6): e2334.

Reiman, A., J. E. Powell, K. J. Flavell, R. G. Grundy, J. R. Mann, S. Parkes, D. Redfern, L. S. Young and P. G. Murray (2003). "Seasonal differences in the onset of the EBV-positive and -negative forms of paediatric Hodgkin's lymphoma." Br J Cancer **89**(7): 1200-1201.

Reske, A., G. Pollara, C. Krummenacher, B. M. Chain and D. R. Katz (2007). "Understanding HSV-1 entry glycoproteins." Rev Med Virol **17**(3): 205-215.

Reyland, M. E. (2009). "Protein kinase C isoforms: Multi-functional regulators of cell life and death." Front Biosci (Landmark Ed) **14**: 2386-2399.

Reynolds, A. E., L. Liang and J. D. Baines (2004). "Conformational changes in the nuclear lamina induced by herpes simplex virus type 1 require genes U(L)31 and U(L)34." J Virol **78**(11): 5564-5575.

Reynolds, A. E., B. J. Ryckman, J. D. Baines, Y. Zhou, L. Liang and R. J. Roller (2001). "UL31 and UL34 Proteins of Herpes Simplex Virus Type 1 Form a Complex That Accumulates at the Nuclear Rim and Is Required for Envelopment of Nucleocapsids." Journal of Virology **75**(18): 8803-8817.

Reynolds, A. E., E. G. Wills, R. J. Roller, B. J. Ryckman and J. D. Baines (2002). "Ultrastructural Localization of the Herpes Simplex Virus Type 1 UL31, UL34, and US3 Proteins Suggests Specific Roles in Primary Envelopment and Egress of Nucleocapsids." Journal of Virology **76**(17): 8939-8952.

Rice, J. A. (1997). "Community health assessment: a new generation." Hosp Technol Ser **16**(4): 1-31.

Rice, S. A. and D. M. Knipe (1990). "Genetic evidence for two distinct transactivation functions of the herpes simplex virus alpha protein ICP27." J Virol **64**(4): 1704-1715.

Robson, M. I., J. I. de Las Heras, R. Czapiewski, P. Le Thanh, D. G. Booth, D. A. Kelly, S. Webb, A. R. Kerr and E. C. Schirmer (2016). "Tissue-Specific Gene Repositioning by Muscle Nuclear Membrane Proteins Enhances Repression of Critical Developmental Genes during Myogenesis." Mol Cell **62**(6): 834-847.

Roger, T., J. Lugrin, D. Le Roy, G. Goy, M. Mombelli, T. Koessler, X. C. Ding, A. L. Chanson, M. K. Reymond, I. Miconnet, J. Schrenzel, P. Francois and T. Calandra (2011). "Histone deacetylase inhibitors impair innate immune responses to Toll-like receptor agonists and to infection." Blood **117**(4): 1205-1217.

Rolls, M. M., P. A. Stein, S. S. Taylor, E. Ha, F. McKeon and T. A. Rapoport (1999). "A visual screen of a GFP-fusion library identifies a new type of nuclear envelope membrane protein." J Cell Biol **146**(1): 29-44.

Rowe, R. K., J. W. Suszko and A. Pekosz (2008). "Roles for the recycling endosome, Rab8, and Rab11 in hantavirus release from epithelial cells." Virology **382**(2): 239-249.

Sabbattini, P., M. Sjoberg, S. Nikic, A. Frangini, P. H. Holmqvist, N. Kunowska, T. Carroll, E. Brookes, S. J. Arthur, A. Pombo and N. Dillon (2014). "An H3K9/S10 methyl-phospho switch modulates Polycomb and Pol II binding at repressed genes during differentiation." Mol Biol Cell **25**(6): 904-915.

Sagou, K., M. Uema and Y. Kawaguchi (2010). "Nucleolin is required for efficient nuclear egress of herpes simplex virus type 1 nucleocapsids." J Virol **84**(4): 2110-2121.

Salloum, S., H. Wang, C. Ferguson, R. G. Parton and A. W. Tai (2013). "Rab18 binds to hepatitis C virus NS5A and promotes interaction between sites of viral replication and lipid droplets." PLoS Pathog **9**(8): e1003513.

Sandri-Goldin, R. M. (2008). "The many roles of the regulatory protein ICP27 during herpes simplex virus infection." Front Biosci **13**: 5241-5256.

Sandri-Goldin, R. M. (2011). "The many roles of the highly interactive HSV protein ICP27, a key regulator of infection." Future Microbiol **6**(11): 1261-1277.

Sato, M., S. Matsubara, A. Miyauchi, H. Ohye, H. Imachi, K. Murao and J. Takahara (1998). "Identification of five novel germline mutations of the MEN1 gene in Japanese multiple endocrine neoplasia type 1 (MEN1) families." J Med Genet **35**(11): 915-919.

Sauer, J. D., K. Sotelo-Troha, J. von Moltke, K. M. Monroe, C. S. Rae, S. W. Brubaker, M. Hyodo, Y. Hayakawa, J. J. Woodward, D. A. Portnoy and R. E. Vance (2011). "The N-ethyl-N-nitrosourea-induced Goldenticket mouse mutant reveals an essential function of Sting in the in vivo interferon response to Listeria monocytogenes and cyclic dinucleotides." Infect Immun **79**(2): 688-694.

Schirmer, E. C., L. Florens, T. Guan, J. R. Yates, 3rd and L. Gerace (2003). "Nuclear membrane proteins with potential disease links found by subtractive proteomics." Science **301**(5638): 1380-1382.

Schirmer, E. C., L. Florens, T. Guan, J. R. Yates, 3rd and L. Gerace (2005). "Identification of novel integral membrane proteins of the nuclear envelope with potential disease links using subtractive proteomics." Novartis Found Symp **264**: 63-76; discussion 76-80, 227-230.

Schirmer, E. C. and R. Foisner (2007). "Proteins that associate with lamins: many faces, many functions." Exp Cell Res **313**(10): 2167-2179.

Schirmer, E. C. and L. Gerace (2005). "The nuclear membrane proteome: extending the envelope." Trends Biochem Sci **30**(10): 551-558.

Schmitz, M. L., M. Kracht and V. V. Saul (2014). "The intricate interplay between RNA viruses and NF-kappaB." Biochim Biophys Acta **1843**(11): 2754-2764.

Schulz, K. S., B. G. Klupp, H. Granzow, L. Passvogel and T. C. Mettenleiter (2015). "Herpesvirus nuclear egress: Pseudorabies Virus can simultaneously induce nuclear envelope breakdown and exit the nucleus via the envelopment-deenvelopment-pathway." Virus Res **209**: 76-86.

Scott, E. S. and P. O'Hare (2001). "Fate of the Inner Nuclear Membrane Protein Lamin B Receptor and Nuclear Lamins in Herpes Simplex Virus Type 1 Infection." Journal of Virology **75**(18): 8818-8830.

Senior, A. and L. Gerace (1988). "Integral membrane proteins specific to the inner nuclear membrane and associated with the nuclear lamina." J Cell Biol **107**(6 Pt 1): 2029-2036.

Sewry, C. A., S. C. Brown, E. Mercuri, G. Bonne, L. Feng, G. Camici, G. E. Morris and F. Muntoni (2001). "Skeletal muscle pathology in autosomal dominant Emery-Dreifuss muscular dystrophy with lamin A/C mutations." Neuropathol Appl Neurobiol **27**(4): 281-290.

Sharma, M., B. J. Bender, J. P. Kamil, M. F. Lye, J. M. Pesola, N. I. Reim, J. M. Hogle and D. M. Coen (2015). "Human cytomegalovirus UL97 phosphorylates the viral nuclear egress complex." J Virol **89**(1): 523-534.

Shiba, C., T. Daikoku, F. Goshima, H. Takakuwa, Y. Yamauchi, O. Koiwai and Y. Nishiyama (2000). "The UL34 gene product of herpes simplex virus type 2 is a tail-anchored type II membrane protein that is significant for virus envelopment." J Gen Virol **81**(Pt 10): 2397-2405.

Shoeman, R. L. and P. Traub (1990). "The in vitro DNA-binding properties of purified nuclear lamin proteins and vimentin." J Biol Chem **265**(16): 9055-9061.

Shu, H. B. and Y. Y. Wang (2014). "Adding to the STING." Immunity **41**(6): 871-873.

Shumaker, D. K., T. Dechat, A. Kohlmaier, S. A. Adam, M. R. Bozovsky, M. R. Erdos, M. Eriksson, A. E. Goldman, S. Khuon, F. S. Collins, T. Jenuwein and R. D. Goldman (2006). "Mutant nuclear lamin A leads to progressive alterations of epigenetic control in premature aging." Proc Natl Acad Sci U S A **103**(23): 8703-8708.

Simmons, A. (2002). "Clinical manifestations and treatment considerations of herpes simplex virus infection." J Infect Dis **186 Suppl 1**: S71-77.

Simpson-Holley, M., J. Baines, R. Roller and D. M. Knipe (2004). "Herpes simplex virus 1 U(L)31 and U(L)34 gene products promote the late maturation of viral replication compartments to the nuclear periphery." J Virol **78**(11): 5591-5600.

Simpson-Holley, M., R. C. Colgrove, G. Nalepa, J. W. Harper and D. M. Knipe (2005). "Identification and functional evaluation of cellular and viral factors involved in the alteration of nuclear architecture during herpes simplex virus 1 infection." J Virol **79**(20): 12840-12851.

Skepper, J. N., A. Whiteley, H. Browne and A. Minson (2001). "Herpes simplex virus nucleocapsids mature to progeny virions by an envelopment --> deenvelopment --> reenvelopment pathway." J Virol **75**(12): 5697-5702.

Smoyer, C. J. and S. L. Jaspersen (2014). "Breaking down the wall: the nuclear envelope during mitosis." Curr Opin Cell Biol **26**: 1-9.

Sola, I., C. Galan, P. A. Mateos-Gomez, L. Palacio, S. Zuniga, J. L. Cruz, F. Almazan and L. Enjuanes (2011). "The polypyrimidine tract-binding protein affects coronavirus RNA accumulation levels and relocalizes viral RNAs to novel cytoplasmic domains different from replication-transcription sites." J Virol **85**(10): 5136-5149.

Soliman, T. M., R. M. Sandri-Goldin and S. J. Silverstein (1997). "Shuttling of the herpes simplex virus type 1 regulatory protein ICP27 between the nucleus and cytoplasm mediates the expression of late proteins." J Virol **71**(12): 9188-9197.

Somech, R., S. Shaklai, O. Geller, N. Amariglio, A. J. Simon, G. Rechavi and E. N. Gal-Yam (2005). "The nuclear-envelope protein and transcriptional repressor LAP2beta interacts with HDAC3 at the nuclear periphery, and induces histone H4 deacetylation." J Cell Sci **118**(Pt 17): 4017-4025.

Soo, K. Y., M. Halloran, V. Sundaramoorthy, S. Parakh, R. P. Toth, K. A. Southam, C. A. McLean, P. Lock, A. King, M. A. Farg and J. D. Atkin (2015). "Rab1-dependent ER-Golgi transport dysfunction is a common pathogenic mechanism in SOD1, TDP-43 and FUS-associated ALS." Acta Neuropathol **130**(5): 679-697.

Soullam, B. and H. J. Worman (1993). "The amino-terminal domain of the lamin B receptor is a nuclear envelope targeting signal." J Cell Biol **120**(5): 1093-1100.

Speese, S. D., J. Ashley, V. Jokhi, J. Nunnari, R. Barria, Y. Li, B. Ataman, A. Koon, Y. T. Chang, Q. Li, M. J. Moore and V. Budnik (2012). "Nuclear envelope budding enables large ribonucleoprotein particle export during synaptic Wnt signaling." Cell **149**(4): 832-846.

Stancheva, I. and E. C. Schirmer (2014). "Nuclear envelope: connecting structural genome organization to regulation of gene expression." Adv Exp Med Biol **773**: 209-244.

Stannard, L. M., S. Himmelhoch and S. Wynchank (1996). "Intra-nuclear localization of two envelope proteins, gB and gD, of herpes simplex virus." Arch Virol **141**(3-4): 505-524.

Stender, J. D. and C. K. Glass (2013). "Epigenomic control of the innate immune response." Curr Opin Pharmacol **13**(4): 582-587.

Sun, W., Y. Li, L. Chen, H. Chen, F. You, X. Zhou, Y. Zhou, Z. Zhai, D. Chen and Z. Jiang (2009). "ERIS, an endoplasmic reticulum IFN stimulator, activates innate immune signaling through dimerization." Proc Natl Acad Sci U S A **106**(21): 8653-8658.

Tabb, D. L., W. H. McDonald and J. R. Yates, 3rd (2002). "DTASelect and Contrast: tools for assembling and comparing protein identifications from shotgun proteomics." J Proteome Res **1**(1): 21-26.

Tanaka, Y. and Z. J. Chen (2012). "STING specifies IRF3 phosphorylation by TBK1 in the cytosolic DNA signaling pathway." Sci Signal **5**(214): ra20.

Tandon, R., E. S. Mocarski and J. F. Conway (2015). "The A, B, Cs of herpesvirus capsids." Viruses **7**(3): 899-914.

Taniura, H., C. Glass and L. Gerace (1995). "A chromatin binding site in the tail domain of nuclear lamins that interacts with core histones." J Cell Biol **131**(1): 33-44.

Taylor, M. P., O. Kobiler and L. W. Enquist (2012). "Alphaherpesvirus axon-to-cell spread involves limited virion transmission." Proc Natl Acad Sci U S A **109**(42): 17046-17051.

Tokuyasu, K. T. (1973). "A technique for ultracryotomy of cell suspensions and tissues." J Cell Biol **57**(2): 551-565.

Torrisi, M. R., C. Di Lazzaro, A. Pavan, L. Pereira and G. Campadelli-Fiume (1992). "Herpes simplex virus envelopment and maturation studied by fracture label." J Virol **66**(1): 554-561.

Tran, D., A. Chalhoub, A. Schooley, W. Zhang and J. K. Ngsee (2012). "A mutation in VAPB that causes amyotrophic lateral sclerosis also causes a nuclear envelope defect." J Cell Sci **125**(Pt 12): 2831-2836.

Ullrich, O., S. Reinsch, S. Urbe, M. Zerial and R. G. Parton (1996). "Rab11 regulates recycling through the pericentriolar recycling endosome." J Cell Biol **135**(4): 913-924.

Ungar, D. and F. M. Hughson (2003). "SNARE protein structure and function." Annu Rev Cell Dev Biol **19**: 493-517.

Ungricht, R., M. Klann, P. Horvath and U. Kutay (2015). "Diffusion and retention are major determinants of protein targeting to the inner nuclear membrane." J Cell Biol **209**(5): 687-703.

Ungricht, R. and U. Kutay (2015). "Establishment of NE asymmetry-targeting of membrane proteins to the inner nuclear membrane." Curr Opin Cell Biol **34**: 135-141.

Upadya, M. H., J. J. Aweya and Y. J. Tan (2014). "Understanding the interaction of hepatitis C virus with host DEAD-box RNA helicases." World J Gastroenterol **20**(11): 2913-2926.

Vanden Berghe, W., M. N. Ndlovu, R. Hoya-Arias, N. Dijsselbloem, S. Gerlo and G. Haegeman (2006). "Keeping up NF-kappaB appearances: epigenetic control of immunity or inflammation-triggered epigenetics." Biochem Pharmacol **72**(9): 1114-1131.

Wagenaar, F., J. M. Pol, B. Peeters, A. L. Gielkens, N. de Wind and T. G. Kimman (1995). "The US3-encoded protein kinase from pseudorabies virus affects egress of virions from the nucleus." J Gen Virol **76 (Pt 7)**: 1851-1859.

Wandinger-Ness, A. and M. Zerial (2014). "Rab proteins and the compartmentalization of the endosomal system." Cold Spring Harb Perspect Biol **6**(11): a022616.

Wang, L., K. S. Jeng and M. M. Lai (2011). "Poly(C)-binding protein 2 interacts with sequences required for viral replication in the hepatitis C virus (HCV) 5' untranslated region and directs HCV RNA replication through circularizing the viral genome." J Virol **85**(16): 7954-7964.

Wang, Y., A. J. Herron and H. J. Worman (2006). "Pathology and nuclear abnormalities in hearts of transgenic mice expressing M371K lamin A encoded by an LMNA mutation causing Emery-Dreifuss muscular dystrophy." Hum Mol Genet **15**(16): 2479-2489.

Washburn, M. P., D. Wolters and J. R. Yates, 3rd (2001). "Large-scale analysis of the yeast proteome by multidimensional protein identification technology." Nat Biotechnol **19**(3): 242-247.

Weidmann, M., U. Meyer-Konig and F. T. Hufert (2003). "Rapid detection of herpes simplex virus and varicella-zoster virus infections by real-time PCR." J Clin Microbiol **41**(4): 1565-1568.

Wen, K. W. and B. Damania (2010). "Kaposi sarcoma-associated herpesvirus (KSHV): molecular biology and oncogenesis." Cancer Lett **289**(2): 140-150.

Whitley, R. J. and B. Roizman (2001). "Herpes simplex virus infections." Lancet **357**(9267): 1513-1518.

Wild, P., M. Engels, C. Senn, K. Tobler, U. Ziegler, E. M. Schraner, E. Loepfe, M. Ackermann, M. Mueller and P. Walther (2005). "Impairment of nuclear pores in bovine herpesvirus 1-infected MDBK cells." J Virol **79**(2): 1071-1083.

Wild, P., C. Senn, C. L. Manera, E. Sutter, E. M. Schraner, K. Tobler, M. Ackermann, U. Ziegler, M. S. Lucas and A. Kaech (2009). "Exploring the nuclear envelope of herpes simplex virus 1-infected cells by high-resolution microscopy." J Virol **83**(1): 408-419.

Wilkie, G. S., N. Korfali, S. K. Swanson, P. Malik, V. Srsen, D. G. Batrakou, J. de las Heras, N. Zuleger, A. R. Kerr, L. Florens and E. C. Schirmer (2011). "Several novel nuclear envelope transmembrane proteins identified in skeletal muscle have cytoskeletal associations." Mol Cell Proteomics **10**(1): M110 003129.

Wills, E., F. Mou and J. D. Baines (2009). "The U(L)31 and U(L)34 gene products of herpes simplex virus 1 are required for optimal localization of viral glycoproteins D and M to the inner nuclear membranes of infected cells." J Virol **83**(10): 4800-4809.

Wisner, T. W., C. C. Wright, A. Kato, Y. Kawaguchi, F. Mou, J. D. Baines, R. J. Roller and D. C. Johnson (2009). "Herpesvirus gB-induced fusion between the virion envelope and outer nuclear membrane during virus egress is regulated by the viral US3 kinase." J Virol **83**(7): 3115-3126.

Wollert, T., D. Yang, X. Ren, H. H. Lee, Y. J. Im and J. H. Hurley (2009). "The ESCRT machinery at a glance." J Cell Sci **122**(Pt 13): 2163-2166.

Worman, H. J., C. D. Evans and G. Blobel (1990). "The lamin B receptor of the nuclear envelope inner membrane: a polytopic protein with eight potential transmembrane domains." J Cell Biol **111**(4): 1535-1542.

Worman, H. J. and E. C. Schirmer (2015). "Nuclear membrane diversity: underlying tissue-specific pathologies in disease?" Curr Opin Cell Biol **34**: 101-112.

Worman, H. J., J. Yuan, G. Blobel and S. D. Georgatos (1988). "A lamin B receptor in the nuclear envelope." Proc Natl Acad Sci U S A **85**(22): 8531-8534.

Wright, C. C., T. W. Wisner, B. P. Hannah, R. J. Eisenberg, G. H. Cohen and D. C. Johnson (2009). "Fusion between perinuclear virions and the outer nuclear membrane requires the fusogenic activity of herpes simplex virus gB." J Virol **83**(22): 11847-11856.

Wu, J. and Z. J. Chen (2014). "Innate immune sensing and signaling of cytosolic nucleic acids." Annu Rev Immunol **32**: 461-488.

Wu, W., F. Lin and H. J. Worman (2002). "Intracellular trafficking of MAN1, an integral protein of the nuclear envelope inner membrane." J Cell Sci **115**(Pt 7): 1361-1371.

Yamauchi, Y., C. Shiba, F. Goshima, A. Nawa, T. Murata and Y. Nishiyama (2001). "Herpes simplex virus type 2 UL34 protein requires UL31 protein for its relocation to the internal nuclear membrane in transfected cells." J Gen Virol **82**(Pt 6): 1423-1428.

Ye, Q. and H. J. Worman (1996). "Interaction between an integral protein of the nuclear envelope inner membrane and human chromodomain proteins homologous to Drosophila HP1." J Biol Chem **271**(25): 14653-14656.

Zeev-Ben-Mordehai, T., D. Vasishtan, C. A. Siebert, C. Whittle and K. Grunewald (2014). "Extracellular vesicles: a platform for the structure determination of membrane proteins by Cryo-EM." Structure **22**(11): 1687-1692.

Zenner, H. L., S. Yoshimura, F. A. Barr and C. M. Crump (2011). "Analysis of Rab GTPase-activating proteins indicates that Rab1a/b and Rab43 are important for herpes simplex virus 1 secondary envelopment." J Virol **85**(16): 8012-8021.

Zerial, M. and H. McBride (2001). "Rab proteins as membrane organizers." Nat Rev Mol Cell Biol **2**(2): 107-117.

Zhang, Y., Z. Wen, M. P. Washburn and L. Florens (2011). "Improving proteomics mass accuracy by dynamic offline lock mass." Anal Chem **83**(24): 9344-9351.

Zhao, S., X. Ge, X. Wang, A. Liu, X. Guo, L. Zhou, K. Yu and H. Yang (2015). "The DEAD-box RNA helicase 5 positively regulates the replication of porcine reproductive and respiratory syndrome virus by interacting with viral Nsp9 in vitro." Virus Res **195**: 217-224.

Zhong, B., Y. Yang, S. Li, Y. Y. Wang, Y. Li, F. Diao, C. Lei, X. He, L. Zhang, P. Tien and H. B. Shu (2008). "The adaptor protein MITA links virus-sensing receptors to IRF3 transcription factor activation." Immunity **29**(4): 538-550.

Zhong, B., L. Zhang, C. Lei, Y. Li, A. P. Mao, Y. Yang, Y. Y. Wang, X. L. Zhang and H. B. Shu (2009). "The ubiquitin ligase RNF5 regulates antiviral responses by mediating degradation of the adaptor protein MITA." Immunity **30**(3): 397-407.

Zhu, M., T. Fang, S. Li, K. Meng and D. Guo (2015). "Bipartite Nuclear Localization Signal Controls Nuclear Import and DNA-Binding Activity of IFN Regulatory Factor 3." J Immunol **195**(1): 289-297.

Zimmerberg, J. and K. Gawrisch (2006). "The physical chemistry of biological membranes." Nat Chem Biol **2**(11): 564-567.

Zufferey, R., T. Dull, R. J. Mandel, A. Bukovsky, D. Quiroz, L. Naldini and D. Trono (1998). "Self-inactivating lentivirus vector for safe and efficient in vivo gene delivery." J Virol **72**(12): 9873-9880.

Zuleger, N., S. Boyle, D. A. Kelly, J. I. de las Heras, V. Lazou, N. Korfali, D. G. Batrakou, K. N. Randles, G. E. Morris, D. J. Harrison, W. A. Bickmore and E. C. Schirmer (2013). "Specific nuclear envelope transmembrane proteins can promote the location of chromosomes to and from the nuclear periphery." Genome Biol **14**(2): R14.

Zuleger, N., D. A. Kelly, A. C. Richardson, A. R. Kerr, M. W. Goldberg, A. B. Goryachev and E. C. Schirmer (2011). "System analysis shows distinct mechanisms and common principles of nuclear envelope protein dynamics." J Cell Biol **193**(1): 109-123.

Zuleger, N., A. R. Kerr and E. C. Schirmer (2012). "Many mechanisms, one entrance: membrane protein translocation into the nucleus." Cell Mol Life Sci **69**(13): 2205-2216.

Zuleger, N., N. Korfali and E. C. Schirmer (2008). "Inner nuclear membrane protein transport is mediated by multiple mechanisms." Biochem Soc Trans **36**(Pt 6): 1373-1377.

Appendix

Please, kindly refer to the electronic copy (CD) in order to have a detailed information of the proteomic dataset.